

PROCESSING AND CHARACTERIZATION OF CARBON NANOTUBE  
BASED CONDUCTIVE POLYMER COMPOSITES

A THESIS SUBMITTED TO  
THE GRADUATE SCHOOL OF NATURAL AND APPLIED SCIENCES  
OF  
MIDDLE EAST TECHNICAL UNIVERSITY

BY

SERTAN YEŞİL

IN PARTIAL FULFILLMENT OF THE REQUIREMENTS  
FOR  
THE DEGREE OF DOCTOR OF PHILOSOPHY  
IN  
CHEMICAL ENGINEERING

MAY 2010

Approval of the thesis:

**PROCESSING AND CHARACTERIZATION OF CARBON NANOTUBE BASED  
CONDUCTIVE POLYMER COMPOSITES**

submitted by **SERTAN YEŞİL** in partial fulfillment of the requirements for the degree of **Doctor of Philosophy in Chemical Engineering Department, Middle East Technical University** by,

Prof. Dr. Canan Özgen  
Dean, Graduate School of **Natural and Applied Sciences**

\_\_\_\_\_

Prof. Dr. Gürkan Karakaş  
Head of Department, **Chemical Engineering**

\_\_\_\_\_

Assoc. Prof. Dr. Göknur Bayram  
Supervisor, **Chemical Engineering Dept., METU**

\_\_\_\_\_

**Examining Committee Members:**

Prof. Dr. Ülkü Yılmaz  
Chemical Engineering Dept., METU

\_\_\_\_\_

Assoc. Prof. Dr. Göknur Bayram  
Chemical Engineering Dept., METU

\_\_\_\_\_

Prof. Dr. Leyla Aras  
Chemistry Dept., METU

\_\_\_\_\_

Prof. Dr. Ayşe Nilgün Akın  
Chemical Engineering Dept., Kocaeli University

\_\_\_\_\_

Prof. Dr. Zuhale Küçükayavuz  
Chemistry Dept., METU

\_\_\_\_\_

**Date:**

**28.05.2010**

\_\_\_\_\_

**I hereby declare that all information in this document has been obtained and presented in accordance with academic rules and ethical conduct. I also declare that, as required by these rules and conduct, I have fully cited and referenced all material and results that are not original to this work.**

Name, Last name: Sertan Yeşil

Signature:

## ABSTRACT

### PROCESSING AND CHARACTERIZATION OF CARBON NANOTUBE BASED CONDUCTIVE POLYMER COMPOSITES

Yeşil, Sertan

Ph.D., Department of Chemical Engineering

Supervisor: Assoc. Prof. Dr. Göknur Bayram

May 2010, 265 pages

The aim of this study was to improve the mechanical and electrical properties of conductive polymer composites. For this purpose, different studies were performed in this dissertation. In order to investigate the effects of the carbon nanotube (CNT) surface treatment on the morphology, electrical and mechanical properties of the composites, poly(ethylene terephthalate) (PET) based conductive polymer composites were prepared by using as-received, purified and modified carbon nanotubes in a twin screw extruder.

During the purification of carbon nanotubes, surface properties of carbon nanotubes were altered by purifying them with nitric acid ( $\text{HNO}_3$ ), sulfuric acid ( $\text{H}_2\text{SO}_4$ ), ammonium hydroxide ( $\text{NH}_4\text{OH}$ ) and hydrogen peroxide ( $\text{H}_2\text{O}_2$ ) mixtures. Electron Spectroscopy for Chemical Analysis (ESCA) results indicated the removal of metallic catalyst residues from the structure of carbon nanotubes and increase in the oxygen content of carbon nanotube surface as a result of purification procedure. Surface structure of the purified carbon nanotubes was also modified by treatment with sodium dodecyl sulfate (SDS), poly(ethylene glycol) (PEG) and diglycidyl ether of Bisphenol A (DGEBA). Fourier Transformed Infrared Spectroscopy (FTIR) spectra of the carbon nanotube samples indicated the existence of functional groups on the surfaces of carbon nanotubes after modification. All composites prepared with purified and modified carbon nanotubes

had higher electrical resistivities, tensile and impact strength values than those of the composite based on as-received carbon nanotubes, due to the functional groups formed on the surfaces of carbon nanotubes during surface treatment.

In order to investigate the effects of alternative composite preparation methods on the electrical and mechanical properties of the composites, in-situ microfiber reinforced conductive polymer composites consisting of high density polyethylene (HDPE), poly(ethylene terephthalate) and carbon nanotubes were prepared in a twin screw extruder followed by hot stretching of PET/CNT phase in HDPE matrix. Composites were produced by using as-received, purified and PEG treated carbon nanotubes. SEM micrographs of the hot stretched composites pointed out the existence of in-situ PET/CNT microfibers dispersed in HDPE matrix up to 1 wt. % carbon nanotube loadings. Electrical conductivity values of the microfibrillar composites were higher than that of the composites prepared without microfiber reinforcement due to the presence of continuous PET/CNT microfibers with high electrical conductivity in the structure.

To investigate the potential application of conductive polymer composites, the effects of surfactant usage and carbon nanotube surface modification; on the damage sensing capability of the epoxy/carbon nanotube/glass fiber composite panels during mechanical loadings were studied. Surface modification of the carbon nanotubes was performed by using hexamethylene diamine (HMDA). 4-octylphenol polyethoxylate (nonionic) (Triton X-100) and cetyl pyridinium chloride (cationic) (CPC) were used as surfactants during composite preparation. Electrical resistivity measurements which were performed during the impact, tensile and fatigue tests of the composite panels showed the changes in damage sensing capabilities of the composites. Surface treatment of carbon nanotubes and the use of surfactants decreased the carbon nanotube particle size and improved the dispersion in the composites which increased the damage sensitivity of the panels.

**Key words:** Conductive polymer composites, carbon nanotubes, surface properties, electrical conductivity, mechanical properties, microfiber reinforced composites, damage sensing capability

## ÖZ

# KARBON NANOTÜP BAZLI İLETKEN POLİMER KOMPOZİTLERİNİN İŞLENMESİ VE KARAKTERİZASYONU

Yeşil, Sertan

Doktora, Kimya Mühendisliği Bölümü

Tez Yöneticisi: Doç. Dr. Gökür Bayram

Mayıs 2010, 265 sayfa

Bu çalışmanın amacı iletken polimer kompozitlerinin elektriksel ve mekanik özelliklerini geliştirmektir. Bu amaçla, tez kapsamında farklı çalışmalar yapılmıştır. Karbon nanotüp (CNT) yüzey işlemlerinin kompozitlerin morfoloji, elektriksel ve mekanik özellikleri üzerindeki etkilerini incelemek için, poli(etilen tereftalat) (PET) bazlı polimer kompozitleri; işlem görmemiş, saflaştırılmış ve modifiye edilmiş karbon nanotüpler kullanılarak çift vidalı ekstrüderde hazırlanmıştır.

Karbon nanotüp saflaştırma işlemleri sırasında, karbon nanotüplerin yüzey özellikleri nitrik asit ( $\text{HNO}_3$ ), sülfürik asit ( $\text{H}_2\text{SO}_4$ ), amonyum hidroksit ( $\text{NH}_4\text{OH}$ ) ve hidrojen peroksit karışımları kullanılarak değiştirilmiştir. Kimyasal analiz için elektron spektroskopu (ESCA) sonuçları saflaştırma prosedürleri sonucunda metalik katalizör artıklarının karbon nanotüp yapısından uzaklaştırıldığını ve karbon nanotüp yüzeyindeki oksijen miktarının arttığını göstermiştir. Saflaştırılmış karbon nanotüplerin yüzey yapısı ayrıca, sodyum dodesil sülfat (SDS), poli(etilen glikol) (PEG) ve Bisfenol A diglisidil eter (DGEBA) kullanılarak da modifiye edilmiştir. Karbon nanotüp örneklerinin Fourier dönüşümlü kızılötesi spektroskopisi (FTIR), karbon nanotüp yüzeylerinde kimyasal modifikasyondan sonra oluşan fonksiyonel grupları göstermiştir. Yüzey işlemleri süresince karbon nanotüplerin yüzeyinde oluşan fonksiyonel gruplar sayesinde, bu karbon nanotüpler kullanılarak hazırlanan

kompozitler, işlem görmemiş karbon nanotüpler kullanılarak hazırlananlara göre daha yüksek elektriksel direnç, çekme ve darbe dayanımlarına sahiptirler.

Alternatif kompozit hazırlama yöntemlerinin kompozitlerin elektriksel ve mekanik özellikleri üzerindeki etkilerini inceleyebilmek için, yüksek yoğunluklu polietilen (HDPE), poli(etilen tereftalat) ve karbon nanotüpleri içeren mikrofiber ile güçlendirilmiş iletken polimer kompozitleri, çift vidalı ekstrüderde, ekstrüzyon ve ardından sıcak çekme yöntemiyle hazırlanmıştır. Kompozitler, işlem görmemiş, saflaştırılmış ve PEG ile modifiye edilmiş karbon nanotüpler kullanılarak üretilmişlerdir. Sıcak çekilmiş kompozitlerin SEM mikrografları ağırlıkça %1 CNT kompozisyonuna kadar, HDPE matriks içerisinde dağılmış PET/CNT mikrofiberlerinin varlığına işaret etmiştir. Mikrofiber ile güçlendirilmiş kompozitlerin elektriksel iletkenlik değerlerinin, yapıdaki yüksek elektriksel iletkenliğe sahip PET/CNT mikrolifleri sayesinde, mikrofiber güçlendirme yöntemiyle hazırlanmamış kompozitlere göre daha yüksek olduğu görülmüştür.

İletken polimer kompozitlerinin uygulama potansiyelini incelemek için, yüzey aktif maddesi kullanımının ve karbon nanotüp yüzey modifikasyonunun, epoksi/karbon nanotüp/cam fiber kompozit panellerinin mekanik yüklemeler sırasındaki hasar algılama kapasiteleri üzerindeki etkileri araştırılmıştır. Karbon nanotüp yüzey modifikasyonu 1,6-diaminohekzan (HMDA) kullanılarak yapılmıştır. Kompozitler hazırlanırken yüzey aktif maddesi olarak 4-oktilfenol polietoksilat (Triton X-100) (noniyonik) ve setilpiridinyum klorür (CPC) (katyonik) kullanılmıştır. Kompozit panellerin darbe, çekme ve yorulma testleri sırasında uygulanan elektriksel direnç ölçümleri, kompozitlerin hasar algılama kapasiteleri arasındaki farkları göstermiştir. Karbon nanotüp yüzey modifikasyonu ve yüzey aktif maddesi kullanımı, karbon nanotüp parçacıklarının boyutlarını küçültmüştür ve kompozit içerisinde homojen dağılımlarını sağlayarak, panellerin hasar algılama kapasitelerini arttırmıştır.

**Anahtar Kelimeler:** İletken polimer kompozitleri, karbon nanotüpler, yüzey özellikleri, elektriksel iletkenlik, mekanik özellikler, mikrofiber ile güçlendirilmiş kompozitler, hasar algılama kapasitesi

***To my beloved family and wife***

## ACKNOWLEDGEMENTS

I would like to express my deepest gratitude to my supervisor Assoc. Prof. Dr. Gökür Bayram for her valuable guidance, advices, encouragements and support during this study. It was a pleasing honor for me to work with her and I sincerely appreciate the time and effort she has taken during my supervision.

I also wish to thank to Prof. Dr. Ülkü Yılmaz, Prof. Dr. Leyla Aras and Prof. Dr. Ayşe Nilgün Akın for their worthy opinions and valuable guidance throughout the thesis research. I am thankful to Assist. Prof. Dr. Valeria La Saponara from the University of California at Davis for giving me the opportunity to work in her laboratory.

For their great services, I would like to thank to Cengiz Tan from Department of Metallurgical and Materials Engineering for SEM analyses, Necmi Avcı from Department of Metallurgical and Materials Engineering for XRD analyses; Mihrican Açıkgöz from Department of Chemical Engineering for DSC and TGA analyses and Dr. Necati Özkan from central laboratory for melt viscosity analyses.

I would like to acknowledge Dr. Özcan Köysüren for his great help both in research and experiments.

I would sincerely thank to İlknur Çakar and Fatma Işık Çoşkunses for their endless friendship, support, and help in all parts of my life, making my stay in METU happy and memorable and being always right beside me.

The friendly and helpful contributions of the polymer group encouraged me during my studies. I want to thank my previous lab mates Dr. Mert Kılınç, Dr. Işıl Işık Gülsaç, Dr. Güralp Özkoç, Aslı Tolga, Elif Alyamaç, Ceren Kurtuluş, Saniye Gülersönmez, Filiz Cengiz, Damla Eroğlu and my present lab mates Canan

Yeniova, Sibel Dönmez, Berk Baltacı, Tijen Seyidođlu, Wisam Abdallah, who have been a constant source of support for me.

I would like to express my sincere appreciation to my wife Ezgi Aktaş Yeşil for her unlimited love, patience and encouragement till the end of my study. I am forever grateful for the love and support of my parents, Gülay and Refik Yeşil and my sister Selcan Yeşil. At every step of my life they were just beside me with their endless support. I am dedicating this work to them, whose love always encouraged me.

Special thanks to TÜBİTAK for supporting me throughout my graduate study by the National Scholarship Program for Ph.D. students. In addition, this thesis work is supported by the BAP-08-11-DPT2002K120510, DPT project and MİSAG 271, TÜBİTAK project.

# TABLE OF CONTENTS

ABSTRACT.....	iv
ÖZ .....	vi
ACKNOWLEDGEMENTS .....	ix
TABLE OF CONTENTS .....	xi
LIST OF FIGURES .....	xvii
LIST OF TABLES.....	xxvii
NOMENCLATURE.....	xxx
CHAPTERS	
1 INTRODUCTION.....	1
2 BACKGROUND .....	9
2.1 Conductive Polymer Composites.....	9
2.1.1 Conductive Fillers.....	12
2.1.1.1 Carbon Nanotubes.....	13
2.1.2 Polymer Matrices.....	16
2.1.2.1 Poly(ethylene terephthalate) (PET).....	16
2.1.2.2 High Density Polyethylene (HDPE).....	18
2.1.2.3 Epoxy Resins.....	18
2.1.3 Fiber Reinforcements.....	20
2.1.3.1 Glass Fibers.....	21
2.1.4 Polymer Composites and Blends.....	22
2.1.4.1 In-situ Microfiber Reinforcement of Polymer Composites.....	24
2.1.5 Preparation Methods of Polymer Composites and Blends.....	27
2.1.5.1 Extrusion.....	27
2.1.5.2 Injection Molding.....	30
2.1.5.3 Compression Molding.....	32
2.1.5.4 Solvent Assisted Ultrasonication.....	33
2.1.5.5 Hand Lay-up.....	34

2.1.6	Surface Treatment of Carbon Nanotubes.....	35
2.1.6.1	Purification of Carbon Nanotubes.....	37
2.1.6.2	Surface Treatment of Carbon Nanotubes with Low Molecular Weight Chemicals.....	38
2.1.6.2.1	Poly(ethylene glycol) (PEG).....	40
2.1.6.2.2	Diglycidyl ether of Bisphenol A (DGEBA)..	41
2.1.6.2.3	Hexamethylene diamine (HMDA).....	42
2.1.6.3	Surface Treatment of Carbon Nanotubes with Surfactants.....	42
2.1.7	Surface Energy Measurements of Composite Constituents.....	45
2.1.7.1	Interfacial Strength, Work of Adhesion and Selective Localization of Carbon Nanotube.....	46
2.2	Experimental Techniques for Material Characterization.....	47
2.2.1	Electrical Conductivity Measurements of Composites.....	47
2.2.2	Mechanical Properties of Composites.....	49
2.2.2.1	Tensile Test.....	49
2.2.2.2	Fatigue Test.....	52
2.2.2.3	Impact Test.....	53
2.2.3	Melt Viscosity Measurements.....	56
2.2.4	Scanning Electron Microscopy and Optical Microscopy.....	59
2.2.5	Differential Scanning Calorimetry Analysis.....	61
2.2.6	Fourier Transformed Infrared Spectroscopy.....	63
2.2.7	Electron Spectroscopy for Chemical Analysis.....	63
2.2.8	X-Ray Diffraction Analysis.....	64
2.2.9	Nuclear Magnetic Resonance Spectroscopy.....	66
2.2.10	Thermogravimetric Analysis.....	68
2.2.11	Electro-Mechanical Tests for Damage Sensing.....	68
2.3	Previous Studies.....	69
3	EXPERIMENTAL .....	73
3.1	Surface Treatment of Carbon Nanotubes and Poly(ethylene terephthalate)/Carbon Nanotube Composites.....	73
3.1.1	Surface Treatment of Carbon Nanotubes .....	73
3.1.1.1	Purification of Carbon Nanotubes.....	74

3.1.1.1.1	Procedures of Carbon Nanotube Purification.....	74
3.1.1.2	Surface Modification of Carbon Nanotube with Low Molecular Weight Chemicals.....	75
3.1.1.2.1	Procedures of Carbon Nanotube Surface Modification.....	76
3.1.2	Poly(ethylene terephthalate)/Carbon Nanotube Composites.....	77
3.2	Microfiber Reinforced High Density Polyethylene/Poly(ethylene terephthalate)/Carbon Nanotube Composites.....	80
3.3	Characterization Methods for the Carbon Nanotube and Conductive Polymer Composite Samples.....	83
3.3.1	Surface Energy Measurements.....	83
3.3.2	Fourier Transformed Infrared Spectroscopy.....	84
3.3.3	Electron Spectroscopy for Chemical Analysis.....	84
3.3.4	X-Ray Diffraction Analysis.....	85
3.3.5	Scanning Electron Microscopy.....	85
3.3.6	Thermogravimetric Analysis.....	86
3.3.7	Quantitative Assessment of Carboxylic Acid Groups Analysis.....	86
3.3.8	Electrical Resistivity Measurements.....	87
3.3.9	Tensile Tests.....	88
3.3.10	Impact Tests.....	88
3.3.11	Differential Scanning Calorimetry.....	89
3.3.12	Nuclear Magnetic Resonance Spectroscopy.....	89
3.3.13	Melt Viscosity Measurements.....	90
3.4	Epoxy/Carbon Nanotube Composites and Epoxy/Carbon Nanotube/Glass Fiber Composite Panels.....	90
3.4.1	Surface Treatment of Carbon Nanotubes.....	92
3.4.2	Preparation of Epoxy/Carbon Nanotube Composites .....	92
3.4.3	Preparation of Epoxy/Carbon Nanotube/Glass Fiber Composite Panels.....	93
3.4.4	Characterization Methods for the Carbon Nanotube and Composite Samples.....	95

3.4.4.1	Fourier Transformed Infrared Spectroscopy.....	95
3.4.4.2	X-Ray Diffraction Analysis.....	95
3.4.4.3	Suspension Stability Analysis of Carbon Nanotube Samples.....	96
3.4.4.4	Scanning Electron Microscopy and Optical Microscopy.....	96
3.4.4.5	Electrical Resistivity Measurements.....	96
3.4.4.6	Tensile Tests.....	97
3.4.4.7	Fatigue Tests.....	98
3.4.4.8	Impact Tests.....	98
3.4.4.9	Electro-Mechanical Tests.....	99
4	RESULTS AND DISCUSSION.....	101
4.1	Surface Treatment of Carbon Nanotubes and Poly(ethylene terephthalate)/Carbon Nanotube Composites.....	101
4.1.1	Purification of Carbon Nanotubes and Poly(ethylene terephthalate)/Carbon Nanotube Composites.....	102
4.1.1.1	Surface Energy Measurements of Carbon Nanotubes.....	102
4.1.1.2	Fourier Transformed Infrared Spectroscopy of Carbon Nanotubes.....	104
4.1.1.3	Electron Spectroscopy for Chemical Analysis of Carbon Nanotubes.....	106
4.1.1.4	X-Ray Diffraction and Scanning Electron Microscopy Analyses of Carbon Nanotubes.....	109
4.1.1.5	Electrical Resistivity Measurements of Composites.....	112
4.1.1.6	Tensile and Impact Tests of Composites.....	114
4.1.1.7	Scanning Electron Microscopy of Composites.....	117
4.1.2	Surface Modification of Carbon Nanotubes and Poly(ethylene terephthalate)/Carbon Nanotube Composites.....	118
4.1.2.1	Surface Energy Measurements of Carbon Nanotubes.....	118

4.1.2.2	Quantitative Assessment of Carboxylic Acid Groups Analysis on Carbon Nanotube Surfaces.....	119
4.1.2.3	Fourier Transformed Infrared Spectroscopy of Carbon Nanotubes.....	120
4.1.2.4	Electron Spectroscopy for Chemical Analysis of Carbon Nanotubes.....	122
4.1.2.5	X-Ray Diffraction and Scanning Electron Microscopy Analyses of Carbon Nanotubes.....	126
4.1.2.6	Thermogravimetric Analyses of Carbon Nanotubes.....	128
4.1.2.7	Surface Energy Measurements Composites.....	129
4.1.2.8	Fourier Transformed Infrared and Nuclear Magnetic Resonance Spectroscopy of Composites.....	130
4.1.2.9	Electrical Resistivity Measurements of Composites.....	135
4.1.2.10	Tensile and Impact Tests of Composites.....	137
4.1.2.11	Differential Scanning Calorimetry Analysis of Composites.....	142
4.1.2.12	Scanning Electron Microscopy of Composites....	143
4.2	Microfiber Reinforced High Density Polyethylene/Poly(ethylene terephthalate)/Carbon Nanotube Composites.....	146
4.2.1	Microfiber Reinforced High Density Polyethylene/Poly(ethylene terephthalate)/Carbon Nanotube Composites Prepared with As-Received Carbon Nanotubes.....	146
4.2.1.1	Surface Energy Measurements and Selective Localization of Carbon Nanotubes .....	146
4.2.1.2	Scanning Electron Microscopy of Composites.....	149
4.2.1.3	Electrical Resistivity Measurements of Composites.....	156
4.2.1.4	Tensile and Impact Tests of Composites.....	159
4.2.1.5	Differential Scanning Calorimetry Analysis of Composites.....	164
4.2.2	Microfiber Reinforced High Density Polyethylene/Poly(ethylene terephthalate)/Carbon Nanotube Composites Prepared with Surface Treated Carbon Nanotubes.....	166

4.2.2.1	Interfacial Tension and Wetting Coefficient Calculations.....	166
4.2.2.2	Melt Viscosity Measurements.....	167
4.2.2.3	Scanning Electron Microscopy of Composites.....	168
4.2.2.4	Electrical Resistivity Measurements of Composites.....	174
4.2.2.5	Tensile and Impact Tests of Composites.....	176
4.3	Epoxy/Carbon Nanotube Composites and Epoxy/Carbon Nanotube/Glass Fiber Composite Panels.....	180
4.3.1	Characterization of Carbon Nanotubes .....	180
4.3.1.1	Fourier Transformed Infrared Spectroscopy of Carbon Nanotubes.....	180
4.3.1.2	X-Ray Diffraction and Scanning Electron Microscopy Analyses of Carbon Nanotubes.....	181
4.3.1.3	Suspension Stability Analysis of Carbon Nanotubes.....	183
4.3.2	Characterization of Epoxy/Carbon Nanotube Composites.....	185
4.3.2.1	Scanning Electron Microscopy and Optical Microscopy of Composites.....	185
4.3.2.2	Electrical Resistivity Measurements of Composites.....	188
4.3.2.3	Tensile Tests of Composites.....	190
4.3.3	Characterization of Epoxy/Carbon Nanotube/Glass Fiber Composite Panels.....	193
4.3.3.1	Tensile Tests of Composite Panels.....	193
4.3.3.2	Impact Tests of Composite Panels.....	196
4.3.3.3	Electro-Mechanical Characterization During Impact Tests of Composite Panels.....	198
4.3.3.4	Electro-Mechanical Characterization During Tensile Tests of Composite Panels.....	201
4.3.3.5	Electro-Mechanical Characterization During Fatigue Tests of Composite Panels.....	202

5	CONCLUSIONS.....	205
	5.1 Purification of Carbon Nanotubes and Poly(ethylene terephthalate)/Carbon Nanotube Composites.....	205
	5.2 Surface Modification of Carbon Nanotubes and Poly(ethylene terephthalate)/Carbon Nanotube Composites.....	206
	5.3 Microfiber Reinforced High Density Polyethylene/Poly(ethylene terephthalate)/Carbon Nanotube Composites Prepared with As-Received Carbon Nanotubes.....	207
	5.4 Microfiber Reinforced High Density Polyethylene/Poly(ethylene terephthalate)/Carbon Nanotube Composites Prepared with Surface Treated Carbon Nanotubes.....	207
	5.5 Epoxy/Carbon Nanotube Composites and Epoxy/Carbon Nanotube/Glass Fiber Composite Panels.....	208
6	RECOMMENDATIONS.....	209
	REFERENCES.....	211
	APPENDICES	
	A. MECHANICAL PROPERTIES.....	232
	B. ESCA SPECTRA.....	239
	C. SOLID STATE NMR.....	246
	D. DSC THERMOGRAMS.....	250
	CURRICULUM VITAE.....	261

## LIST OF FIGURES

### FIGURES

Figure 2.1 Energy gaps in conductors, semiconductors and insulators.....	10
Figure 2.2 Schematic representation of the percolation theory.....	11
Figure 2.3 Schematic representations of carbon nanotube types.....	13
Figure 2.4 Three types of single walled carbon nanotubes with different chirality..	15
Figure 2.5 Chemical structure of poly(ethylene terephthalate).....	17
Figure 2.6 Two steps in the polymerization of poly(ethylene terephthalate).....	17
Figure 2.7 Chemical structure of polyethylene.....	18
Figure 2.8 Epoxy prepolymer formed from bisphenol A and epichlorohydrin.....	19
Figure 2.9 Cure of an epoxy resin by reaction of the prepolymer with an amine...20	
Figure 2.10 Different glass fiber forms.....	21
Figure 2.11 Schematic presentation of the essential steps during manufacturing of microfiber reinforced composites.....	25
Figure 2.12 Schematic of the industrial relevant extrusion and hot-stretching line.....	26
Figure 2.13 Sketch of an extrusion line.....	27
Figure 2.14 Parts of a single screw extruder.....	28
Figure 2.15 Parts of a single screw extruder.....	29
Figure 2.16 Classification of twin screw extruders.....	30
Figure 2.17 Sequence of operations for a reciprocating screw machine.....	31
Figure 2.18 Pressure change during the injection molding cycle.....	32
Figure 2.19 Schematic of a compression molding operation.....	33
Figure 2.20 Hand lay-up techniques.....	35

Figure 2.21 General procedure for carbon nanotube surface treatment.....	36
Figure 2.22 Functionalization possibilities for carbon nanotubes: (a) oxidized carbon nanotube functionalization, (b) covalent sidewall functionalization, (c) noncovalent functionalization with surfactants, (d) noncovalent functionalization with polymers.....	39
Figure 2.23 Amidation of oxidized carbon nanotube surface.....	40
Figure 2.24 Chemical structure of poly(ethylene glycol).....	41
Figure 2.25 Chemical structure of diglycidyl ether of Bisphenol A.....	41
Figure 2.26 Chemical structure of hexamethylene diamine.....	42
Figure 2.27 Schematic illustration of a surfactant.....	43
Figure 2.28 Schematic illustration of critical micelle concentration.....	44
Figure 2.29 Chemical structures of the surfactants used in this study.....	45
Figure 2.30 Collinear four point probe showing current flow and voltage measurement.....	48
Figure 2.31 Two point probe arrangement.....	49
Figure 2.32 Typical dogbone shaped tensile test specimen; where $L_0$ is the gauge length, $W_0$ is the initial width, $T_0$ is the initial thickness of the specimen.....	50
Figure 2.33 Schematic representation of tensile test.....	50
Figure 2.34 Engineering data from tensile tests.....	51
Figure 2.35 Typical tensile test curves for polymeric materials.....	52
Figure 2.36 Load and displacement curves during fatigue tests.....	53
Figure 2.37 Schematic drawing of the charpy impact tester.....	54
Figure 2.38 Schematic of the falling weight impact tower.....	55
Figure 2.39 Typical impact energy and inelastic energy curves for the composite materials obtained during falling weight impact test.....	56
Figure 2.40 Schematic representation of a capillary viscometer.....	57
Figure 2.41 Pressure profile in capillary viscometer.....	58
Figure 2.42 Schematic representation of a SEM.....	60
Figure 2.43 Schematic representation of an optical microscope.....	61

Figure 2.44 Typical DSC curve for poly(ethylene terephthalate).....	62
Figure 2.45 Basic components of a FTIR.....	63
Figure 2.46 Schematic of a ESCA spectrometer showing all the necessary components.....	64
Figure 2.47 Basic features of a typical XRD experiment.....	66
Figure 2.48 Schematic of a NMR spectrometer.....	67
Figure 2.49 Online electrical resistivity measurement system during tensile testing.....	69
Figure 3.1 A photograph of the co-rotating twin screw extruder.....	77
Figure 3.2 A photograph of the grinder.....	78
Figure 3.3 A photograph of the compression molding device.....	79
Figure 3.4 A photograph of the injection molding device.....	79
Figure 3.5 Experimental set-up for the preparation of the microfiber reinforced composites.....	81
Figure 3.6 Transformation of PET or PET/CNT domains into ellipsoids during image analyses of the samples.....	86
Figure 3.7 A photograph of the Keithley 2400 constant current source meter.....	87
Figure 3.8 A photograph of the Shimadzu Autograph AG-100 KNIS MS tensile testing machine.....	88
Figure 3.9 A photograph of the Ceast Resil Impactor 6967 impact testing machine.....	89
Figure 3.10 Equipments for the preparation of the epoxy/carbon nanotube composite samples (a) vacuum chamber, (b) silicone mold for the electrical resistivity measurement samples, (c) silicone mold for the tensile testing samples.....	93
Figure 3.11 General procedure for the preparation of composite panels.....	94
Figure 3.12 A photograph of the Keithley 199 constant current source meter.....	97
Figure 3.13 A photograph of the MTS 810 tensile testing instrument.....	98
Figure 3.14 A photograph of the Instron Dynatup 9250G impact tester.....	99
Figure 3.15 Electro-mechanical tests (a) during tensile and fatigue tests, (b) during impact test.....	100

Figure 3.16 Placement of the copper electrodes on the tensile, fatigue and impact specimens for the electro-mechanical tests.....	100
Figure 4.1 FTIR spectra of as-received and purified carbon nanotube samples.....	105
Figure 4.2 ESCA O1s spectra of as-received and purified carbon nanotube samples .....	107
Figure 4.3 XRD patterns of as-received and purified carbon nanotube samples.....	110
Figure 4.4 SEM micrographs of selected as-received and purified carbon nanotube samples.....	111
Figure 4.5 Electrical resistivity values of PET/CNT composites prepared with as-received and purified carbon nanotubes.....	112
Figure 4.6 Tensile strength values of neat PET and PET/CNT composites prepared with as-received and purified carbon nanotubes.....	115
Figure 4.7 Tensile modulus values of neat PET and PET/CNT composites prepared with as-received and purified carbon nanotubes.....	115
Figure 4.8 Impact strength values of neat PET and PET/CNT composites prepared with as-received and purified carbon nanotubes.....	116
Figure 4.9 SEM micrographs of PET/ASCNT and PET/CNT2 composites.....	117
Figure 4.10 FTIR spectra of carbon nanotube samples.....	121
Figure 4.11 ESCA O1s spectra of carbon nanotube samples.....	123
Figure 4.12 Possible interaction mechanisms between PEG and purified carbon nanotubes.....	125
Figure 4.13 Possible interaction mechanisms between DGEBA and purified carbon nanotubes.....	125
Figure 4.14 XRD patterns of carbon nanotube samples.....	126
Figure 4.15 SEM micrographs of the carbon nanotube samples.....	127
Figure 4.16 TGA graphs of carbon nanotube samples; (a) ASCNT, (b) pCNT, (c) SDSCNT, (d) DGEBA/CNT, (e) PEG400CNT, (f) PEG1000CNT.....	129
Figure 4.17 FTIR spectra of the neat PET and PET/CNT composites.....	132
Figure 4.18 NMR spectra of the neat PET and PET/CNT composites.....	133
Figure 4.19 Possible interaction mechanisms between PEGCNT and PET.....	134

Figure 4.20 Possible interaction mechanisms between DGEBCNT and PET.....	134
Figure 4.21 Electrical resistivity values of PET/CNT composites.....	135
Figure 4.22 Effect of carbon nanotube concentration on the electrical resistivity values of PET/CNT composites.....	137
Figure 4.23 Tensile strength values of neat PET and PET/CNT composites.....	138
Figure 4.24 Tensile modulus values of neat PET and PET/CNT composites.....	139
Figure 4.25 Impact strength values of neat PET and PET/CNT composites.....	139
Figure 4.26 Effect of carbon nanotube concentration on the tensile strength values of PET/CNT composites.....	140
Figure 4.27 Effect of carbon nanotube concentration on the tensile modulus values of PET/CNT composites.....	141
Figure 4.28 Effect of carbon nanotube concentration on the impact strength values of PET/CNT composites.....	141
Figure 4.29 SEM micrographs of 0.5 wt. % carbon nanotube containing PET/CNT composites (Micrographs on the right hand side are the magnified images of the micrographs on the left hand side).....	144
Figure 4.30 SEM micrographs of PET/CNT composites (a) and (b) PET/ASCNT (1 wt. %), (c) and (d) PET/ASCNT (4 wt. %), (e) and (f) PET/pCNT (1 wt. %), (g) and (h) PET/pCNT (4 wt. %), (i) and (j) PET/PEG1000CNT (1 wt. %), (k) and (l) PET/PEG1000CNT (4 wt. %) (Micrographs on the right hand side are the magnified images of the micrographs on the left hand side).....	145
Figure 4.31 Shear viscosity vs. shear rate graphs for HDPE, PET and PET/ASCNT composites.....	148
Figure 4.32 SEM micrographs of the HDPE/PET/ASCNT (70/30/0.5) composite system.....	148
Figure 4.33 SEM micrographs of the HDPE/PET/ASCNT (60/40/0.5) composite system.....	149
Figure 4.34 SEM micrographs of the selected blend samples (HDPE/PET) (a) 80/20 (b) 70/30 (c) 50/50 (etched by trifluoro acetic acid).....	150
Figure 4.35 SEM micrographs of the selected composite samples (HDPE/PET/CNT) (a) 80/20/0.5 (b) 70/30/0.5 (c) 50/50/0.5 (etched by trifluoro acetic acid).....	151

Figure 4.36 SEM micrographs of the selected hot-stretched samples [(a), (a')] 90/10/0.5 microfiber [(b), (b')] 80/20/0.5 microfiber [(c), (c')] 70/30/0.5 microfiber [(d), (d')] 50/50/0.5 microfiber (etched by hot xylene).....	154
Figure 4.37 SEM micrographs of the selected molded samples (a) 80/20/0.5 microfiber (210) (b) 80/20/0.5 microfiber (210) (etched by hot xylene) (c) 80/20/0.5 microfiber (240) (etched by hot xylene) (d) 80/20/0.5 microfiber (280) (etched by trifloro acetic acid) (e) 80/20/0.5 (etched by trifloro acetic acid).....	155
Figure 4.38 Electrical resistivity values of the microfibrillar and conventional composites.....	156
Figure 4.39 Electrical resistivity values of the microfiber reinforced composites molded at different temperatures.....	158
Figure 4.40 Tensile strength values of the composites and blends.....	160
Figure 4.41 Tensile modulus values of the composites and blends.....	161
Figure 4.42 Tensile strength values of the microfiber reinforced composites molded at different temperatures.....	161
Figure 4.43 Tensile modulus values of the microfiber reinforced composites molded at different temperatures.....	162
Figure 4.44 Impact strength values of the composites and blends.....	163
Figure 4.45 Impact strength values of the microfiber reinforced composites molded at different temperatures.....	164
Figure 4.46 Shear viscosity vs. shear rate graphs for HDPE, PET and PET/CNT composites.....	168
Figure 4.47 SEM micrographs of the HDPE/PET/CNT composites a) 0.25 wt.% ASCNT, b) 1.5 wt.% ASCNT, c) 0.25 wt.% pCNT, d) 1.5 wt.% pCNT, e) 0.25 wt.% PEG1000CNT, f) 1.5 wt.% PEG1000CNT (samples were directly taken from the extruder die without hot-stretching and etched with trifluoro acetic acid).....	169
Figure 4.48 SEM micrographs of the microfibrillar HDPE/PET/CNT composite systems containing 0.5 wt. % pCNT and PEG1000CNT containing (molded at 280°C and show the selective localization of pCNT and PEG1000CNT in PET phase).....	171
Figure 4.49 SEM micrographs of the hot-stretched HDPE/PET/CNT composites a) 0.25 wt.% ASCNT, b) 0.5 wt.% ASCNT, c) 1 wt.% ASCNT, d) 1.5 wt.% ASCNT, e) 0.25 wt.% pCNT, f) 0.5 wt.% pCNT, g) 1 wt.% pCNT, h) 1.5 wt.% pCNT, i) 0.25 wt.% PEG1000CNT, j) 0.5 wt.% PEG1000CNT, k) 1 wt.% PEG1000CNT, l) 1.5 wt.% PEG1000CNT (etched with hot xylene).....	172

Figure 4.50 SEM micrographs of the microfibrillar HDPE/PET/CNT composites a) 0.25 wt.% ASCNT, b) 1.5 wt.% ASCNT, c) 0.25 wt.% pCNT, d) 1.5 wt.% pCNT, e) 0.25 wt.% PEG1000CNT, f) 1.5 wt.% PEG1000CNT (molded at 210°C and etched with hot-xylene).....	173
Figure 4.51 Electrical resistivity values of the microfibrillar HDPE/PET/CNT composites a) effect of carbon nanotube surface treatment and amount (molded at 210°C), b) effect of molding temperature at 0.75 wt.% carbon nanotube containing microfibrillar composites.....	175
Figure 4.52 Tensile strength, modulus and impact strength values of the microfibrillar HDPE/PET/CNT composites and HDPE/PET blend.....	177
Figure 4.53 Tensile strength, modulus and impact strength values of the microfibrillar HDPE/PET/CNT composites containing 0.75 wt. % carbon nanotube and HDPE/PET blends (effect of molding temperature).....	179
Figure 4.54 FTIR spectra of the carbon nanotube samples.....	181
Figure 4.55 XRD patterns of carbon nanotube samples.....	182
Figure 4.56 SEM micrographs of carbon nanotube samples.....	182
Figure 4.57 Suspension stabilities of the carbon nanotube samples in acetone and ethyl alcohol (EA) with and without surfactant assistance.....	184
Figure 4.58 SEM micrographs of the epoxy/CNT (0.5 wt. %) composites.....	186
Figure 4.59 Optical microscopy images of the epoxy/CNT (0.5 wt. %) composites.....	187
Figure 4.60 Effect of carbon nanotube concentration on the electrical resistivity values of epoxy/ASCNT composites.....	188
Figure 4.61 Electrical resistivity values of the composites containing 0.5 wt.% carbon nanotubes .....	189
Figure 4.62 Effect of carbon nanotube concentration on the tensile strength values of epoxy/ASCNT composites.....	190
Figure 4.63 Effect of carbon nanotube concentration on the tensile modulus values of epoxy/ASCNT composites.....	191
Figure 4.64 Tensile strength values of the composites containing 0.5 wt. % carbon nanotubes.....	192
Figure 4.65 Tensile modulus values of the composites containing 0.5 wt. % carbon nanotubes.....	193
Figure 4.66 SEM micrographs of the composite panel in which CPC assisted 0.5 wt. % carbon nanotubes containing epoxy/mCNT composite is used as matrix.....	194

Figure 4.67 Tensile strength values of the composite panels prepared by using neat epoxy and 0.5 wt. % carbon nanotubes containing epoxy based composites as matrix.....	195
Figure 4.68 Tensile modulus values of the composite panels prepared by using neat epoxy and 0.5 wt. % carbon nanotubes containing epoxy based composites as matrix.....	195
Figure 4.69 Poisson's ratio values of the composite panels prepared by using neat epoxy and 0.5 wt. % carbon nanotubes containing epoxy based composites as matrix.....	196
Figure 4.70 The change in the impact energy of the panels prepared with (a) epoxy/ASCNT, (b) CPC assisted epoxy/mCNT as matrices during the impact test at different impact energies.....	197
Figure 4.71 Inelastic energy curves of the panels prepared with epoxy/ASCNT and CPC assisted epoxy/mCNT as matrices.....	198
Figure 4.72 Electrical resistivity changes (a) on the surfaces, (b) through the cross-sectional areas of the epoxy/ASCNT and CPC assisted epoxy/mCNT based panels for different transferred impact energies.....	200
Figure 4.73 Electrical resistivity changes of the composite panels during static tensile tests.....	202
Figure 4.74 Residual strain change of the composite panels during fatigue tests.....	203
Figure 4.75 Electrical resistivity changes of the composite panels during fatigue tests (a) vs. number of load cycles (b) vs. residual strains.....	204
Figure B.1 ESCA spectrum of ASCNT.....	239
Figure B.2 ESCA spectrum of CNT1.....	240
Figure B.3 ESCA spectrum of CNT2.....	240
Figure B.4 ESCA spectrum of CNT3.....	241
Figure B.5 ESCA spectrum of CNT4.....	241
Figure B.6 ESCA spectrum of CNT5.....	242
Figure B.7 ESCA spectrum of CNT6.....	242
Figure B.8 ESCA spectrum of CNT7.....	243
Figure B.9 ESCA spectrum of CNT8.....	243
Figure B.10 ESCA spectrum of SDSCNT.....	244

Figure B.11 ESCA spectrum of DGEBA/CNT.....	244
Figure B.12 ESCA spectrum of PEG400/CNT.....	245
Figure B.13 ESCA spectrum of PEG1000/CNT.....	245
Figure C.1 <sup>13</sup> C NMR spectrum of PET.....	246
Figure C.2 <sup>13</sup> C NMR spectrum of PET/ASCNT composite.....	247
Figure C.3 <sup>13</sup> C NMR spectrum of PET/pCNT composite.....	247
Figure C.4 <sup>13</sup> C NMR spectrum of PET/SDSCNT composite.....	248
Figure C.5 <sup>13</sup> C NMR spectrum of PET/DGEBA/CNT composite.....	248
Figure C.6 <sup>13</sup> C NMR spectrum of PET/PEG400/CNT composite.....	249
Figure C.7 <sup>13</sup> C NMR spectrum of PET/PEG1000/CNT composite.....	249
Figure D.1 DSC thermogram of HDPE.....	250
Figure D.2 DSC thermogram of HDPE/PET (80/20) blend.....	251
Figure D.3 DSC thermogram of HDPE/PET (70/30) blend.....	251
Figure D.4 DSC thermogram of HDPE/PET (50/50) blend.....	252
Figure D.5 DSC thermogram of microfiber reinforced HDPE/PET/ASCNT (80/20/0.5) composite.....	252
Figure D.6 DSC thermogram of microfiber reinforced HDPE/PET/ASCNT (70/30/0.5) composite.....	253
Figure D.7 DSC thermogram of microfiber reinforced HDPE/PET/ASCNT (50/50/0.5) composite.....	253
Figure D.8 DSC thermogram of microfiber reinforced HDPE/PET/ASCNT (80/20/0.5) composite molded at 210 °C.....	254
Figure D.9 DSC thermogram of microfiber reinforced HDPE/PET/ASCNT (80/20/0.5) composite molded at 240 °C.....	254
Figure D.10 DSC thermogram of microfiber reinforced HDPE/PET/ASCNT (80/20/0.5) composite molded at 280 °C.....	255
Figure D.11 DSC thermogram of microfiber reinforced HDPE/PET/ASCNT (70/30/0.5) composite molded at 210 °C.....	255
Figure D.12 DSC thermogram of microfiber reinforced HDPE/PET/ASCNT (50/50/0.5) composite molded at 210 °C.....	256

Figure D.13 DSC thermogram of conventional HDPE/PET/ASCNT (80/20/0.5) composite.....	256
Figure D.14 DSC thermogram of PET.....	257
Figure D.15 DSC thermogram of PET/ASCNT (0.5 wt. %) composite.....	257
Figure D.16 DSC thermogram of PET/pCNT (0.5 wt. %) composite.....	258
Figure D.17 DSC thermogram of PET/SDSCNT (0.5 wt. %) composite.....	258
Figure D.18 DSC thermogram of PET/DGEBACNT (0.5 wt. %) composite.....	259
Figure D.19 DSC thermogram of PET/PEG400CNT (0.5 wt. %) composite.....	259
Figure D.20 DSC thermogram of PET/PEG1000CNT (0.5 wt. %) composite.....	260

## LIST OF TABLES

### TABLES

Table 2.1 Theoretical and experimental properties of carbon nanotubes.....	14
Table 3.1 Properties of commercial grade multi walled carbon nanotubes.....	74
Table 3.2 Properties and suppliers of the surface modifiers.....	76
Table 3.3 Properties of commercial grade poly(ethylene terephthalate).....	77
Table 3.4 Properties of commercial grade high density polyethylene.....	80
Table 3.5 Surface energy components of probe liquids, (mN/m).....	84
Table 3.6 Information for the materials used during the production of the composites and panels.....	91
Table 3.7 Chemicals used for the preparation of the epoxy/carbon nanotube composites.....	91
Table 4.1 Surface energy components of the as-received and purified carbon nanotube samples (mN/m).....	103
Table 4.2 Peaks and chemical structures corresponding to these peaks in ESCA O1s spectra and oxygen to carbon (O/C) ratios of as-received and purified carbon nanotube samples.....	108
Table 4.3 Interplanar spacings ( $d_{002}$ ) (Å) and crystalline lengths ( $L_c$ ) (Å) of as-received and purified carbon nanotube samples.....	110
Table 4.4 Surface energy components of carbon nanotube samples and work of adhesion values between carbon nanotubes and PET (mN/m).....	119
Table 4.5 Results of the titrations for carboxylic acid groups assessment.....	120
Table 4.6 Peaks and chemical structures corresponding to these peaks in ESCA O1s spectra of carbon nanotube samples.....	124
Table 4.7 Surface energy components of the neat PET and PET/CNT composites (mN/m).....	130
Table 4.8 Thermal properties of neat PET and PET/CNT composites.....	143

Table 4.9 Surface energy components of HDPE, PET and ASCNT (mN/m).....	147
Table 4.10 Image analyses results of the selected samples.....	152
Table 4.11 DSC results of the selected samples.....	165
Table A.1 Tensile strength, tensile modulus, elongation at break and impact strength values of neat PET and PET/CNT composites prepared with as-received and purified carbon nanotubes at 0.5 wt. % carbon nanotube loading.....	232
Table A.2 Tensile strength, tensile modulus, elongation at break and impact strength values of PET/CNT composites prepared with modified carbon nanotubes at 0.5 wt. % carbon nanotube loading.....	233
Table A.3 Tensile strength, tensile modulus, elongation at break and impact strength values of PET/CNT composites prepared with as-received, purified and PEG1000 treated carbon nanotubes at different carbon nanotube loadings.....	233
Table A.4 Tensile strength, tensile modulus, elongation at break and impact strength values of conventional HDPE/PET blends, HDPE/PET/CNT composites prepared with as-received carbon nanotubes.....	234
Table A.5 Tensile strength, tensile modulus, elongation at break and impact strength values of microfiber reinforced HDPE/PET/CNT composites prepared with as-received carbon nanotubes and molded at different temperatures.....	235
Table A.6 Tensile strength, tensile modulus, elongation at break and impact strength values of microfiber reinforced HDPE/PET blend and HDPE/PET/CNT composites at (80/20 HDPE/PET ratio) prepared with as-received, purified and PEG1000 treated carbon nanotubes.....	236
Table A.7 Tensile strength, tensile modulus and elongation at break values of neat epoxy and epoxy/CNT composites prepared with as-received carbon nanotubes at different compositions.....	237
Table A.8 Tensile strength, tensile modulus and elongation at break values of epoxy/CNT composites prepared with as-received and modified carbon nanotubes at 0.5 wt.% carbon nanotube loading.....	237
Table A.9 Tensile strength, tensile modulus, elongation at break and Poisson's ratio values of glass fiber reinforced composite panels prepared by using neat epoxy and epoxy/CNT composites (0.5 wt.%) as matrix.....	238

## NOMENCLATURE

A	Area, cm <sup>2</sup>
A <sub>0</sub>	Initial cross – sectional area of tensile specimen, mm <sup>2</sup>
B	Widening of diffraction line
d <sub>avg</sub>	Average diameter of PE//CNT phase in the composites, micron
d <sub>002</sub>	Interplanar spacing between carbon nanotube aggregates, nm
E <sub>g</sub>	Energy gap, eV
F	Force measured during tensile testing, N
I	Electrical current, Volt
K	Scherrer constant
L	Length of the capillary, mm
L <sub>c</sub>	Crystallite length along the c-axis of carbon nanotube
L <sub>0</sub>	Gauge length of tensile test specimen, mm
m <sub>CNT</sub>	Carbon nanotube sample weight, g
N	Number of applied strain cycles during fatigue test
N <sub>HCl</sub>	Normality of HCl solution, N
N <sub>NaOH</sub>	Normality of NaOH solution, N
n	Power law index of the material
P	Injection molding pressure, bar
Q	Volumetric flow rate of the polymer melt, cm <sup>3</sup> /s
R	Electrical resistance, Ohm
R <sub>c</sub>	Contact resistances between the probes and the material, Ohm
R <sub>i</sub>	Electrical resistivity measured during and after the tests, Ohm
R <sub>mat</sub>	Material resistance, Ohm
R <sub>o</sub>	Electrical resistivity measured before the tests, Ohm
R <sub>sp</sub>	Spreading resistance, Ohm
R <sub>T</sub>	Total resistance, Ohm
R <sub>w</sub>	Wire and probe resistances, Ohm
S	Cross-sectional area, cm <sup>2</sup>
T <sub>c</sub>	Cold crystallization temperature, °C

$T_g$	Glass transition temperature, °C
$T_m$	Melting temperature, °C
$T_0$	Initial thickness of tensile test specimen, mm
$V$	Electrical potential, Ampere
$V_{HCl}$	Volume of HCl solution used for the titration of the filtrate, ml
$V_{NaOH}$	Volume of NaOH solution added to carbon nanotube suspension, ml
$w$	Wetting coefficient
$w_{poly}$	Fraction of polymer phase in the composites
$W_a$	Work of adhesion, mN/m
$W_0$	Initial width of tensile test specimen, mm
$X_c$	Percent crystallinities of the polymer phases
$\Delta L$	Change in the tensile specimens gauge length, mm
$\Delta P$	Pressure drop through a capillary, bar
$\Delta H_m^o$	Melting energy of the 100% crystal structure, J/g
$\Delta H_c$	Cold crystallization energy, J/g
$\Delta H_m$	Melting energy, J/g
$\Delta R$	Percent changes in the electrical resistivities of the specimens
[COOH]	Carboxylic acid concentration, (mol COOH/g nanotube)

### Greek Letters

$\rho$	Volumetric electrical resistivity, Ohm.cm
$\gamma$	Shear rate, s <sup>-1</sup>
$\gamma_{Solid}$	Total surface energy, mN/m
$\gamma_{Solid}^d$	Dispersive component of total surface energy, mN/m
$\gamma_{Solid}^A$	Acidic component of total surface energy, mN/m
$\gamma_{Solid}^B$	Basic component of total surface energy, mN/m
$\gamma_{Solid}^p$	Polar component of total surface energy, mN/m
$\gamma_{Liquid}$	Total surface energy of the probe liquid, mN/m
$\gamma_{Liquid}^d$	Dispersive component of the probe liquid surface energy, mN/m
$\gamma_{Liquid}^A$	Acidic component of the probe liquid surface energy, mN/m
$\gamma_{Liquid}^B$	Basic component of the probe liquid surface energy, mN/m
$\gamma_{1-2}$	The interfacial tensions between two composite constituents, mN/m
$\gamma_{f-A}$	Interfacial tension between the polymer A and filler, mN/m
$\gamma_{f-B}$	Interfacial tension between the polymer B and filler, mN/m

$\gamma_{A-B}$	Interfacial tension between two polymers, mN/m
$\theta$	Diffraction angle of beam of radiation, °
$\theta_{\text{Liquid}}$	Contact angle values of the probe liquids, °
$\sigma$	Engineering stress, MPa
$\varepsilon$	Empirical parameter for entrance corrections in capillary viscometers
$\varepsilon_T$	True strain in the transverse direction
$\varepsilon_L$	True strain in the longitudinal direction
$\nu$	Poisson's ratio
$\eta$	Melt viscosity, Pa.s
$\tau_w$	Shear stress at the capillary wall, kPa
$\Phi$	Apparent shear rate, s <sup>-1</sup>
$\lambda$	wavelength of radiation, nm
$\delta_{\text{PEG}}$	Hildebrand parameter of poly(ethylene glycol), MPa <sup>1/2</sup>
$\delta_{\text{DGEBEA}}$	Hildebrand parameter of diglycidyl ether of Bisphenol-A, MPa <sup>1/2</sup>
$\delta_{\text{PET}}$	Hildebrand parameter of poly(ethylene terephthalate), MPa <sup>1/2</sup>

### Abbreviations

ASCNT	As-received carbon nanotube
ATR	Attenuated Total Reflectance
CNT	Carbon nanotube
CNT1	Purified carbon nanotube in HNO <sub>3</sub> /H <sub>2</sub> SO <sub>4</sub> (1:3 by volume) mixture for 15 minutes
CNT2	Purified carbon nanotube in HNO <sub>3</sub> /H <sub>2</sub> SO <sub>4</sub> (1:3 by volume) mixture for 30 minutes
CNT3	Purified carbon nanotube in HNO <sub>3</sub> /H <sub>2</sub> SO <sub>4</sub> (1:3 by volume) mixture for 60 minutes
CNT4	Purified carbon nanotube in HNO <sub>3</sub> /H <sub>2</sub> SO <sub>4</sub> (1:3 by volume) mixture for 120 minutes
CNT5	Purified carbon nanotube in HNO <sub>3</sub> /H <sub>2</sub> SO <sub>4</sub> (1:1 by volume) mixture for 30 minutes
CNT6	Purified carbon nanotube in HNO <sub>3</sub> /H <sub>2</sub> SO <sub>4</sub> (3:1 by volume) mixture for 30 minutes
CNT7	Purified carbon nanotube in NH <sub>4</sub> OH for 30 minutes

CNT8	Purified carbon nanotube in $\text{NH}_4\text{OH}/\text{H}_2\text{O}_2$ (1:1 by volume) mixture for 30 minutes
CMC	Critical micelle concentration
CPC	Cetyl pyridinium chloride
DGEBA	Diglycidyl ether of bisphenol A
DGEBACNT	Carbon nanotube treated with diglycidyl ether of bisphenol A
DIM	Diiodomethane
DMT	Dimethyl terephthalic acid
DSC	Differential Scanning Calorimetry
EG	Ethylene glycol
ESCA	Electron Spectroscopy for Chemical Analysis
FA	Formamide
FTIR	Fourier Transformed Infrared Spectroscopy
HDPE	High density polyethylene
HMDA	Hexamethylene diamine
LCP	Liquid crystalline polymers
mCNT	Carbon nanotube treated with hexamethylene diamine
MWCNT	Multiwalled carbon nanotube
NMR	Nuclear Magnetic Resonance
PEG	Poly(ethylene glycol)
PEG400CNT	Carbon nanotube treated with poly(ethylene glycol) which has a molecular weight of 400 g/mole
PEG1000CNT	Carbon nanotube treated with poly(ethylene glycol) which has a molecular weight of 1000 g/mole
pCNT	Purified carbon nanotube in $\text{HNO}_3/\text{H}_2\text{SO}_4$ (1:1 by volume) mixture for 30 minutes
PET	Poly(ethylene terephthalate)
SDS	Sodium dodecyl sulfate
SDSCNT	Carbon nanotube treated with sodium dodecyl sulfate
SEM	Scanning Electron Microscopy
SWCNT	Single walled carbon nanotube
TGA	Thermogravimetric Analysis
Triton X-100	4-octylphenol polyethoxylate
VARTM	Vacuum assisted resin transfer molding
XRD	X-Ray Diffraction

# CHAPTER 1

## INTRODUCTION

Composite materials are defined as the combination of two or more materials to give a unique combination of properties. The main components of a composite are the matrix and filler materials. The fillers can be fibers, particulates, or whiskers, and the matrix materials can be metals, plastics, or ceramics. Composites prepared with a polymer matrix have become more common and are widely used in various industries such as; automotive components, sporting goods, aerospace parts, consumer goods, in the marine and oil industries [1, 2].

In recent years, there is a great interest in industry on electrically semiconductor materials with superior mechanical properties and thermal stability [3]. Conductive polymer composites can be an alternative for this kind of materials. They are generally a synergetic combination of conductive filler and insulating polymer matrix. They exhibit a series of features, such as a percolation phenomenon, sensitivity to pressure, temperature and gas, improved electrical, mechanical and thermal properties. As a result of these unique properties they have received significant attention for use in various engineering applications such as sensors, antistatic coatings, electromagnetic interference shielding materials and electrolytes in the fuel cells [4, 5]. The crucial point in conductive polymer composite preparation is the establishment of the proper balance among the electrical, mechanical and thermal properties by applying appropriate processing methods and altering the properties of the composite constituents [6, 7].

The properties of the polymer composites depend on the properties of the individual components, type, shape, size and amount of the filler, dispersion of the filler in the matrix, degree of adhesion between the polymer matrix and the

conductive filler. Thus a great variety of properties can be established by altering these factors [8].

Carbon nanotubes are fullerene related structures which consist of rolled graphene sheets into cylinders, closed at either end with caps containing pentagonal or hexagonal rings [4]. They attract great interest due to their remarkable physical properties, such as high thermal, electrical conductivities and outstanding tensile strength [9]. Since their graphitic sidewalls have low amount of defects and chemically reactive functional groups on them, carbon nanotubes are chemically inert and their commercial use becomes limited due to weak interfacial interactions and poor dispersion capability. Therefore, activating and modifying the surface of carbon nanotubes are essential for the usage of carbon nanotubes in various application areas [10-13].

Poly(ethylene terephthalate) (PET) is a semi crystalline thermoplastic polymer with excellent chemical resistance, thermal stability, melt mobility, and spinnability. It has been used in a wide variety of fields including packaging, electrical, automotive, textile and construction industries [14-16]. It is also considered as a good matrix for polymeric composite materials due to its outstanding properties mentioned above [17, 18]. Carbon nanotubes are thought to be high potential fillers to improve the electrical, mechanical and thermal properties of the polymers with their exceptional physical properties [19-21]. However, there are very important limitations to achieve optimal enhancement of properties in carbon nanotube containing PET based composites [22]. These limitations are the poor interfacial adhesion between the carbon nanotubes and polymer, inadequate dispersion of carbon nanotubes in polymer matrix [23]. The interfacial adhesion between carbon nanotubes and matrix polymers can be improved by increasing the reactivity of carbon nanotubes. This can be achieved by increasing the number of defect sites and creating functional groups on carbon nanotube surface via chemical functionalization of carbon nanotubes [24, 25]. Enhanced interactions result in better load transfer and carbon nanotube dispersion in the composites which improve the mechanical properties [26-28].

Weak van der Waals interactions, mechanical interlocking and covalent bonding are three main potential mechanisms of load transfer from the polymer matrix to

carbon nanotubes. Among these three mechanisms, the contributions of the first two to the load transfer are limited. However, covalent bonds between functional groups on the outer shell of carbon nanotubes and the matrix polymer have been suggested as being responsible for the observed interfacial strength between the nanotubes and matrix in various researches [29-31]. In order to increase the covalent bonding between carbon nanotubes and polymer matrix in the composite, surface treatment of carbon nanotubes is performed with various chemicals before the preparation of polymer composites. General procedure for the carbon nanotube surface modification is to oxidize the carbon nanotubes with strong acids or bases firstly which usually refers to the purification. The purpose of purification procedure is two fold; to remove the metallic catalyst residues, which arise from the carbon nanotube synthesis and to create oxygen containing carboxyl and hydroxyl functional groups on carbon nanotube surfaces. These functional groups are reactive sites of the surface of carbon nanotubes during further chemical modifications. They can also improve the polymer-carbon nanotube interfacial interactions [32]. After the purification step carbon nanotubes are treated with various chemicals with different functional groups. The type of the surface modifier can be determined according to the matrix polymer that will be used for the preparation of polymer composites [33-70].

The covalent attachment of carboxyl and hydroxyl functional groups during purification can improve the efficiency of load transfer and dispersion in the composite. However, it should be noted that purification also introduces defects (dangling bonds) on carbon nanotube surfaces and damages the perfect crystalline structure of carbon nanotubes. This destruction yields to a decrease in mechanical strength and electrical conductivity of the carbon nanotubes and affects the properties of the prepared composites, since they both depend on the filler, matrix properties and the interphase between them [37, 38]. Therefore, there should be a trade off between the degree of carbon nanotube surface functionalization and bulk properties of carbon nanotube during the application of the purification procedure. The extent of each of these effects is dependent on the purification conditions [7, 39]. This balance can be achieved by optimizing the purification medium and period.

Polymer blends are the combination of homopolymers or copolymers which are, in most cases, thermodynamically immiscible [71]. Since, they can combine the useful properties of each blend component; immiscible blends are generally preferred over miscible blends [72]. However, the unfavorable interactions at the molecular level between the blend constituents lead to an unstable morphology when compared to their components in most immiscible blends which results in poor mechanical properties [73, 74]. High density polyethylene (HDPE)/ Poly(ethylene terephthalate) (PET) blend systems are widely studied in the literature due to their industrial importance [75-78]. HDPE is used mainly for films, pipe, blown bottles, and other consumer containers [72]. Lower cost and the resistance of HDPE to high processing temperatures needed for PET (230°C–270°C) under suitable conditions make HDPE/PET blends convenient materials in industrial applications [74]. However, HDPE and PET are also inherently incompatible due to their nonpolar and polar characteristics [79] and exhibit poor mechanical properties. This problem can be solved by preparing polymer blends under different processing conditions and creating blends with desirable morphologies [80].

Conductive polymer composites are usually prepared by incorporating conductive fillers into polymer matrix through melt mixing either by using an extruder or an internal mixer. However; in order to obtain high electrical conductivity with this method, high loadings of the conductive fillers are usually required, which may result in poor mechanical properties and high cost [81-85]. In the literature, several processing techniques have been used to lower the percolation threshold, in which electrical conductivity of composite increases by several orders of magnitude with the formation of current conductive structures [82]. These techniques are in situ polymerization of the polymer in the presence of conductive particles [86] and selective localization of conductive filler in one of the phases or at the interface of a polymer blend composed of two polymer constituents, in which filler forms the conductive network in the dispersed phase and this phase also constitutes continuous conductive structure in the major phase, which is called as double percolation [87, 88]. However, in situ polymerization technique is hard to apply in the industrial scale and the incompatible nature of the polymer constituents of the composite lowers the mechanical properties in the second technique.

At this point, a suitable processing technique must be performed for preparation of the conductive polymer composites with lower filler loadings and better mechanical properties. The processing technique may change the morphology, which affects the properties of the polymer composites. It has been established that fibrillar morphology can greatly improve the mechanical properties of the polymer blends when the mechanical properties of the dispersed fiber phase is superior when compared to polymer matrix [77]. Moreover, composites containing conductive fibers have lower percolation thresholds than the ones having spherical conductive particles [9, 77]. In situ formed microfibrils in polymer blends can be generated, by using the microfiber reinforced composites concept which was proposed by Fakirov et.al. for the first time [89]. In order to form a microfiber structure in a polymer blend, two polymers with different melting point temperatures should be used. Polymer with higher melting point temperature forms the dispersed microfibers in the polymer matrix with lower melting point [90]. An elongational flow field and lower melt viscosity of the dispersed microfiber phase can accumulate the higher aspect ratio microfiber formation [91]. In previous works two-step strategy was used to prepare the in situ microfibrillar blends. During the first melt mixing and hot-stretching step at the processing temperature of the dispersed polymer phase, the microfibrillar morphology of this polymer is developed. Then during the second step, the blend containing microfibrils is processed through injection molding at the processing temperature of the lower melting temperature polymer and the microfibrillar structure of the dispersed phase is maintained in the structure [92–94]. The electrical and mechanical properties of the blends are mainly affected by the amount, size and distribution of the dispersed microfibers in the matrix, processing conditions, hot stretching speed and molding temperature [90-103].

Conductive polymer composites can also be produced with fiber and carbon nanotube reinforcements by using thermosetting polymers. There is an increase of composite materials for load-bearing applications (e.g. they are used in airplanes such as the Boeing 787, F-35, A-350, vehicular and pedestrian bridges worldwide, mine hunter ships, trains, cars, etc.). Epoxies are epoxide based thermosetting polymers, which are used as matrix for the preparation of the composite structures with carbon fiber and glass fiber reinforcements [104-111]. They are generally produced from a reaction between epichlorohydrin and bisphenol-A. Epoxy resins are cured by mixing and heating them with amine based hardeners. They are very

good adhesives for different kinds of surfaces, their heat contraction is low and they are resistant to chemicals, moisture and heat [104].

Surface treatment of carbon nanotubes with amine based chemicals is a widely used technique in the literature [105]. Diamines are used for enhancing the interfacial interactions between carbon nanotube and epoxy, since one of the amine in the structure reacts with carbon nanotube surface and the other reacts with epoxy resin. Moreover, amine functionality can accelerate and enhance the curing of the epoxy [106]. Surfactants can be used to decrease the carbon nanotube particle size in the composites. Smaller particle size and improved dispersion homogeneity in epoxy matrix of carbon nanotubes can enhance the electrical conductivity and mechanical properties of the composites [107].

Fiber reinforced composite materials have different damage modes when compared to ordinary engineering materials (metals, ceramics and plastics) and these modes are difficult to detect with ordinary techniques [112]. It is very important to determine the damaged parts of the materials during their service lives, since these damages can cause the deterioration of the materials in the future. These inspections are often called as structural health monitoring of the materials. Non destructive techniques such as tap tests, X and N-rays, ultrasonic inspection and eddy current testing are often used for the determination of the damage in the composites. Conventional sensing techniques can be performed by either embedded or attaching sensors on the composite structure, which can raise cost, reduce the durability and result in deteriorating the total composite performance. This problem can be solved if composite material itself behaves like an intrinsic sensor. Conductive carbon nanotube filled composites respond the applied load with the change in electrical conductivity of the composite [113]. However, it should be noted that carbon nanotube dispersion, particle size and fiber-carbon nanotube integration in multiscale composites can directly affect the damage sensing characteristics of the composites. Damage sensing capability of the composites can be determined by means of electro-micromechanical tests which can be defined as a simultaneous measurement of electrical resistance as well as micromechanical properties while applying load [114].

The main aim of this dissertation was to prepare conductive polymer composites with enhanced mechanical and electrical properties. For this purpose, different aspects were investigated in three main sections. First aspect is the surface treatment of carbon nanotubes and their use in PET based composites. The second aspect is the preparation of microfiber reinforced composites containing HDPE, PET and carbon nanotubes. The third aspect is the preparation of glass fiber reinforced epoxy based polymer composites having carbon nanotubes which have been chosen for the potential use in structural health monitoring applications.

In the first part of the carbon nanotube surface treatment studies, the effects of different purification mediums and periods on the properties of the carbon nanotubes and composites based on these carbon nanotubes were investigated. As-received carbon nanotubes were purified by using strong acids (nitric acid ( $\text{HNO}_3$ ) and sulphuric acid ( $\text{H}_2\text{SO}_4$ )) and bases (ammonium hydroxide ( $\text{NH}_4\text{OH}$ ) and hydrogen peroxide ( $\text{H}_2\text{O}_2$ )). Poly(ethylene terephthalate) (PET) based conductive polymer composites were prepared with as received and purified carbon nanotubes. In the second part, the effect of carbon nanotube surface functionality on the properties of the PET based composites were investigated by using as-received, purified, sodium dodecyl sulfate (SDS), poly(ethylene glycol) (PEG), diglycidyl ether of Bisphenol A (DGEBA) treated carbon nanotubes during composite preparation. Carbon nanotube amount in the composites was varied from 0.25 wt.% to 4 wt.% in this part of the research. These composites were characterized in terms of electrical conductivity, mechanical, thermal properties and morphology. Apart from the most of the studies in the literature, possible interaction patterns between the carbon nanotubes and PET were searched by applying Fourier Transformed Infrared Spectroscopy (FTIR) and Nuclear Magnetic Resonance (NMR) analysis to composite samples. All carbon nanotube samples were characterized extensively by means of surface energy measurements, Fourier Transformed Infrared Spectroscopy (FTIR), Electron Spectroscopy for Chemical Analysis (ESCA), X-Ray Diffraction (XRD), Scanning Electron Microscopy (SEM) and Thermogravimetric Analysis (TGA).

Microfiber reinforcement of the polymer composites was performed as an alternative composite preparation method during this research, to improve the electrical and mechanical properties of the composites. In the first part of the

microfiber reinforced composite studies, in-situ microfiber reinforced high density polyethylene HDPE/PET/CNT (as-received) composites were prepared through extrusion and hot stretching. Apart from the most of the studies reported in the literature, carbon nanotube, which is the high aspect ratio conductive filler, was incorporated into the microfiber reinforced polymer composites. The effect of PET content and the molding temperature of the composites on the microfibrillar morphology were mainly investigated. In addition, microfiber composites were compared to conventional melt mixed HDPE/PET blends and HDPE/PET/CNT composites in terms of morphology, electrical, mechanical and thermal properties. In the second part, effects of carbon nanotube purification, PEG treatment and carbon nanotube amount in the composites, on the morphology, electrical, and mechanical properties of the microfiber reinforced polymer composites were investigated. Carbon nanotube amount in the composites was varied from 0.25 wt.% to 1.5 wt.% in this part of the research.

In the last part of the thesis, epoxy/CNT composites and epoxy/CNT/glass fiber composite panels were prepared by using solvent assisted sonication and hand lay-up techniques. Carbon nanotube amount in the composites was varied from 0.25 wt.% to 1 wt.% in this part of the research. Composites were characterized in terms of electrical and mechanical properties. Moreover, damage sensitivities of the composite panels were determined by measuring the electrical resistivity changes of the panels during tensile, fatigue and impact tests. Apart from the studies published in the literature, effects of carbon nanotube surface treatment with hexamethylene diamine (HMDA) and surfactant (4-octylphenol polyethoxylate (Triton X-100) and cetyl pyridinium chloride (CPC)) usage during epoxy/CNT mixture preparation were studied on the damage sensing properties of the composite panels.

## CHAPTER 2

### BACKGROUND

#### 2.1 Conductive Polymer Composites

The electrical conductivity is defined by the ohm's law. Electrical current with a magnitude of  $I$  flows across a material when an electrical potential,  $V$  is applied. The Ohm's relation describes the proportionality of current to the voltage:

$$I = \frac{V}{R} \quad (2.1)$$

where  $R$  is the electrical resistance.  $\rho$  depends on the intrinsic resistivity  $R$  of the material and on the geometry (length ( $l$ ) and area ( $A$ ) through which the current passes) [115]:

$$\rho = \frac{Rl}{A} \quad (2.2)$$

The electrical resistivity is one of the properties of materials that vary most widely, from  $10^{-6}$  to  $10^{18}$  ohm.cm. Conductors have an electrical resistivity range of  $10^{-6}$ - $10^{-3}$  ohm.cm. Semiconductors are in the range of  $10^{-3}$ - $10^7$  ohm.cm. If the electrical resistivity is higher than  $10^{12}$  ohm.cm, then the material is an insulator. Materials with electrical resistivities in the range of  $10^7$ - $10^{12}$  ohm.cm may be called as semi-insulators [3].

Electrical conduction in conductors is achieved by means of electrons in the conduction band. In a metallic (conductor) solid containing an incomplete energy band, the effective number of free electrons is always different from zero [116].

There are empty states just above the Fermi levels, where electrons can be promoted in a conductor solid. The promotion energy is negligibly small so that at any temperature electrons can be found in the conduction band. Current conduction in semiconductors and insulators is provided by electrons in the conduction band and by holes in the valence band. Holes are vacant states which are created when an electron is removed from the valence band. In insulators and semiconductors, there is an energy gap ( $E_g$ ) between the valence and conduction bands which is narrower in semiconductors when compared to the insulators (Figure 2.1). Hence, energy is needed to promote an electron to the conduction band. This energy may come from heat, or energetic radiation [115].

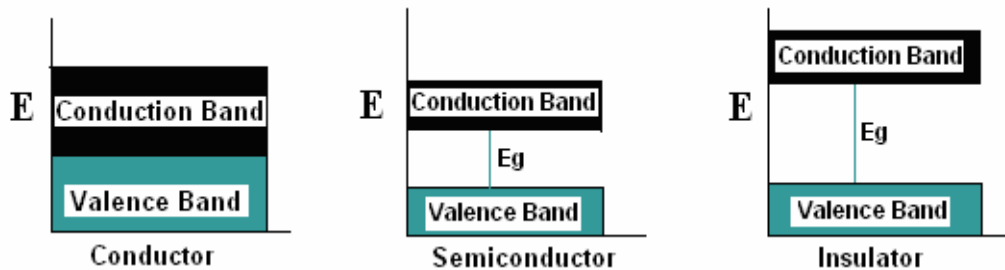


**Figure 2.1** Energy gaps in conductors, semiconductors and insulators [116]

Nowadays engineering applications requires semiconductor materials with good mechanical properties and thermal stability. One example for this kind of materials can be conductive polymer composites. They consist of insulator polymer matrix and the conductive filler particles dispersed in the matrix polymer.

Thermoplastic polymers can be easily shaped by heat and pressure to produce low density, mechanically tough and flexible products for wide range of industrial applications. However, due to the chemical structure, most of the solid polymers contain very small amount of free electrons. Therefore they are very good electrical insulators [117].

The electrical conductivity of the conductive polymer composites is explained by the percolation theory. The mechanism of the electrical conduction is the formation of a continuous filler network throughout the insulating polymer matrix. Conductive path is formed by the free transportation of the electrons along the chains of directly contacting particles and over the spaces between the particles, filled with polymer by tunneling [4]. In this theory the most important parameter is the percolation threshold concentration which is defined as the minimum amount of conductive filler which must be incorporated to an insulating matrix to cause the onset of electrical conductivity in the composite.

Figure 2.2 shows the electrical resistivity change of a conductive polymer composite with respect to the conductive filler amount in the composite. Below the percolation threshold the filler particles can not form continuous conductive networks in the composite. After the filler concentration reaches the percolation threshold the conductive filler chains are formed in the matrix and the composite has higher electrical conductivity.

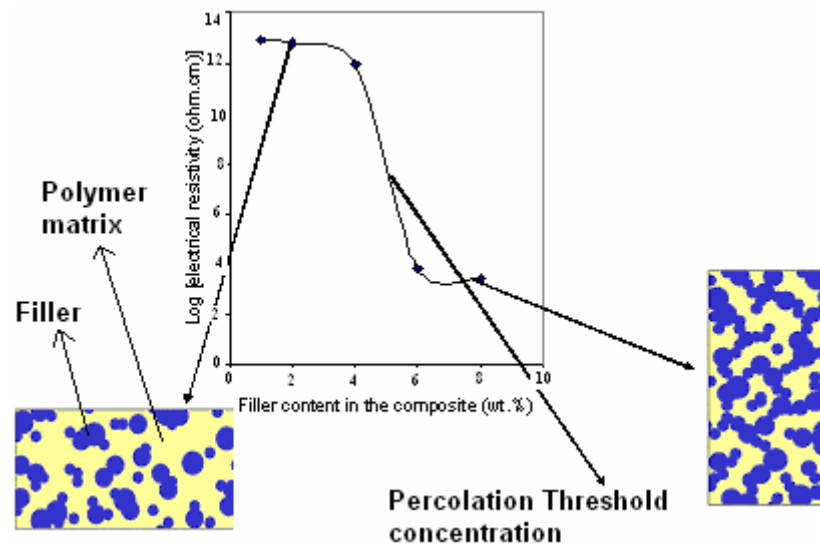


**Figure 2.2** Schematic representation of the percolation theory

At lower filler contents (before the percolation threshold concentration) in the composites, insulating polymer matrix controls the conduction mechanism, since the electrons of conductive fillers have to pass through micro spaces between fillers filled with insulating polymer matrix and the tunneling distance is very high. However, beginning from percolation content, the conductive fillers dominate the conduction mechanism which increases the electrical conductivity of the composite significantly and the direct contact is continued to be provided at higher filler concentrations [4].

Electrical conductivity of conductive polymer composites depend on the conductivity of the separate components, concentration, size and shape of the filler, positions of the fillers with respect to each other in the polymer matrix, contact resistance of the neighboring particles [4]. The conductive filler content of these composites must be as low as possible to meet its electrical requirements. At higher filler concentrations conductive fillers tend to form agglomerates and the composite processing becomes difficult, the mechanical properties of the composite become poorer, the final cost of the material increases. There are several ways to decrease the percolation threshold concentration in polymeric matrices, which are mainly based on the use of additives, the optimization of processing conditions, as well as the size, distribution and surface properties of filler [118].

### 2.1.1 Conductive Fillers

Desired electrical conductivity in the composites can be achieved by blending insulating polymers with different kinds of conductive fillers. Conductive polymer composites are usually prepared by the incorporation of the conductive filler particles, such as carbon black, carbon nanotube, carbon nanofiber, graphite and metal particles, into the insulating polymer matrix [48, 86, 119, 120]. Nowadays, carbon nanotubes are the most commonly used conductive fillers to obtain conductive polymer composites due to the greater tendency of carbon nanotube particles to form a conductive network inside the composites with their smaller particle size and chain like aggregate structures when compared to other

conducting additives. Multi walled carbon nanotubes (MWCNT) were used as conductive filler in the content of this dissertation.

### 2.1.1.1 Carbon Nanotubes

Carbon nanotubes are a new form of carbon, which are configurationally equivalent to two dimensional graphene sheet rolled into a tube. In other words they may be considered as graphene cylinders [121]. Extensive research activities across the world have been conducted on carbon nanotubes since their first observation by Sumio Iijima of the NEC Corporation in 1991 due to their extraordinary mechanical properties and unique electrical properties [122]. Two main types of the carbon nanotubes which are single walled (SWCNT) and multiwalled (MWCNT) carbon nanotubes are shown in Figure 2.3.

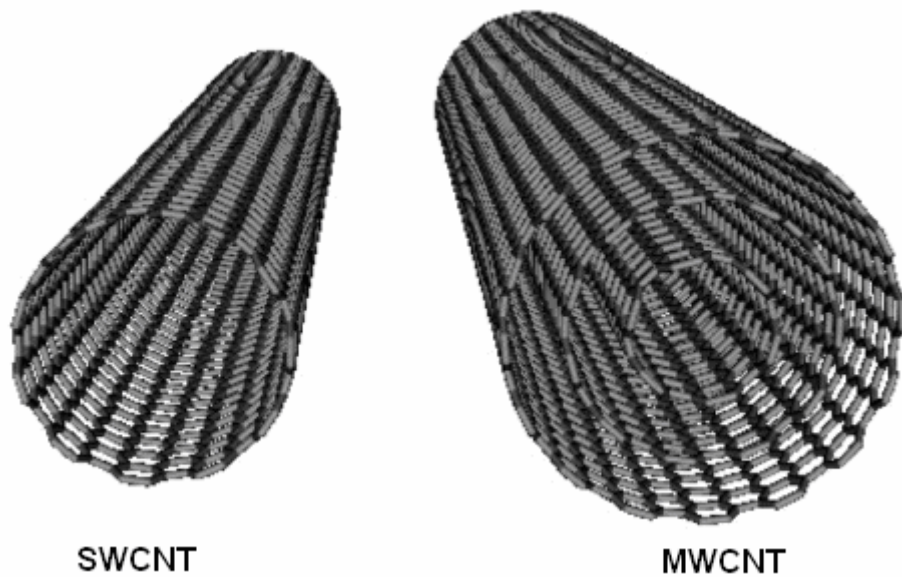


**Figure 2.3** Schematic representations of carbon nanotube types

A single walled carbon nanotube can be described as a rolled - up single graphene sheet in which the edges of the sheet are joined together to form a seamless tube [121]. The diameters of single walled carbon nanotubes vary from 1 to 1.4 nm. Multi walled carbon nanotubes are composed of 2 to 30 concentric graphene layers in diameters from 10 to 50 nm with an aspect ratio more than 1000 [123]. Table 2.1 summarizes some experimental and theoretical properties of carbon nanotubes.

**Table 2.1** Theoretical and experimental properties of carbon nanotubes [43]

<b>Property</b>	<b>CNT</b>
Specific gravity	0.8 g/cm <sup>3</sup> for SWCNT; 1.8 g/cm <sup>3</sup> for MWCNT (theoretical)
Elastic modulus	1 TPa for SWCNT; 0.3 – 1 TPa for MWCNT
Strength	50–500 GPa for SWCNT; 10–60 GPa for MWCNT
Resistivity	5–50 μΩ cm
Thermal conductivity	3000 W m <sup>-1</sup> K <sup>-1</sup> (theoretical)
Magnetic susceptibility	22 x 10 <sup>6</sup> EMU/g (perpendicular with plane), 0.5 x 10 <sup>6</sup> EMU/g (parallel with plane)
Thermal stability	>700 °C (in air); 2800 °C (in vacuum)
Specific surface area	10–20 m <sup>2</sup> /g

In the last two decades, great progress has been made toward applications of carbon nanotubes, including; materials for chemical, biological separation, purification, and catalysis; energy storage such as hydrogen storage, fuel cells, and the lithium battery; and devices such as probes, sensors, and actuators for molecular imaging, sensing, and manipulation; transistors, memories, logic devices, and other nanoelectronic devices; field emission devices for x-ray instruments, flat panel display, and other vacuum nanoelectronic applications [122]. In some special applications, such as sensors, antistatic coatings, electromagnetic interference shielding materials and electrolytes in the fuel cells,

high-performance lightweight structural materials are required, and they can be developed by adding carbon nanotubes into polymers and preparing conductive polymer composites. Moreover, carbon nanotubes can be either conducting or semi conducting due to the topological defects from the fullerene-like end caps. Thus, the electronic and physico-mechanical properties of carbon nanotubes are dependent upon their dimensions, helicity or chirality [43]. By changing the direction in the roll-up of the graphene sheets, carbon nanotubes with zig zag (roll-up in  $(n, 0)$  direction), chiral (roll-up in  $(n, m)$  direction), and arm chair (roll-up in  $(m, m)$  direction) chiralities can be created (Figure 2.4).

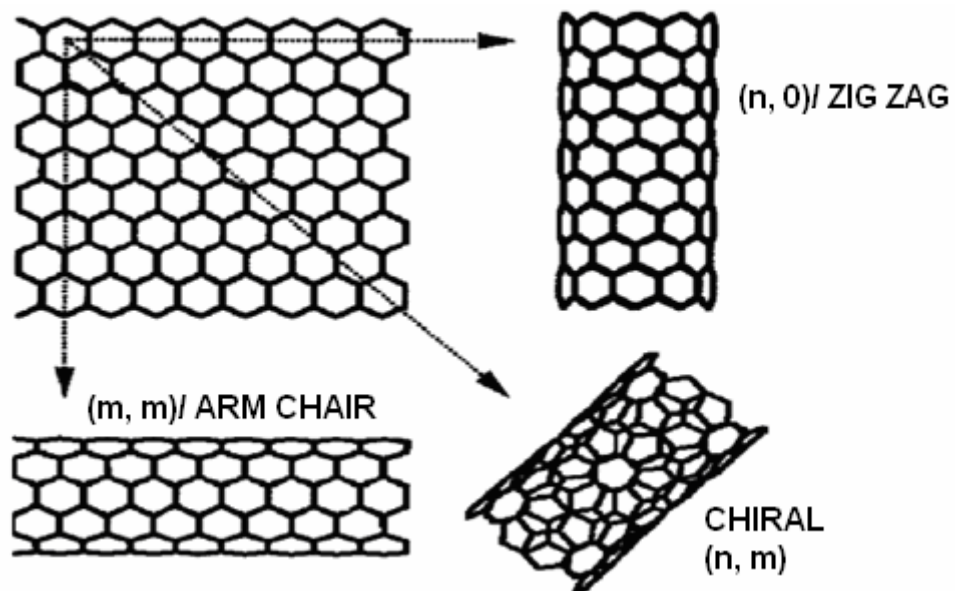


**Figure 2.4** Three types of single walled carbon nanotubes with different chirality [122]

Carbon nanotubes can be synthesized by three main processes. In arc discharge process an arc discharge between two graphite rods is ignited which results in the consumption of one of the electrode and the synthesized carbon nanotubes can be collected from the different positions of the reactor. Single walled and multiwalled carbon nanotubes can be grown with different yields depending on the gas

atmosphere in this process. During the laser ablation method, a graphite target loaded with a catalyst is positioned in a tube furnace and irradiated by a laser. Carbon nanotubes are deposited at the end of the tube furnace (cooler zone) with high yield. In catalytic chemical vapor deposition process, a tube furnace is loaded with metal catalyst and it is fed with a carbon containing gas or gas mixture. At the temperature range of 500–1000°C, carbon nanotubes are deposited on the catalyst surfaces [122].

## 2.1.2 Polymer Matrices

The polymer matrix in the composite is the continuous phase and it has two main functions. It protects the reinforcing fillers against the outside effects such as abrasion, mechanical damage, environmental corrosion and it also provides uniform load distribution to the reinforcing constituents if proper adhesion between the matrix and the fillers is accomplished. The thermo-mechanical characteristics of the composites are also determined by the matrices, heat resistance and thermal properties of the polymer matrices are also important for the composite performance [124].

In each part of this dissertation, different types of polymers were used as matrix to prepare conductive polymer composites. In the first part, poly(ethylene terephthalate) (PET) was utilized for the preparation of the carbon nanotube containing polymer composites. In the second part, microfiber reinforced polymer composites were processed by extrusion and hot stretching the PET/CNT phase in high density polyethylene (HDPE) matrix. In the last part, glass fiber reinforced composite panels were prepared by using neat epoxy and epoxy/CNT mixtures.

### 2.1.2.1 Poly(ethylene terephthalate) (PET)

Poly(ethylene terephthalate) (PET) (Figure 2.5) is an industrially important polyester which is used as a consumer fiber since 1953 [125]. PET retains good

mechanical properties at temperatures up to 150–175°C due to its high crystalline melting point and glass transition temperature. Its chemical and solvent resistance is also good. Its crease resistance, work recovery and low moisture absorption also increase its uses in different industrial applications. These properties result from the stiffness of the polymer chains which results in high modulus and insusceptibility of the interchain bonds to moisture. The major application areas of PET are in fiber, bottle and film industries [126].

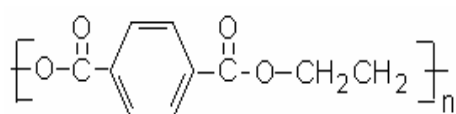


**Figure 2.5** Chemical structure of poly(ethylene terephthalate)

The production of commercial PET is achieved through two successive ester interchange reactions (Figure 2.6). The first step is the ester interchange of dimethyl terephthalic acid (DMT) and ethylene glycol (EG) at temperatures near 200°C. In the second stage, the temperature increment causes the formation of high molecular weight PET during which ethylene glycol is distilled off [125].

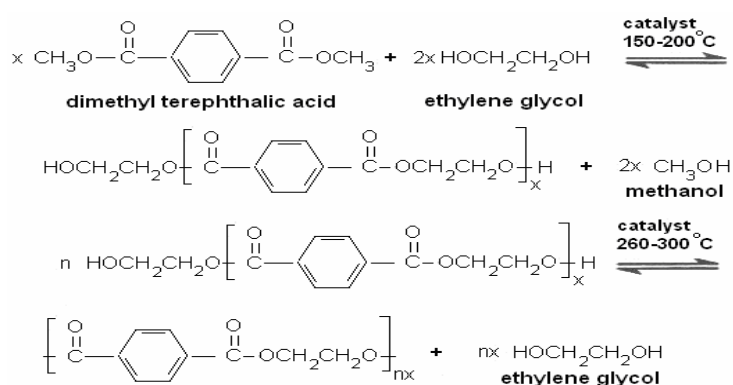


**Figure 2.6** Two steps in the polymerization of poly(ethylene terephthalate) [125]

### 2.1.2.2 High Density Polyethylene (HDPE)

High density polyethylene (HDPE) (Figure 2.7) is a typical thermoplastic with a glass transition temperature below room temperature. Low molecular weight HDPE is slightly brittle, the high molecular weight HDPE is more ductile and has higher impact resistance. The tensile strength and modulus of HDPE are relatively low due to the weak intermolecular forces between the nonpolar molecules in the polymer chain. Commercial HDPE is soluble in hot xylene. HDPE has a melting point of at least 125°C because of its weak intermolecular forces and high flexibility [127]. The typical commercial applications of HDPE are blow-molded containers, crates, pails, drums, gas tanks and blown films [125]. HDPE can be synthesized in several ways; such as radical polymerization of ethylene at extremely high pressures, coordination polymerization of ethylene and polymerization of ethylene with supported metal-oxide catalysts [126].

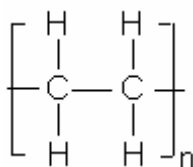


**Figure 2.7** Chemical structure of polyethylene

### 2.1.2.3 Epoxy Resins

The epoxy resin term is used to describe polyphenol derivatives which are defined by ring opening of oxirane rings [127]. Epoxy resins have low shrinkage upon curing, good mechanical and electrical properties, high chemical and corrosion resistance [125]. They can adhere well to substrates such as wood or metal due to the presence of polar hydroxyl pendant groups in their structure [127]. The main applications for epoxy resins include protective coatings and adhesives [125]. Epoxy based composites are used to manufacture tools for aircrafts and

automobiles [127]. Epoxy resins can also be used in both molding and laminating techniques to make glass fiber reinforced composite panels with superior mechanical properties [126].

Bisphenol A is the most widely used phenol for epoxy resin production. Epoxies are formed by two stage process. In the first stage, a low molecular weight prepolymer is prepared by a base catalyzed step-growth reaction of a dihydroxy compound (Bisphenol A) with epichlorohydrin (Figure 2.8) [125]. During a separate curing step, the prepolymer molecular weight is increased and the network structure is formed. Amines may be used as curing agent to cause ring opening of the epoxide end groups through nucleophilic addition [125] (Figure 2.9).

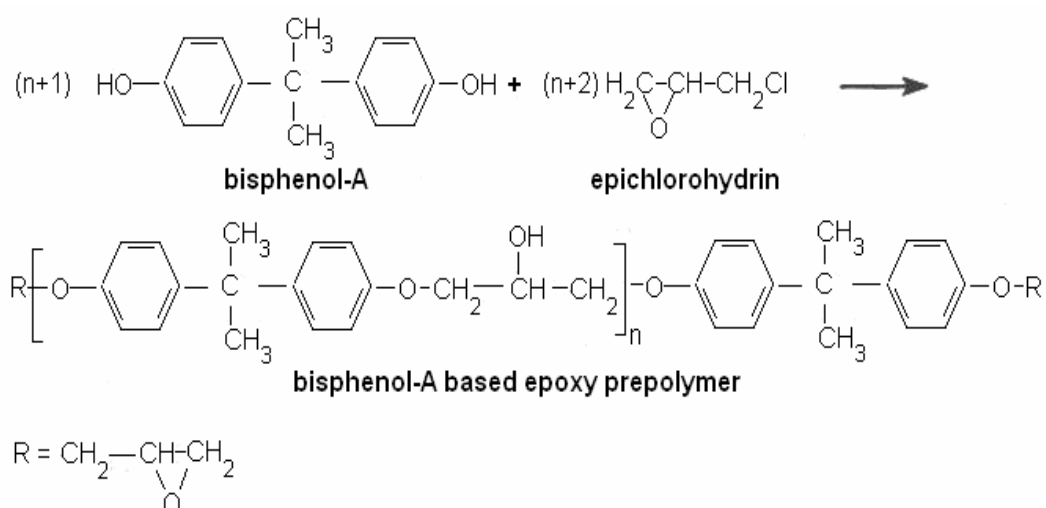


**Figure 2.8** Epoxy prepolymer formed from bisphenol A and epichlorohydrin [125]

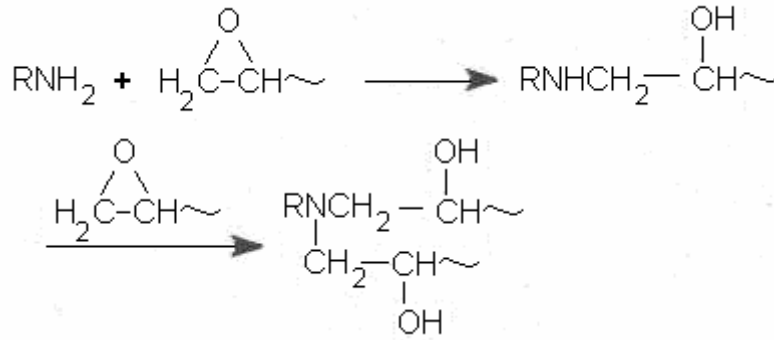


**Figure 2.9** Cure of an epoxy resin by reaction of the prepolymer with an amine [125]

### 2.1.3 Fiber Reinforcements

Fiber reinforcements are important constituents of composite materials and give all the necessary stiffness and strength to the composite. The most common reinforcements are glass, carbon, aramid and boron fibers and their diameters are in the range of 5 – 20  $\mu\text{m}$ . The flexibility and small diameters of the fibers makes them to conform to various shapes. In general, fibers are made into strands for weaving or winding operations. They are wound around a bobbin and collectively called a roving for delivery purposes. An untwisted bundle of carbon fibers is called tow [1].

Reinforcement of polymeric matrices has certain aspects. In the polymer matrix composites, the polymer matrix is expected to coat the fiber surfaces and there are physical and chemical interactions at the polymer-fiber interface [124]. Fibers for composite materials can be obtained in many forms, from continuous fibers to discontinuous fibers, long fibers to short fibers, organic fibers to inorganic fibers. The most widely used fiber materials in fiber-reinforced plastics are glass fibers [1].

### 2.1.3.1 Glass Fibers

Glass is an amorphous material composed of silica network. The four main types of the glass fibers are high alkali (A glass) grade, electrical (E glass) grade, chemically resistant modified E glass (ECR glass) grade and high strength (S glass) grade. E glass fiber is the most widely used one for the reinforcement purposes in the polymer composites. Glass fibers are obtained after cooling the melt spun to the rigid condition without the crystallization of glass. After the preparation of the continuous glass fibers, they are transformed into various forms, such as (continuous or woven) rovings, yarns for textile applications, chopped strands, mats and preforms (Figure 2.10) [124].

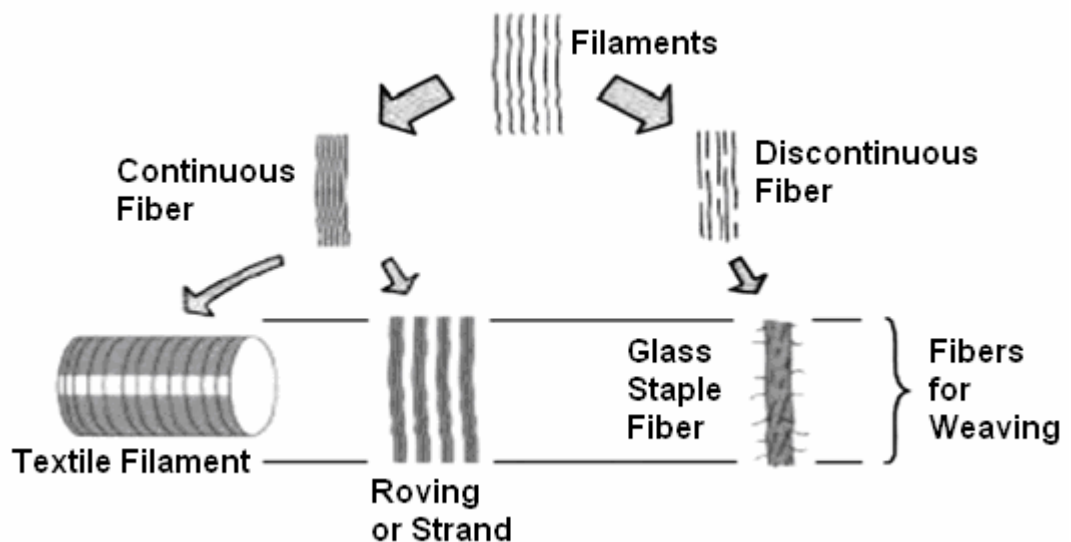


**Figure 2.10** Different glass fiber forms [128]

In composite applications of the glass fibers, a proper fiber finishing and application of a coupling agent to the surface of fiber is required. The functions of the coupling agent are; to protect it from damage during processing, to aid the processing and to promote the matrix–fiber adhesion. Coupling agents may be film forming organics and polymers, adhesion promoter silane coupling agents or chemical

modifiers. The sizing formulation depends on the type of the polymer matrix used for the composite preparation [124].

#### 2.1.4 Polymer Composites and Blends

Polymer composites consist of polymer matrix and fillers differing in composition on a macro scale with two distinct phases having recognizable interfaces between them [124]. Fillers in the polymer composites might have certain geometries such as fibers, flakes, spheres and particulates. Reinforcing fibers are found in different forms, from long continuous fibers to woven fabric and mat [1]. Fiber reinforced thermoset laminates are usually classified as high performance polymer composites. The particulate filled composites are usually based on a thermoplastic polymer matrix and they are classified as lower performance polymer composites when compared to continuous fiber reinforced composites [129].

The properties of the polymer composites depend on the inherent properties, size, shape of the fillers; composition of the composite; the interaction of composite components at the interface; and the method of fabrication. The fillers in the polymer composites can be classified as reinforcements, fillers or reinforcing fillers. Reinforcements usually increase composite's modulus and strength due to their higher stiffness and strength. Besides the mechanical reinforcement, fillers in the polymer composites affect the electrical, thermal and optical properties. In the composites filled with discontinuous fillers, the fillers (short fibers, flakes or particulates) can be arranged in the composite in different orientations, multiple geometric patterns and sizes. These are formed by the selected processing and shaping methods (extrusion and injection molding for thermoplastic matrices) [129]. Especially, the filler size is the most important criterion that affects the properties of the composites. The larger particulate filler agglomerates in the composites act as stress concentrated areas and accelerate the rupture of the composite structure and decrease the mechanical strength [8]. Moreover it is stated that small size of particle is a required criterion for filler particles to build an electrically conductive composite at lower filler concentrations [4].

Recently, a new area in the composite science has established to overcome the limitations of traditional micrometer scale filler loaded polymer composites and nanoscale additive filled polymer composites have been developed [130]. Polymer nanocomposites are the combination of a polymer matrix and additives that have at least one dimension in the nanometer range. The additives can be one-dimensional such as carbon nanotubes and carbon nanofibers, two-dimensional such as layered silicates and clay, or three dimensional including spherical particles like carbon black. Polymer nanocomposites have attracted considerable interests, due to their outstanding mechanical properties like elastic stiffness and strength with only a small amount of the nanofillers (usually less than 5 wt.%). This is due to the large surface area to volume ratio of nano fillers when compared to those of micro and macro fillers. Other superior properties of polymer nanocomposites include electrical, optical and magnetic properties, barrier resistance, flame retardancy and scratch, wear resistance [131].

Polymer composites based on thermoplastic and thermosetting polymers with different kinds of fillers can be prepared by using melt intercalation, solution intercalation, roll milling, emulsion polymerization, high shear mixing, in-situ polymerization, hand – lay up, spray up and resin transfer molding techniques [1, 132–134].

Polymer blends are prepared by mixing of two or more different polymers together. The polymer mixtures which do not contain conductive fillers or fiber reinforcements are called as blends throughout the thesis. The combination of these polymers makes it possible to achieve various property combinations of the final material. Polymer blends can be classified as chemical and physical blends. Copolymers are examples of chemical blends which involve chemical bonding between blend phases. Physical blending of two amorphous polymers can produce either a homogeneous mixture at the molecular level or a heterogeneous phase separated blend. Two totally separated phases can be obtained by demixing of polymer chains, and this leads to macro phase separation in polymer blends. Some specific types of organized structures may be formed in block copolymers due to micro phase separation of block chains within one block copolymer molecule [135].

Blending may be used to reduce the overall cost, to improve the processability or to improve the impact resistance [125]. However, binary blends of immiscible polymers generally exhibit poor mechanical properties due to a coarse and often unstable morphology [84]. Unfavorable interactions exist at the molecular level leads to a great interfacial tension between the polymer phases of the blend which makes dispersion of the components during processing difficult. This results in an unstable morphology (coalescence of phases) and poor interfacial adhesion between the phases of the polymer blend [78]. Therefore it is essential to control and stabilize a desired type of morphology in a polymer blend in order to generate polymeric materials with favorable properties [84]. Microfiber reinforced polymer blends can be an example for this strategy. It has been established that fibrillar morphology can greatly improve the mechanical properties of the polymer blends when the mechanical properties of the dispersed fiber phase is higher compared to polymer matrix [77]. In situ formed microfibrils in polymer blends can be generated, by using the microfiber reinforced blends concept [89]. Incorporation of conductive fillers into immiscible polymer blends improves the electrical conductivity at much lower filler contents due to a double percolation phenomenon. Double percolation means the percolation of the conductive filler within one phase of a polymer blend (first percolation), which itself percolates in the blend (second percolation) [84]. In the case of microfiber reinforced polymer blends, when the conductive filler locates selectively in the dispersed microfibrillar phase of the blend then the obtained composite may have high electrical conductivity, due to the double percolation phenomena in a polymer blend.

Polymer blends can be prepared by using the melt compounding, mechanical mixing, latex blending, solvent film casting and copolymerization.

#### 2.1.4.1 In-situ Microfiber Reinforcement of Polymer Composites

Microfiber reinforced composites are developed on the basis of polymer blends. Processing of an incompatible polymer pair in which the dispersed phase forms in situ microfibers in the matrix is the preferable way to achieve the desired properties. One way of preparing these blends is mixing thermotropic liquid

crystalline polymers (LCP) with thermoplastics. Thermotropic LCP are essentially rigid rod long chain molecules with some irregularity or flexibility and this molecular structure allows these materials to exhibit molecular order in a liquid mesophase. LCP are quite attractive as a potential dispersed microfibrillar phase for microfiber reinforced materials due to the highly orientated nature of LCP which produces highly anisotropic physical properties [136]. However the LCP are often too expensive for general engineering applications. In order to overcome this problem, a new type of processing route with two thermoplastic polymers is developed for the preparation of the microfiber reinforced composites. This preparation route consists of three main steps (Figure 2.11). The mixing step includes melt blending with extrusion or internal mixer of two immiscible polymers. After the mixing step, hot-stretching of the extrudate with good orientation of the two phases is performed. In the last step, isotropization of the composite is performed by thermal treatment at temperature between the melting points of the two blend constituents [136–139].

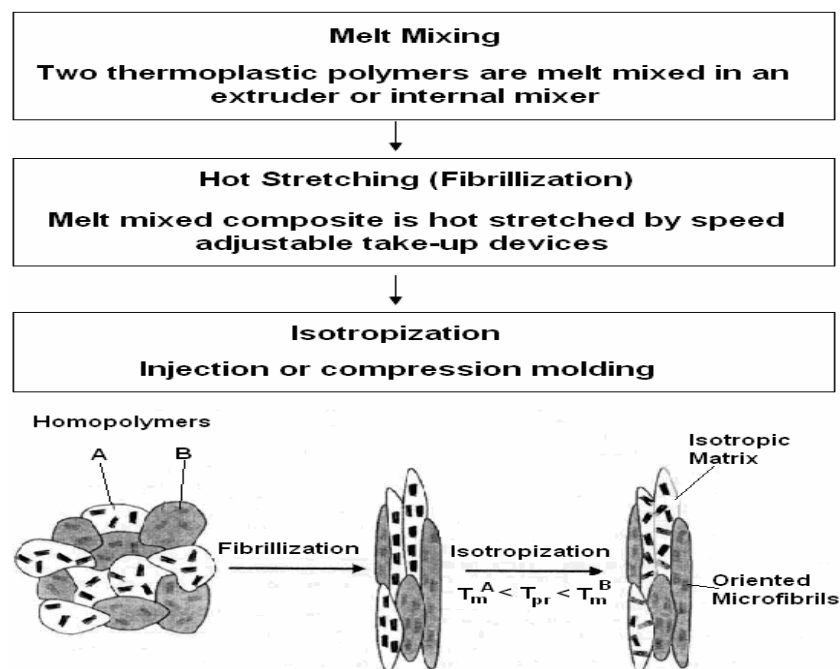


**Figure 2.11** Schematic presentation of the essential steps during manufacturing of microfiber reinforced composites [139]

Microfiber reinforced conductive polymer composites are generally prepared by extrusion of an incompatible thermoplastic polymer pair with conductive filler in which the conductive particles selectively locate in the dispersed polymer phase and the dispersed polymer/conductive filler phase forms microfibers in situ by hot stretching (Figure 2.12). In this method, polymer matrices should have a distinct difference between their melting temperatures and melt viscosities. Polymer with higher melting point and lower melt viscosity is the dispersed phase in which the conductive filler particles distribute, and forms the microfibers in the matrix polymer with lower melting point. The isotropization step is performed at a temperature below the melting point of the microfiber phase in order to preserve the microfibrillar morphology via injection or compression molding. The properties of these composites are mainly dependent on the amount, size and distribution of the dispersed polymer/conductive filler microfibers in the matrix, processing conditions, hot stretching speed and molding temperature [5, 90, 95, 140]. Microfiber reinforced conductive polymer composites might have high electrical conductivity, lower percolation threshold and better mechanical properties, due to the selective localization of the conductive filler in microfiber phase, double percolation phenomena in a polymer blend and reinforcement of microfibers.

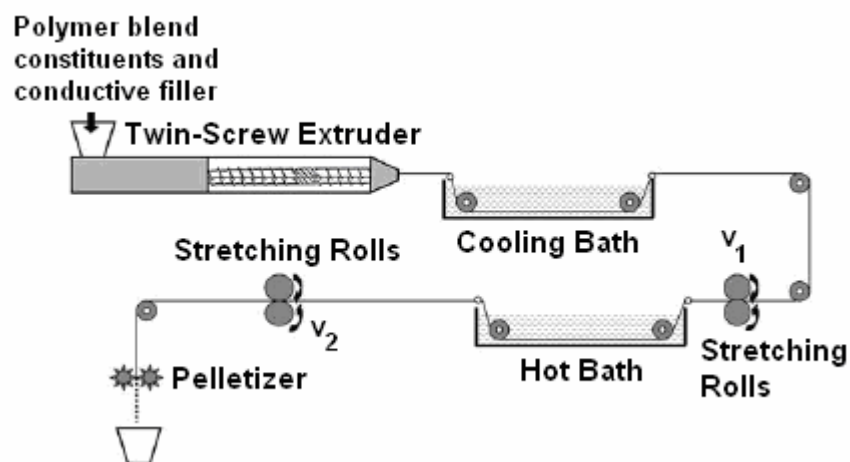


**Figure 2.12** Schematic of the industrial relevant extrusion and hot-stretching line [136]

## 2.1.5 Preparation Methods of Polymer Composites and Blends

Polymer composites and blends can be prepared by using basic polymer processing methods. Thermoplastic polymer processing may be divided into two broad areas. The first one is the conversion of the polymer into pellet or powder form after melt processing. The second type describes the process of converting polymeric materials into useful articles of desired shapes [141]. Different polymer composite preparation methods were used in this dissertation. PET/CNT and microfiber reinforced HDPE/PET/CNT composites were processed by using a twin screw extruder. The test samples of these composites for the characterization experiments were prepared with injection and compression molding techniques. During the production of the epoxy/CNT/glass fiber composite panels, epoxy/CNT mixtures were prepared by using solvent assisted sonication technique. Composite panels for the tensile, fatigue and impact tests were obtained by applying hand lay-up technique.

### 2.1.5.1 Extrusion

Extrusion is the most widely used polymer processing operation. During extrusion process thermoplastic materials in powder or granular form are transformed into a continuous uniform melt, which is shaped into uniform cross-sectional area by forcing it through a die [141]. After the die a whole array of units for cooling, stretching and cutting can be attached to the extrusion unit (Figure 2.13) [142].

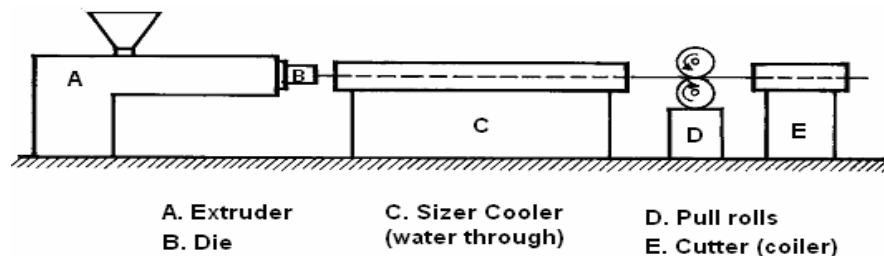


**Figure 2.13** Sketch of an extrusion line [141]

Figure 2.14 shows the schematic representation of the various parts of a single screw extruder. It essentially consists of the barrel, the polymer and additives are fed to the barrel from the hopper part, which is at the rear end. The polymer melt conveys to the die which is at the front end of the extruder during the operation. The screw, which is the moving part of the extruder, is designed to pick up, mix, compress, and move the polymer as it changes from solid granules to a viscous melt. Motor operating through a gear reducer supplies the power which turns the screw in the barrel [141].

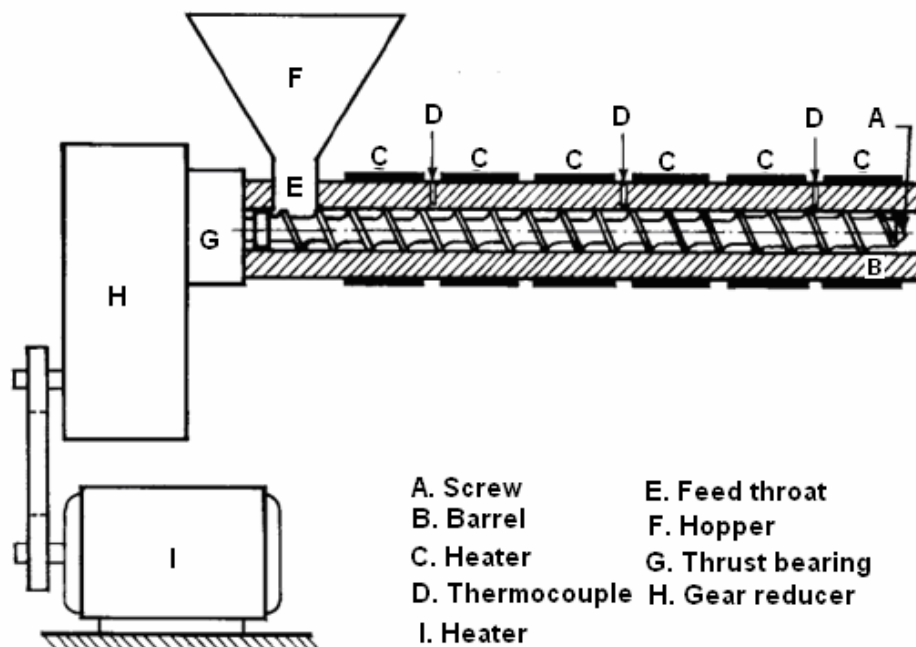


**Figure 2.14** Parts of a single screw extruder [141]

The barrel part can be divided into feed, compression and metering sections (Figure 2.15). The solid feed is conveyed from the feed section to the compression section with the rotation of the screw. There are electric heaters attached to the compression zone of the barrel and the resin begins to melt with the help of them. The resin is completely melted as it reaches the metering section and the shear action of the rotating screw against the inner wall of the barrel forces the polymer

melt coming out from the die section. The extrudate is shaped into the desired form as it comes out the die [125].

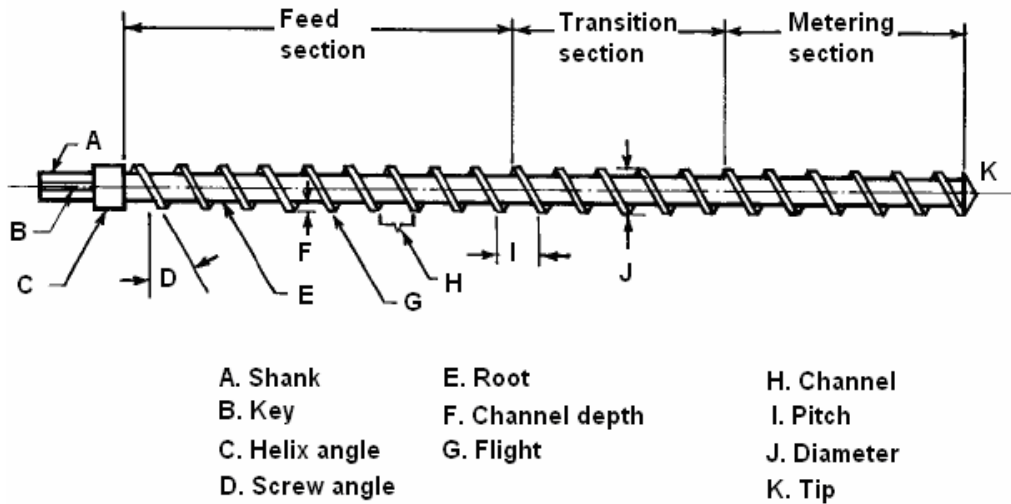


**Figure 2.15** Parts of a single screw extruder [141]

Various modifications of the single screw design are possible. Multiscrew extruders are also widely used for specialized applications for which the single screw designs are inefficient. Screw configuration for multiscrew extruders may involve intermeshing, corotating, or counter rotating screws (Figure 2.16) [141]. Most twin screw extruders perform the same elementary polymer processing steps as single screw extruders. However, the unique time varying screw to screw interactions that take place in them particularly affect the elementary steps of melting and mixing inside the extruder. The twin-screw extruders have important advantages over single screw extruders, which enable them to carry out the melting and mixing steps more efficiently and uniformly owing to the additional mechanisms mentioned above [143].

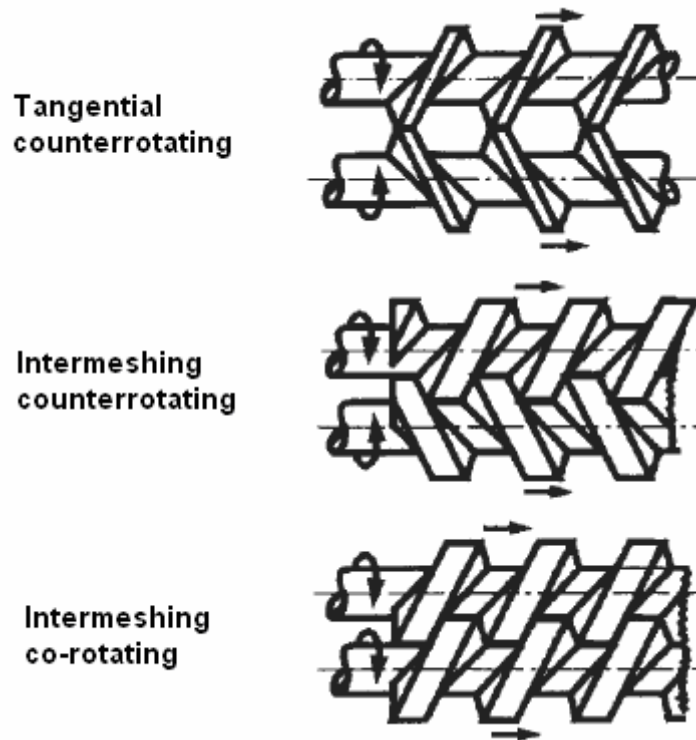


**Figure 2.16** Classification of twin screw extruders [143]

### 2.1.5.2 Injection Molding

Injection molding is the predominant process for the production of thermoplastics in the finished forms. It is used for making complex plastic parts at very high production rates. It is an automated process and usually has a process cycle time of 20 to 60 s [1]. Injection molding consists of three steps, firstly the polymer pellets are heated until it melts. After this, the melt is injected into mold and held cooled under pressure until the polymer melt solidifies. Finally, the mold opens and the product is ejected (Figure 2.17). High quality and cost-effective parts can be obtained if these functions are performed automatically under suitable conditions. Injection pressure, back-pressure, melt temperature, mold temperature, and shot size are the process variables, which affect the quality of injection molded parts. Injection molding machines have injection and the clamp units to perform the cyclical steps during the injection molding process [141].

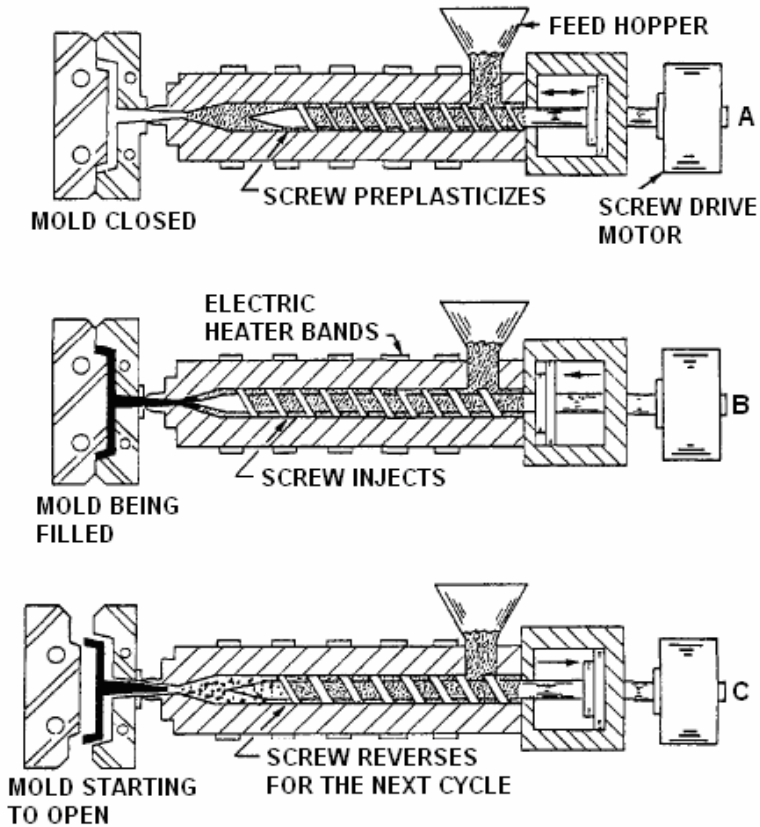


**Figure 2.17** Sequence of operations for a reciprocating screw machine [144]

The pressure change during the injection molding cycle can be shown graphically as in Figure 2.18. The pressure ( $P$ ) increases at a relatively slow rate during the filling stage. During the packing stage shrinkage is decreased by maintaining a high pressure. Finally, the pressure in the mold relaxes during the cooling stage [145]. In most cases, approximately 50% of the process cycle time is taken by the cooling time for the part. The cooling time depends on the size and shape of the part, wall thickness, and temperature settings on the machine [1].

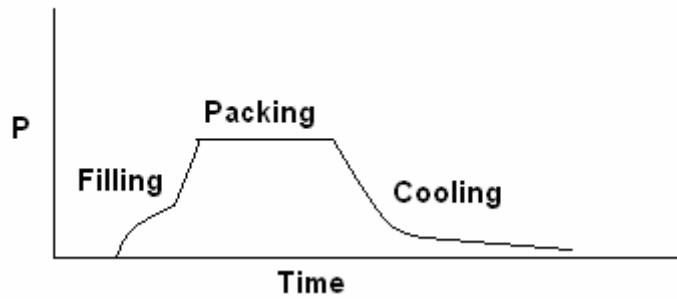


**Figure 2.18** Pressure change during the injection molding cycle [145]

### 2.1.5.3 Compression Molding

Compression molding is the least expensive and simplest of all polymer processing operations [125]. The compression molding machine is based on a hydraulic press providing the pressure, and a heated mold which is made of two parts [142]. During the compression molding process, first the polymer resin is placed in the bottom half of the preheated mold and the top half of the mold is placed over the bottom half. Next, the pressure is applied to cause the molten polymer to completely fill the mold cavity while the excess resin is forced out of the mold (Figure 2.19) [125]. After an appropriate time, the mold is opened and the part is ejected while still hot and allowed to cool outside (for fast cooling quenching can be applied) [141]. Material flow and the final properties of the molded part depend on the mold temperature, pressure applied during the molding and cooling, so they must be adequately controlled.

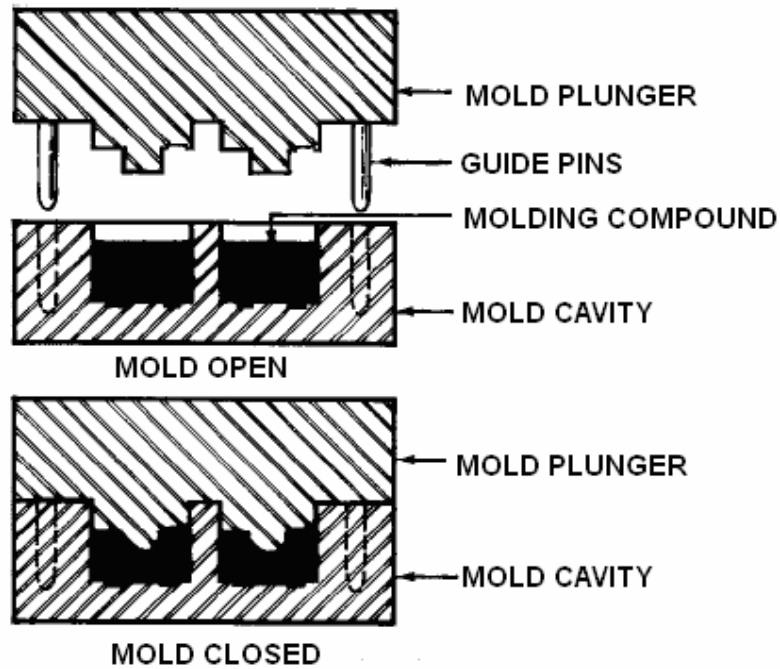


**Figure 2.19** Schematic of a compression molding operation [141]

#### 2.1.5.4 Solvent Assisted Ultrasonication

Carbon nanotubes are very cohesive materials owing to the van der Waals interactions between the carbon atoms in their structure. It is difficult to disperse them in the liquids, such as water, organic solvents or polymeric resins due to the strong agglomeration tendency of the carbon nanotubes. Carbon nanotubes can be utilized to their maximum potential in their applications by applying a simple, reliable and scalable process for deagglomeration of carbon nanotubes. Ultrasonication can be an effective method to obtain discrete and single dispersed carbon nanotubes in the liquid materials. For liquids, which have viscosity up to 100,000 cP, ultrasonication can be used for dispersing the carbon nanotubes, since bonding forces between the carbon nanotubes can be overcome by the liquid jet streams resulting from ultrasonic cavitations [146, 147].

Solvent assisted ultrasonication technique for dispersing carbon nanotubes in epoxy resin consists of three main steps. Firstly, epoxy resin and carbon

nanotubes are dissolved in a solvent and premixed by a standard stirrer. Next, high energy ultrasonication is applied to this mixture until it homogenizes and a well dispersed carbon nanotube based suspension is obtained. Finally, solvent is evaporated from the suspension by applying proper amount of heat. Resulting epoxy/carbon nanotube mixture can be used for further applications.

#### 2.1.5.5 Hand Lay-up

Hand lay-up is a widely used processing method for fiber reinforced materials. The major advantage of this method is that it is a very simple process so that ordinary equipment is needed and the molds may be made from plastics, wood or metal sheets [148]. In this process, liquid resin is applied to the mold after spraying the release agent on the mold surface and then reinforcement is placed on top. A roller is used to impregnate the fiber with the resin. The roller compresses the fibers and removes the air bubbles trapped in the resin [149]. After this, another resin and reinforcement layer is applied until a suitable thickness builds up. Curing takes place at room temperature generally but heat is sometimes applied to accelerate it.

The process is very flexible, so that it allows the user to optimize the part by placing different types of fabric and mat materials. However, quality of the composite is highly dependent on operator skills and the quality control in the hand lay-up process is relatively difficult [1]. Hand lay-up techniques can be classified as basic, vacuum bag and pressure bag molding (Figure 2.20). In the vacuum bag molding a flexible bag is placed over the lay-up and the vacuum is applied between the molding and the bag. The vacuum bag sucks the composite constituents and it squeezes the air bubbles, excess resin from the composite. In the pressure bag molding process, a similar principle is applied except that pressure is applied on the bag [148].

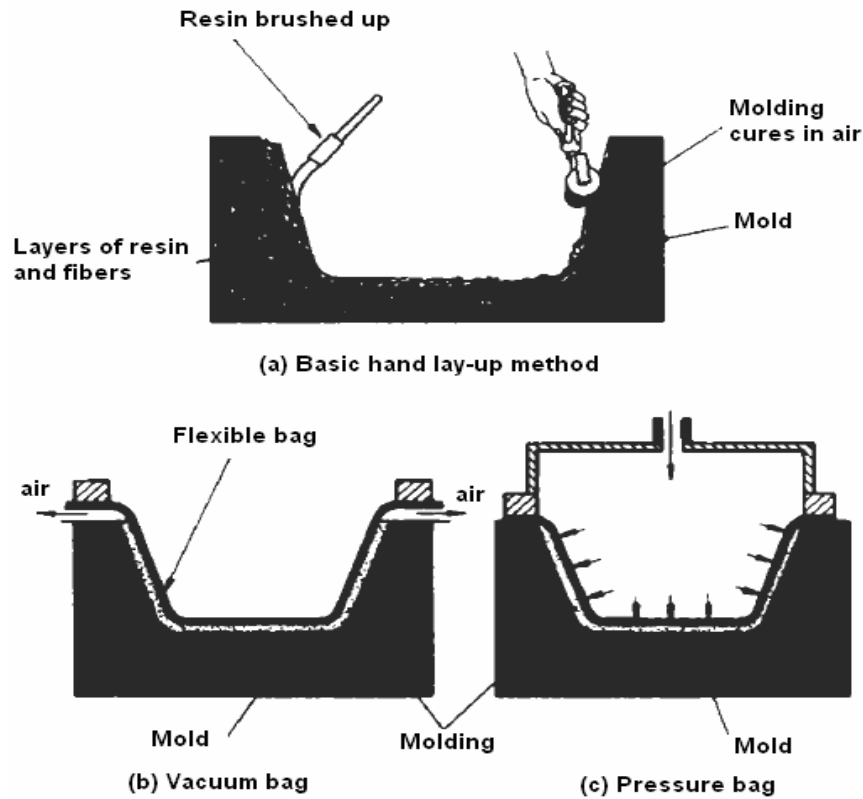


**Figure 2.20** Hand lay-up techniques [148]

### 2.1.6 Surface Treatment of Carbon Nanotubes

There has been an extensive research on carbon nanotubes since their discovery by Iijima in 1991, because of their unique structure, mechanical and electrical properties [60]. Conductive polymer composites containing carbon nanotube exhibit high electrical conductivity and improved mechanical properties at lower filler contents [84]. However, carbon nanotubes are chemically inert, due to the low amount of defects sites and functional chemical groups on their surfaces. The use of carbon nanotubes in the conductive polymer composites might have some disadvantages due to poor dispersion capability and weak interfacial interactions. These can lower the mechanical and electrical properties of the composites in some cases. Therefore, activating and modifying the carbon nanotube surface before composite preparation is an essential procedure [13]. Dispersion capability of carbon nanotubes and the interfacial adhesion between carbon nanotubes and

matrix polymers can be improved by increasing the reactivity of carbon nanotubes. This can be achieved by increasing the number of defect sites and functional groups on carbon nanotube surface [32]. Any change in the surface chemistry of carbon nanotube might alter the final properties of the carbon nanotube based composites [27, 33].

Carbon nanotubes are assembled as ropes or bundles, and there are some catalyst residuals, bucky onions, spheroidal fullerenes, amorphous carbon, polyhedron graphite nano-particles, and other forms of impurities in as grown carbon nanotubes. Thus, purification treatments are needed before chemical functionalization of carbon nanotubes [43]. General procedure for the carbon nanotube surface treatment consists of two steps. These steps can be identified as purification (oxidation) and chemical treatment procedures (Figure 2.21).

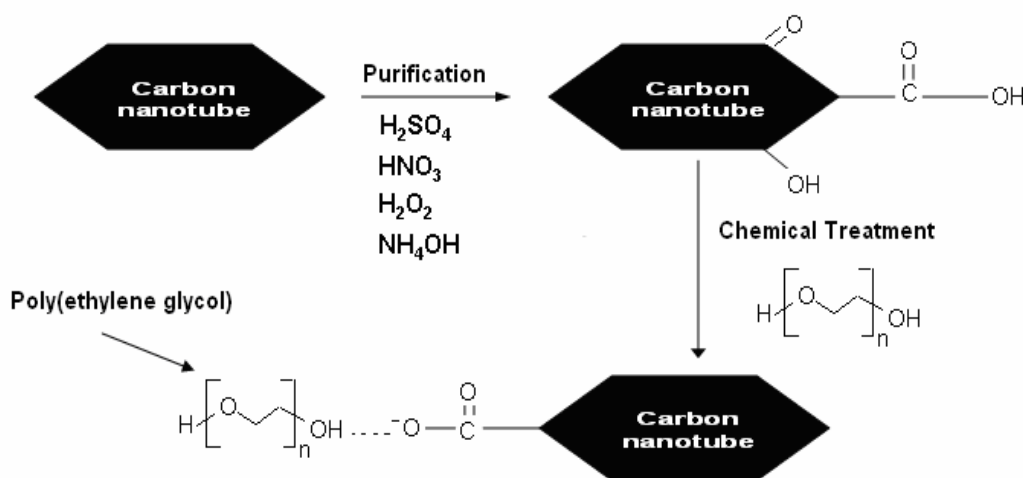


**Figure 2.21** General procedure for carbon nanotube surface treatment

Carboxyl, hydroxyl and quinone groups on the carbon nanotube outer walls can be produced with covalent modification of carbon nanotubes by using oxidizing acid or base mixtures. These functional groups can be attached to various chemicals through different interactions, such as esterification, amidation, or acid–base

chemistry. Noncovalent modification involves the use of surfactants or low molecular weight polymer wrapping on the carbon nanotube surface. Although noncovalent modification does not cause damage to the walls of the carbon nanotubes or alter their properties, the interactive forces between the carbon nanotubes and surrounding molecules are relatively weak when compared to the covalent modification [150]. Surface treatment can also improve the solubility of the carbon nanotubes in certain organic solvents and water.

#### 2.1.6.1 Purification of Carbon Nanotubes

Carbon nanotube derivization can be achieved by the formation of carboxyl and hydroxyl groups on the carbon nanotube surface as a result of acid and base purification procedures which also remove the metallic catalyst as well as amorphous, microcrystalline carbon produced as an impurity during carbon nanotube synthesis [129]. General purification procedures of carbon nanotubes are categorized as controlled oxidation, chemical treatment and filtration methods. Carbon nanotube purification with acid and base mixtures is generally performed by using nitric acid ( $\text{HNO}_3$ ), sulfuric acid ( $\text{H}_2\text{SO}_4$ ), hydrochloric acid ( $\text{HCl}$ ), potassium hydroxide ( $\text{KOH}$ ), hydrogen peroxide ( $\text{H}_2\text{O}_2$ ) and ammonium hydroxide ( $\text{NH}_4\text{OH}$ ).

The chemical oxidation during the purification of carbon nanotubes consist of two main steps. The oxidants attack the graphene structure by electrophilic reactions and generate active sites such as hydroxyl and quinone during the defect generating step. The success of this step depends on the oxidant's ability to generate hydroxyl groups and to transform them into carboxyl groups. During the defect consuming step, the graphene structure of the tube can be destroyed by the oxidation of the generated active sites in defect generating step. The defect consuming step mostly counts on the ability of the oxidant to etch and destroy the graphite like structure around already generated carboxyl and their neighborhood groups [151]. The second step can affect the intrinsic electronic and mechanical properties of the carbon nanotubes. So, purification medium, duration, conditions and method should be optimized accordingly, in order to perform the impurity

removal and surface oxidation of carbon nanotubes without causing severe damages on the graphitic wall structure of carbon nanotubes.

The electrical and mechanical properties of polymer/carbon nanotube composites have been also shown to be affected by various conditions of carbon nanotube purification. The electrical resistivity of carbon nanotube filled composites increases by ascending the carbon nanotube polarity due to the presence of hydroxyl and carboxyl groups introduced by chemical treatment. Moreover the conductivity of composites decreases as time and temperature of carbon nanotube oxidation in acid mixtures increase. The reinforcement ability of carbon nanotubes increases in polymer composites when they are treated in acidic mixtures [152]. On the other hand, there is very little information on the structural alteration of carbon nanotubes under basic oxidative treatments. It is shown that, for the composites prepared by using carbon nanotubes treated with basic mixtures, electrical conductivity enhances due to the minor damages of the carbon nanotubes graphitic sidewalls [153].

#### 2.1.6.2 Surface Treatment of Carbon Nanotubes with Low Molecular Weight Chemicals

Chemical treatment of the carbon nanotube surfaces can be performed with low molecular weight chemicals through noncovalent and covalent attachment of the materials to the carbon nanotube surface (Figure 2.22). Silane coupling agents [33], functional amines [10, 42], vinyl monomers [43], polymeric and oligomeric materials [44, 46] are the most widely used chemicals for the surface treatment of the carbon nanotubes. Among the various approaches of the covalent surface modification, esterification or amidation of oxidized carbon nanotubes and side wall covalent attachment of functional groups approaches are generally applied [57]. Noncovalent attachment is based mainly on van der Waals forces, and is controlled by thermodynamic criteria. The noncovalent attachment for some polymer chains and surfactants is called as wrapping [66].

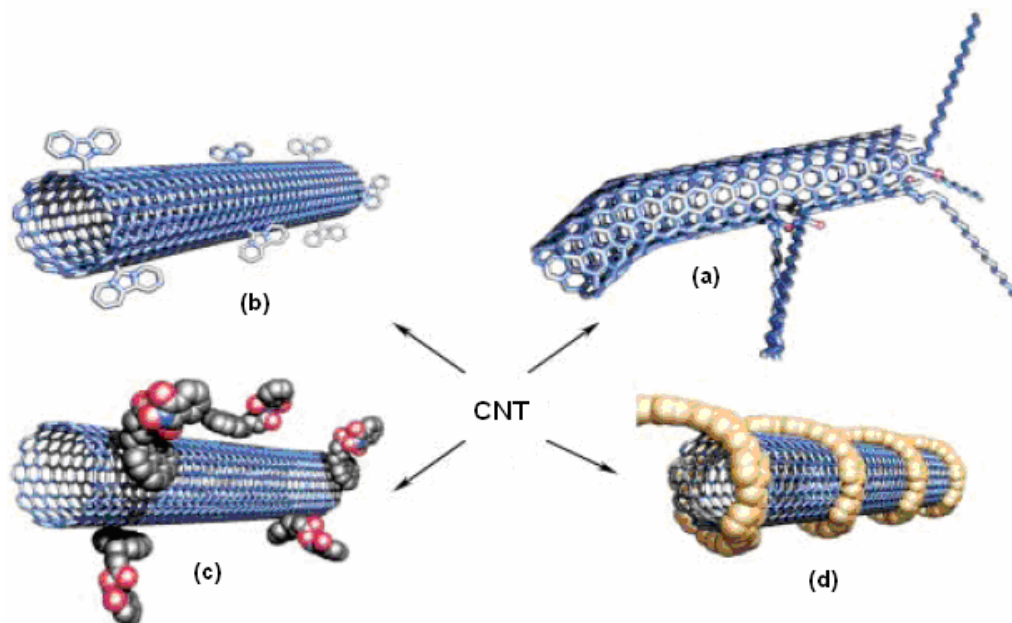


**Figure 2.22** Functionalization possibilities for carbon nanotubes: (a) oxidized carbon nanotube functionalization, (b) covalent sidewall functionalization, (c) noncovalent functionalization with surfactants, (d) noncovalent functionalization with polymers [154]

During the covalent attachment of the modifiers on the oxidized carbon nanotubes, the carboxyl groups on the carbon nanotube surface can react with the reactive groups of the modifier. Ester or amide linkages can be formed between the carbon nanotube surface and modifier (Figure 2.23). In the side wall covalent attachment, the surface modifiers can directly form covalent bonds with the defect sites (dangling bonds) of the carbon nanotube surface.

In this dissertation poly(ethylene glycol) (PEG) with different molecular weights, diglycidyl ether of Bisphenol A (DGEBA) and hexamethylene diamine (HMDA) were used for the surface treatment of carbon nanotubes.

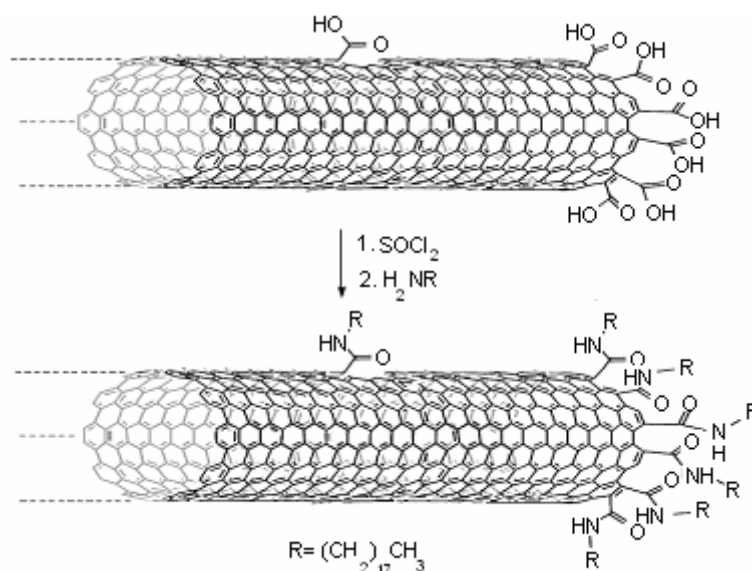


**Figure 2.23** Amidation of oxidized carbon nanotube surface [154]

#### 2.1.6.2.1 Poly(ethylene glycol) (PEG)

Poly(ethylene glycol) (PEG) (Figure 2.24) is synthesized by the condensation polymerization of ethylene oxide and water. Its general formula is  $\text{H}(\text{OCH}_2\text{CH}_2)_n\text{OH}$ , where  $n$  is the average number of repeating oxyethylene groups which ranges typically from 4 to about 180. It is also known as poly(ethylene oxide) (PEO) or polyoxyethylene (POE). PEG can be in liquid or solid form at the room temperature according to their molecular weights. PEG is soluble in water, methanol, benzene, dichloromethane. They can be coupled to hydrophobic molecules to produce nonionic surfactants. PEG is non-toxic, odorless, neutral, lubricating, nonvolatile and nonirritating. They are used to make emulsifying agents and detergents, and as plasticizers, humectants, and water-soluble textile lubricants [155].

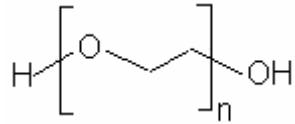


**Figure 2.24** Chemical structure of poly(ethylene glycol)

#### 2.1.6.2.2 Diglycidyl ether of Bisphenol A (DGEBA)

Diglycidyl ether of Bisphenol A (DGEBA) (Figure 2.25) is the primary chemical building block for the broad spectrum of materials referred to generally as epoxy resins. It can be synthesized through the reaction between bisphenol A and epichlorohydrin. Low molecular weight DGEBA resins are liquids and higher molecular weight resins are more viscous liquids or solids. DGEBA is a colorless liquid with a low flash point which is insoluble in water. It has a low vapor pressure and mild odor. The epoxide groups in the structure of DGEBA are very reactive with various chemical groups which enhance its use as adhesive and matrix material in composite structures [125, 127].

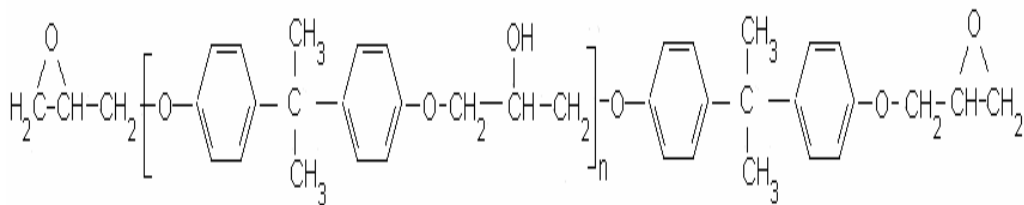


**Figure 2.25** Chemical structure of diglycidyl ether of Bisphenol A [70]

### 2.1.6.2.3 Hexamethylene diamine (HMDA)

Hexamethylene diamine (HMDA) (Figure 2.26) is synthesized by the hydrogenation of adiponitrile. Its molecular formula is  $\text{H}_2\text{N}(\text{CH}_2)_6\text{NH}_2$  which is a hexamethylene hydrocarbon chain terminated by the amine functional groups. It is a colorless solid with a strong amine odor. HMDA is generally used for the production of polymers (especially nylon66), due to its bifunctional structure [156].

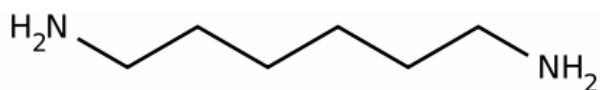


**Figure 2.26** Chemical structure of hexamethylene diamine

### 2.1.6.3 Surface Treatment of Carbon Nanotubes with Surfactants

Surfactants are generally defined as wetting agents which lower the surface tension of a liquid or decrease the interfacial tension between two liquids. A surfactant is characterized by its tendency to adsorb at surfaces or interfaces. They can adsorb on solid–vapor, solid–liquid, solid–solid, liquid–vapor and liquid–liquid interfaces. Surfactant molecules consist of at least two hydrophilic and hydrophobic parts. The hydrophilic part is referred as head group and hydrophobic part as the tail (Figure 2.27). The hydrophobic part of the surfactant may be branched or linear. The hydrophilic head group is usually attached to the end of the alkyl chain. The degree of chain branching, the position of the polar group and the length of the chain are the parameters that affect the properties of the surfactants [157].

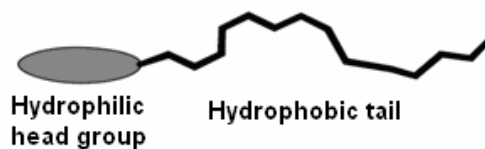


**Figure 2.27** Schematic illustration of a surfactant [157]

Surfactant treatment has two main functions in the carbon nanotube filled polymer composites. It lowers the surface tension of the carbon nanotubes which prevents the formation of aggregates and improves the wettability of carbon nanotubes by polymer with the aid of functional groups or miscible parts on the long tail. Moreover, carbon nanotubes might overcome van der Waals attractions by electrostatic or steric repulsive forces promoted by surfactants [65]. Surfactant selection for composite preparation depends on four basic criteria: a) head group charge of the surfactant, b) head group size of the surfactant (small head group size is preferred mostly for better interaction), c) alkyl chain length of surfactant (longer alkyl chain lengths improve carbon nanotube coverage since surfactant molecules are present along the length of the carbon nanotube) and d) presence of benzene ring in the surfactant structure (pi like stacking of the benzene rings onto the surface of graphite is believed to improve the coverage of the carbon nanotube surface by surfactant) [65].

Surfactants can be classified according to their head group charges. The polar head groups of the surfactants may be ionic and nonionic. Moreover, the ionic head groups can be anionic and cationic. Different types of surfactants act on the carbon nanotube surface in distinct ways. In ionic surfactants, generally hydrophobic tails (alkyl tails) adsorb on the carbon nanotube surface and hydrophilic heads create the electrostatic repulsions between similar groups of the other surfactant molecules and this overcome the van der Waals interactions between carbon nanotubes. In nonionic surfactants, head groups tend to be located on the carbon nanotube surface, affording a similar nature to the carbon nanotubes and the polymer matrix. This should lower the attractive potential between the nanofiller particles [63–67].

The critical micelle concentration (CMC) is defined as the concentration of surfactants above which micelles are spontaneously formed (Figure 2.28). Surfactant molecules normally orient the hydrophobic groups to the surface when a surfactant adsorbs at hydrophobic surface, and the hydrophilic (polar) groups are exposed to the water. Therefore, the micelles are polar aggregates with water solubility since as they form in the water the hydrophobic groups directed to the interior of the cluster and polar head groups orient toward the water [157]. To improve the carbon nanotube dispersion, surfactants should be added in amounts exceeding their critical micelle concentration [67]. At low surfactant concentrations the amount may be low to produce efficient coating and induce electrostatic repulsion. However, surfactant concentration should not exceed critical micelle concentration too much since large micelle aggregates can not interact efficiently with carbon nanotube bundles (depletion attraction).

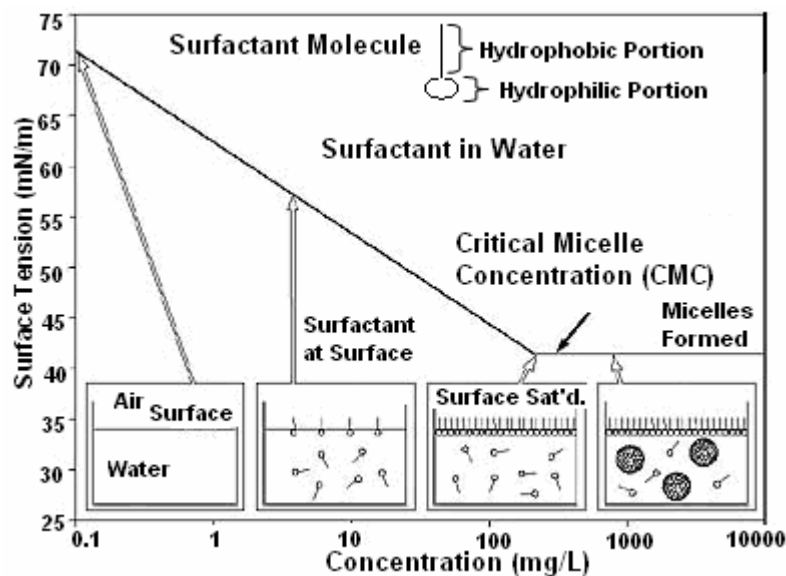


**Figure 2.28** Schematic illustration of critical micelle concentration

In this dissertation, three types of surfactants were used during the carbon nanotube surface treatment studies (Figure 2.29). During the preparation of the PET/CNT composites sodium dodecyl sulfate (anionic) (SDS) was used as a

surface modifier. Moreover, cetyl pyridinium chloride (cationic) (CPC) and 4-octylphenol polyethoxylate (nonionic) (Triton X-100) surfactants were used for improving the carbon nanotube dispersion in epoxy/carbon nanotube mixtures.

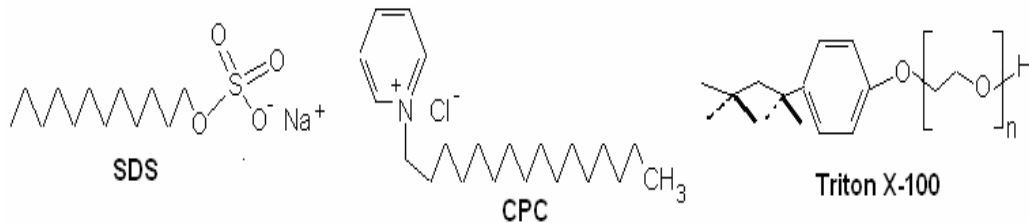


**Figure 2.29** Chemical structures of the surfactants used in this study

### 2.1.7 Surface Energy Measurements of Composite Constituents

Surface treatment of carbon nanotubes alters the surface structure which can be noticed from the changes in the surface energy components of the particles. Moreover, when carbon nanotube particles are mixed with an immiscible polymer blend; it can be dispersed in one of the polymer phases or at the interface between the polymers. Surface energies of the polymers and conductive filler; mainly determine the location of the conductive filler in the composite.

The surface energy components of the carbon nanotube and the matrix polymers at the room temperature can be determined by measuring the contact angles of the certain probe liquids on the samples of the filler and polymers [158, 159].

The dispersive ( $\gamma_{\text{Solid}}^{\text{d}}$ ), acidic ( $\gamma_{\text{Solid}}^{\text{A}}$ ) and basic ( $\gamma_{\text{Solid}}^{\text{B}}$ ) components of the total surface energy can be calculated with ‘Young Equation’ (Equation 2.3), by using contact angles of probe liquids measured on the sample surfaces [158]:

$$(1 + \cos \theta_{\text{Liquid}}) \gamma_{\text{Liquid}} = 2[(\gamma_{\text{Liquid}}^{\text{d}} \gamma_{\text{Solid}}^{\text{d}})^{1/2} + (\gamma_{\text{Liquid}}^{\text{A}} \gamma_{\text{Solid}}^{\text{B}})^{1/2} + (\gamma_{\text{Liquid}}^{\text{B}} \gamma_{\text{Solid}}^{\text{A}})^{1/2}] \quad (2.3)$$

in which  $\theta_{\text{Liquid}}$  is the contact angle values of the probe liquid,  $\gamma_{\text{Liquid}}$  is the total surface energy of the probe liquid,  $\gamma_{\text{Liquid}}^{\text{d}}$  is the dispersive component of the probe liquid surface energy,  $\gamma_{\text{Liquid}}^{\text{A}}$  is the acidic component of the probe liquid surface energy and  $\gamma_{\text{Liquid}}^{\text{B}}$  is the basic component of the probe liquid surface energy. Polar component of the surface energy ( $\gamma_{\text{Solid}}^{\text{P}}$ ) consists of electron acceptor ( $\gamma_{\text{Solid}}^{\text{A}}$ ) and electron donor components ( $\gamma_{\text{Solid}}^{\text{B}}$ ).

$$\gamma_{\text{Solid}}^{\text{P}} = 2(\gamma_{\text{Solid}}^{\text{A}}\gamma_{\text{Solid}}^{\text{B}})^{1/2} \quad (2.4)$$

Moreover, the total surface energy,  $\gamma_{\text{Solid}}$ , can be calculated by using dispersive ( $\gamma_{\text{Solid}}^{\text{d}}$ ), and polar components ( $\gamma_{\text{Solid}}^{\text{P}}$ ).

$$\gamma_{\text{Solid}} = \gamma_{\text{Solid}}^{\text{d}} + \gamma_{\text{Solid}}^{\text{P}} \quad (2.5)$$

#### 2.1.7.1 Interfacial Strength, Work of Adhesion and Selective Localization of Carbon Nanotube

The interfacial tensions between two composite constituents ( $\gamma_{1-2}$ ) can be determined by using the surface energy components of the materials from general equation with harmonic mean:

$$\gamma_{1-2} = \gamma_1 + \gamma_2 - 4\left[\left(\frac{\gamma_1^{\text{d}}\gamma_2^{\text{d}}}{\gamma_1^{\text{d}} + \gamma_2^{\text{d}}}\right) + \left(\frac{\gamma_1^{\text{P}}\gamma_2^{\text{P}}}{\gamma_1^{\text{P}} + \gamma_2^{\text{P}}}\right)\right] \quad (2.6)$$

where  $\gamma_i$  is total surface energy,  $\gamma_i^{\text{d}}$  is the dispersive component of the total surface energy;  $\gamma_i^{\text{P}}$  is the polar component of the surface energy.

Surface energies of the polymers and carbon nanotube determine the location of the filler in the polymer composite. Generally, the lower interfacial tension between the polymer and carbon nanotube makes the adsorption of the filler by the polymer easier. Sumita et al. proposed that the selective localization of the filler in a polymer blend can be estimated by the wetting coefficient ( $w$ ), which is defined by the following equation [160];

$$w = (\gamma_{f-B} - \gamma_{f-A}) / \gamma_{A-B} \quad (2.7)$$

where  $\gamma_{f-A}$  is the interfacial tension between the polymer A and filler,  $\gamma_{f-B}$  is the interfacial tension between the polymer B and filler and  $\gamma_{A-B}$  is the interfacial tension between two polymers. If  $w$  is greater than 1, the filler particles locate within polymer A. If  $w$  is less than -1, the filler particles locate within polymer B. Otherwise the filler particles distribute at the interface [160].

Work of adhesion ( $W_a$ ) values between matrix polymers (1) and carbon nanotubes (2) can be calculated for the composites from the following equation by using the surface energy components of the materials [158];

$$W_a = 2[(\gamma_1^d \gamma_2^d)^{1/2} + (\gamma_1^A \gamma_2^B)^{1/2} + (\gamma_1^B \gamma_2^A)^{1/2}] \quad (2.8)$$

where  $\gamma_i^d$  is the dispersive component of the total surface energy,  $\gamma_i^A$  is the acidic component of the total surface energy and  $\gamma_i^B$  is the basic component of the total surface energy.

## 2.2 Experimental Techniques for Material Characterization

In this dissertation, conductive polymer composite and carbon nanotube samples were characterized in terms of various electrical, mechanical, thermal, spectroscopic and thermal characterization methods.

### 2.2.1 Electrical Conductivity Measurements of Composites

Electrical measurements on semiconductors are routinely performed for the analyses of wide range of semiconductor properties. These routine methods for the electrical characterization of semiconductors can be related to the measurements of the electrical resistivity, carrier mobility and carrier type. One of the most important characteristics of a semiconductor material is its electrical resistivity and

it can be measured by applying four point probe, two point probe (spreading resistance) and Hall – Van der Pauw methods [161].

The four point probe technique (Figure 2.30) is the most common technique for the measurements of semiconductor material resistivity and sheet resistance. It is an absolute measurement and it is sometimes used to provide standards for the other resistivity measurements [162, 163].

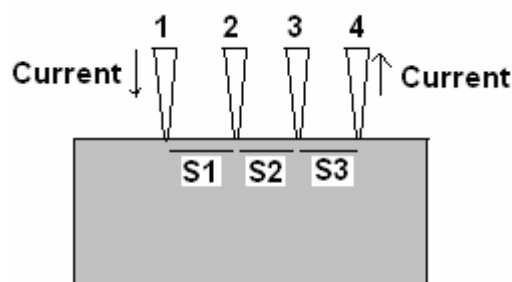


**Figure 2.30** Collinear four point probe showing current flow and voltage measurement [162]

The volume resistivity  $\rho$  is given by the relationship (Equation 2.9) [162] when the probe spacings are equal to each other ( $S1 = S2 = S3 = S$ ).

$$\rho = (2\pi SF) \times (V / I) \quad (2.9)$$

where,  $F$  is the correction factor which depends on the sample geometry,  $V$  is the voltage drop and  $I$  is the current.

Two point probe technique (Figure 2.31) is easier to conduct since two probes need to be manipulated. However, the interpretation of the measured data is harder when compared to the four point probe technique [163]. The total resistance  $R_T$  is given by Equation 2.10;

$$R_T = V/I = 2R_w + 2R_c + 2R_{mat} \quad (2.10)$$

where,  $R_w$  is the wire and probe resistances,  $R_c$  is the contact resistances between the probes and the material and  $R_{mat}$  is the resistance of the material. The spreading resistance ( $R_{sp}$ ), which results from the current transportation between the probe and material, also exists during the measurements [162]. The total resistance measured from the two point probe technique is the sum of these resistances. The volume resistivity  $\rho$  with two point probe technique can be calculated from the following relationship;

$$\rho = (V/I) \times (S/L) \quad (2.11)$$

in which  $V$  is the voltage drop,  $I$  is the current,  $L$  is the length and  $S$  is the cross sectional area of the sample.

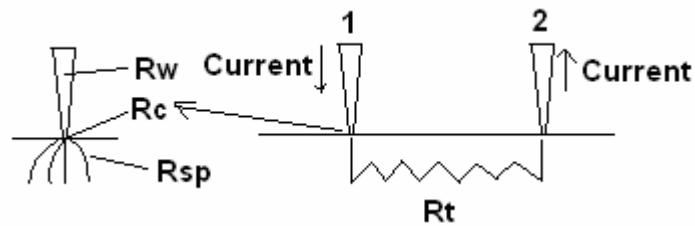


**Figure 2.31** Two point probe arrangement [162]

## 2.2.2 Mechanical Properties of Composites

### 2.2.2.1 Tensile Test

Tensile test measures the force response when a sample is strained at a constant deformation rate. This test provides the characterization of the mechanical

properties of a polymeric material in terms of modulus, strength and elongation to failure. Dogbone shaped specimens (Figure 2.32) are used in the typical tensile testing of polymers and polymer composites [125].

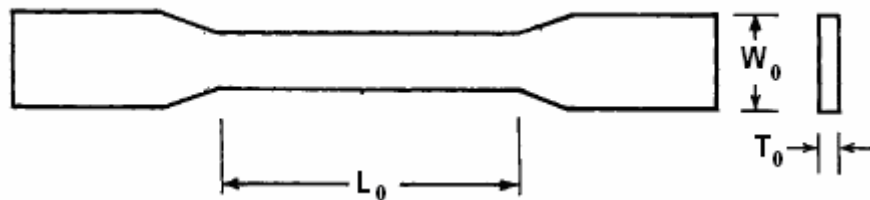


**Figure 2.32** Typical dogbone shaped tensile test specimen; where  $L_0$  is the gauge length,  $W_0$  is the initial width,  $T_0$  is the initial thickness of the specimen [141]

During the tensile testing, one end of the specimen is clamped to the testing machine and pulled at a constant rate of elongation from the other end (Figure 2.33). During a successful test the failure happens at the center of the bar, where the stress is highest, not at the grip sites due to the shape of the tensile specimen which prevents the premature failures during testing [125].

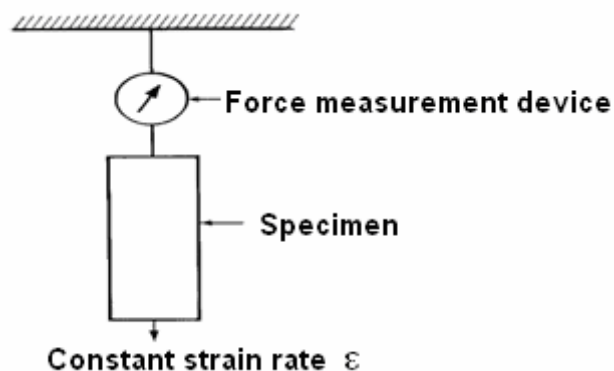


**Figure 2.33** Schematic representation of tensile test [141]

Usually the tensile response is plotted as engineering stress ( $\sigma$ ) versus engineering strain ( $\epsilon$ ) (Figure 2.34). Engineering stress can be calculated from the following relation;

$$\sigma = \frac{F}{A_0} \quad (2.12)$$

where,  $F$  is the force measured during testing and  $A_0$  is the initial cross-sectional area. Engineering strain can be calculated from Equation 2.13;

$$\epsilon = \frac{\Delta L}{L_0} \quad (2.13)$$

where  $\Delta L$  is the change in the sample's gauge length when the sample is exposed to elongation and  $L_0$  is the initial gauge length of the sample. Sample length changes can be determined from tensile testing machine settings or by an extensometer. Poisson's ratio ( $\nu$ ), which is defined as the ratio of the true strain in the transverse direction ( $\epsilon_T$ ), to the true strain in the longitudinal direction ( $\epsilon_L$ ) can also be calculated from the data obtained by the extensometers or strain gauges [125].

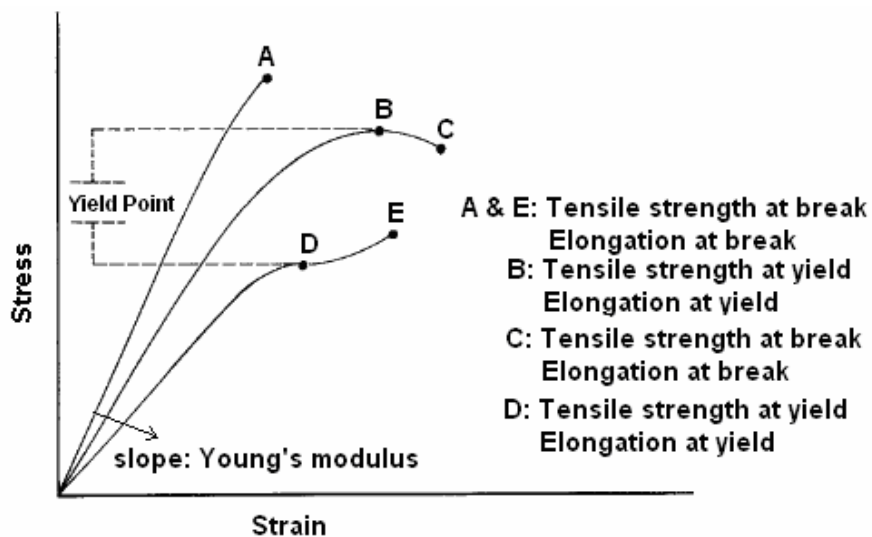


**Figure 2.34** Engineering data from tensile tests [141]

Polymeric materials can be classified as soft and weak, hard and brittle, soft and tough, hard and strong, hard and tough according to their tensile test responses (Figure 2.35). The strength of the material indicates the ability to sustain load. Young's modulus (elastic modulus) is the slope of the initial portion of the stress vs. strain curve and it determines whether the material is soft or hard. Toughness is a measure of the material's ability to absorb energy and undergo extensive plastic deformation without rupturing. It is determined by calculating the area under the stress vs. strain curve [141, 164].

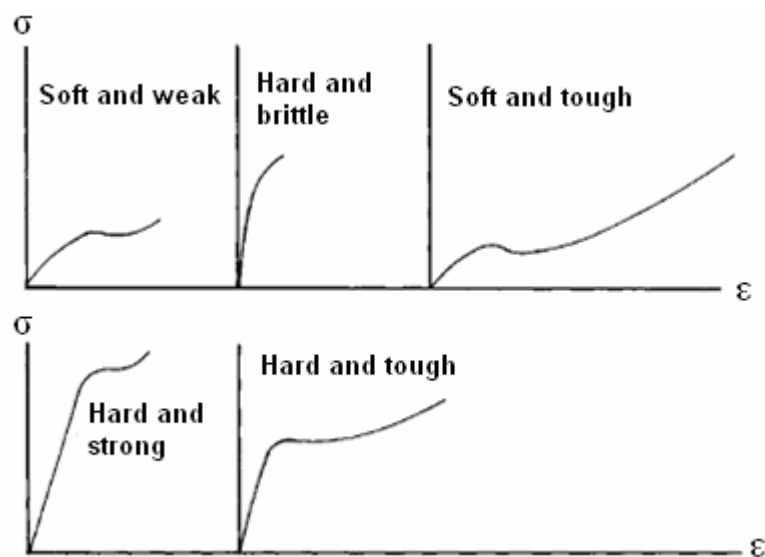


**Figure 2.35** Typical tensile test curves for polymeric materials [141]

### 2.2.2.2 Fatigue Test

Materials frequently fail by fatigue due to the application of cyclic load on them during their service lives. The microscopic cracks around the stress concentrated areas within the material or on the surface are initiated by these cyclic loads. Eventually, these cracks propagate and lead the material to eventual failure [164]. The information from the fatigue tests is very important for the engineering and

composite materials considered for load bearing applications where periodic loading may be encountered [125].

During fatigue tests, the number of applied strain cycles (N) before the complete failure of the specimen is determined at a predetermined stress level. This number of cycles is called as the fatigue life of the material [125]. In the fatigue tests the loading level is hold constant by the testing machine. However, a plastic deformation of the sample, which continues to stay in the body of the samples due to the exposed load cycles during the fatigue tests, occurs and it is called as residual strain (Figure 2.36). The fatigue lives of the materials decrease with increasing frequency of oscillation and decreasing temperature [125].

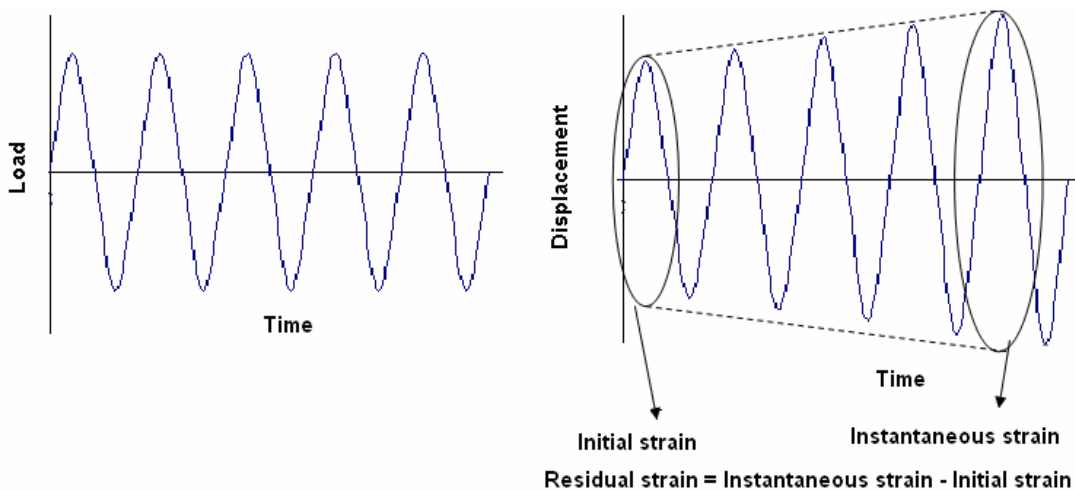


**Figure 2.36** Load and displacement curves during fatigue tests

### 2.2.2.3 Impact Test

Polymers and composites may also fail during their service lives due to the effects of rapid stress loading (impact loads). Materials ability to withstand these loads can be tested with various test methods [141]. Two major types of impact tests are categorized as bending beam and falling weight [164].

Izod and Charpy impact tests are the most common examples of bending beam tests, in which a small bar of polymer is struck with a heavy pendulum (Figure 2.37). During the Izod test the bar is held vertically by gripping one end in a vice and the other free end is struck by the pendulum. In the Charpy test the bar is supported near its ends in a horizontal plane [164]. The required energy to break the sample is determined from the loss in the kinetic energy of the hammer [125].

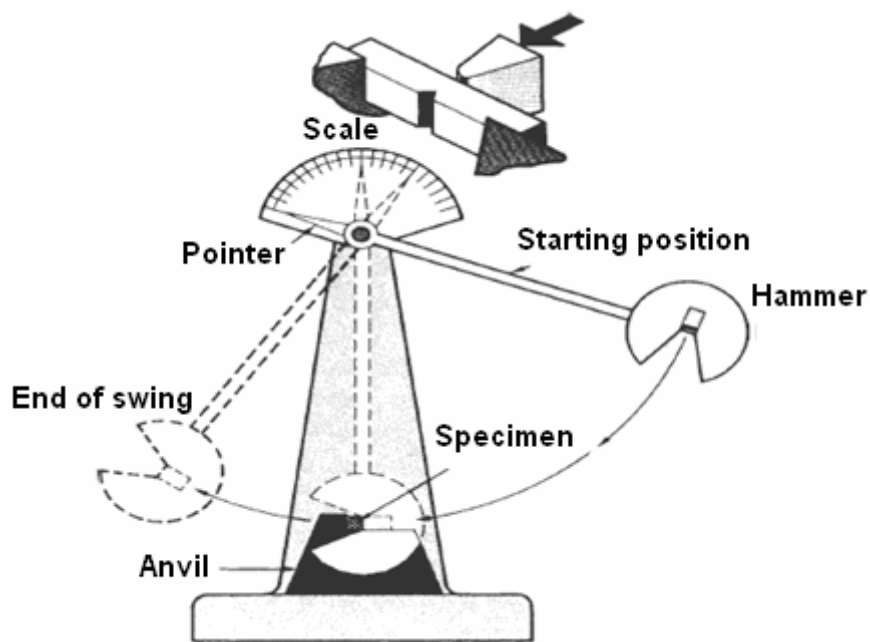


**Figure 2.37** Schematic drawing of the Charpy impact tester [164]

During the falling weight tests (Figure 2.38), a well calibrated weight is released from a known height from the impact specimen and it gains a kinetic energy during its downfall. This kinetic energy transfers into impact energy when the weight hits the specimen's surface. Energy for the failure of the specimen can be calculated from the weight of the falling part and height from which it is dropped [125].

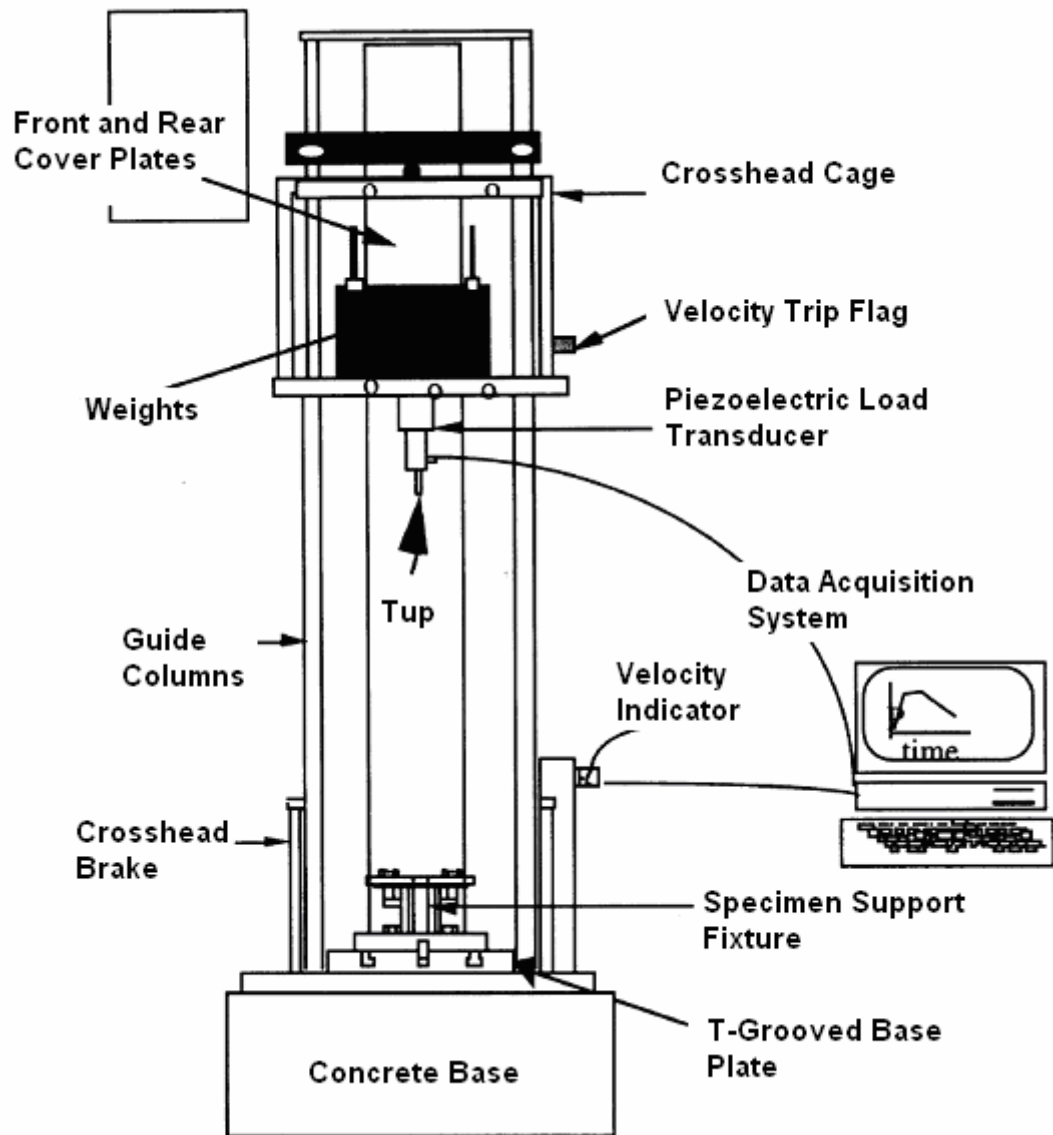


**Figure 2.38** Schematic of the falling weight impact tower [165]

In the falling weight test, most of the impact energy transferred to the specimen is absorbed by the panel, the remaining energy is returned to the drop weight surface and it is called as inelastic returned energy. Majority of the absorbed energy is distributed inside the material irreversibly and damages the panel, rest of the absorbed energy is stored inside the panel elastically (reversibly) [165]. The sum of the absorbed and returned energies is equal to the transferred impact energy (Figure 2.39). These energies can be calculated from the impact energy vs. time

curves of the samples. Inelastic energy curves of the composite panels are constructed by plotting the inelastic return energies with respect to the transferred impact energies and these curves mainly consist of two major regions; elastic–inelastic yield and complete puncture regions (Figure 2.39) [165].

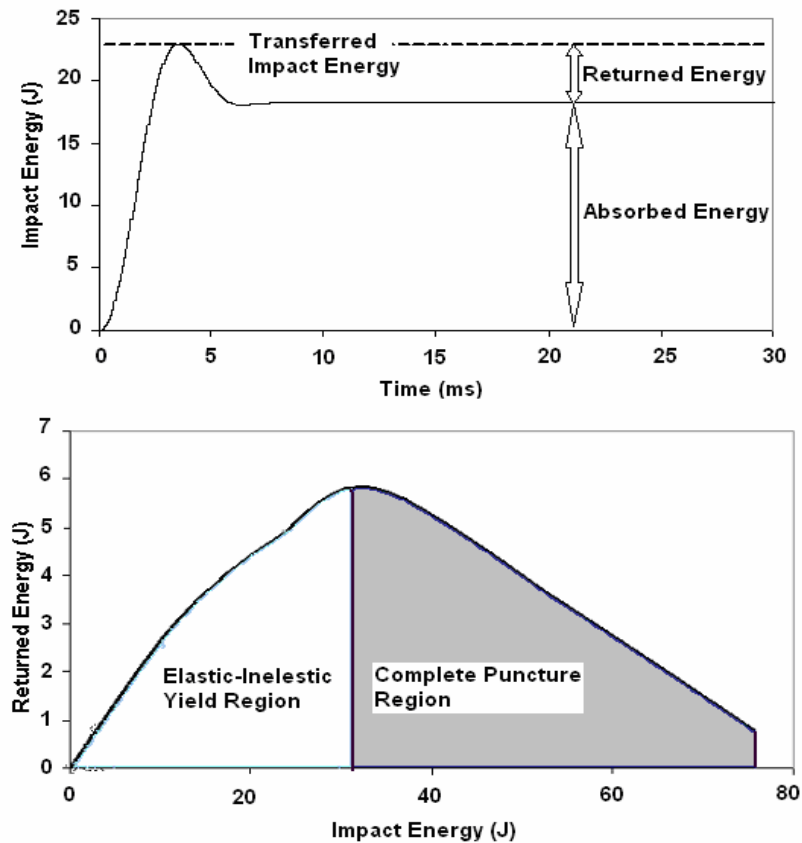


**Figure 2.39** Typical impact energy and inelastic energy curves for the composite materials obtained during falling weight impact test

### 2.2.3 Melt Viscosity Measurements

The pressure flow through a capillary tube may be used to determine the melt viscosity ( $\eta$ ) of a polymer melt as a function of shear rate ( $\dot{\gamma}$ ). This method is called as capillary rheometry and it can be used over the shear rate range from

1 to  $10^5 \text{ s}^{-1}$ . This shear rate range occupies the most polymer processing operations. During the capillary rheometer operation, volumetric flow rate ( $Q$ ) of the polymer melt and the pressure drop ( $\Delta P$ ) through a capillary with known dimensions are measured. In the apparatus, the capillary is attached to a reservoir containing the polymer melt and pressurization of the reservoir forces the polymer melt through the capillary (Figure 2.40) [125].

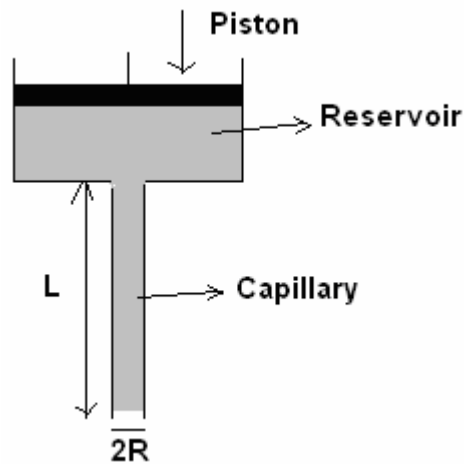


**Figure 2.40** Schematic representation of a capillary viscometer

The shear stress at the capillary wall ( $\tau_w$ ) can be calculated as follows;

$$\tau_w = \frac{R\Delta P}{2L} \quad (2.14)$$

where,  $\Delta P$  is the pressure drop,  $R$  is the radius of the capillary and  $L$  is the length of the capillary.

The apparent shear rate ( $\Phi$ ) can be calculated from the following relationship;

$$\Phi = \frac{4Q}{\pi R^3} \quad (2.15)$$

where,  $Q$  is the volumetric flow rate and  $R$  is the radius of the capillary. The relationship between the shear rate ( $\dot{\gamma}$ ) and the apparent shear rate ( $\Phi$ ) depend on fluid model. For Newtonian fluids  $\dot{\gamma}_w \equiv \Phi$ . For power law fluids, the shear rate at the capillary wall can be calculated from the following relationship;

$$\dot{\gamma}_w = \frac{3n+1}{4n} \Phi \quad (2.16)$$

where,  $n$  is the power law index of the material and  $\Phi$  is the apparent shear rate. The melt viscosity ( $\eta$ ) of the any fluid can be calculated from the ratio of the shear stress at the wall ( $\tau_w$ ) and shear rate at the wall ( $\dot{\gamma}_w$ ) (Equation 2.17).

$$\eta = \frac{\tau_w}{\dot{\gamma}_w} \quad (2.17)$$

It should be noted that, a significant pressure drop might occur at the entrance region of the capillary and the pressure drop profile can not be linear over the entire length of the capillary (Figure 2.41). The experimental data from the rheometer should be corrected for these entrance effects [125].

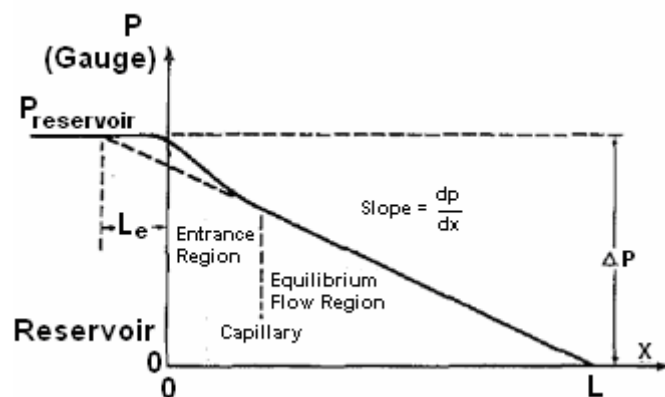


**Figure 2.41** Pressure profile in capillary viscometer [166]

Bagley has suggested that the entrance effects on the shear stress can be corrected by the following relationship;

$$\tau_w^c = \frac{R\Delta P}{2(L + \varepsilon R)} \quad (2.18)$$

where,  $\tau_w^c$  is the corrected shear stress at the wall, R is the capillary radius,  $\Delta P$  is the pressure drop, L is the length of the capillary,  $\varepsilon$  is the empirical parameter, which can be obtained by extrapolating the plot of  $\Delta P$  vs. (L/R) to zero  $\Delta P$  at constant  $\gamma$  for the capillaries with the different lengths [125].

#### 2.2.4 Scanning Electron Microscopy and Optical Microscopy

Scanning electron microscopy (SEM) provides a highly magnified image of the material's surface. The high resolution surface morphology of a polymer composite or blend can be achieved by using SEM. The resolution of the SEM can approach a few nm and it can operate at magnifications that are easily adjusted from about 10X - 300000X. Besides the topographical morphology, the chemical composition on the material surface can be obtained with the help of SEM [167].

In the SEM, a source of electrons is focused (in vacuum) into a fine probe that is rastered over the surface of the specimen (Figure 2.42). A number of interactions occur that can result in the emission of electrons or photons from (or through) the surface during the penetration of the electrons to the material. A reasonable fraction of the electrons emitted can be collected by appropriate detectors, and the output can be used to modulate the image of the material surface [167].

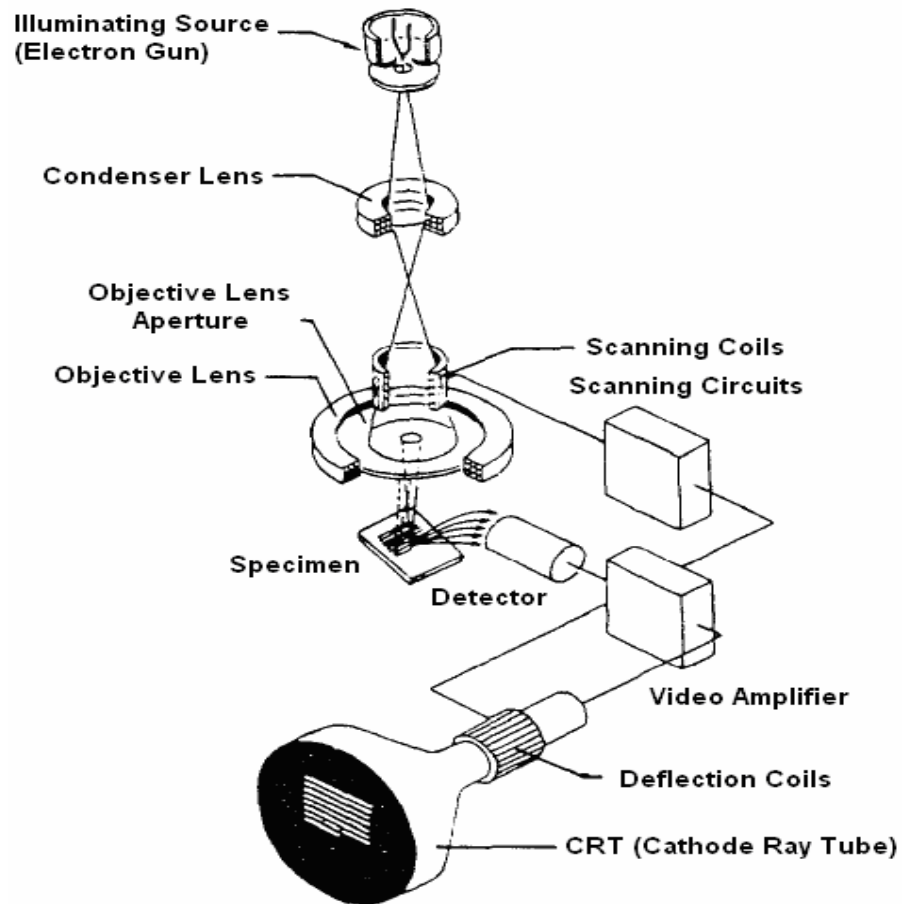


**Figure 2.42** Schematic representation of a SEM [168]

Samples in the SEM can be examined for general morphology, as freeze fractured surfaces or as microtome blocks of solid bulk samples. Solvent etching, which can be used for the polymer blends with the constituents having large solubility difference in a particular solvent,  $\text{OsO}_4$  staining and  $\text{RuO}_4$  staining are the methods to achieve the contrast during analysis. In addition, the SEM can be used to study liquids or temperature sensitive polymers on a cryostage [168].

Optical microscopy (Figure 2.43) is a valuable technique for examining the texture of the materials which are opaque or which can be prepared as thin films by casting on a microscope slide. The examination is performed by the transmitted light [126]. Particulate filled composite materials are usually analyzed with a polarizing microscope set up for transmitted light. This allows one to determine the

shape, size, dispersion state, color, pleochroism, refractive indices, and birefringence [167].

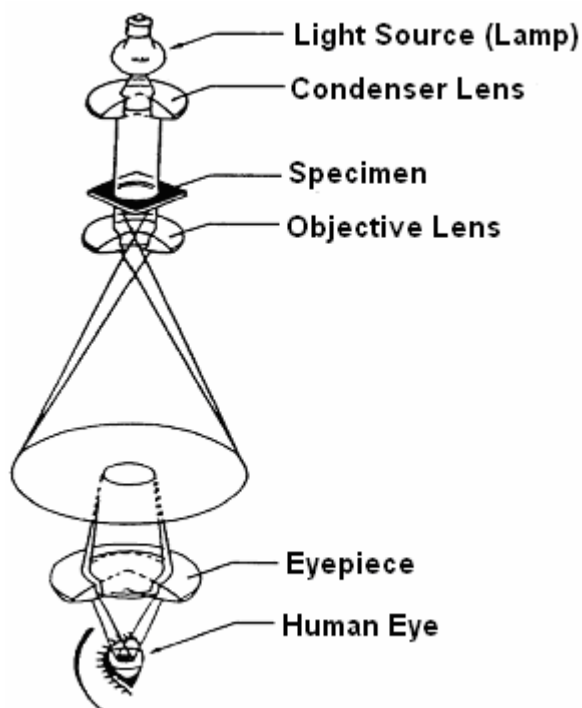


**Figure 2.43** Schematic representation of an optical microscope [168]

### 2.2.5 Differential Scanning Calorimetry Analysis

Differential Scanning Calorimetry (DSC) measures the heat energy per unit mass from a polymer sample, which has a weight of less than 10 mg usually, in a sealed aluminum pan. The samples are referenced to an empty pan in order to maintain a zero temperature differential between them during programmed heating and cooling temperature scans. Transition temperatures of the polymers, such as glass transition temperature ( $T_g$ ), cold crystallization temperature ( $T_c$ ) and melting temperature ( $T_m$ ) can be characterized by this technique (Figure 2.44) [168].  $T_g$  is the temperature at which an amorphous material becomes rigid and below which, it softens.  $T_m$  is the melting temperature at which crystals in a material disintegrate

and liquefy [169]. DSC can also be used for studying the kinetics of chemical reactions, oxidation and decomposition. The measured heat of fusion can be converted to % crystallinity of the polymer phase, if the heat of fusion for the 100 % crystalline polymer is known [168]. Percent crystallinities ( $X_c$ ) of the polymer phases in the composites can be calculated by using the equation below;

$$X_c = [(\Delta H_m - \Delta H_c) / (\Delta H_m^0 w_{poly})] \times 100 \quad (2.19)$$

where  $\Delta H_m^0$  (J/g) is the melting energy of the 100% crystal structure, ( $\Delta H_c$  (J/g) is the cold crystallization energy, ( $\Delta H_m$  (J/g) is the melting energy obtained from the DSC analysis of the sample and  $w_{poly}$  is the fraction of polymer phase in the composite.

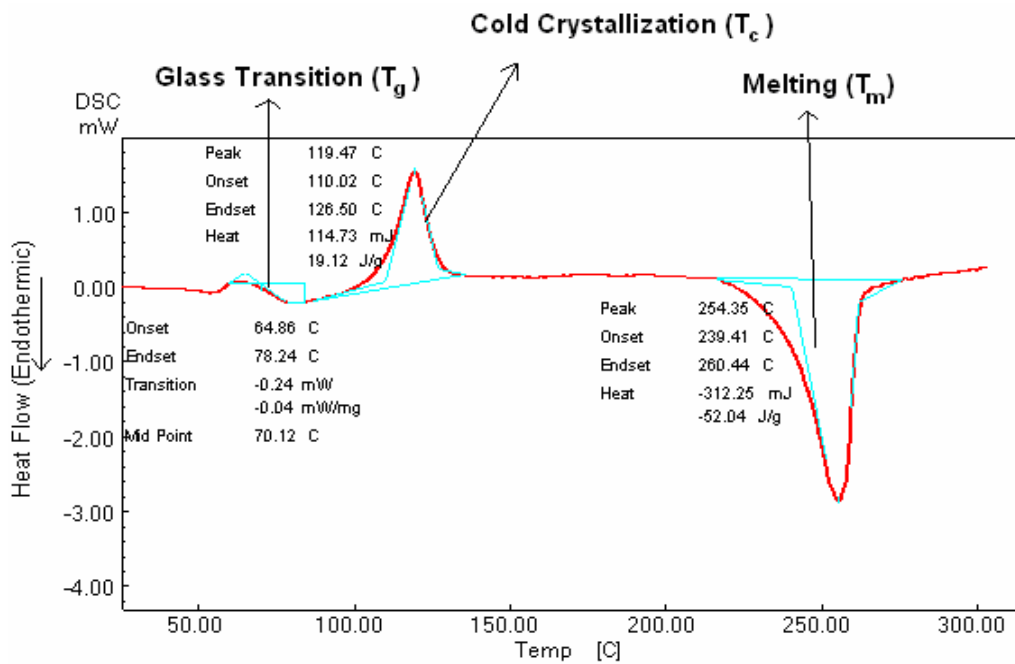


**Figure 2.44** Typical DSC curve for poly(ethylene terephthalate)

## 2.2.6 Fourier Transformed Infrared Spectroscopy

Fourier Transformed Infrared Spectroscopy (FTIR) (Figure 2.45) is the most widely used method of infrared spectroscopy. In this method as the infrared (IR) radiation passes through a sample, some of the IR radiation is absorbed by the sample and some of it is transmitted through the sample. The resulting spectrum represents the molecular absorption and transmission and this creates a molecular fingerprint of the sample [167]. This makes infrared spectroscopy useful for qualitative identification of various functionalities. The chemical groups of the sample can be identified by the presence of the absorption bands. The intra molecular and intermolecular bondings determine the location of the absorption band of a chemical group in the FTIR spectrum of the sample [125]. For quantitative analyses, FTIR requires the use of well characterized standards [168].

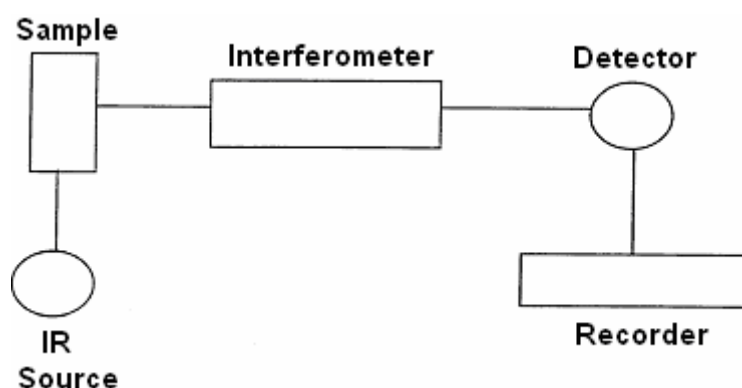


**Figure 2.45** Basic components of a FTIR [168]

## 2.2.7 Electron Spectroscopy for Chemical Analysis

Electron Spectroscopy for Chemical Analysis (ESCA) (Figure 2.46) is also known as the X-Ray Photoelectron Spectroscopy (XPS). Electron binding energies are sensitive to the chemical state of the atoms on the material surface. ESCA sends soft X rays (photons) to the material surface, which ejects photoelectrons from the

sample. Electrons originating from the core levels of the sample identify the elements and chemical groups present, from their binding energies. Small chemical shifts in the binding energies also provide additional chemical state information. Moreover, the relative concentrations of the different elements present can be determined from relative peak intensities. ESCA identifies all elements except hydrogen and helium atoms from a depth ranging from around 2 monolayers to 25 monolayers. Typical values for ESCA peaks in the 500–1400 eV kinetic energy range are 5 to 10 monolayers. This surface sensitivity, combined with quantitative and chemical state analysis capabilities have made ESCA one of the most broadly applicable general surface analysis technique [167].

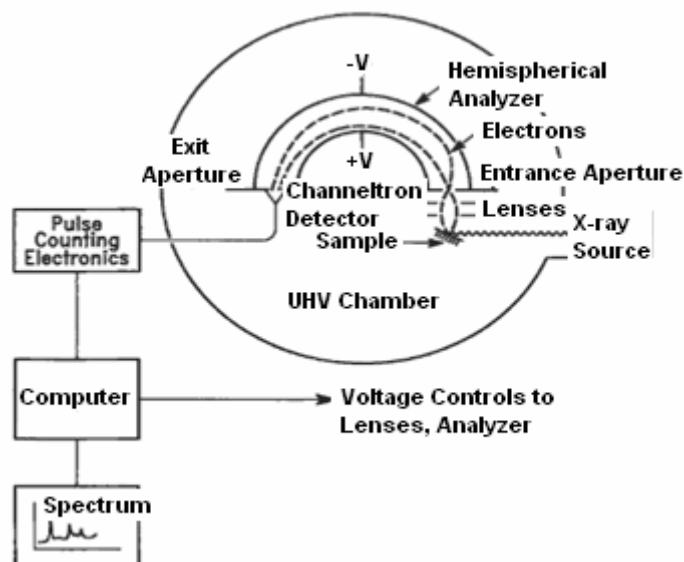


**Figure 2.46** Schematic of a ESCA spectrometer showing all the necessary components [167]

### 2.2.8 X-Ray Diffraction Analysis

X-Ray Diffraction (XRD) is widely used technique for material characterization which can provide the information about both the crystalline and amorphous states.

It uses the X-Rays which are high energy photons with short wavelengths that can interact with electrons. The photons will be absorbed, transmitted and scattered due to the interactions with electrons, when an X-Ray beam is focused on a material. These interactions yield in a scattering pattern which is a function of scattering angle ( $2\theta$ ) (Figure 2.47). This pattern provides information about the electron-density distribution (positions of atoms in the material). There are two types of X-Ray scattering; wide angle X-Ray scattering (WAXS) is used for the investigation of small scale structures, small angle X-Ray scattering (SAXS) is used to study large scale morphological structures [125].

XRD can also be used to determine the detailed microstructure of the carbon based conductive fillers, such as carbon nanotubes. Interplanar spacing between carbon nanotube aggregates ( $d_{002}$ ) can be calculated by using the Bragg equation [170]:

$$n\lambda = 2d_{002} \sin \theta \quad (2.20)$$

where  $n$  is equal to one for monochromatic radiation,  $\lambda$  is wavelength of radiation,  $d_{002}$  is interlayer spacing between graphene layers and  $\theta$  is diffraction angle of beam of radiation corresponding with Bragg's maximum. Crystallite length along the c-axis ( $L_c$ ) of carbon nanotube was calculated by using the Scherrer equation [171]:

$$L_c = K\lambda / B \cos \theta \quad (2.21)$$

in which  $K$  is Scherrer constant, equal to 0.89,  $L_c$  is crystallite length along the c-axis of carbon nanotube,  $\lambda$  is wavelength of radiation,  $\theta$  is diffraction angle of beam of radiation corresponding with Bragg's maximum,  $B$  is widening of diffraction line measured in the middle of its maximum intensity.

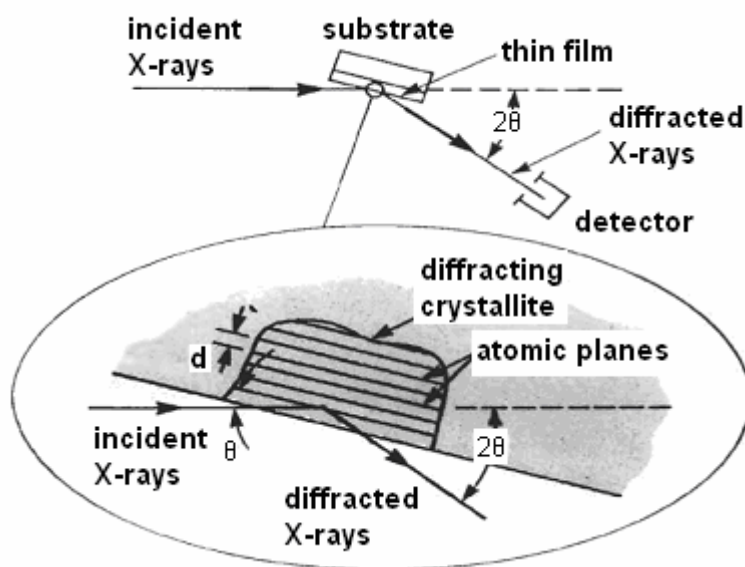


**Figure 2.47** Basic features of a typical XRD experiment [167]

### 2.2.9 Nuclear Magnetic Resonance Spectroscopy

Nuclear Magnetic Resonance (NMR) (Figure 2.48) is a spectrometric technique for determining chemical structures [168]. The nuclei of certain atoms are considered to spin. The spinning of these charged particles or circulation of charge generates a magnetic moment along the axis of spin, so that these nuclei act like tiny magnets. The nucleus of hydrogen ( $^1\text{H}$ ) is the one of greatest interest for what is referred to as  $^1\text{H}$ -NMR, which is useful for the broad spectrum of organic molecules. However, another nucleus ( $^{13}\text{C}$ ), which forms the basis for  $^{13}\text{C}$ -NMR, is very useful for studying polymers and resins [169].

In NMR spectroscopy, the measurement concentrates on the precise energy differences between such nuclear magnetic states. These differences are measured by applying electromagnetic waves in the radio frequency region (1 – 600 MHz) and measuring the frequency at which transitions occur between the states [167]. The chemical structure of the sample can be interpreted by the minor spectral shifts due to chemical environment and they are normally expressed in terms of part-per-million shifts from the reference frequency of a standard [168].

NMR has the advantage of being element selective and inherently quantitative. Since the signal from the NMR experiment is a direct reflection of the local environment of the element under study and NMR can also provide structural insights on a molecular level. This feature is particularly useful in the structural analysis of highly disordered, amorphous, and compositionally complex systems [167].

NMR instrumentation consists of three major components which are the magnet, the spectrometer console, and the probe. NMR probes are used to transfer the radio frequency pulse to the sample and to detect the nuclear induction signal after the pulse. Magic angle spinning NMR (MAS-NMR) experiments require special probes, enabling very fast sample rotation within the magnet. MAS is mostly done on powdered samples packed within cylindrical containers (rotors) that are machined from single-crystal alumina, zirconia, or silicon nitride with precise dimensions [167].

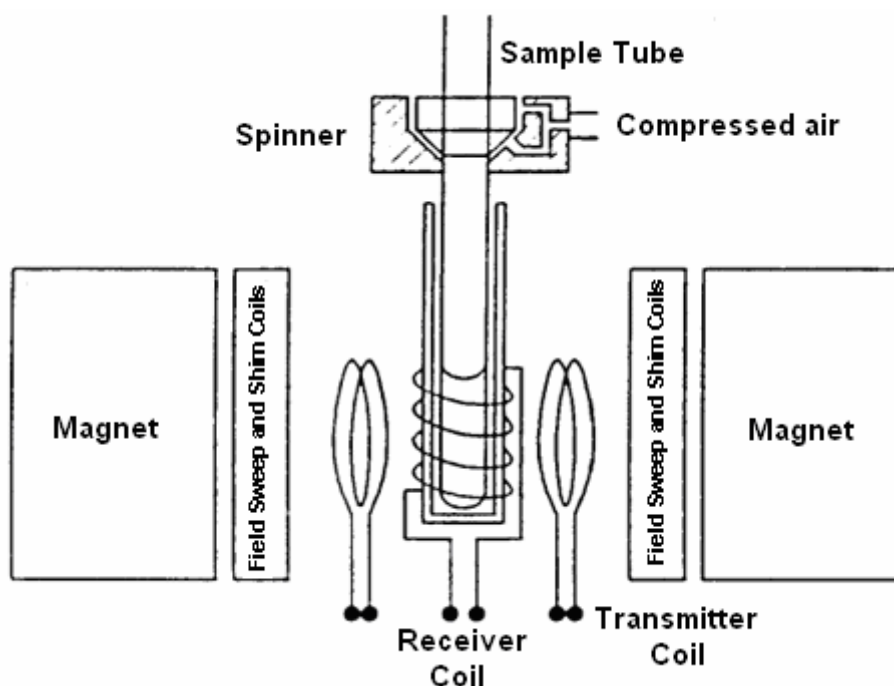


**Figure 2.48** Schematic of a NMR spectrometer [168]

### 2.2.10 Thermogravimetric Analysis

Thermogravimetric Analysis (TGA) is a type of thermal analyses which examines the mass change of a sample as a function of temperature in the scanning mode or as a function of time in the isothermal mode. TGA devices are configured for the vacuum and variable atmospheres. Thermal events such as desorption, absorption, sublimation, vaporization, oxidation, reduction and decomposition cause a change in the mass of the sample during the TGA analysis. The decomposition characteristics (where the major mass loss occurs in the sample during testing) and thermal stability of materials can be investigated by using TGA under a variety of conditions to examine the kinetics of the physico chemical processes occurring in the sample [172]. Moreover, the amounts of materials in a mixture can be detected if the materials are chemically different and have distinct decomposition temperatures [169].

In a typical TGA design, specimen is placed in the refractory pan which is placed in the hot zone of the furnace and suspended from a high precision balance. A thermocouple is placed in the vicinity of the sample without touching it, not to interfere with free float of the balance. The balances are electronically compensated so that the specimen pan does not move when the specimen's weight changes [173].

### 2.2.11 Electro-Mechanical Tests for Damage Sensing

Electro-mechanical tests can be used as an economical nondestructive evaluation (NDE) method for sensing micro damage in the carbon nanotube or carbon fiber reinforced composite panels, the characterization of interfacial properties, and other nondestructive behavior since the composite panel can act as an intrinsic sensor itself due to the electrical conductivity induced by the reinforcing fillers [174]. Electrical resistivity with micro failure mechanisms and nondestructive characteristics can be studied to provide the correlation between interfacial adhesion and electrical properties, since these composites respond to the applied load with the change in the electrical resistivity [113]. In this method damage

sensing capacity of the composites can be determined by means of online electrical resistivity and mechanical property measurements (Figure 2.49). This electrical method can be used to study variety of damage mechanisms such as; delamination or matrix cracking under static or dynamic loading conditions [175].

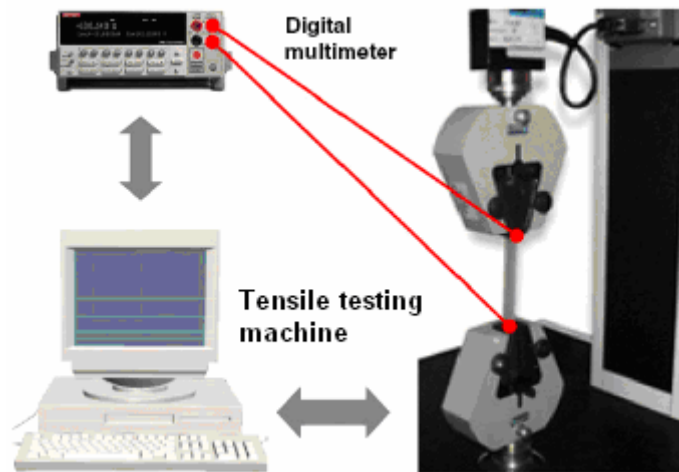


**Figure 2.49** Online electrical resistivity measurement system during tensile testing [113]

### 2.3 Previous Studies

Various surface modification techniques are applied to carbon nanotubes in order to alter the surface chemical structure of carbon nanotubes and improve the carbon nanotube based composite properties. Generally two main approaches are performed for the surface modification of carbon nanotubes. Covalent modification of carbon nanotubes by using oxidizing strong acid and base mixtures to produce carboxyl and hydroxyl groups on the carbon nanotubes outer walls [40, 41], followed by the further treatment with amines [10, 42], silane coupling agents [33], formaldehyde [43], vinyl monomers [43], polymeric and oligomeric materials [44, 46] is used widely in the literature. The functional groups attached on carbon nanotube surfaces can improve the interfacial interactions with different types of

polymer matrices, such as epoxy [47, 48], polycarbonate [49], polyethylene [50, 51], polymethyl methacrylate [52], polypropylene [53], polystyrene [54], polyvinyl alcohol [55], poly(ethylene terephthalate) [16, 18, 22, 56]. The noncovalent modification of carbon nanotubes can be performed by attaching molecules or polymer chains on surfaces of carbon nanotubes. The noncovalent attachment can alter the nature of the carbon nanotubes surface and make it more compatible with the polymer matrix [57]. Polymers such as poly(acrylic acid) [58, 59], polyvinylpyrrolidone [60], poly(4-styrenesulfonate) [61] and polyaniline [62] are used as modifiers during the noncovalent treatment of the surfaces of carbon nanotubes.

Chemical treatment of carbon nanotubes with surfactants can help to form individual carbon nanotubes instead of agglomerates and this can also improve the electrical and mechanical properties of the composites [63]. However, this improvement can be more efficient if the functionality of carbon nanotube match the chemistry of the matrix [64, 65]. During noncovalent treatment of carbon nanotubes the graphitic wall structure is not altered and the intrinsic electrical and mechanical properties of carbon nanotubes are conserved. However, the forces between the attached modifier and carbon nanotube might be weak, thus the efficiency of the load transfer in the composites might be low [66].

In the literature, there are few studies about the surface treatment of carbon nanotubes with sodium dodecyl sulfate (SDS), poly(ethylene glycol) (PEG) and diglycidyl ether of Bisphenol A (DGEBA) and their usage in the polymer composites. Vaisman et.al. suggested SDS as an effective surfactant to disperse the carbon nanotubes in water soluble polymers when it is used above its critical micelle concentration [67]. Yang et.al. showed that carbon nanotube reinforced polyimide composites assisted with PEG exhibit individual carbon nanotube dispersion at high amount of filler loadings (43 wt.%) [68]. Blighe et.al. produced polyurethane based composite films at different filler loadings with PEG functionalized carbon nanotubes range from the stiffer to more ductile when compared to neat polyurethane [69]. Liao et.al. showed that the flexural strength and the bulk electrical conductivity of the carbon nanotube/polypropylene nanocomposite bipolar plates are higher than those of the original composite bipolar plates prepared with untreated carbon nanotubes, by adding 8 phr of DGEBA functionalized carbon nanotubes [70].

High-performance polymer composites can be formulated by introducing particulate fillers into microfiber reinforced polymer blends. Li et.al. manufactured microfibrillar-reinforced material based on fibrillized blends of poly(ethylene terephthalate) / polypropylene (PP), and TiO<sub>2</sub> nanoparticles. Differential scanning Calorimetry (DSC) analysis confirmed the heterogeneous nucleating effect of the TiO<sub>2</sub> nanoparticles on the PET microfibrils [96]. Electrically conductive materials with high conductivity and lower percolation threshold values can be obtained in a microfiber reinforced composites with only a small concentration of particulate conductive fillers, if a double percolation is present. This may be achieved when the conductive particles, localized preferentially in microfiber polymer phase, having a concentration equal to or larger than the electric percolation threshold and the microfiber/filler phase is continuous in matrix polymer [6, 97]. Dai et.al. showed that the PET phases formed well-defined microfibrils, and carbon black (CB) particles localized in the surfaces of the PET microfibrils, which led to a very low percolation threshold concentration in microfiber reinforced HDPE/PET/CB composites [98]. Garmabi et.al. established that the PP/polyamide 6 (PA6)/CB composite with microfibrillar conducting network can be prepared by using melt spinning process. The percolation threshold of the system reduced when aspect ratio of the conducting phase was increased by developing microfibrillar morphology. Mechanical strength of microfibrillar composites were increased up to 80% in comparison to pure PP when processing conditions were optimized [99, 100].

Carbon nanotubes can also be a good candidate as conductive filler and reinforcement for microfibrillar polymer composites due to their unique properties [101, 102]. Moreover incorporation of carbon nanotubes into polymer blends might increase the compatibility between the polymer phases [96]. Li et.al. produced carbon nanotube filled microfibrillar polymer composite based on polycarbonate and HDPE by using a shear controlled orientation in injection molding. Tensile properties of the samples were considerably increased compared to their conventional samples, especially in the presence of 0.5 wt% of carbon nanotube [103].

Fiber reinforced polymer composites filled with carbon nanotubes have drawn significant attention in the field of advanced, high performance materials in various

application areas. They are known as multiscale composites since they are composed of microscale fibers and nanoscale nanotubes [108, 109]. Solvent assisted sonication technique has been widely used to predisperse carbon nanotubes in the resin before composite fabrication in the literature [108]. The integration of epoxy/carbon nanotube mixture with fiber fabric are performed by, resin transfer molding (RTM), vacuum-assisted resin transfer molding (VARTM) and hand lay-up techniques [110]. Some improvements in mechanical properties of multiscale composites have been achieved with the addition of carbon nanotubes into epoxy matrix. However, the combination of the improved matrix properties with the continuous fiber reinforcements is a challenging task and limited by many factors [108, 111]. At this point carbon nanotube surface chemistry and dispersion in the polymer matrix becomes more important to enhance the mechanical properties of fiber reinforced composites.

## **CHAPTER 3**

### **EXPERIMENTAL**

Experimental procedures and the details of the material characterization are explained in four separate sections in this dissertation. In the first section, materials and methods for the carbon nanotube surface treatment and PET/CNT composite preparation are described. In the second section, materials and methods for the preparation of microfiber reinforced HDPE/PET/CNT composites are explained. In the third part, characterization methods for the carbon nanotube and conductive polymer composite samples, which are prepared in the first two sections, are given. Finally, in the last part, materials, methods for the preparation of the epoxy/CNT composites, epoxy/CNT/glass fiber composite panels and characterization methods are explained.

#### **3.1 Surface Treatment of Carbon Nanotubes and Poly(ethylene terephthalate)/Carbon Nanotube Composites**

##### **3.1.1 Surface Treatment of Carbon Nanotubes**

Surface treatment studies of carbon nanotubes will be explained in two subsections. In the first part, carbon nanotube purification with strong acids, strong bases and with their mixtures will be described. In the second part, surface modification of carbon nanotube with low molecular weight chemicals will be explained.

### 3.1.1.1 Purification of Carbon Nanotubes

Purification of multi walled carbon nanotubes, delivered by Nanocyl, were performed by using nitric acid (HNO<sub>3</sub>) (JT Baker 65 %), sulfuric acid (H<sub>2</sub>SO<sub>4</sub>) (JT Baker 95 %), ammonium hydroxide (NH<sub>4</sub>OH) (JT Baker 30 %) and hydrogen peroxide (H<sub>2</sub>O<sub>2</sub>) (JT Baker 30 %) and by using the mixtures of them. Table 3.1 summarizes the properties of commercial grade multi walled carbon nanotubes.

**Table 3.1** Properties of commercial grade multi walled carbon nanotubes

<b>Material</b>	<b>Trade name and Supplier</b>	<b>Specifications</b>
Multi walled carbon nanotube	Nanocyl 7000; Nanocyl (Belgium)	Average Diameter, 10 nm Electrical Resistivity, 10 <sup>-4</sup> ohm.cm Surface Area, 250 m <sup>2</sup> /g

#### 3.1.1.1.1 Procedures of Carbon Nanotube Purification

5 g. portion of as-received carbon nanotubes (ASCNT) were added to 200 ml of purification medium. Next, the mixture was sonicated in an ultrasonic bath (Bandelin Sonorex) (Figure 3.1) at 80 °C. After the sonication, mixture was diluted with distilled water 1:5 by volume and it was filtered with the 0.2 µm pore sized filter paper in order to recover the carbon nanotubes from the solution. Filtered carbon nanotubes were washed with excess hot and cold distilled water until no residual acid or base was present (pH of the filtrate water is greater than 5). Finally, carbon nanotubes were dried in the oven for 24 hours at 100 °C. During purification experiments carbon nanotubes were treated at the following eight different purification conditions; in order to observe the effects of purification medium and duration on the carbon nanotube and composite properties. In the first part, carbon nanotubes were sonicated in HNO<sub>3</sub>/H<sub>2</sub>SO<sub>4</sub> (1:3 by volume) mixture, which is the generally used mixture during carbon nanotube purification in the literature, for 15

(CNT1), 30 (CNT2), 60 (CNT3) and 120 (CNT4) minutes. In the second part, sonication period was kept constant at 30 minutes, HNO<sub>3</sub>/H<sub>2</sub>SO<sub>4</sub> (1:1 by volume) (CNT5), HNO<sub>3</sub>/H<sub>2</sub>SO<sub>4</sub> (3:1 by volume) (CNT6) mixtures were used as the other purification mediums. Finally, basic mediums; NH<sub>4</sub>OH (CNT7) and NH<sub>4</sub>OH/H<sub>2</sub>O<sub>2</sub> (1:1 by volume) (CNT8), were used during the 30 minutes purification of carbon nanotubes. At the end of the purification experiments, carbon nanotubes purified in the HNO<sub>3</sub>/H<sub>2</sub>SO<sub>4</sub> (1:1 by volume) medium for 30 minutes, were selected as raw materials for the experiments on carbon nanotube surface modification with low molecular weight chemicals.

### 3.1.1.2 Surface Modification of Carbon Nanotubes with Low Molecular Weight Chemicals

In this part of the carbon nanotube surface treatment studies, first carbon nanotubes were purified in HNO<sub>3</sub>/H<sub>2</sub>SO<sub>4</sub> (1:1 by volume) medium for 30 minutes (pCNT) according to the procedure explained before. After the purification step, surface modification of carbon nanotubes were performed with sodium dodecyl sulfate (SDS), diglycidyl ether of Bisphenol A (DGEBA), poly(ethylene glycol) (PEG) with 400 and 1000 g/mole molecular weight, separately. Suppliers, chemical structures and some of the physical properties of the surface modifiers are shown in Table 3.2.

**Table 3.2** Properties and suppliers of the surface modifiers

<b>Material</b>	<b>Supplier</b>	<b>Specifications</b>
Sodium dodecyl sulfate	Sigma Aldrich	Molecular Weight, 288 g/mole Melting Temperature, 204°C CMC, 7-10 mM
Diglycidyl ether of bisphenol A	Hexion	Epoxide Equivalent Weight, 185-192 g/eq. Density, 1.17 g/ml at 25 °C
Poly(ethylene glycol)	Sigma Aldrich	Molecular Weight, 400, 1000 g/mole Density, 1.12 g/ml at 20 °C

#### 3.1.1.2.1 Procedures of Carbon Nanotube Surface Modification

During surface treatment with sodium dodecyl sulfate, 200 ml 10 mmol/L distilled water/SDS solution were prepared. Purified carbon nanotubes were added into this solution and sonicated in ultrasonic bath for 4 hours at 80°C.

During surface treatment with diglycidyl ether of Bisphenol A, purified carbon nanotubes were sonicated in 200 ml acetone/10 ml DGEBA solution at 80°C for 5 hours. Potassium hydroxide (KOH) was used as catalyst.

During surface treatment with poly(ethylene glycol), first 200 ml 0.04 M Nickel chloride (NiCl<sub>2</sub>)/distilled water solution was prepared. Purified carbon nanotubes and 10 ml PEG with 400 or 1000 g/mole molecular weight were added to the solution. This mixture was sonicated in ultrasonic bath for 4 hours at 80°C.

At the end of the sonication, modified carbon nanotubes (SDSCNT, DGEBCNT, PEG400CNT and PEG1000CNT) were filtered with the 0.2 µm pore sized filter paper in order to recover the carbon nanotubes from the solution, washed with distilled water and dried at 100°C for 24 hours.

### 3.1.2 Poly(ethylene terephthalate)/Carbon Nanotube Composites

In this part of the dissertation, amorphous poly(ethylene terephthalate), delivered by AdvanSA, was used for the processing of the conductive polymer composites. Table 3.3 summarizes the properties of commercial grade PET.

**Table 3.3** Properties of commercial grade poly(ethylene terephthalate)

<b>Material</b>	<b>Trade name and Supplier</b>	<b>Specifications</b>
Poly(ethylene terephthalate)	Melinar; AdvanSA (Turkey)	Melting Temperature, 255°C Electrical Resistivity, $10^{14}$ ohm.cm Density, 1.4 g/cm <sup>3</sup>

During composite preparation, PET pellets were compounded with as received, purified and modified carbon nanotubes in a co-rotating twin screw extruder (Thermo PRISM TSE-16-TC, L/D = 24) shown in Figure 3.1. The amount of carbon nanotubes in the composites was 0.5 wt. %.



**Figure 3.1** A photograph of the co-rotating twin screw extruder

The extrusion processes were performed with the temperature profile of 230-255-260-265-270 °C and at a screw speed of 120 rpm. Prior to the extrusion processes, PET pellets were ground into powder form by using a Wiley mill intermediate model grinder (Arthur H. Thomas Co., Philadelphia) (Figure 3.2). PET powder and carbon nanotubes were mixed at predefined weights and fed from the main feeder of the extruder during composite preparation. Before the extrusion and molding processes, PET powder and composite pellets were dried in a vacuum oven for 24 hours at 90° C.



**Figure 3.2** A photograph of the grinder

Specimens of composites for tensile, impact testing and electrical conductivity measurements were prepared by using injection and compression molding devices at 280°C. During compression molding (Figure 3.3), samples were preheated and molded at 50 bar oil pressure for 1.5 minutes and 150 bar oil pressure for 1 minute, respectively. Compression molded samples were quenched to room temperature by tap water. Injection moldings (DSM Micro 10 cc Injection Molding Machine) (Figure 3.4) of the samples were performed at 15 bar and 30 °C mold temperature.

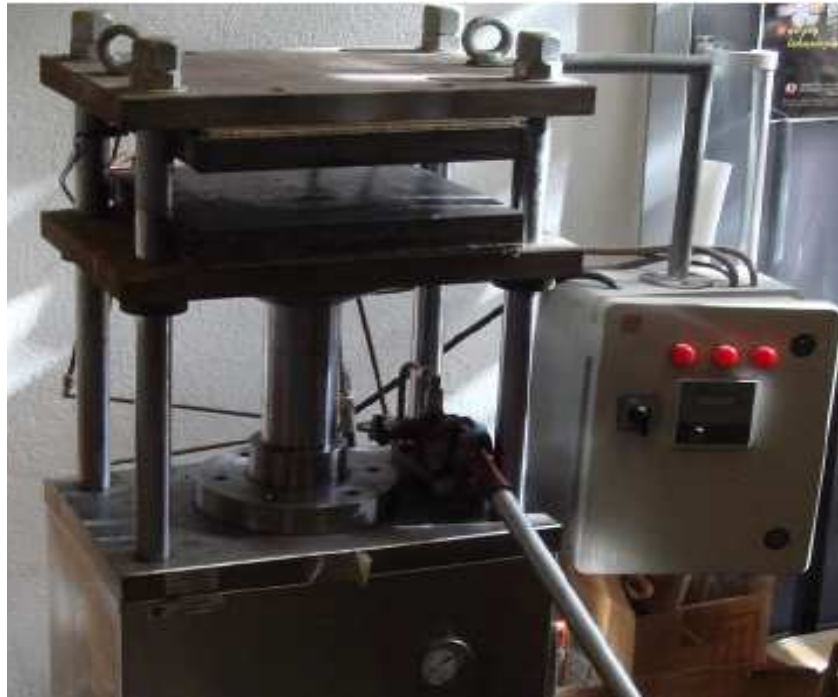


**Figure 3.3** A photograph of the compression molding device



**Figure 3.4** A photograph of the injection molding device

Moreover, the effect of carbon nanotube concentration on the electrical and mechanical properties of PET/CNT composites were investigated by compounding PET with ASCNT, pCNT and PEG1000CNT in the co-rotating twin screw extruder to obtain 0.25, 0.5, 1, 2 and 4 wt. % of carbon nanotube containing composites. The extrusion and molding processes of the composites were performed with the same devices and according to the procedures explained before.

### 3.2 Microfiber Reinforced High Density Polyethylene/Poly(ethylene terephthalate)/Carbon Nanotube Composites

In this part of the dissertation; high density polyethylene delivered by PETKİM, poly(ethylene terephthalate) and multi walled carbon nanotubes were used for the preparation of the composites and blends. Some of the properties of commercial grade HDPE are given in Table 3.4.

**Table 3.4** Properties of commercial grade high density polyethylene

<b>Material</b>	<b>Trade name and Supplier</b>	<b>Specifications</b>
High density polyethylene	Petilen S0464; PETKİM (Turkey)	Melting Temperature: 140°C Electrical Resistivity: 10 <sup>18</sup> ohm.cm Density: 0.964 g/cm <sup>3</sup>

Microfiber reinforced composites and conventional systems were prepared in a two step extrusion process. Before blending, HDPE and PET pellets were dried in a vacuum oven at 60 °C for 4 hours and at 90 °C for 24 hours, respectively. During the first extrusion, HDPE and PET were mixed in a corotating twin screw extruder (Thermoprism TSE 16 TC, L/D = 24). The HDPE/PET ratios were selected as 90/10, 80/20, 70/30, 60/40 and 50/50. HDPE/PET blends, which were obtained in

first extrusion, were mixed with ASCNT in the second extrusion and the mixture from the extruder die was hot stretched by using a speed adjustable take-up device (Siemens Micromaster 440) in order to form the PET/ASCNT microfibers in the HDPE matrix at the hot stretching speed of 5.8 m/min (Figure 3.5). The hot-stretching ratio (the ratio of the cross-sectional areas of extrudate to hot stretched sample which was drawn by the take-up device) was 19.6, since it was the ultimate speed of the take-up device at which continuous microfibrillar composite processing with uniform dimensions could be performed. The HDPE/PET part was  $(100 - x) \%$  of the composite, where  $x$  was the ASCNT amount in the composite and it was kept constant as 0.5 wt. %. The carbon nanotube amount in the PET phase of the HDPE/PET/CNT composites were 5, 2.5, 1.67, 1.25 and 1 wt. % for the HDPE/PET ratios of 90/10, 80/20, 70/30, 60/40 and 50/50, respectively. Conventional composites and blends were prepared at the same compositions with the microfiber reinforced composites according to the same procedure given above without the hot-stretching process. Extrusion processes were performed at a barrel temperature profile of 190–210–230–250–270 °C, and a screw speed of 120 rpm.

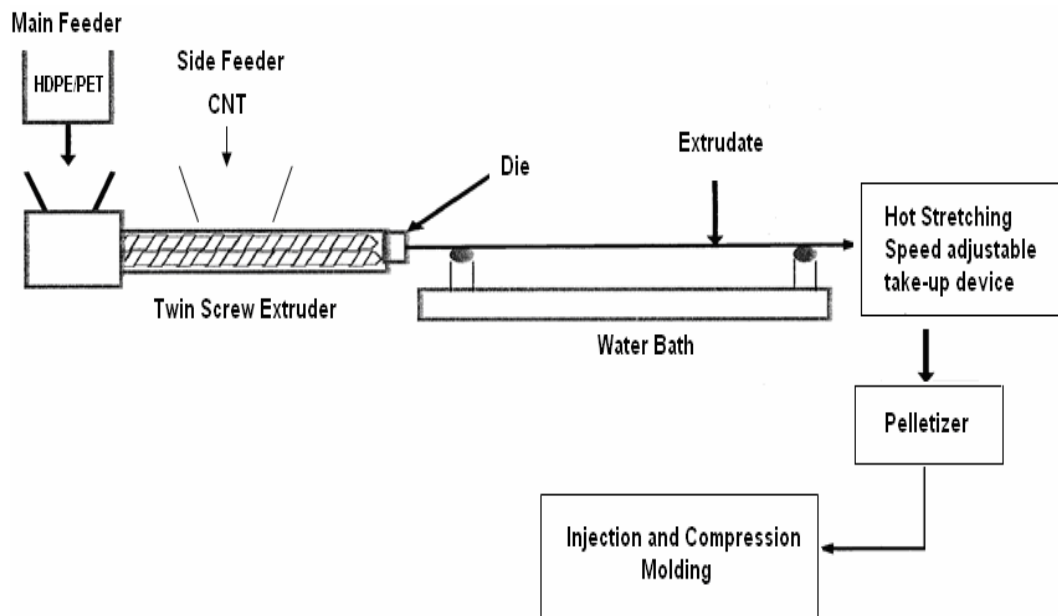


**Figure 3.5** Experimental set-up for the preparation of the microfiber reinforced composites

In the second part of the microfiber reinforced composite studies, microfiber reinforced polymer composites were also prepared in a two step extrusion process. Firstly, HDPE and PET were blended in the co-rotating twin screw extruder (Thermoprism TSE 16 TC, L/D = 24) at a fixed (80/20 by weight) HDPE/PET ratio, since this ratio resulted in better mechanical properties in the first part of the studies. During second extrusion HDPE/PET blends were mixed with ASCNT, pCNT, PEG1000CNT at 0.25, 0.5, 0.75, 1, 1.5 wt. % concentrations. The HDPE/PET part was  $(100-x)$  % of the composites, where x was the CNT amount in the composites. The carbon nanotube amounts in the PET phase of the HDPE/PET/CNT composites were 1.25, 2.5, 3.75, 5 and 7.5 wt. % for the carbon nanotube loadings of 0.25, 0.5, 0.75, 1 and 1.5 wt. %, respectively. The procedure and the experimental conditions for the microfiber reinforced composite preparation were the same as the first part of the studies.

Specimens for tensile, impact testing and electrical conductivity measurements were prepared by using injection and compression molding devices, respectively, at 210°C. The PET based microfibers were considered to be preserved at this temperature because of the high melting point of PET (~255°C). In order to observe the effect of molding temperature on microfiber structure, composites were also molded at 240°C and 280°C. During compression molding, samples were preheated and molded at 50 bar oil pressure for 1.5 min. and 150 bar oil pressure for 1 min., respectively. Compression molded samples were quenched to room temperature by tap water. Injection moldings (DSM Micro 10 cc Injection Molding Machine) of the samples were conducted under 15 bar pressure and at 30 °C mold temperature. Conventional composites and blends were molded at the same conditions used for the microfiber reinforced composites.

Injection and compression moldings of the microfiber reinforced composites, which were prepared in the second part of the studies, were performed at 210°C. Furthermore, the effect of molding temperature on the composite properties was investigated by molding the microfibrillar composites at 280°C. The procedure and the experimental conditions for the microfiber reinforced composite moldings were the same as the first part of the studies.

### 3.3 Characterization Methods for the Carbon Nanotube and Conductive Polymer Composite Samples

In the poly(ethylene terephthalate)/carbon nanotube composites prepared with surface treated carbon nanotubes and microfiber reinforced high density polyethylene/poly(ethylene terephthalate)/carbon nanotube composites studies, carbon nanotube and composite samples were characterized in terms of various characterization methods. Carbon nanotube samples were characterized by means of surface energy measurements, Fourier Transformed Infrared Spectroscopy (FTIR), Electron Spectroscopy for Chemical Analysis (ESCA), X-Ray Diffraction (XRD) analysis, Scanning Electron Microscopy (SEM) and Thermogravimetric Analysis (TGA) and quantitative assessment of carboxylic acid groups analysis. The techniques used for the characterization of the composite samples were surface energy measurement analysis, electrical resistivity measurements, tensile, and impact testing, Scanning Electron Microscopy (SEM), Differential Scanning Calorimetry (DSC) analysis, Fourier Transformed Infrared Spectroscopy (FTIR), Nuclear Magnetic Resonance (NMR) spectroscopy and melt viscosity measurements.

#### 3.3.1 Surface Energy Measurements

Surface energy components ( $\gamma_{\text{Solid}}$ : total surface energy,  $\gamma_{\text{Solid}}^{\text{d}}$ : dispersive component of total surface energy,  $\gamma_{\text{Solid}}^{\text{P}}$ : polar component of total surface energy,  $\gamma_{\text{Solid}}^{\text{A}}$ : acidic component of total surface energy,  $\gamma_{\text{Solid}}^{\text{B}}$ : basic component of total surface energy) of the carbon nanotube samples, PET/CNT composites, neat HDPE and PET were determined by measuring the contact angles of probe liquids on sample surfaces according to the Sessile drop method. Contact angle measurements of the composites and neat polymers were conducted on the compression and injection molded samples. Carbon nanotube particles were pressed as discs with 12 mm diameter and 1 mm thickness under 150 bar oil pressure by using the compression molding machine, and contact angles of probe liquids were determined from these pressed surfaces [159]. Diiodomethane (DIM), ethylene glycol (EG) and formamide (FA) were used as probe liquids. DIM was

selected to calculate the dispersive component of total surface energy. Meanwhile, EG and FA were used to calculate the polar component of total surface energy. Surface energy components of probe liquids are given in Table 3.5 [158].

**Table 3.5** Surface energy components of probe liquids, (mN/m)

<b>Probe Liquid</b>	$\gamma_{\text{Liquid}}$	$\gamma_{\text{Liquid}}^{\text{d}}$	$\gamma_{\text{Liquid}}^{\text{p}}$	$\gamma_{\text{Liquid}}^{\text{A}}$	$\gamma_{\text{Liquid}}^{\text{B}}$
DIM	50.80	50.80	-	-	-
EG	48.00	29.00	19.00	3.00	30.10
FA	58.00	39.00	19.00	2.30	39.60

### 3.3.2 Fourier Transformed Infrared Spectroscopy

Fourier Transformed Infrared Spectroscopy (FTIR) (Shimadzu IRPrestige 21) was used to investigate the presence of reactive groups on the carbon nanotube surfaces, resulted from the purification and surface treatment of carbon nanotubes. The infrared spectra of carbon nanotubes pressed with KBr were recorded in the range of 400-4000  $\text{cm}^{-1}$ . The FTIR spectra of the neat PET and PET/CNT composites were recorded with Attenuated Total Reflectance (ATR) apparatus.

### 3.3.3 Electron Spectroscopy for Chemical Analysis

Surface chemical structure of carbon nanotube samples were also analyzed by Electron Spectroscopy for Chemical Analysis (ESCA) with a Specs model spectrometer (aluminum radiation at 1 W). The high resolution spectrum of oxygen and carbon (O1s and C1s) were recorded with pass energy of 48 eV under  $10^{-5}$  Pa vacuum. A non-linear background was removed from the spectra and they were fitted by using curve fitting program of XPSPeak41.

### 3.3.4 X-Ray Diffraction Analysis

X-ray diffraction (XRD) patterns of carbon nanotube samples were obtained with a twin tube X-ray diffractometer (100 kV Philips (PW/1050)) providing CuK $\alpha$  radiation ( $\lambda=0.15418$  nm) at 40 kV and 40 mA.

### 3.3.5 Scanning Electron Microscopy

Morphological analyses of the carbon nanotube samples and PET/CNT composites were performed by using a Scanning Electron Microscope (SEM) (Zeiss Supra 50 V). The SEM micrographs of the PET/CNT composites were obtained from the impact fractured surfaces of the injection molded specimens. The morphological analyses of the microfiber reinforced composites (HDPE/PET/CNT) studies were conducted by using a Scanning Electron Microscope (JEOL JSM-6400). Before the SEM analyses, composite samples were coated with a thin layer of gold to prevent the accumulation of static electric field during imaging.

Prior to morphological analysis selected samples were etched in hot xylene at 135°C for 45 minutes in order to remove the HDPE phase from the composites and observe microfibrillar morphology easier. In addition, some of the samples were etched in trifluoro acetic acid at room temperature for 6 hours, for determining the size of the PET and PET/CNT phases. Since trifluoro acetic acid etching removes the PET and PET/CNT phase from the composites, these phases are observed as hollow spherical particles dispersed in HDPE phase in the SEM micrographs. Domain sizes of the PET and PET/CNT phases in the blends and composites were determined from the SEM micrographs by using image analysis software (Image J). Two SEM micrographs were analyzed for each sample and at least 300 hollow spherical particles were taken into account. The total area of the black holes in the samples was determined by using the image analysis software by transforming these black holes into ellipsoids and calculating the total area of these ellipsoids (Figure 3.6). Finally, the average diameters of the PET and PET/CNT phases were calculated by using the total area calculated from these analyses.

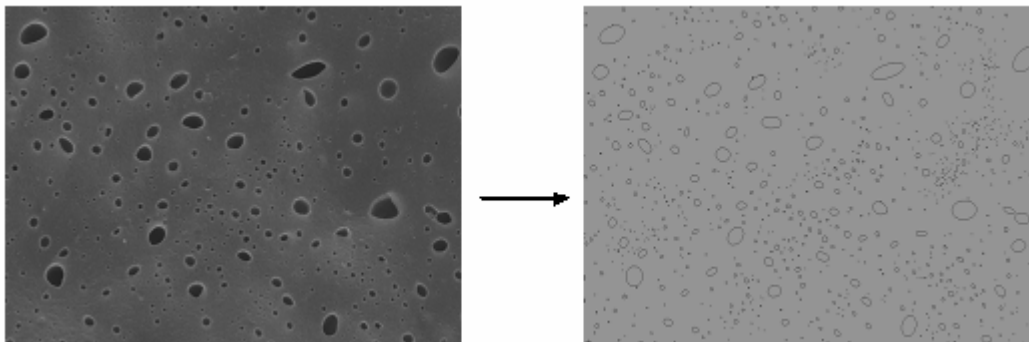


**Figure 3.6** Transformation of PET or PET/CNT domains into ellipsoids during image analyses of the samples

### 3.3.6 Thermogravimetric Analysis

The thermal stability of carbon nanotube samples and the presence of the surface modifiers on the carbon nanotube surfaces were investigated with Thermogravimetric Analysis (TGA) by using a Shimadzu DTG-60/DTG-60A thermal analyzer. The temperature range of the analysis was from 30°C to 1400°C. Heating rates of the samples were 25°C/min.

### 3.3.7 Quantitative Assessment of Carboxylic Acid Groups Analysis

Carbon nanotubes were analyzed quantitatively to determine carboxylic groups (COOH) concentration on the carbon nanotube surfaces after surface treatment. During the analysis, first carbon nanotubes were put into distilled water, and bath sonicated for 1 h. After this, 50 ml. solution of 0.01 N NaOH was added and the mixture was stirred overnight. The mixture was then filtered and washed with distilled water. The filtrate was titrated with 0.01 N HCl solutions to determine the NaOH amount in the filtrate [66]. The difference in the amounts of NaOH added to the carbon nanotube suspension and left in the filtrate solution showed the amount of NaOH molecules that were attached to the carbon nanotube samples. The

carboxylic acid concentration [COOH] (mol COOH/g nanotube) on carbon nanotubes were calculated from the following equation;

$$[\text{COOH}] = [(V_{\text{NaOH}} N_{\text{NaOH}}) - (V_{\text{HCl}} N_{\text{HCl}})] / m_{\text{CNT}} \quad (3.1)$$

where  $V_{\text{NaOH}}$  (ml) was the volume of NaOH added to carbon nanotube suspension,  $V_{\text{HCl}}$  (ml) was the volume of HCl used for the titration of the filtrate,  $N_{\text{NaOH}}$ ,  $N_{\text{HCl}}$  were the normalities of the solutions (0.01 N) and  $m_{\text{CNT}}$  (g) was the carbon nanotube sample weight.

### 3.3.8 Electrical Resistivity Measurements

The electrical resistivity measurements of the compression molded composites were performed according to two point probe method, which was connected to a Keithley 2400 constant current source meter (Figure 3.7). For better electrical contact, copper wires were placed into the samples during compression molding. Resistivity measurements were conducted at room temperature by contacting the probes to the copper wires. The averages of five measurements were reported for each composite.

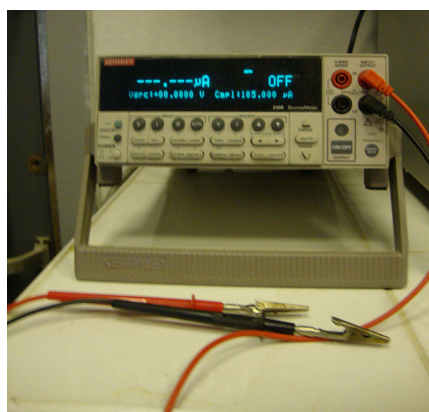


**Figure 3.7** A photograph of the Keithley 2400 constant current source meter

### 3.3.9 Tensile Tests

The tensile properties were investigated by using a Shimadzu Autograph AG-100 KNIS MS universal tensile testing instrument (Figure 3.8), according to ISO 527-2 5A standards at room temperature. Injection molded tensile specimens had a thickness of 2 mm, a width of 4 mm and a gauge length of 20 mm. According to the gauge length and a strain rate of  $0.1 \text{ min}^{-1}$ , the crosshead speed of testing instrument was selected as 2 mm/min. Five specimens of each sample were tested and the averages of these tests were reported with standard deviations (Appendix A, Tables A.1-A.6). All tensile strength and elongation values reported in the dissertation were measured at the break point.



**Figure 3.8** A photograph of the Shimadzu Autograph AG-100 KNIS MS tensile testing machine

### 3.3.10 Impact Tests

Impact strength of the samples were determined by using a Ceast Resil Impactor 6967 impact testing device (Figure 3.9) according to ASTM D 5942 standards, instrumented with a 7.5 J hammer, at room temperature. Injection molded impact specimens had a thickness of 4 mm, a width of 10 mm and a length of 80 mm. Five

specimens of each sample were tested and the averages of these tests were reported with standard deviations (Appendix A, Tables A.1-A.6).



**Figure 3.9** A photograph of the Ceast Resil Impactor 6967 impact testing machine

### 3.3.11 Differential Scanning Calorimetry Analysis

Thermal properties of the composites were investigated by using a Differential Scanning Calorimeter (DSC) (Shimadzu DSC-60) with heating rate of 5 °C/min in a temperature range from 30 °C to 300 °C. Glass transition ( $T_g$ ), cold crystallization ( $T_c$ ) and melting ( $T_m$ ) temperatures of polymer phases in the composites were determined from the DSC thermograms (Appendix D).  $\Delta H_m^0$  values of the HDPE and PET are used as 207 J/g and 138 J/g, respectively during percent crystallinity calculations [176].

### 3.3.12 Nuclear Magnetic Resonance Spectroscopy

Solid state Nuclear Magnetic Resonance (NMR) analysis of neat PET and PET/CNT composites was performed with CP/MAS  $^{13}\text{C}$  NMR (Bruker

Superconducting FT.NMR Spectrometer Avance TM 300 MHz WB) in the chemical shift range from -40 to 250 ppm. Samples were ground into powder form before the analyses.

### 3.3.13 Melt Viscosity Measurements

Melt viscosities of the HDPE, PET and PET/CNT composites were determined by using a Dynisco LCR-7001 capillary viscometer at 260°C in a shear rate range from 10 to 600 1/s. In the first part of the microfiber reinforced composite studies, the carbon nanotube content of the HDPE/PET/CNT composite systems is constant (0.5 wt. %), but the carbon nanotube amount in PET phase differs as PET composition changes from 10 to 50 wt. %. Hence, the melt viscosities of PET/CNT composites containing 1, 1.25, 2.5 and 5 wt. % carbon nanotube were measured and illustrated. In the second part of the microfiber reinforced composite studies, the HDPE/PET ratio of the HDPE/PET/CNT composite systems is constant (80/20 by weight), but the carbon nanotube amount in PET phase differs as carbon nanotube composition changes from 0.25 to 1.5 wt. %. Hence, the melt viscosities of PET/CNT composites containing 1.25, 3.75 and 7.5 wt. % carbon nanotube were measured and illustrated.

## 3.4 Epoxy/Carbon Nanotube Composites and Epoxy/Carbon Nanotube/Glass Fiber Composite Panels

The preparation and characterization of carbon nanotubes, epoxy/CNT composites and epoxy/CNT/glass fiber composite panels, samples were performed in the Mechanical and Aerospace Engineering Department of University of California at Davis. Hence, the preparation methods were selected according to the availability of equipments. The composite panels prepared in this study are designated to be used in the aerospace applications. In this study; epoxy resin delivered by Proset, multi walled carbon nanotubes and glass fiber delivered by Applied Vehicle Technology were used for the production of the composites and panels. Some of

the physical properties of these materials are shown in Table 3.6. Chemicals used for the preparation of the epoxy/CNT composites are given in Table 3.7.

**Table 3.6** Information for the materials used during the production of the composites and panels

<b>Material</b>	<b>Supplier</b>	<b>Specifications</b>
Epoxy/Hardener	Proset 117LV/237; Proset (USA)	Density, 1.08 g/cm <sup>3</sup> Viscosity, 36 Pa.s Glass Transition Temp., 86°C
Glass Fiber	AVT 7715; Applied Vehicle Technology (USA)	Weight, 245.8 g/m <sup>2</sup> Thickness, 0.229 mm Poisson's Ratio, 0.25

**Table 3.7** Chemicals used for the preparation of the epoxy/CNT composites

<b>Function</b>	<b>Material</b>	<b>Supplier</b>
Surface Modifier	Hexamethylene diamine (HMDA) (H <sub>2</sub> N(CH <sub>2</sub> ) <sub>6</sub> NH <sub>2</sub> )	Alfa Aesar
Nonionic Surfactant	4-octylphenol polyethoxylate (Triton X-100) (C <sub>14</sub> H <sub>22</sub> O(C <sub>2</sub> H <sub>4</sub> O) <sub>10</sub> )	Integra Chemical Company
Cationic Surfactant	Cetyl Pyridinium Chloride (CPC) (C <sub>21</sub> H <sub>38</sub> NCl)	MP Biomedicals
Solvent	Acetone (OC(CH <sub>3</sub> ) <sub>2</sub> )	Sigma-Aldrich
Solvent	Ethyl Alcohol (C <sub>2</sub> H <sub>5</sub> OH)	Sigma-Aldrich

### 3.4.1 Surface Treatment of Carbon Nanotubes

0.2 g. of as-received carbon nanotube (ASCNT) were mixed with 5 wt. % hexamethylene diamine (HMDA) containing 200 ml. solution. This mixture was sonicated in an ultrasonic bath (Fisher Scientific FS30D) at 25 °C for 2 hours. The sonicated mixture was stirred at 120 °C for 5 days by using a magnetic stirrer. After the stirring process, carbon nanotubes were filtered out from the solution by using a 0.2 µm pore sized filter paper (Millipore Isopore) and washed with the excess water and ethyl alcohol in order to remove the residual unreacted diamine from the carbon nanotube surface. Finally modified carbon nanotubes (mCNT) were dried at 100 °C for 24 hours.

### 3.4.2 Preparation of Epoxy/Carbon Nanotube Composites

Epoxy/CNT composites were prepared with the help of solvent assisted sonication technique. In the first part, effects of carbon nanotube concentration were investigated by preparing epoxy/ASCNT composites including 0.25, 0.5, 0.75 and 1 wt. % ASCNT. In the second part, carbon nanotube amount in the composites were kept constant at 0.5 wt.%. During composite preparation carbon nanotubes were mixed with solvent (acetone or ethyl alcohol) firstly and if a surfactant was used, Triton X-100 or CPC was added to this mixture. The mixture was sonicated at 25 °C for 60 minutes. After the first sonication epoxy resin was added and the mixture was sonicated 30 minutes more. Then, solvent was evaporated by stirring the mixture at 50 °C for 6 hours. Finally the hardener was added and mixed for 5 minutes. This mixture was degassed in a vacuum chamber (Figure 3.10 (a)) for 60 minutes in order to get rid of the air bubbles. Epoxy/CNT mixtures were poured into silicone molds for the preparation of the electrical (Figure 3.10 (b)) and mechanical (Figure 3.10 (c)) test's specimens. Curing of the composites was performed at room temperature for 15 hours and at 82°C for 8 hours in a vacuum oven (Yamato DKN600). The amount of surfactant used during the composite processing was determined according to the critical micelle concentrations (CMC) of the surfactants. Tenfold of the CMC was used for the both surfactants (CMC of Triton X-100 is 2 mM [177] and CMC of CPC is 1 mM [67]). Ethyl alcohol was used as

solvent during the preparation of the composites with CPC (CPC is not soluble in acetone). Acetone was used as solvent during the preparation of all the other composites due to its higher volatility. After the characterization studies of carbon nanotubes and epoxy/CNT composites, CPC was observed to be a more effective surfactant for the preparation of the composites than Triton X-100. Hence, it was selected as the surfactant during the production of the glass fiber reinforced composite panels.

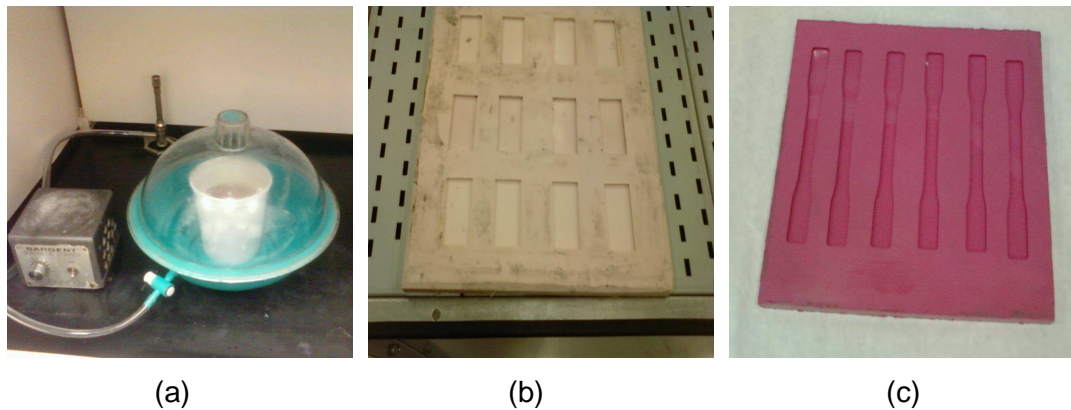


**Figure 3.10** Equipments for the preparation of the epoxy/CNT composite samples (a) vacuum chamber, (b) silicone mold for the electrical resistivity measurement samples, (c) silicone mold for the tensile testing samples

### 3.4.3 Preparation of Epoxy/Carbon Nanotube/Glass Fiber Composite Panels

The composite panels were prepared separately by hand lay-up for the tensile, fatigue and impact tests. The panels which were used during the tensile and fatigue tests were prepared from 9 layers of unidirectional glass fiber with a  $[(0, 90)_4, 0]$  stacking sequence. The preparation of these panels were performed by using neat epoxy, 0.5 wt. % carbon nanotube containing epoxy/ASCNT, epoxy/mCNT, CPC assisted epoxy/ASCNT and epoxy/mCNT mixtures as matrices. The panels which were used during the impact tests were prepared from 15 layers

of unidirectional glass fiber with a  $[(0, 90)_7, 0]$  stacking sequence. The preparation of impact test panels were performed by using 0.5 wt. % carbon nanotube containing epoxy/ASCNT and CPC assisted epoxy/mCNT mixtures as matrices. All the epoxy/CNT mixtures were prepared according to the procedure which is explained in the preparation of epoxy/CNT composites section and the curing of the panels were also performed at room temperature for 15 hours and then at 82°C for 8 hours under vacuum. The samples for the mechanical and electro – mechanical tests were obtained by cutting from the panels. The general procedure for the preparation of the glass fiber reinforced panels is shown in Figure 3.11.

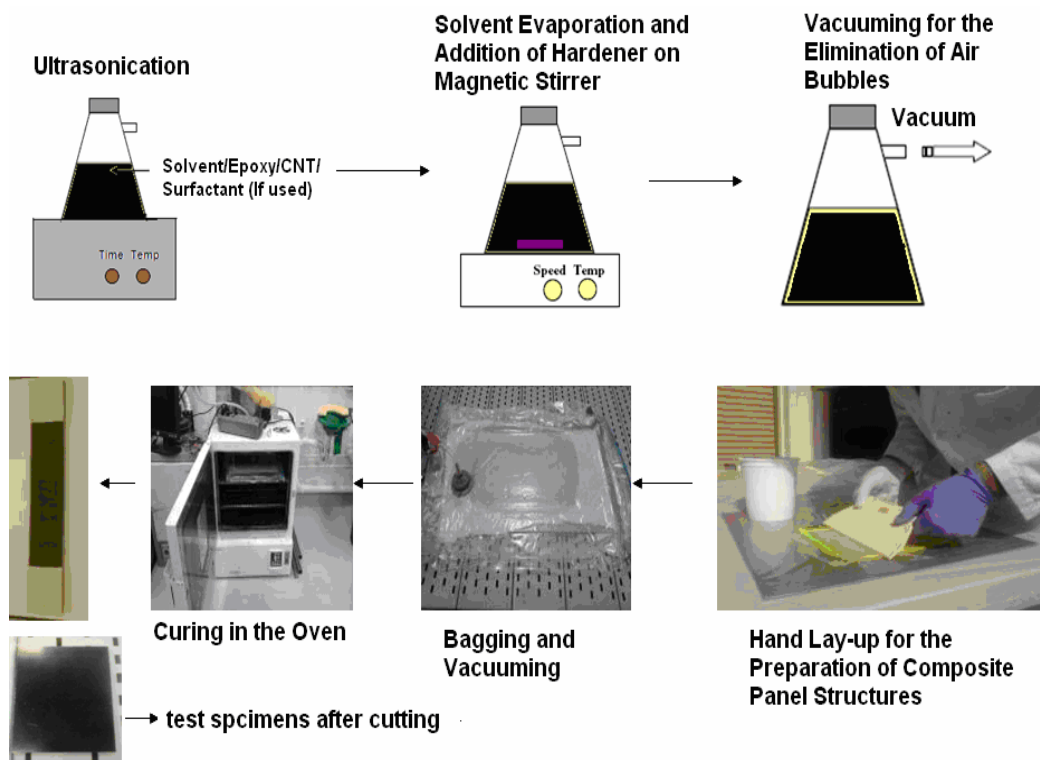


**Figure 3.11** General procedure for the preparation of composite panels

### 3.4.4 Characterization Methods for the Carbon Nanotube and Composite Samples

The characterization methods used in this part of the dissertation were selected according to the availability of the equipments in the Mechanical and Aerospace Engineering Department of University of California at Davis. Carbon nanotube samples were characterized by means of Fourier Transformed Infrared Spectroscopy (FTIR), X-Ray Diffraction (XRD) analysis, suspension stability analysis, and Scanning Electron Microscopy (SEM). The techniques used for the characterization of the composite samples were Scanning Electron Microscopy (SEM), optical microscopy, electrical resistivity measurements, tensile, fatigue, impact testing, and electro-mechanical testing.

#### 3.4.4.1 Fourier Transformed Infrared Spectroscopy

Generation of chemical functional groups on carbon nanotube samples after surface treatment was confirmed by using Fourier Transformed Infrared Spectroscopy (FTIR). The wave number range during FTIR analysis was between  $400\text{ cm}^{-1}$  and  $4000\text{ cm}^{-1}$ . The analyses were performed by using a Shimadzu IRPrestige 21 spectrometer.

#### 3.4.4.2 X-Ray Diffraction Analysis

X-ray diffraction (XRD) patterns of carbon nanotube samples were obtained by using a twin tube X-ray diffractometer (Scintag XDS 2000 providing  $\text{CuK}\alpha$  radiation ( $\lambda=0.15418\text{ nm}$ ) at 45 kV and 40 mA.

#### 3.4.4.3 Suspension Stability Analysis of Carbon Nanotube Samples

Suspension stabilities of the carbon nanotube samples in acetone and ethyl alcohol (EA) were determined by sonicating the 0.05 g. carbon nanotubes in 5 ml. solvent for 60 minutes and taking the pictures of the suspensions during definite time intervals (after 5 minutes, 60 minutes, 240 minutes, 24 hours, 48 hours). The effect of surfactant usage on the stabilities of the suspensions was also investigated by preparing Triton X-100 and CPC assisted epoxy/CNT mixtures.

#### 3.4.4.4 Scanning Electron Microscopy and Optical Microscopy

The morphological analyses of the carbon nanotube samples and composites were performed by using a Scanning Electron Microscope (SEM) (Philips EDAX XLFEG). Moreover, dispersion homogeneities of the carbon nanotubes in epoxy/CNT composites were determined with optical microscopy (Nikon metallographs equipped with CCD cameras).

#### 3.4.4.5 Electrical Resistivity Measurements

The electrical resistivities of the composites were measured with two point probe method, which was connected to a Keithley 199 (Figure 3.12) constant current source meter. The measurements were performed by contacting the copper electrodes, which were embedded into samples before curing, to the probes of the source meter.



**Figure 3.12** A photograph of the Keithley 199 constant current source meter

#### 3.4.4.6 Tensile Tests

Tensile properties of the epoxy/CNT composites were investigated by using a MTS 810 universal tensile testing instrument (Figure 3.13), according to ASTM 638-03 standards. The specimens had a thickness of 2.7 mm, a width of 13 mm and a gauge length of 50 mm. According to the gauge length and a strain rate of  $0.1 \text{ min}^{-1}$ , the crosshead speed of testing instrument was selected as 5 mm/min. Tensile properties of the glass fiber reinforced composite panels were investigated according to the ASTM D3039 standards. The specimens had a thickness of 2.8 mm, a width of 25 mm and a gauge length of 155 mm. The crosshead speed of the testing instrument was selected as 2 mm/min. Five specimens of each sample were tested and the averages of these tests were reported with standard deviations (Appendix A, Tables A.7-A.9). All tensile strength and elongation values reported in the dissertation were measured at the break point.



**Figure 3.13** A photograph of the MTS 810 tensile testing instrument

#### 3.4.4.7 Fatigue Tests

The fatigue tests of the composite panels were also performed with MTS 810 universal tensile testing instrument at 10 Hz frequency. The dimensions of the specimens were the same as the dimensions of the tensile test samples. During the load cycles the ratio of the minimum load to maximum load was selected as 0.7 ( $R=0.7$ ) for all specimens.

#### 3.4.4.8 Impact Tests

The impact tests of the composite panels were conducted by using an Instron Dynatup 9250G instrument (Figure 3.14) according to the ASTM D7136 standards. The dimensions of the specimens were 80 mm width, 4 mm thickness and 130 mm length. During the tests the panels were impacted at 5 different energy levels (10J, 20J, 30J, 50J and 70J).



**Figure 3.14** A photograph of the Instron Dynatup 9250G impact tester

#### 3.4.4.9 Electro-Mechanical Tests

The electrical resistivity changes of the composite panels during the tensile, fatigue tests (Figure 3.15 (a)) and impact tests (Figure 3.15 (b)) were measured by two point probe method with the help of the copper electrodes which were placed on the edges, top and bottom surfaces of specimens (Figure 3.16). Silver paste was used in order to decrease the contact resistance between the copper electrodes and sample surface. The percent changes ( $\Delta R$ ) in the electrical resistivities of the specimens were calculated according to the relationship:

$$\Delta R = [(R_i - R_0) / R_0] \times 100 \quad (3.2)$$

where,  $R_0$  is the electrical resistivity measured between the electrodes before the tests and  $R_i$  is the electrical resistivity measured between the electrodes during and after the tests. The specimens for tensile and fatigue electro-mechanical tests have dimensions with a thickness of 2.8 mm, a width of 25 mm and a gauge length 155

mm. The dimensions of the specimens for impact electro-mechanical tests were 80 mm width, 4 mm thickness and 130 mm length.

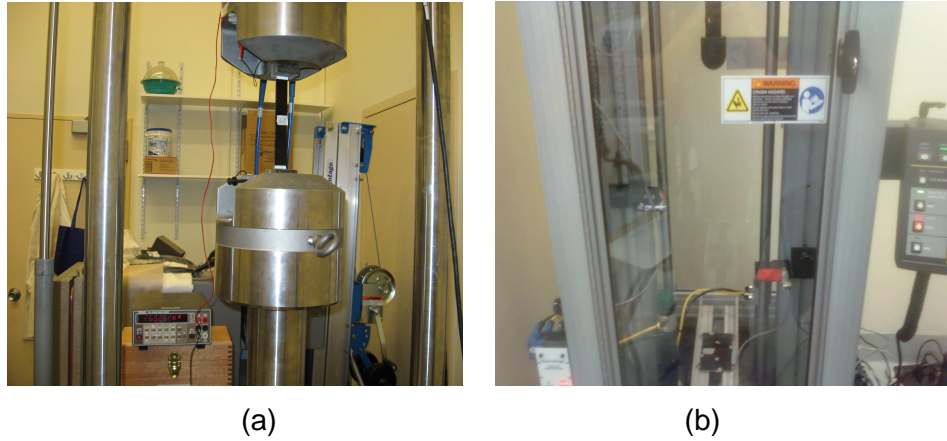


**Figure 3.15** Electro-mechanical tests (a) during tensile and fatigue tests, (b) during impact test

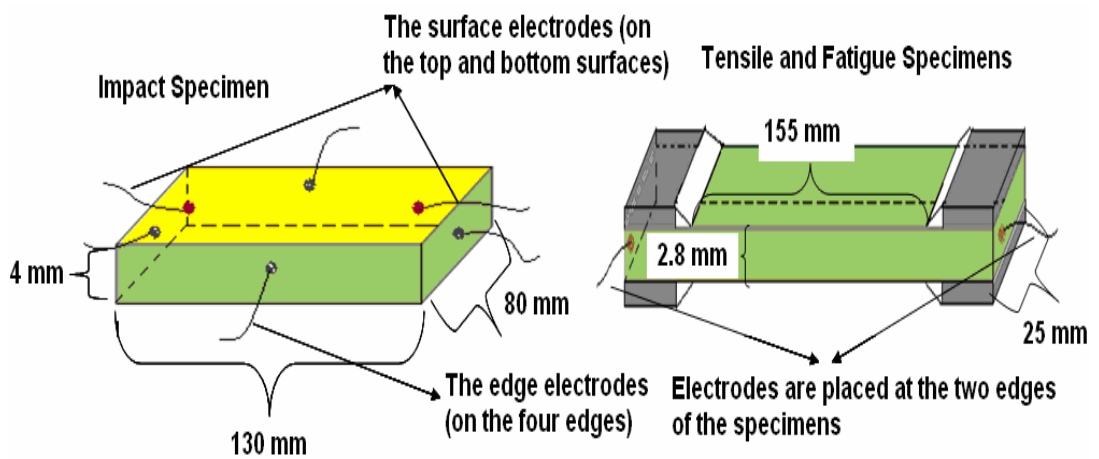


**Figure 3.16** Placement of the copper electrodes on the tensile, fatigue and impact specimens for the electro-mechanical tests

## CHAPTER 4

### RESULTS AND DISCUSSION

The main aim of this dissertation is to prepare conductive polymer composites with improved electrical and mechanical properties. For this purpose, carbon nanotube surface treatment and different processing methods were performed during the preparation of the composites. The results of these studies are explained in three main parts in this chapter. In the first part, characterization results of the carbon nanotube surface treatment and PET/CNT composites are explained. The second part contains the characterization results of the microfiber reinforced HDPE/PET/CNT composites. The final part includes the characterization results of the epoxy/CNT composites and epoxy/CNT/glass fiber composite panels.

#### 4.1 Surface Treatment of Carbon Nanotubes and Poly(ethylene terephthalate)/Carbon Nanotube Composites

Surface treatment studies of carbon nanotube and preparation of PET based composites will be explained in two subsections. In the first part, the characterization results of the carbon nanotube purification with strong acids, strong bases, with their mixtures and usage of these carbon nanotubes in the composites will be described. In the second part, the characterization results of surface modification of carbon nanotube with low molecular weight chemicals and PET/CNT composites prepared by using purified and modified carbon nanotubes will be explained.

#### 4.1.1 Purification of Carbon Nanotubes and Poly(ethylene terephthalate)/Carbon Nanotube Composites

The results of the characterization experiments of the purified carbon nanotube and PET/CNT conductive polymer composite samples will be explained in this section of the dissertation.

##### 4.1.1.1 Surface Energy Measurements of Carbon Nanotubes

The alteration in the surface properties and creation of new functional groups on the surface of carbon nanotubes directly change the contact angles between the carbon nanotube surface and probe liquids due to the differences in the carbon nanotube surface wettings by probe liquids. This change differ the surface energy components (Equations 2.3-2.5) of purified carbon nanotubes with respect to each other and when compared to ASCNT (Table 4.1). Acidic component ( $\gamma_{\text{Solid}}^{\text{A}}$ ) of the surface energy increases as the treatment time increases in  $\text{HNO}_3/\text{H}_2\text{SO}_4$  (1:3) mixture (CNT 1-4), due to the acidic carboxyl groups formed on the carbon nanotube surface during acid treatment [178]. The formation of these groups is also observed in the FTIR and ESCA spectra of carbon nanotubes. 15 minutes of purification seem to be short for the formation of new functional groups on carbon nanotube surface, since no significant change in the polar components of surface energy is observed for CNT1. On the other hand, the acidic component of CNT4 is nearly two times that of ASCNT. Total surface energy of carbon nanotubes ( $\gamma_{\text{Solid}}$ ) remain constant, while basic component ( $\gamma_{\text{Solid}}^{\text{B}}$ ) decreases with rising treatment time due to the growing number of oxygen containing carboxylic acid functional groups present on the surface [178]. Sulfuric acid is a strong acid, and an oxidizing agent. The main contribution, for the formation of carboxyl and hydroxyl functional groups on the surface, is from  $\text{H}_2\text{SO}_4$  in acidic mixture, since the acidic component of the surface energy decreases as  $\text{H}_2\text{SO}_4$  concentration in the  $\text{HNO}_3/\text{H}_2\text{SO}_4$  mixtures descends (CNT2, CNT5, and CNT6).

After basic purification with  $\text{NH}_4\text{OH}$  (CNT7) basic component of the surface energy ascends much when compared to that of ASCNT. However purification with

NH<sub>4</sub>OH/H<sub>2</sub>O<sub>2</sub> mixture does not cause an increase in the basic component of the surface energy, and the polar component of the CNT8 is the lowest among all the purified carbon nanotube types in this study due to the deficient sonication time to form the chemical groups on carbon nanotube surface in a less oxidative basic purification medium. The dispersive component of the surface energy ( $\gamma_{\text{Solid}}^{\text{d}}$ ) of purified carbon nanotubes are lower than that of ASCNT (except CNT3 and CNT5), which may arise from the decrease in the effective surface area of carbon nanotubes after surface treatment [179].

**Table 4.1** Surface energy components of the as-received and purified carbon nanotube samples (mN/m)

Code of Material	Treatment Parameters	$\gamma_{\text{Solid}}$	$\gamma_{\text{Solid}}^{\text{d}}$	$\gamma_{\text{Solid}}^{\text{p}}$	$\gamma_{\text{Solid}}^{\text{A}}$	$\gamma_{\text{Solid}}^{\text{B}}$
ASCNT	-	46.14	35.67	10.47	2.17	12.62
	HNO <sub>3</sub> /H <sub>2</sub> SO <sub>4</sub>					
CNT1	(1:3) (15 min.)	41.31	31.76	10.55	2.23	12.48
	HNO <sub>3</sub> /H <sub>2</sub> SO <sub>4</sub>					
CNT2	(1:3) (30 min.)	48.32	35.44	12.88	3.73	11.35
	HNO <sub>3</sub> /H <sub>2</sub> SO <sub>4</sub>					
CNT3	(1:3) (60 min.)	47.29	35.92	11.37	3.82	8.47
	HNO <sub>3</sub> /H <sub>2</sub> SO <sub>4</sub>					
CNT4	(1:3) (120 min.)	43.98	33.21	10.77	4.05	7.16
	HNO <sub>3</sub> /H <sub>2</sub> SO <sub>4</sub>					
CNT5	(1:1) (30 min.)	47.67	35.70	11.97	3.24	11.07
	HNO <sub>3</sub> /H <sub>2</sub> SO <sub>4</sub>					
CNT6	(3:1) (30 min.)	44.71	32.24	12.47	3.04	12.80
	NH <sub>4</sub> OH					
CNT7	(30 min.)	45.04	31.56	13.48	2.23	20.38
	NH <sub>4</sub> OH/H <sub>2</sub> O <sub>2</sub>					
CNT8	(1:1) (30 min.)	42.23	31.96	10.27	2.29	11.53

#### 4.1.1.2 Fourier Transformed Infrared Spectroscopy of Carbon Nanotubes

Figure 4.1 displays the FTIR spectra of ASCNT and purified carbon nanotubes. There are certain peaks in the FTIR spectra of all the carbon nanotube samples which belong to the carbon nanotube phonon modes and these peaks are observed at the same wave number for all of the samples. As reported before in the literature the bands at  $2912\text{ cm}^{-1}$  can be discounted as being due to  $\text{CH}_2$  stretching and observed in all carbon nanotube samples [38]. The peak at  $1500\text{ cm}^{-1}$  might be attributed to aromatic  $\text{C}=\text{C}$  stretching [7]. The peaks at  $1571$  and  $1602\text{ cm}^{-1}$  are the characteristic stretching vibrations of  $\text{C}-\text{C}$  bonds related to the expected carbon nanotubes phonon modes [13, 38]. Small peaks at  $1080\text{ cm}^{-1}$  and  $3440\text{ cm}^{-1}$  indicate the presence of  $-\text{OH}$  groups on the surface and it is an evidence for the presence of hydroxyl functional groups in carbon nanotube surface before any surface treatment [13]. The peak at  $2370\text{ cm}^{-1}$  is also observed for all samples and it represents the  $\text{CO}_2$  absorption in air.

Purification with strong acids and bases cause some changes in FTIR spectra of the samples. Some new peaks appear and intensities of some peaks increase. After purification, the presence of peaks at around  $1180$  and  $1718\text{ cm}^{-1}$  corresponding to the stretching modes of the carboxylic acid groups [180, 181],  $1637\text{ cm}^{-1}$  corresponding to the H-bonded carbonyl groups ( $\text{C}=\text{O}$ ) that conjugate with ( $\text{C}=\text{C}$ ) in the graphene wall, indicate the formation of carboxylic acid ( $\text{COOH}$ ) functional groups on carbon nanotubes surface. Also the peaks around  $1240$ ,  $1740$  and  $1427\text{ cm}^{-1}$  can be attributed to  $\text{C}-\text{N}$  stretching vibrations [32, 34],  $\text{C}=\text{O}$  stretching mode and  $\text{C}-\text{H}$  bending vibrations [34]. It is observed that at certain purification conditions, the intensities of the peaks corresponding to carboxyl and hydroxyl groups generally become higher (CNT 2-5), which might be stated as these purifications are more effective than the rest of the purification procedures in terms of carbon nanotube surface treatment and formation of functional groups on the carbon nanotube surface.

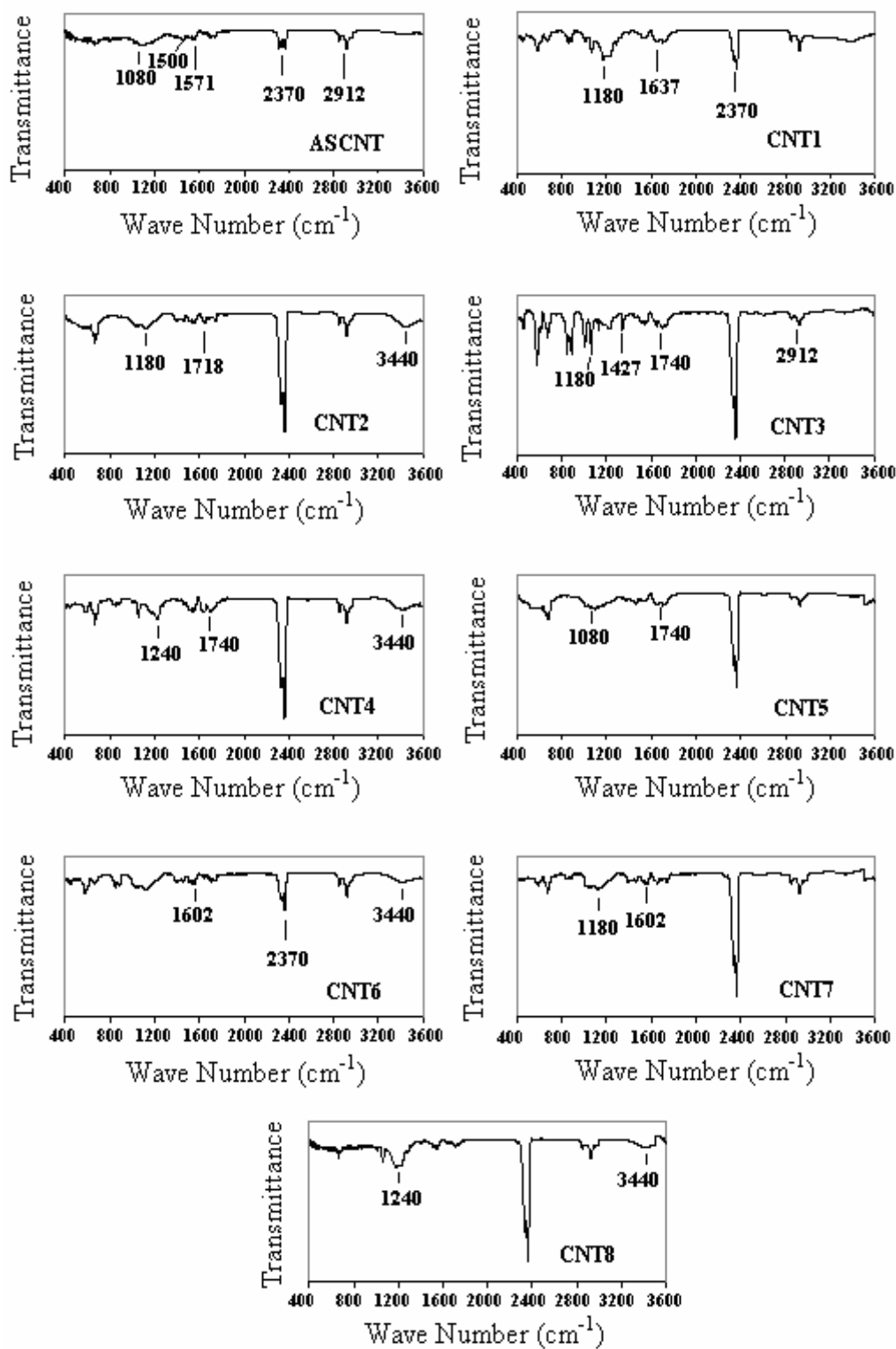


**Figure 4.1** FTIR spectra of as-received and purified carbon nanotube samples

#### 4.1.1.3 Electron Spectroscopy for Chemical Analysis of Carbon Nanotubes

ESCA spectra of ASCNT and purified carbon nanotubes are shown in Figure 4.2. O1s spectrum of ASCNT is fitted to two peaks corresponding to metal oxides (Oxygen atoms bonded to the metallic catalyst residues present on the carbon nanotube) [182], C=O or C-O and to a small peak corresponding to oxygen from adsorbed H<sub>2</sub>O, which can be stated as a small amount of oxygen is present on the carbon nanotubes surface in different chemical structures before any surface treatment [183]. After purification, O1s spectra of purified carbon nanotubes are fitted to peaks for C=O, C-O, C-O-C, OH, O-C=O and hydroxide or carbonate bound to NH<sub>4</sub> types of oxygen generally, which can explain the oxidation effect of the purification mediums and formation of carboxyl and hydroxyl groups on the carbon nanotubes surface. These functional groups are beneficial in terms of increasing the chemical compatibility between carbon nanotube and poly(ethylene terephthalate) (PET). Some of the hydroxyl groups present on carbon nanotube surfaces might be attributed to water contamination results from the washing of carbon nanotubes with distilled water after purification. The peaks appeared in the ESCA spectra and the chemical structures corresponding to these peaks for all carbon nanotube samples are explained in Table 4.2.

Intensities (electron counts) of the peaks in the O1s spectra of purified carbon nanotube samples are higher than that of ASCNT, which indicate the increase in the number of oxygen containing functional groups on the carbon nanotube surface. This result figures out that, purification with acids and bases are successful in terms of formation of hydroxyl and carboxyl based functional groups on the surfaces of carbon nanotubes [182]. Moreover, increment in purification duration for HNO<sub>3</sub>/H<sub>2</sub>SO<sub>4</sub> (1:3) mixture, results in an increase in the intensities of the peaks in O1s spectrum of carbon nanotube samples (CNT 1-4), which indicates the higher oxidation occurring at longer purification periods. On the other hand any decrease in the H<sub>2</sub>SO<sub>4</sub> content of the acidic purification medium (CNT2, CNT5 and CNT6) descend the intensities of the peaks, due to the less effective oxidation. The carbon-nitrogen interactions which are observed in FTIR spectra (Figure 4.1) is also seen in the ESCA spectra as hydroxide or carbonate bound to NH<sub>4</sub>. This confirms the presence of nitrogen based chemical groups on the surfaces of carbon nanotubes.

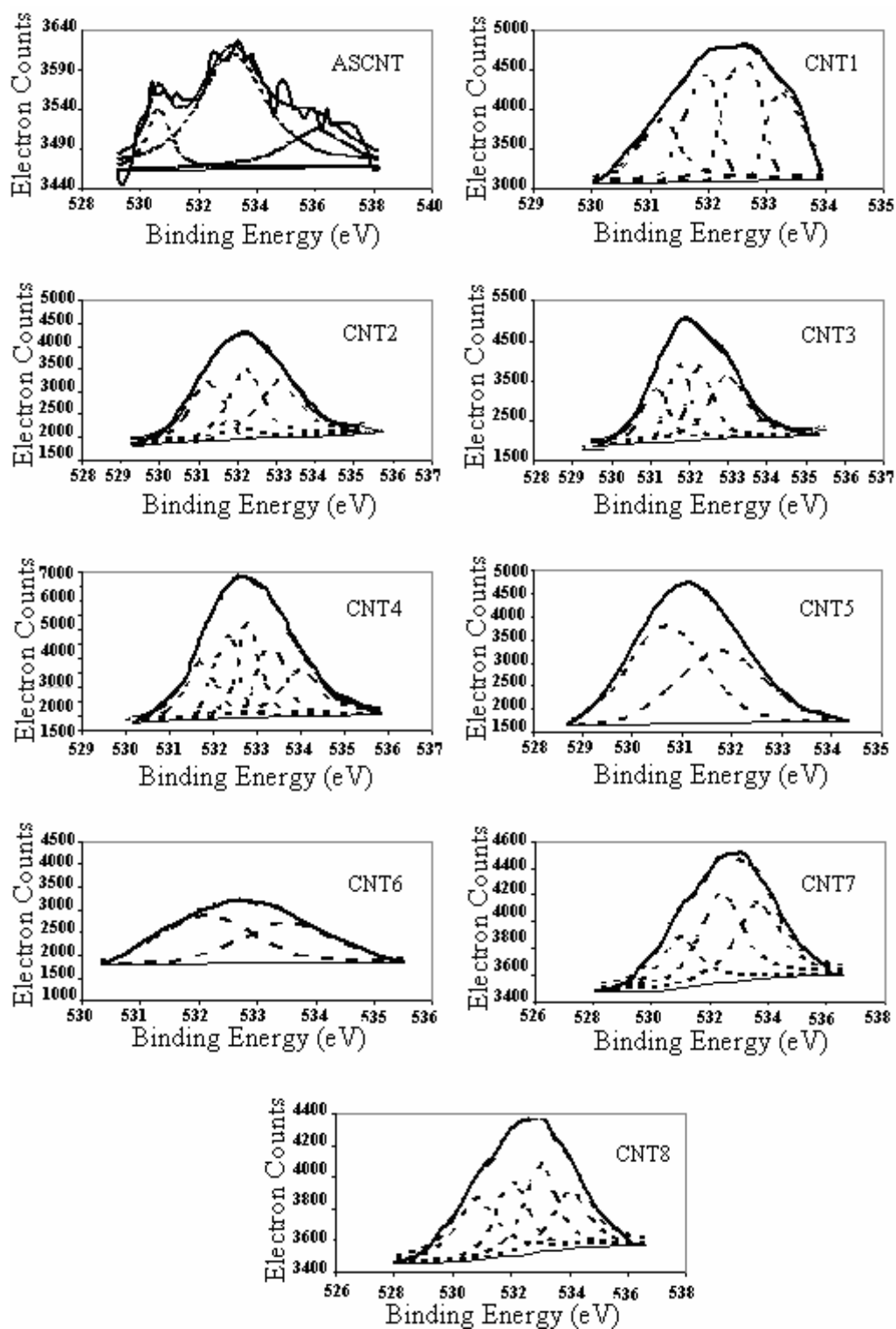


**Figure 4.2** ESCA O1s spectra of as-received and purified carbon nanotube samples

**Table 4.2** Peaks and chemical structures corresponding to these peaks in ESCA O1s spectra and oxygen to carbon (O/C) ratios of as-received and purified carbon nanotube samples

<b>Code of Material</b>	<b>Peaks (eV)</b>	<b>O/C ratio</b>
<b>ASCNT</b>	530.4: Oxygen bonded to the metallic catalyst residues, 532.9: C=O or C-O, 535.9: Oxygen from adsorbed H <sub>2</sub> O	0.03
<b>CNT1</b>	531.1: C=O, 531.8: OH, 532.6: C=O or C-O 533.4: C-O-C	0.22
<b>CNT2</b>	531.6: OH, 532.6: C=O or C-O, 533.5: C-O-C 532.1: C=O, O-C=O and C=O (esters, anhydrides)	0.51
<b>CNT3</b>	531.8: OH, 532.5: C=O or C-O, 533.4: C-O-C	0.54
<b>CNT4</b>	531.7: OH, 532.8: C=O, 533.4: C-O-C, 534.1: C-O 532.2: C=O, O-C=O and C=O (esters, anhydrides)	0.97
<b>CNT5</b>	530.8: Hydroxide or carbonate bound to NH <sub>4</sub> 532.1: C=O, O-C=O and C=O (esters, anhydrides)	0.33
<b>CNT6</b>	532.1: C=O, O-C=O and C=O (esters, anhydrides) 533.4: C-O-C	0.10
<b>CNT7</b>	530.8: Hydroxide or carbonate bound to NH <sub>4</sub> , 533.3: C-O-C 532.1: C=O, O-C=O and C=O (esters, anhydrides)	0.06
<b>CNT8</b>	530.8: Hydroxide or carbonate bound to NH <sub>4</sub> , 531.8: OH, 532.7: C=O or C-O, 533.7: C-O-C	0.04

Basic purification results in the formation of oxygen based chemical groups on the surface of carbon nanotube to a certain extent. However this formation is more effective in acidic treatment than the basic one, since intensities of the peaks in the CNT7 and CNT8 O1s spectra are lower than those of carbon nanotubes purified by using acids. Oxygen to carbon ratios (O/C) on the surface of the carbon nanotube samples, are calculated by taking the ratio of the areas under the O1s and C1s curves in ESCA spectra for each sample [183] and are shown in Table 4.2. The areas under the O1s and C1s curves are determined by integrating the wide scan ESCA spectra data of the each carbon nanotube sample (Appendix B). These

ratios also reveal the oxidation efficiency of the different purification conditions. Oxygen to carbon ratio increases enormously with increasing treatment time for HNO<sub>3</sub>/H<sub>2</sub>SO<sub>4</sub> (1:3) mixture. In addition, a decrease in H<sub>2</sub>SO<sub>4</sub> content of the acidic purification mixture results in a sharp decrease in oxygen to carbon ratio of carbon nanotube samples (CNT2, CNT5, and CNT6). Basic purifications increased oxygen to carbon ratio on the surface slightly, when compared to ASCNT. Apart from ASCNT, no peaks for metal oxides were observed in ESCA spectra of the samples, which mean that the catalyst residues were removed successfully during purification.

#### 4.1.1.4 X-Ray Diffraction and Scanning Electron Microscopy Analyses of Carbon Nanotubes

Figure 4.3 shows the XRD patterns of as-received and purified carbon nanotubes. It can be seen that, XRD patterns of ASCNT and purified carbon nanotubes are similar to each other, which means that the purified carbon nanotubes have the same graphitic cylinder wall structure with as received carbon nanotubes [184]. However, there are some changes in the crystalline structure of the carbon nanotubes after purification. The small changes in the interplanar spacing between the carbon nanotube aggregates ( $d_{002}$ ) (Equation 2.20) (Table 4.3) of purified carbon nanotubes do not cause a significant change in the position of the characteristic peak at around 26°. Also, this peak is sharper for ASCNT than those of the purified carbon nanotube samples (CNT 2-4). The change in the sharpness of this peak is due to the damage in the crystalline constitution of the samples. Purification conditions which are more effective in terms of carbon nanotube oxidation infest the crystallinity of carbon nanotubes. As the purification period for HNO<sub>3</sub>/H<sub>2</sub>SO<sub>4</sub> (1:3) mixture increase the sharpness of the peak decrease due to the longer exposure of carbon nanotubes to severe acidic conditions [171]. The crystallite length ( $L_c$ ) (Equation 2.21) and interplanar spacing between the carbon nanotube aggregates ( $d_{002}$ ) are not calculated for the samples CNT 2-4. The main peaks at 26° are very broad for these samples which indicate the increase in the disordered amorphous carbon content of the carbon nanotube samples. Therefore, it is meaningless to apply the calculation methods, which are used for the ordered

graphitic structures, to the CNT 2-4 samples. Since the crystalline constitution is important for final electrical and mechanical properties of carbon nanotubes and composites based on these carbon nanotubes [16], there should be a balance between the carbon nanotube surface oxidation and the preservation of crystalline structure. Besides, purification with acidic mixtures which contains lower amount of  $H_2SO_4$  (CNT5 and CNT6) and bases (CNT7 and CNT8) do not cause a significant change in crystallite length of carbon nanotubes, due to more applicable treatment conditions.

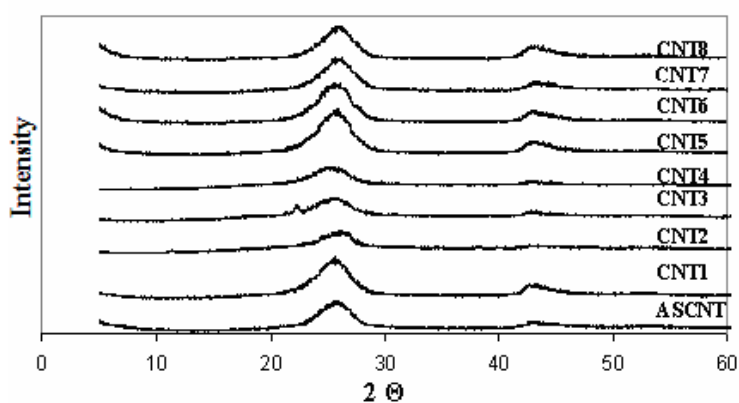


**Figure 4.3** XRD patterns of as-received and purified carbon nanotube samples

**Table 4.3** Interplanar spacings ( $d_{002}$ ) (Å) and crystallite lengths ( $L_c$ ) (Å) of as-received and purified carbon nanotube samples

Code of Material	$2\theta$	B	$d_{002}$	$L_c$
ASCNT	25.98	2.74	3.43	0.51
CNT1	25.44	3.00	3.50	0.48
CNT5	25.94	2.94	3.44	0.48
CNT6	25.54	2.82	3.48	0.50
CNT7	25.72	2.77	3.46	0.49
CNT8	25.76	2.80	3.45	0.50

The change in the structure of the carbon nanotube samples due to rough purification can also be observed in SEM micrographs (Figure 4.4). Micrograph of ASCNT showed that carbon nanotubes are randomly entangled in untreated carbon nanotube. 120 minutes purified carbon nanotubes in  $\text{HNO}_3/\text{H}_2\text{SO}_4$  (1:3) mixture (CNT4) has a more compact morphology in which tubes are joined to each other due to the dissolution of carbon nanotube bundles in purification medium, when compared to that of ASCNT. On the other hand, SEM micrographs of the other purified carbon nanotube samples resemble that of ASCNT.

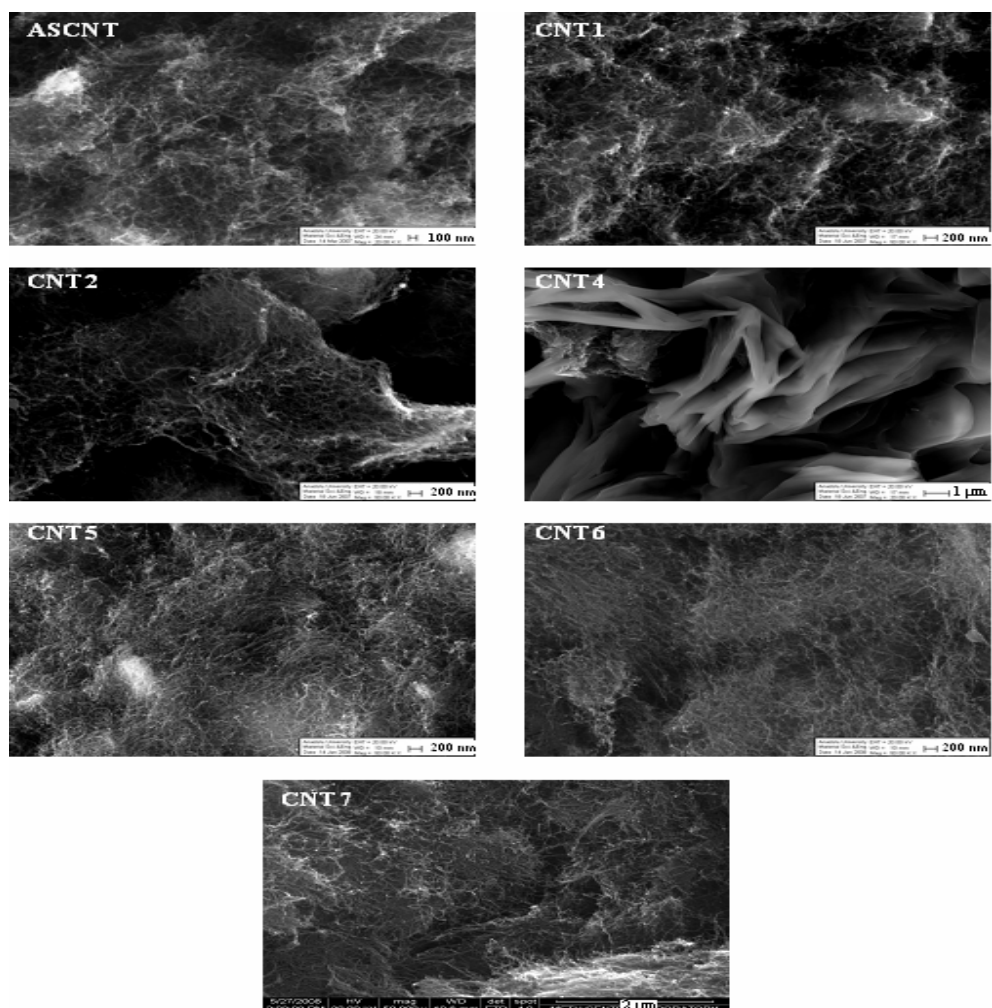


**Figure 4.4** SEM micrographs of selected as-received and purified carbon nanotube samples

#### 4.1.1.5 Electrical Resistivity Measurements of Composites

Characterization experiments of the as-received and purified carbon nanotube samples showed the differences of carbon nanotubes in terms of surface properties and morphology with each other. After the characterization of carbon nanotube samples, PET/CNT composites based on as-received and purified carbon nanotubes were characterized in terms of electrical resistivity, mechanical properties and morphology. Electrical resistivity values of PET/CNT composites are shown in Figure 4.5. Electrical resistivity values of all composites are below  $10^4$  ohm.cm, which confirm that, the carbon nanotube concentration (0.5 wt. %) in the composites is higher than the percolation threshold concentration since electrical resistivity values of all composites already outgone from insulator range to semiconductor region. At the percolation threshold the formation of conductive carbon nanotube networks occur, the conductive filler particles can contact each other and conduct the electrical current throughout the composite [4].

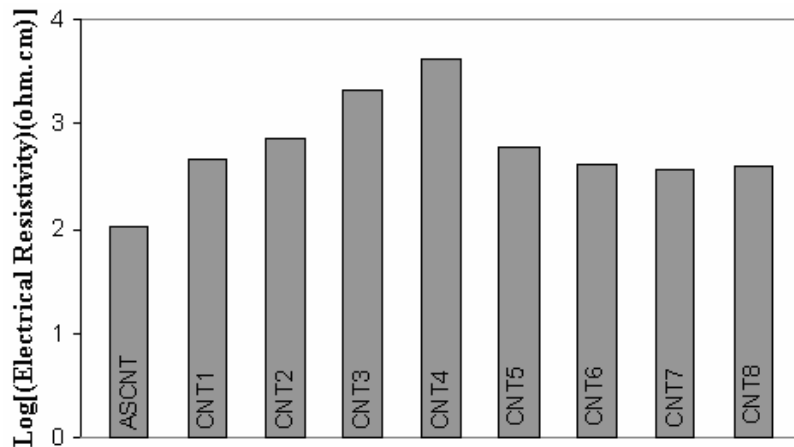


**Figure 4.5** Electrical resistivity values of PET/CNT composites prepared with as-received and purified carbon nanotubes

Electrical resistivity values of the composites including purified carbon nanotubes are higher than that of PET/ASCNT composite. There might be several reasons for

this consequence. After purification, carboxyl and hydroxyl groups (Table 4.2) present on the carbon nanotube surface may increase the intrinsic electrical resistivity of the individual carbon nanotube, due to the electrically insulating oxide layer, resulted from the oxidation of carbon based structures. When these purified carbon nanotubes are incorporated in a polymer matrix, this insulating region on the surface limits the transportation of electrons effectively at the carbon nanotube contact points and this increase the electrical resistivities of the composites [32, 37]. Composite which is prepared with CNT2 has higher electrical resistivity when compared to those of the composites based on CNT5 and CNT6, due to the more effective oxidation during purification (Figure 4.2). Purification with base mixtures results in the lowest electrical resistivity among the composite systems based on purified carbon nanotubes, as a result of the lower oxygen content on carbon nanotube surface (Table 4.2).

Purification with strong acids damages the crystalline structure of carbon nanotube and this also decreases the intrinsic electrical conductivity of individual carbon nanotube [48]. XRD patterns of carbon nanotube samples reveal this damage in crystalline structure (Figure 4.3) and this destruction ascend as the purification time increase in  $\text{HNO}_3/\text{H}_2\text{SO}_4$  (1:3) mixture (Table 4.3). As a result of these damages in carbon nanotube structure, electrical resistivity values of the composites based on purified carbon nanotubes increase as the chemical treatment time gets longer. There is an approximately ten-fold difference between the electrical resistivity values of PET/CNT1 and PET/CNT4 composites.

Interactions between carbon nanotubes and PET increase after purification, due to the presence of functional groups on the surfaces of carbon nanotubes. Carboxyl and hydroxyl functional groups on the surfaces of carbon nanotubes can interact with the reactive end groups of PET. This might be another reason for the decrease in this electrical conductivity of the composites including purified carbon nanotubes [185]. Advanced reactivity between carbon nanotubes and PET can increase the wetting of carbon nanotubes by PET and improve the dispersion of carbon nanotube particles in the polymer matrix. Conductive nanotube particles can be surrounded by insulating polymer matrix easily as the interactions between filler and polymer increase. At this point, the polymer phase have the same function with the insulating oxide layer and it decreases the conductivity of the

composite, since it descends the number of contact points between the conductive filler particles [186].

#### 4.1.1.6 Tensile and Impact Tests of Composites

The reinforcement effect of the carbon nanotube particles in the polymer composites depends on four main points. These are large aspect ratio, good dispersion, alignment and effective load transfer from polymer to carbon nanotube at the interphase. Among these four main factors, the most important one for carbon nanotube reinforcement in the composite is that external stresses applied to the composite are efficiently transferred to the carbon nanotubes [26]. In other words the mechanical properties of the polymer composites strongly depend on the extent of the interfacial interactions between the polymer matrix and the filler.

Carbon nanotube is a very strong material with an ultimate tensile strength and modulus [43]. However, PET/CNT composites generally suffer from the weak mechanical properties due to the poor dispersion capability and interfacial adhesion of carbon nanotubes in the polymer matrix [22]. A sharp decrease in the tensile strength value of the PET based composite with respect to neat PET can be observed after the addition of ASCNT (Figure 4.6). This reduction can be explained in terms of the weak interfacial adhesion between PET and inert carbon nanotube surface, which causes debonding and pull outs of carbon nanotubes from the surrounding matrix [7]. Also, poor dispersion and agglomeration of carbon nanotube particles in the polymer matrix, due to the incompetent shear applied during extrusion as a result of the low melt viscosity of PET might cause the noticeable decrease in tensile strength. Carbon nanotube addition into PET improves the tensile modulus due to the reinforcement effect of rigid fibrillar particles with high aspect ratio (Figure 4.7) [187]. However, this enhancement is limited in the PET/ASCNT composite due to the reasons which are discussed above. Tensile strength, modulus and impact strength values of the composites prepared with purified carbon nanotubes are higher than those of the PET/ASCNT composite (Figures 4.6, 4.7 and 4.8). Oxygen containing carboxyl and hydroxyl groups and defect sites on the carbon nanotube surface increase the mechanical

interlocking and covalent bonding between carbon nanotubes and the PET matrix. These interactions between composite constituents improve the efficiency of load transfer from the PET to carbon nanotubes [188].

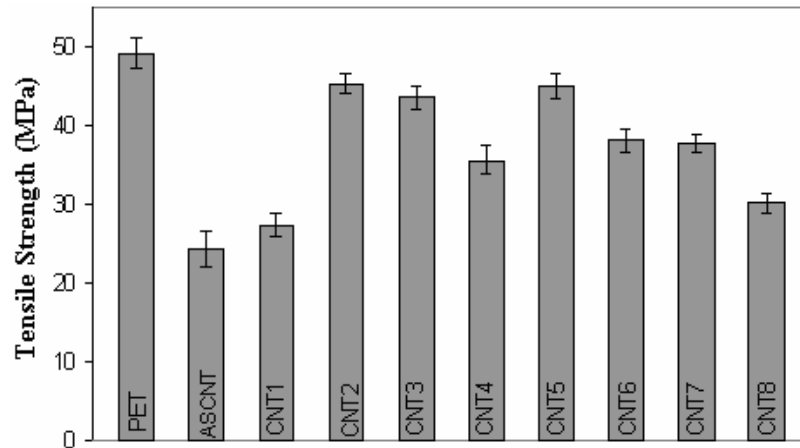


**Figure 4.6** Tensile strength values of neat PET and PET/CNT composites prepared with as-received and purified carbon nanotubes

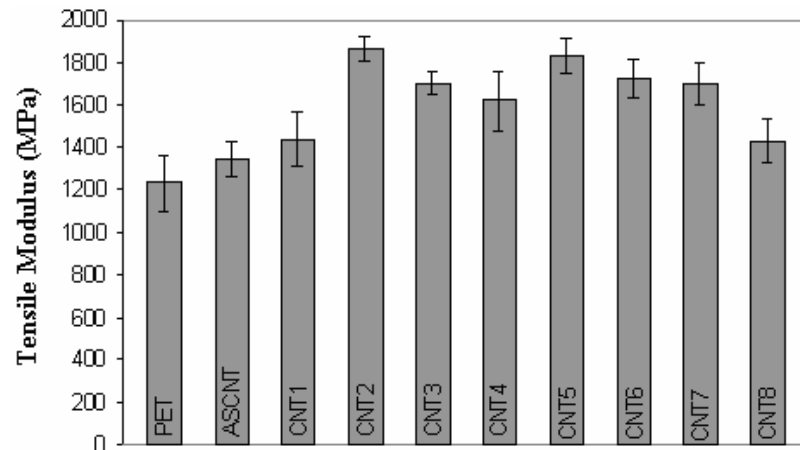


**Figure 4.7** Tensile modulus values of neat PET and PET/CNT composites prepared with as-received and purified carbon nanotubes

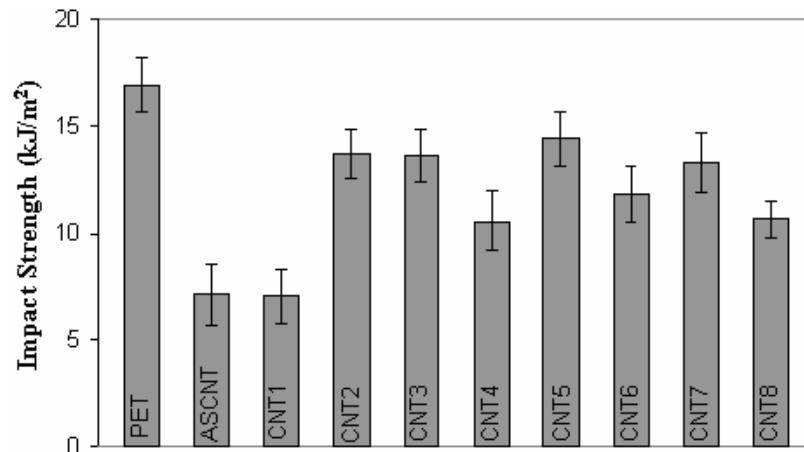


**Figure 4.8** Impact strength values of neat PET and PET/CNT composites prepared with as-received and purified carbon nanotubes

Tensile strength of the composite based on CNT2 show a maximum and as the sonication time is increased in  $\text{HNO}_3/\text{H}_2\text{SO}_4$  (1:3) purification medium, a decrease in these properties is observed due to the breakdown in the crystalline structure which is observed in X-Ray and SEM analysis (Table 4.3 and Figure 4.4). PET/CNT3 and PET/CNT4 composites have lower tensile strength and modulus values when compared to CNT2 filled composite. Damages in the graphitic wall structures of carbon nanotubes decrease the bulk mechanical properties. These directly affect the tensile and impact properties of the polymer composites [26]. Moreover, any decrease in the  $\text{H}_2\text{SO}_4$  concentration of the acidic purification mixture causes a reduction in the tensile strength and modulus of the composites slightly. Tensile and impact strength values of the composites based on CNT2 and CNT5 are close to each other. The oxygen content on the surface of carbon nanotubes are higher for CNT2 (Table 4.2), but the damage in the crystalline structure is lower for CNT5 (Table 4.3). These two factors balances each other and similar mechanical properties are observed for PET/CNT2 and PET/CNT5 composites. However, CNT6 based composite has lower strength values when compared to PET/CNT2 and PET/CNT5 composites due to the lower oxygen content of the surfaces of carbon nanotubes (Table 4.2). Basic purification could not improve the mechanical properties as much as acidic purification do, due to the limited oxidation of carbon nanotubes and chemical compatibility between

composite constituents which decrease the degree of stress transfer in the composite.

#### 4.1.1.7 Scanning Electron Microscopy of Composites

The distribution of carbon nanotubes and their particle size play a distinct role in the determination of electrical and mechanical properties of the composites [187]. Surface treatment helps the carbon nanotube dispersion in the composite due to the ionic repulsions between the chemical groups on the surface and better interfacial adhesion between PET and carbon nanotube. The composite containing ASCNT appears to have less homogeneous carbon nanotube dispersion with larger carbon nanotube agglomerates observable on the fracture surface when compared to the composite based on CNT2 (Figure 4.9).

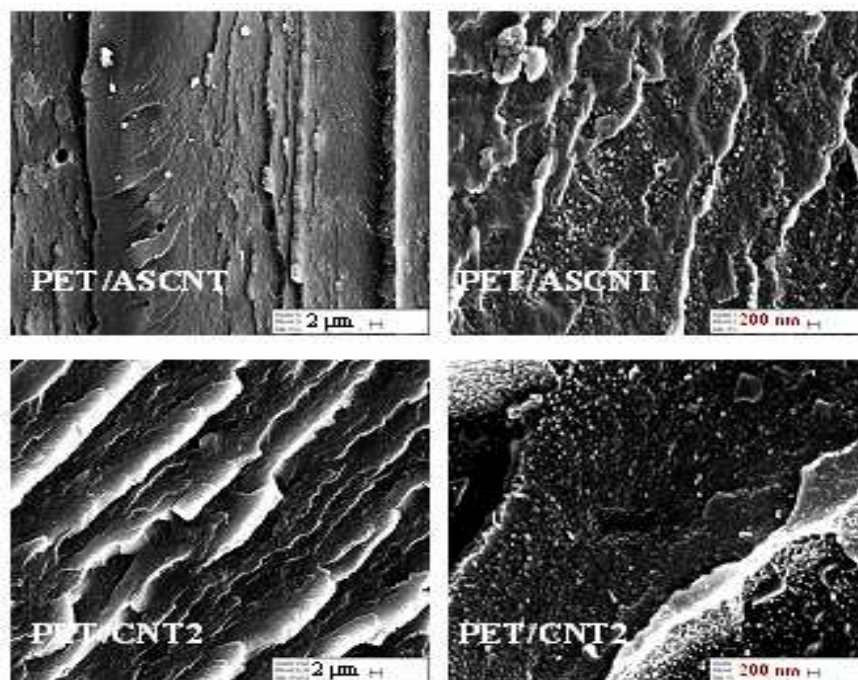


**Figure 4.9** SEM micrographs of PET/ASCNT and PET/CNT2 composites

#### 4.1.2 Surface Modification of Carbon Nanotubes and Poly(ethylene terephthalate)/Carbon Nanotube Composites

General procedure of the carbon nanotube surface modification consists of two consecutive steps. The first step is the purification (oxidation) of carbon nanotubes. The second step is the treatment of the purified carbon nanotubes with low molecular weight chemicals. The details of the characterization experiments performed in the purification step explained in the previous section. The present part of the dissertation deals with the characterization results of the surface treated carbon nanotubes and PET/CNT composites based on these carbon nanotubes.

##### 4.1.2.1 Surface Energy Measurements of Carbon Nanotubes

Surface energy components of carbon nanotubes are given in Table 4.4. The surface energy components of purified and surface treated carbon nanotubes are different from each other and ASCNT. After purification with the strong acid mixture ( $\text{HNO}_3/\text{H}_2\text{SO}_4$  (1:1) (30 min.) (CNT5)), acidic component ( $\gamma_{\text{Solid}}^{\text{A}}$ ) of the surface energy increases due to the formation of carboxyl (COOH) groups on carbon nanotubes [178]. The dispersive component of the total surface energy ( $\gamma_{\text{Solid}}^{\text{d}}$ ) of purified carbon nanotubes is lower than that of ASCNT. Surface treatment with SDS does not cause a significant change in the surface energy components of pCNT (CNT5) owing to the lower extent of interactions between the surfaces of carbon nanotubes and SDS. The reactions between the carboxyl, hydroxyl groups on purified carbon nanotube surface and the reactive groups of the surface modifiers might cause a significant change in the surface energy components of carbon nanotube samples [189]. After surface treatments with PEG and DGEBA, total surface energies of carbon nanotube samples ( $\gamma_{\text{Solid}}$ ) are higher when compared to those of the other samples. PEG treatment results in a sharp increase in the basic component of polar surface energy ( $\gamma_{\text{Solid}}^{\text{B}}$ ) due to the reactions of carboxyl groups on surfaces of carbon nanotubes with hydroxyl end groups of PEG. Higher basic component of polar surface energy in PEG1000CNT sample when compared to PEG400CNT sample shows more effective coverage of the surfaces of carbon nanotubes with the modifier. The distinct changes in polar

component of total surface energy ( $\gamma_{\text{Solid}}^{\text{p}}$ ) and acidic component of polar surface energy ( $\gamma_{\text{Solid}}^{\text{A}}$ ) after DGEBA treatment showed that the functional group in epoxide parts of the modifier can react with pCNT and attach to the carbon nanotube surface. Surface treatments with PEG and DGEBA increase the work of adhesion values (Equation 2.8) when compared to ASCNT and pCNT (Table 4.4), which show that the possible chemical interactions between PET and carbon nanotubes ascend theoretically after modification [158, 190]. Moreover, the attachment of surface modifiers on carbon nanotube surface might improve the mechanical interlocking between carbon nanotube sidewalls and PET which can also enhance the interfacial adhesion in the composite.

**Table 4.4** Surface energy components of carbon nanotube samples and work of adhesion values between carbon nanotubes and PET (mN/m)

<b>Code of Material</b>	$\gamma_{\text{Solid}}$	$\gamma_{\text{Solid}}^{\text{d}}$	$\gamma_{\text{Solid}}^{\text{p}}$	$\gamma_{\text{Solid}}^{\text{A}}$	$\gamma_{\text{Solid}}^{\text{B}}$	$W_a$
<b>ASCNT</b>	46.14	35.67	10.47	2.17	12.62	85.16
<b>pCNT</b>	46.67	34.70	11.97	3.24	11.07	85.60
<b>SDSCNT</b>	46.18	34.45	11.73	3.16	10.89	84.10
<b>DGEBACNT</b>	55.50	39.2	16.30	4.63	14.35	91.80
<b>PEG400CNT</b>	51.01	38.8	12.21	2.14	17.44	90.64
<b>PEG1000CNT</b>	52.28	40.1	12.18	1.78	20.87	92.96

#### 4.1.2.2 Quantitative Assessment of Carboxylic Acid Groups Analysis on Carbon Nanotubes

The results of the quantitative assessment of carboxylic acid groups on carbon nanotube samples are given in Table 4.5 (Equation 3.1). ASCNT has very low amount of carboxyl groups on its surface when compared to purified and treated carbon nanotubes. After purification, concentration of carboxyl groups increases approximately ten times due to the oxidation with strong acids. Surface treatment

decreases the number of carboxylic acid groups on the surface enormously due to the consumption of these groups during reactions between modifiers and carbon nanotubes. The differences in the carboxylic acid group concentrations reveal the efficiency of surface modifications [66]. Reactive hydroxyl and epoxide groups in the structure of PEG and DGEBA possibly react more rapidly with carboxyl groups and make the attachment of these polymers on carbon nanotube surface easier. Modification with PEG1000 results in lower carboxylic acid group concentration when compared to PEG400 due to the better attachment of surface modifier on carbon nanotube surface. Treatment with SDS does not alter the carboxylic acid group concentration significantly due to the lower extent of interactions between SDS and pCNT.

**Table 4.5** Results of the titrations for carboxylic acid groups assessment

<b>Code of Material</b>	<b>V<sub>NaOH</sub> (ml)</b>	<b>V<sub>HCl</sub> (ml)</b>	<b>[COOH] (mol COOH/g nanotube)</b>
<b>ASCNT</b>	50	48	$2.0 \times 10^{-4}$
<b>pCNT</b>	50	25	$2.5 \times 10^{-3}$
<b>SDSCNT</b>	50	27	$2.3 \times 10^{-3}$
<b>DGEBACNT</b>	50	47	$3.0 \times 10^{-4}$
<b>PEG400CNT</b>	50	43	$7.0 \times 10^{-4}$
<b>PEG1000CNT</b>	50	47	$3.0 \times 10^{-4}$

#### 4.1.2.3 Fourier Transformed Infrared Spectroscopy of Carbon Nanotubes

FTIR is the fundamental tool to analyze surface chemistry and the unknown chemical bonding of functional groups of carbon nanotube samples [191]. Figure 4.10 displays the FTIR spectra of carbon nanotube samples. Peaks at  $1080 \text{ cm}^{-1}$  and  $3440 \text{ cm}^{-1}$  indicate the presence of  $-\text{OH}$  (hydroxyl) groups on the surface and it is an evidence for the presence of functional groups on the surface of carbon nanotube before any surface treatment [13]. After purification and SDS treatment,

the presence of peaks at around 1180, 1718  $\text{cm}^{-1}$  indicate the formation of carboxyl (COOH) functional groups on carbon nanotube surface [180, 181]. The peak at 887  $\text{cm}^{-1}$  represents the out of plane deformation vibrations of the alkyl groups attached on carbon nanotube surface. After grafting of PEG on carbon nanotube surface, the stretching absorption peaks of C=O and C-O for the ester group at 1734 and 1056  $\text{cm}^{-1}$  are clearly observed in Figure 1 [191]. The PEG functionalization is also observed by the appearance of the peak at 2929  $\text{cm}^{-1}$  which corresponds to the C-H stretching vibrations of the alkyl group of PEG [192]. Moreover, the increase in the intensity of the peak at 3440  $\text{cm}^{-1}$  might show the increase in the amount of hydroxyl groups on the surface after chemical treatment [105]. DGEBA treatment increases the number of peaks corresponding to ester (peak at around 2546  $\text{cm}^{-1}$ ) and epoxide groups (peaks at around 1774 and 1890  $\text{cm}^{-1}$ ) in FTIR spectrum.

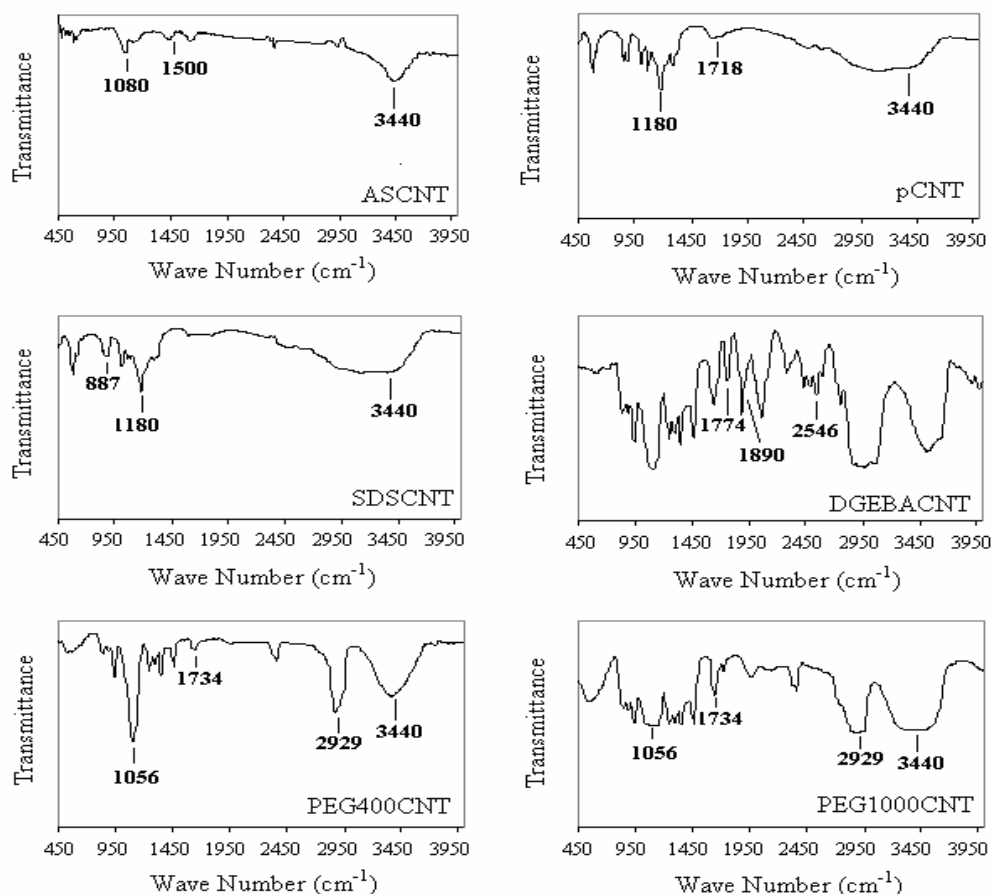


**Figure 4.10** FTIR spectra of carbon nanotube samples

#### 4.1.2.4 Electron Spectroscopy for Chemical Analysis of Carbon Nanotubes

ESCA spectra of carbon nanotube samples are shown in Figure 4.11. After purification, intensity of the spectrum increases when compared to that of ASCNT. This indicates the increase in the amount of oxygen containing functional groups on the carbon nanotube surface. O1s spectra of pCNT and SDSCNT fit the peaks corresponding to the hydroxide or carbonate bound to  $\text{NH}_4$ ,  $\text{O-C=O}$ ,  $\text{OH}$ ,  $\text{C=O}$ ,  $\text{C-O}$  and  $\text{C-O-C}$  groups (Table 4.6), which can show the formation of carboxyl and hydroxyl groups on carbon nanotube surface [182]. Moreover, the peaks corresponding to metal oxides in ESCA spectra disappear after purification, which shows the success of acid treatment of carbon nanotube in terms of the removal of metallic impurities.

The intensities of the O1s spectra of carbon nanotube samples decrease after surface treatment. The reason for this is the presence of modifiers with lower amount of oxygen in their chemical structure when compared to oxidized carbon nanotube surface. Another reason may be the consumption of carboxylic acid groups during the reactions between the purified carbon nanotube surface and modifiers [193, 194] which are also confirmed by the surface energy measurements (Table 4.4) and quantitative assessment of carboxylic acid groups analyses (Table 4.5). The peak at 532.7 eV in ESCA spectra of PEG400CNT and PEG1000CNT samples is a characteristic peak for the PEG showing the presence of the surface modifier on CNT surface. Also the peak corresponding to OH groups in PEG400CNT spectrum might indicate the existence of unreacted hydroxyl groups in PEG structure on carbon nanotube surface. The peak at 533.5 and 534.6 eV in O1s spectrum of DGEBCNT shows the interactions of surface modifier with carbon nanotube surface and between carbon nanotube aggregates.

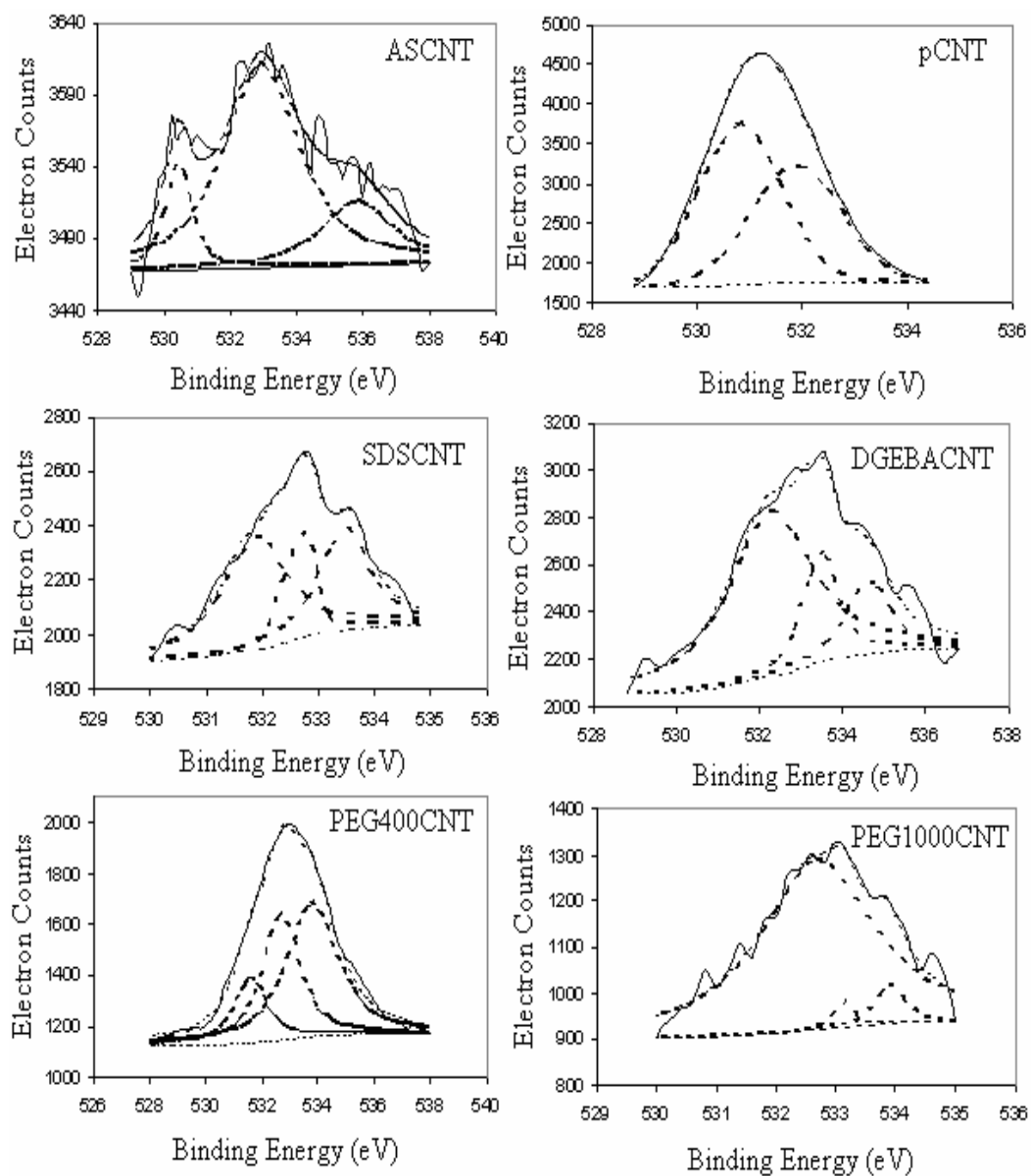


**Figure 4.11** ESCA O1s spectra of carbon nanotube samples

**Table 4.6** Peaks and chemical structures corresponding to these peaks in ESCA O1s spectra of carbon nanotube samples

<b>Code of Material</b>	<b>Peaks (eV)</b>
<b>ASCNT</b>	530.4: Oxygen bonded to the metallic catalyst residues, 532.9: C=O or C-O, 535.9: Oxygen from adsorbed H <sub>2</sub> O
<b>pCNT</b>	530.8: Hydroxide or carbonate bound to NH <sub>4</sub> 532.1: C=O, O-C=O and C=O (esters, anhydrides)
<b>SDSCNT</b>	531.9: OH, 532.6: C=O or C-O, 533.5: C-O-C 532.3: C=O or C-O
<b>DGEBACNT</b>	533.5: C-O-C 534.6: Phenyl-O-(C=O)O-Phenyl
<b>PEG400CNT</b>	531.6: OH, 532.7: PEG, 533.8: C-O-C
<b>PEG1000CNT</b>	532.7: PEG, 533.1: -C=O in HCOOCH <sub>2</sub> CH <sub>3</sub> 533.9: C-O-C

FTIR and ESCA analyses on carbon nanotube samples reveal the possible interaction mechanisms between the purified carbon nanotube and surface modifiers (PEG and DGEBA). PEG can interact with the carboxyl and quinone groups on the CNT surface in three ways (Figure 4.12). One or both hydroxyl groups of PEG can make bonding with either carboxyl or quinone groups on pCNT [195]. Oxygen on main chain of PEG can interact with carboxyl or quinone groups on pCNT. DGEBA interacts with pCNT surface with the help of epoxide groups in two ways (Figure 4.13). One or both hydroxyl groups, which are formed by the opening of epoxide in DGEBA structure at the chain ends, can make bonding with either carboxyl or quinone on pCNT [66]. Total interactions between the surface modifier and carbon nanotubes can be the combination of these modes for both PEG and DGEBA.

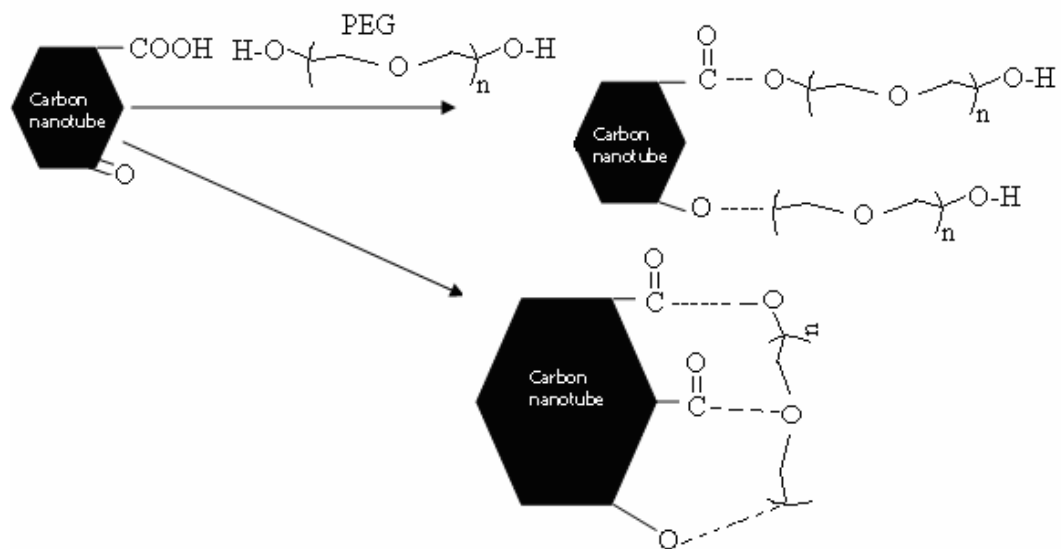


**Figure 4.12** Possible interaction mechanisms between PEG and purified carbon nanotubes

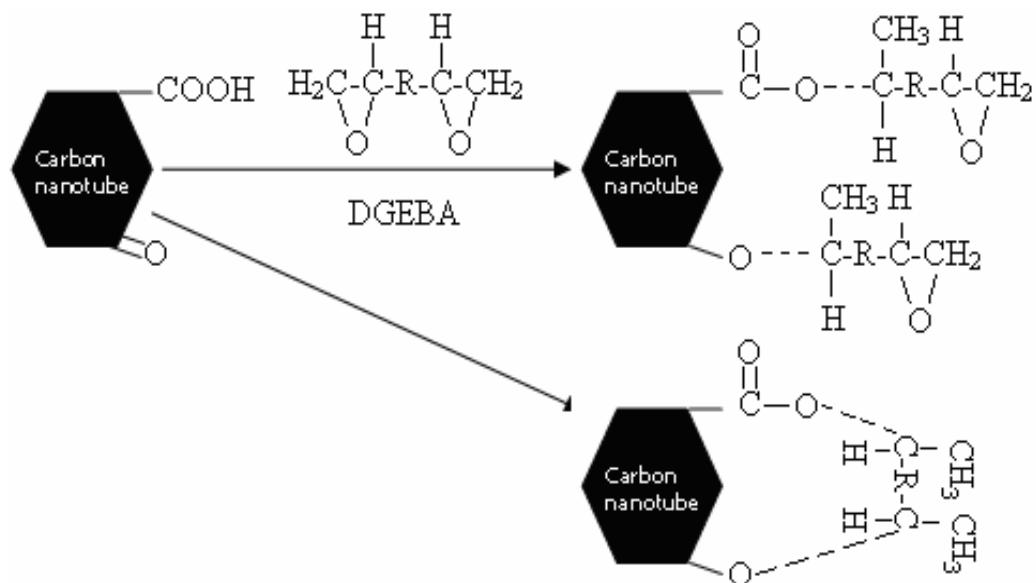


**Figure 4.13** Possible interaction mechanisms between DGEBA and purified carbon nanotubes

#### 4.1.2.5 X-Ray Diffraction and Scanning Electron Microscopy Analyses of Carbon Nanotubes

XRD patterns of carbon nanotube samples are similar to one another and the characteristic peaks at  $26^\circ$  and  $43^\circ$  are observed for all samples (Figure 4.14), which means that the surface treated carbon nanotubes have the same cylinder wall and crystalline structure with untreated carbon nanotubes [31]. The main peak at  $26^\circ$  is sharper for pCNT when compared to that of ASCNT owing to the removal of the disordered amorphous carbon and metallic catalyst particles from the carbon nanotube structure during purification [196]. DGEBA and PEG treatments broadened the two main peaks in XRD spectra owing to the surface modifier layer present on CNT surface. These layers may act like disordered impurities which can decrease the intensities of the main peaks [153].

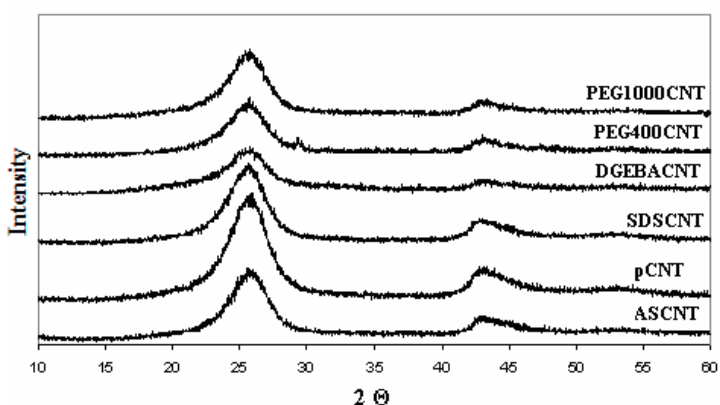


**Figure 4.14** XRD patterns of carbon nanotube samples

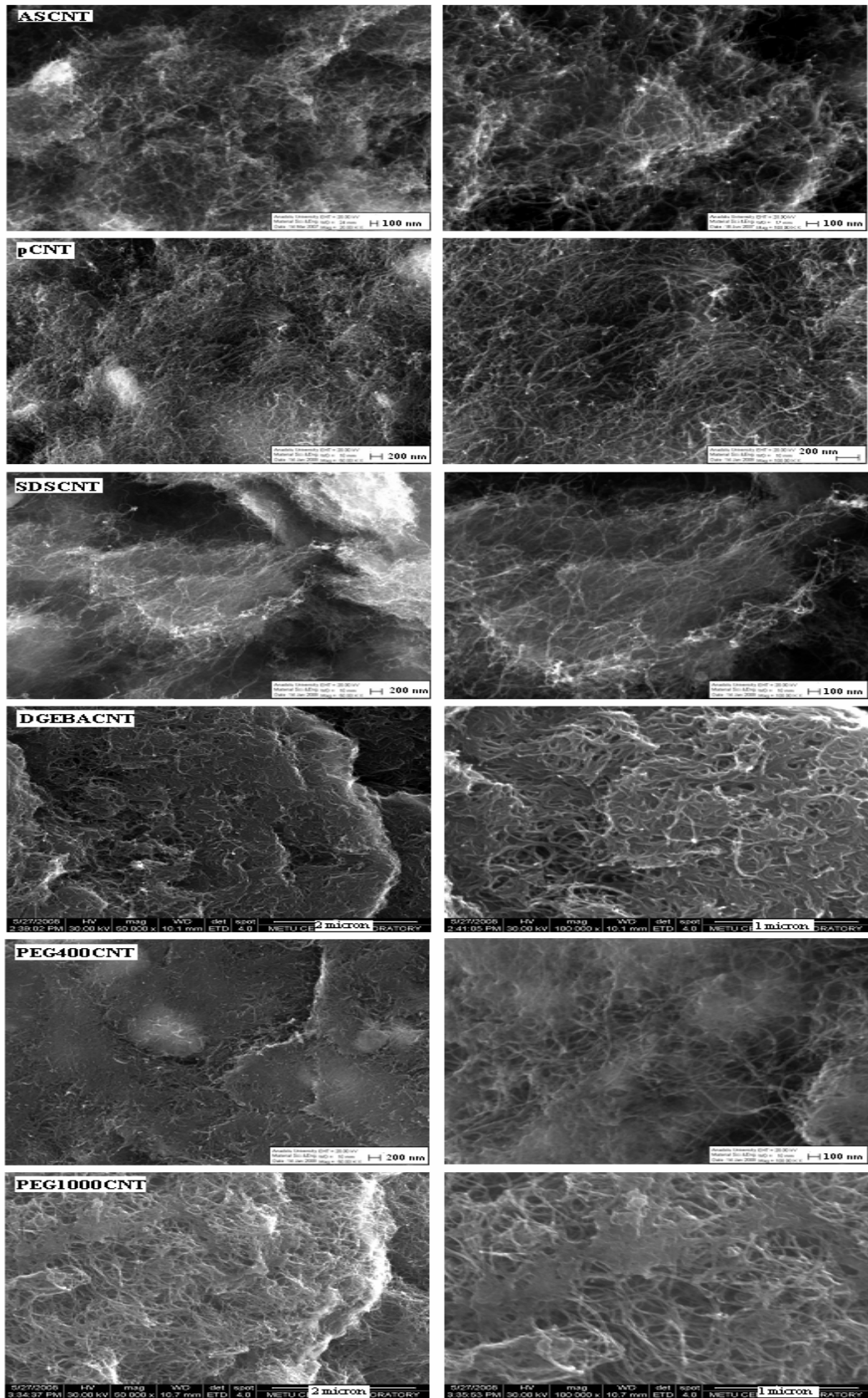
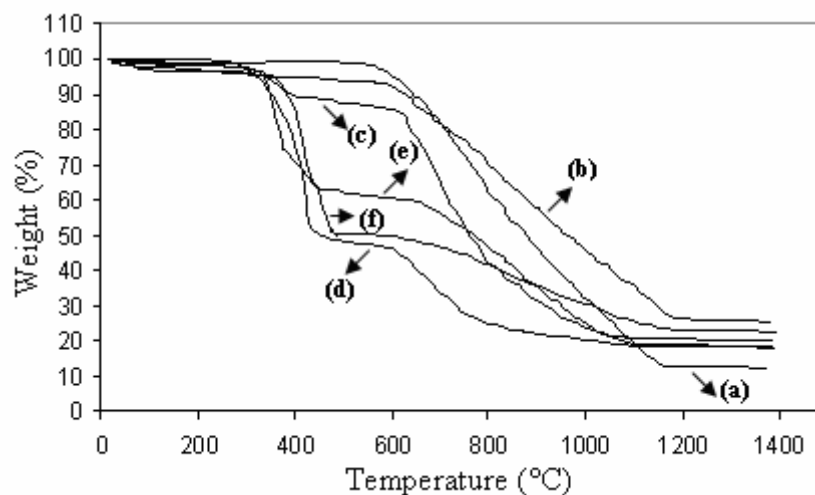


Figure 4.15 SEM micrographs of the carbon nanotube samples

SEM micrographs of ASCNT, pCNT and SDSCNT show that CNT are randomly entangled (Figure 4.15). DGEBA and PEG treated carbon nanotube structure is more compact, tubes are joined to each other and modifier residues can be observed on the carbon nanotube surfaces. No destruction of carbon nanotubes are observed in XRD, SEM analyses after purification and modification, which indicates that carbon nanotubes are strong enough to withstand these kinds of functionalization processes [197].

#### 4.1.2.6 Thermogravimetric Analysis of Carbon Nanotubes

TGA analyses are performed for all carbon nanotube samples to show the existence and determine the amount of organic functional groups on surfaces of carbon nanotubes [191]. The amounts of the surface modifiers on carbon nanotube samples were calculated by subtracting the weight present at the end of the first decomposition from the initial weight of the carbon nanotube sample. The results reveal that the ASCNT has about 87% weight loss between 600 and 1150 °C (Figure 4.16 (a)) due to the degradation of the amorphous carbon, metallic residues and mostly graphitic structure [198]. The graphitic decomposition is also observed for other samples. Total weight losses of the pCNT and modified carbon nanotubes are lower than that of ASCNT due to the absence of the disordered carbon structures and catalyst particles after purification in the structure of carbon nanotubes. TGA curve of pCNT (Figure 4.16 (b)) shows about 7% weight loss from 200 to 550°C because of the decomposition of carboxyl and hydroxyl groups [153]. As a result of the decomposition of SDS, DGEBA and PEG residues on carbon nanotube surfaces, two decomposition regions are observable in the TGA curves of modified carbon nanotubes (Figure 4.16 (c-f)). The decomposition temperature of the organic SDS, DGEBA and PEG molecules are lower than that of the graphite layers, in the range of 250 to 500°C. The surface modifier amount on the CNT surface can be determined by using the results of TGA analyses [66]. The concentrations of the SDS, DGEBA, PEG400 and PEG1000 molecules are estimated as 4 wt. %, 41 wt. %, 33 wt. %, and 43 wt. % respectively, which show that PEG1000 and DGEBA are seemed to be more effective in terms of attachment on surfaces of carbon nanotubes among the surface modifiers used in this study.



**Figure 4.16** TGA graphs of carbon nanotube samples; (a) ASCNT, (b) pCNT, (c) SDSCNT, (d) DGEBA/CNT, (e) PEG400/CNT, (f) PEG1000/CNT

#### 4.1.2.7 Surface Energy Measurements of Composites

The surface energy components of the neat PET and PET based composites are given in Table 4.7. The changes in the surface energy can be a proof for the enhanced interactions between PET and surface treated carbon nanotubes. Total surface energies of the composites generally increase after surface treatment due to the increase in the dispersive component of the total surface energy. Polar component of the total surface energy decreases after surface treatment due to the interaction of the polar end groups of PET with surface modified carbon nanotubes. The increase in the number of reacted carboxylic end groups resulted in a decrease in the polar component of the PET. The change in the polar component of total surface energy is higher for the composites prepared with PEG and DGEBA treated carbon nanotubes. The hydroxyl groups in PEG structure and epoxide groups in DGEBA structure seemed to be more susceptible to react with the carboxylic end group and phenyl group of PET. On the other hand surface energy components of the PET/SDSCNT composite are approximately the same with those of the PET/pCNT composite and SDS seems to be less effective in terms of increasing the interactions between the carbon nanotube and PET.

**Table 4.7** Surface energy components of the neat PET and PET/CNT composites (mN/m)

Sample	$\gamma_{\text{Solid}}$	$\gamma_{\text{Solid}}^{\text{d}}$	$\gamma_{\text{Solid}}^{\text{p}}$	$\gamma_{\text{Solid}}^{\text{A}}$	$\gamma_{\text{Solid}}^{\text{B}}$
PET	36.96	29.06	7.90	4.73	3.30
PET/ASCNT	36.25	27.74	8.51	5.16	3.51
PET/pCNT	39.36	31.53	7.83	4.11	3.73
PET/SDSCNT	39.32	31.34	7.98	4.24	3.76
PET/DGEBACNT	41.70	34.93	6.77	3.57	3.21
PET/PEG400CNT	39.73	32.78	6.95	3.96	3.05
PET/PEG1000CNT	39.88	33.12	6.76	3.78	3.02

#### 4.1.2.8 Fourier Transformed Infrared and Nuclear Magnetic Resonance Spectroscopy of Composites

FTIR spectra of the neat PET and PET based composites are investigated, in order to reveal the possible interaction mechanisms between the PET and carbon nanotubes and it is shown in Figure 4.17. The peak at around  $729\text{ cm}^{-1}$  indicates out of plane deformations of two carbonyl substituents on the aromatic ring of PET. The peak at around  $970\text{ cm}^{-1}$  corresponds to O-CH<sub>2</sub> stretching vibration of ethylene glycol segment of PET. Aromatic skeletal stretching vibrations of PET can be attributed to the peak at around  $1410\text{ cm}^{-1}$ . The peak at around  $1710\text{ cm}^{-1}$  represents the C=O stretching vibrations. After surface treatment generally two peaks showed the main difference in FTIR spectra. The peak at around  $1010\text{ cm}^{-1}$  in the FTIR spectra of the samples is observed after surface treatment. Intensity of the peak at  $1710\text{ cm}^{-1}$  starts to decrease with PET/pCNT composite. It approximately disappears after surface treatments with PEG and DGEBA. It shows the possible interactions between carbon nanotube surface and carboxylic end group of PET [199-201]. Moreover, composites prepared with PEG and DGEBA treated carbon nanotubes show two peaks at around  $2750$  and  $3450\text{ cm}^{-1}$  belong to hydroxyl groups which might indicate the presence of these surface modifiers on CNT surface. SDS treated carbon nanotubes do not show a further interaction

between PET and the FTIR spectrum of this composite just resembles that of the composite prepared with pCNT.

Solid state NMR analyses of neat PET and PET based composites are also performed to understand the possible reaction mechanisms between PET and carbon nanotube surfaces (Appendix C). There are three main peaks in the spectra corresponding to PET which are characteristic for all samples. These peaks are at around 59, 120, 158 ppm and they represent the carbons in the ethylene group of PET, carbons in the aromatic ring of PET, carbons in the carbonyl groups of PET respectively (Figure 4.18). The peaks at 20 ppm and 180 ppm in the spectra of the composites prepared with PEG and DGEBA treated carbon nanotubes correspond to carbons of the  $\text{CH}_3\text{-C-R}$  and  $\text{CH}_3\text{-O-R}$  groups, carbons in the COOR group respectively and they arise from the surface modifiers present on carbon nanotubes surfaces and interaction between PET carboxylic acid end groups and functional groups on the surfaces of carbon nanotubes. The peaks denoted with asterisks (\*) are side spinning bands of the major peaks in the spectra [202]. The intensities of the peaks at 120 ppm and 158 ppm in the spectra of composites prepared with PEGCNT and DGEBA CNT are lower when compared to those of the other samples. The carbonyl and phenyl groups of PET are surrounded by the hydroxyl and epoxide groups present on the surfaces of carbon nanotubes during the interactions. This results in a decrease in the intensities of the peaks at 120 ppm and 158 ppm for these composites. Finally it can be concluded that, FTIR and NMR analyses of the samples indicate the interactions between the carbonyl groups and aromatic group of PET and the hydroxyl groups of PEG on surface of carbon nanotubes (Figure 4.19). Moreover, epoxide group of DGEBA CNT interacts with the carbonyl and phenyl groups of PET (Figure 4.20).

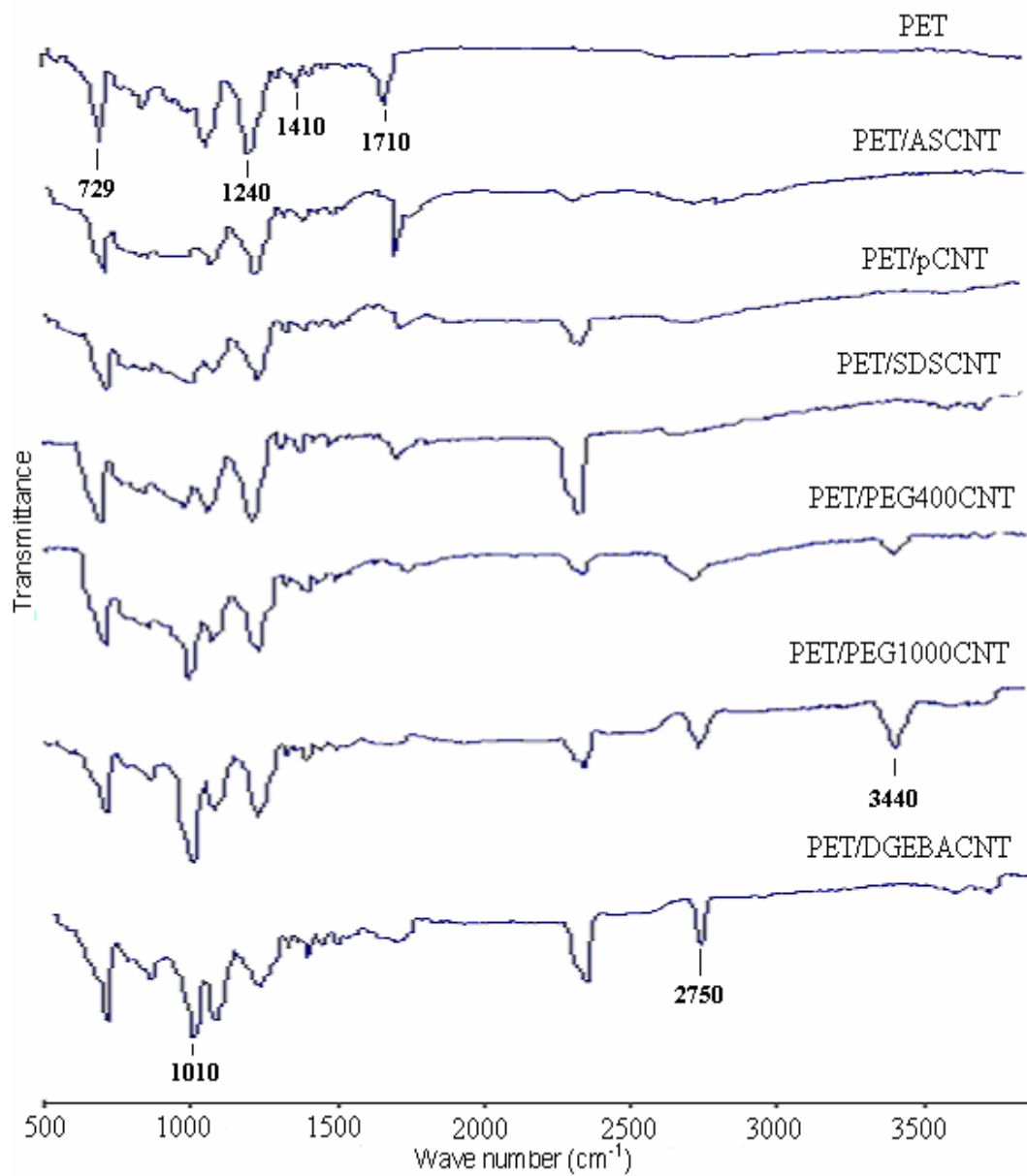


**Figure 4.17** FTIR spectra of the neat PET and PET/CNT composites

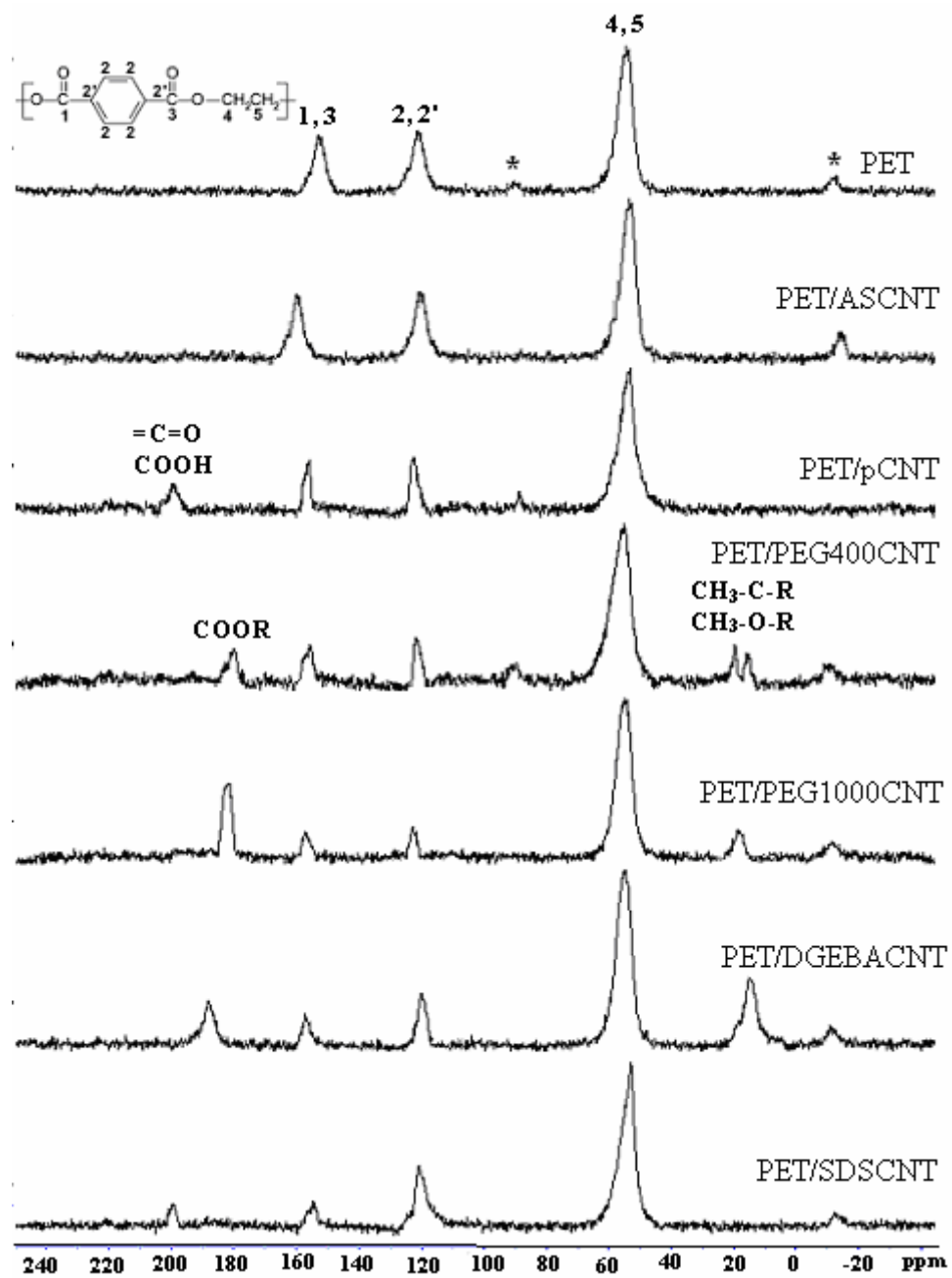
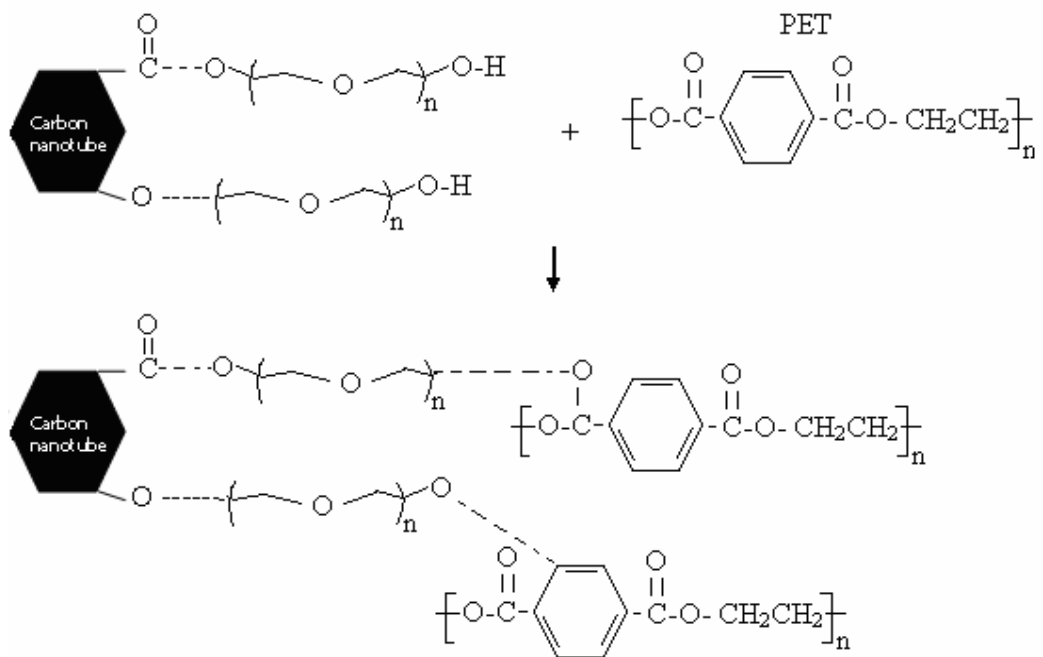
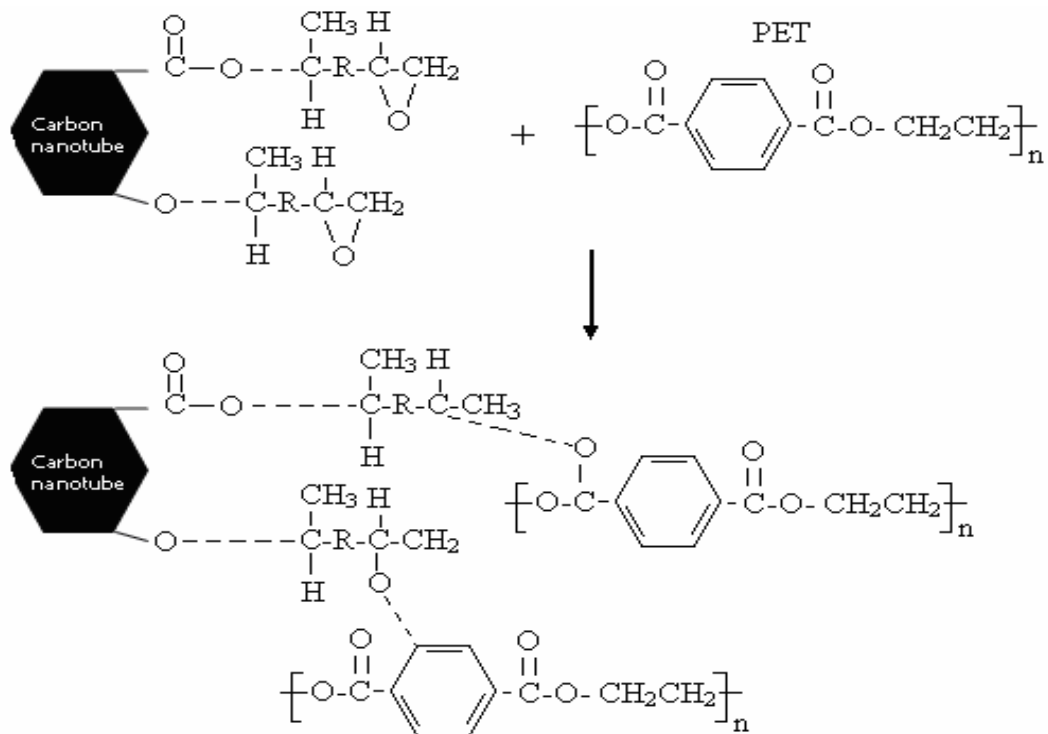


Figure 4.18 NMR spectra of the neat PET and PET/CNT composites



**Figure 4.19** Possible interaction mechanisms between PEGCNT and PET



**Figure 4.20** Possible interaction mechanisms between DGEBCNT and PET

#### 4.1.2.9 Electrical Resistivity Measurements of Composites

The electrical resistivity values of the PET/CNT composites prepared with as-received, purified and modified carbon nanotubes were measured according to the two point probe method. The change of the electrical resistivities of the composites with respect to the type of modifier on the surfaces of carbon nanotubes can be seen in Figure 4.21. The percolation threshold concentrations of all composite systems are lower than 0.5 wt. %, since the electrical resistivity values of all the composites are below  $10^4$  ohm.cm at 0.5 wt. % carbon nanotube loading [203]. After the percolation threshold concentration the composite conductivity mainly depends on the conductivity of the carbon nanotubes. The potential barriers due to the matrix polymer between the conductive carbon nanotube regions become unimportant in our composites [204]. However, it should be noted that the interfacial interactions between the composite constituents and dispersion of carbon nanotubes inside the composite can also have distinct effects on the electrical resistivity values of the composites [4].

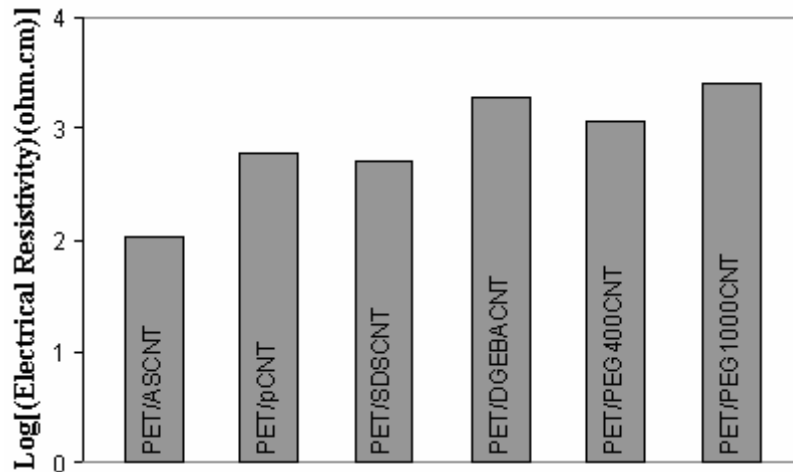


**Figure 4.21** Electrical resistivity values of PET/CNT composites

Electrical resistivity values of the composites based on pCNT and modified carbon nanotubes are higher than those of the composites based on ASCNT, due to the lower electrical conductivity of the carbon nanotubes after surface treatment. As a result of the purification and surface modification, the created oxygen containing functional groups and defects on the carbon nanotube surface might deteriorate the perfect electronic structure of the carbon nanotubes. Insulating oxide and modifier chemical region on the surface does not allow the transportation of electrons effectively which decreases the electrical conductivity of the individual carbon nanotube aggregates [204, 38]. Composites prepared with PEG and DGEBA have higher electrical resistivity than the rest of the composites owing to better attachment of surface modifiers (Figure 4.16) and thicker modifier layer on carbon nanotube surfaces (Figure 4.15). Another reason for the decrease in electrical conductivity of the composites after surface treatment with PEG and DGEBA might be the increase in the interactions between the PET and carbon nanotube particles, due to the presence of functional groups on the carbon nanotube surface (Figures 4.12 and 4.13). These functional groups improve the wetting of carbon nanotubes by PET. Conductive carbon nanotube particles are surrounded by insulating polymer matrix easily as the interactions between filler and polymer increase (Figures 4.17-4.20). The polymer phase has the same function with the insulating oxide layer and it decreases the conductivity of the composite, since it descends the number of contact points between the carbon nanotube particles. The electrical resistivity of the PET/PEG1000CNT composite is nearly 1400 ohm.cm higher than that of the PET/PEG400CNT composite due to the enhanced interactions between PET as a result of the higher amount PEG present on the carbon nanotube surface (Figures 4.16 and 4.21). Finally, the compact microstructure of the carbon nanotubes after surface treatment (Figure 4.15) might decrease the electrical resistivity values of the composites due to the decrease in the effective contact area between carbon nanotubes bundles [205].

The change of the electrical resistivities of the composites with respect to the carbon nanotube amount in the composites and the functionalization of carbon nanotubes can be seen in Figure 4.22. Electrical resistivities of the composites decrease with the increasing amount of conductive filler. This is an expected result since the contact points between the conductive filler particles increase and the conductive pathways are formed, as the filler concentration in the composite is

increased. However the sharp increase in electrical conductivities of the composites is generally limited after 1 wt. % carbon nanotube loading for all carbon nanotube samples when compared to the electrical conductivity increase at lower carbon nanotube loadings, due to the decrease in the contact area between carbon nanotubes as a result of the higher possibility for the formation of larger agglomerates at more intense carbon nanotube concentrations [204]. The percolation threshold concentrations of all composite systems are lower than 0.25 wt.%, since the electrical resistivity values of all the composites are below  $10^6$  ohm.cm at 0.25 wt. % carbon nanotube concentration. Electrical resistivity values of the composites based on pCNT and mCNT are higher than those of the composites based on ASCNT for all compositions, due to the lower intrinsic electrical conductivity of the carbon nanotubes after surface treatment.

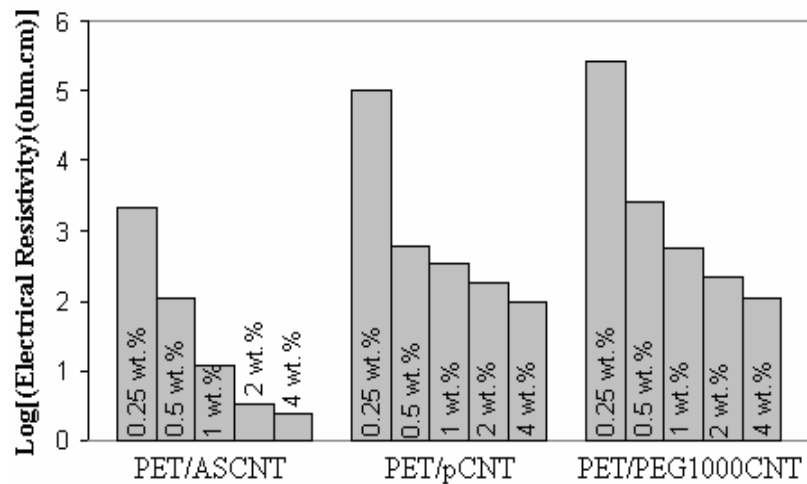


**Figure 4.22** Effect of carbon nanotube concentration on the electrical resistivity values of PET/CNT composites

#### 4.1.2.10 Tensile and Impact Tests of Composites

Tensile strength, modulus and impact strength values of the neat PET and PET/CNT composites are shown in Figures 4.23-4.28. PET/CNT composites

generally suffer from the weak tensile properties when compared to neat PET [206]. Moreover carbon nanotube addition to the thermoplastic polymers decreases the impact strength of these polymers due to the lower impact energy absorbance of the rigid carbon nanotube particles. Tensile strength and modulus values of the composites prepared with pCNT and modified carbon nanotubes are higher than those of PET/ASCNT composite. After purification carboxyl and hydroxyl groups formed on the carbon nanotube surface (Figure 4.10 and Tables 4.5 and 4.6) can react with the carboxyl end groups of PET and increase the chemical compatibility in the composite. Moreover, defect sites on the surfaces of carbon nanotubes can increase the mechanical interlocking and covalent bonding between carbon nanotubes and polymer matrix.

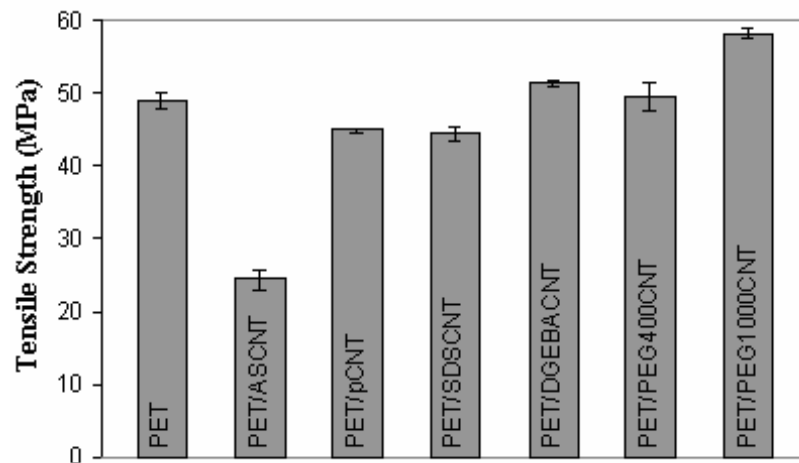


**Figure 4.23** Tensile strength values of neat PET and PET/CNT composites

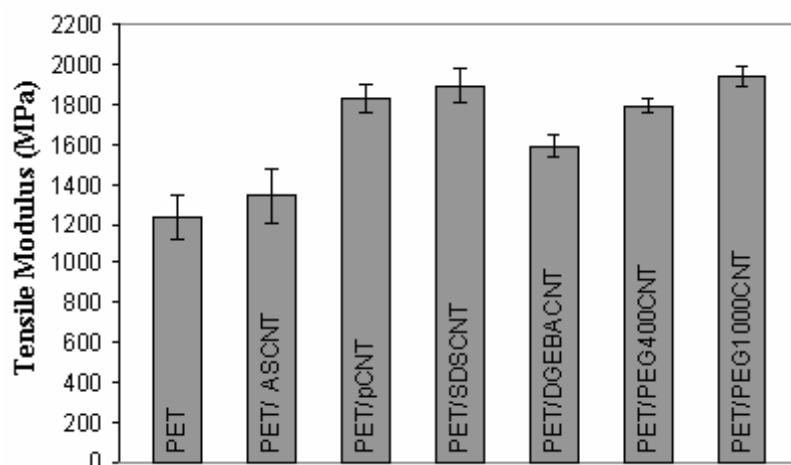


**Figure 4.24** Tensile modulus values of neat PET and PET/CNT composites

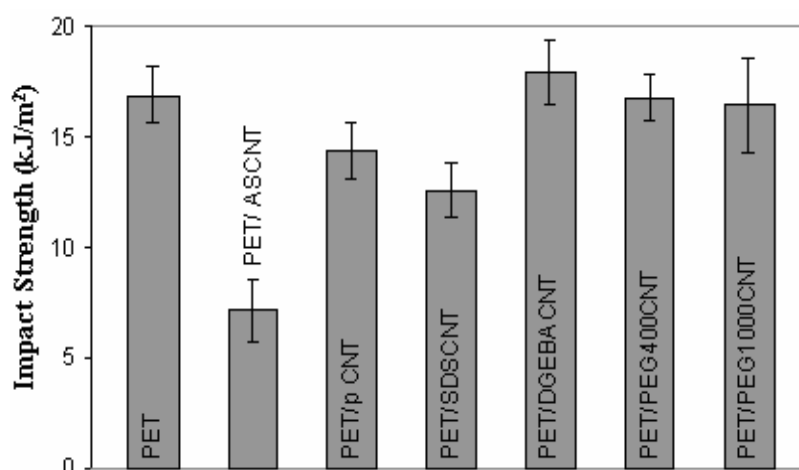


**Figure 4.25** Impact strength values of neat PET and PET/CNT composites

Miscibility of molecules is most favorable for species with similar Hildebrand solubility parameters [69]. As the Hildebrand parameters of PEG, DGEBA and PET are reasonably similar ( $\delta_{\text{PEG}} = 20.2 \text{ MPa}^{1/2}$  [69],  $\delta_{\text{DGEBA}} = 20.9 \text{ MPa}^{1/2}$  [206] and  $\delta_{\text{PET}} = 20.5 \text{ MPa}^{1/2}$  [207]) strong interaction and mixing between the functional groups of the modified carbon nanotubes and the PET is expected. Also, PEG and

DGEBA treated carbon nanotubes have different modes of reaction patterns with PET. The hydroxyl and epoxide end groups of PEG and DGEBA can interact with the carboxyl end groups and aromatic group of PET (Figures 4.19 and 4.20). These interactions between composite constituents improve the efficiency of load transfer from the PET to carbon nanotubes [188]. It is also observed that purification followed by PEG1000 treatment yields a more effective reinforcement than other surface treatments for PET based composites. The reason for this is the enhanced interactions between CNT and PET owing to the improved miscibility between PEG1000CNT surface and PET with the help of the alkyl groups present in PEG structure. Moreover, composites prepared with PEG and DGEBA treated carbon nanotubes have higher impact strength values (Figure 4.25) which may be due to the plasticizing effect induced by the long alkyl chains [208] present in the surface modifier structures.

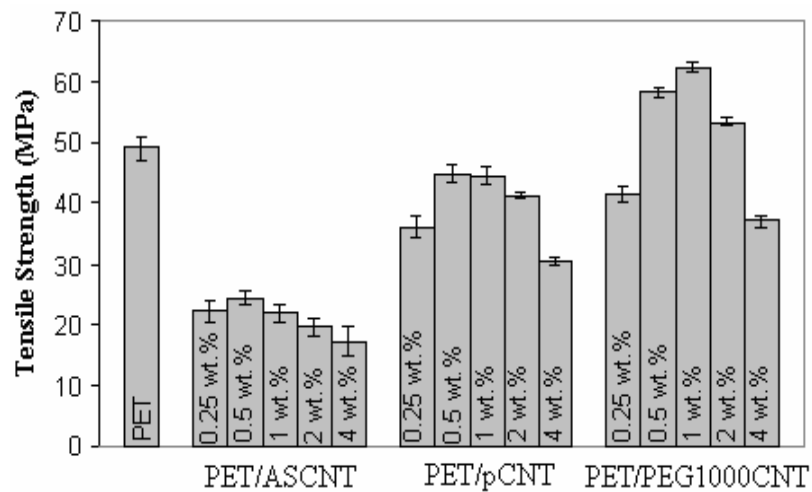


**Figure 4.26** Effect of carbon nanotube concentration on the tensile strength values of PET/CNT composites

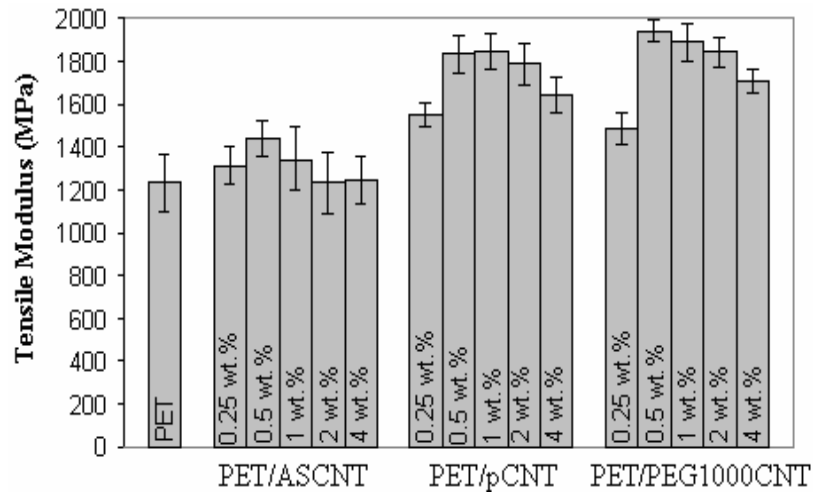


**Figure 4.27** Effect of carbon nanotube concentration on the tensile modulus values of PET/CNT composites

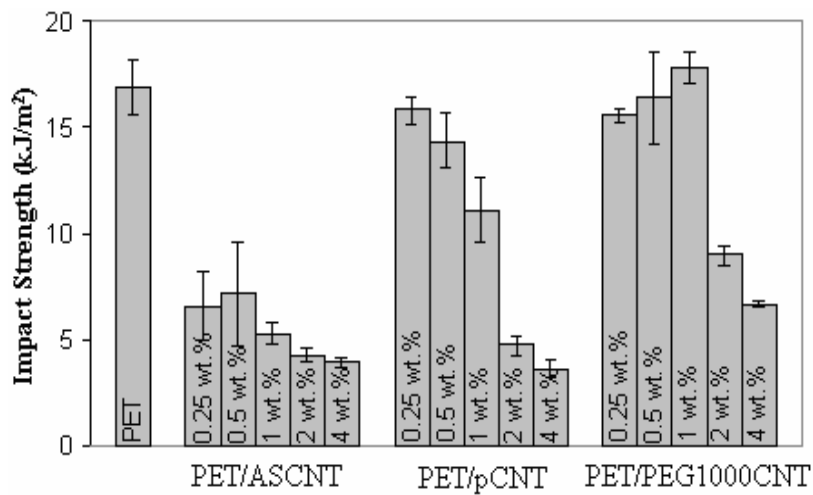


**Figure 4.28** Effect of carbon nanotube concentration on the impact strength values of PET/CNT composites

Mechanical strength of the composites generally decreased after 0.5 wt. % carbon nanotube loading. This might be due to the increase in the carbon nanotube agglomerate size at higher carbon nanotube concentrations [204]. The larger

carbon nanotube agglomerates in the composites act as stress concentrated areas and accelerate the rupture of the composite structure [8].

#### 4.1.2.11 Differential Scanning Calorimetry Analysis of Composites

Thermal properties of the neat PET and PET/carbon nanotube composites are investigated by using Differential Scanning Calorimetry (DSC) (Appendix D) and they are shown in Table 4.8. Thermal properties of the neat PET and PET/ASCNT composite are close to each other. The reason for this might be the lack of interactions between the ASCNT and PET. Carbon nanotube particles behave as a distinct phase in the composite and do not interfere with the thermal properties of PET. On the other hand, glass transition, crystallization and melting temperatures of the composites prepared with pCNT and modified carbon nanotubes are lower than those of the neat PET and PET/ASCNT composite. Enhanced interactions between the treated carbon nanotubes and PET directly affect the thermal properties. The plasticizing effect of the surface modifiers present on the carbon nanotube surface after modification might cause a decrease in the glass transition temperature. PET/DGEBACNT composite have the lowest glass transition temperature among all samples, owing to the higher amount of modifier present on carbon nanotube surface (Figure 4.16). Moreover, the difference in the mechanical properties of the composites might be due to the difference in the crystallinities of the composites prepared with ASCNT and surface modified carbon nanotubes [209]. The presence of carbon nanotube in PET phase increases the percent crystallinity due to the nucleation effect [210, 211]. Tensile strength of the composites increase as the percent crystallinities of the composites also ascend (Figure 4.23 and Table 4.8).

**Table 4.8** Thermal properties of neat PET and PET/CNT composites

Sample	T <sub>g</sub> (°C)	T <sub>c</sub> (°C)	T <sub>m</sub> (°C)	X <sub>c</sub> (%)
PET	70	119	254	23.8
PET/ASCNT	72	118	256	25.6
PET/pCNT	68	116	254	28.6
PET/SDSCNT	65	107	251	27.3
PET/DGEBACNT	62	106	251	28.9
PET/PEG400CNT	66	107	252	29.5
PET/PEG1000CNT	63	105	250	31.8

#### 4.1.2.12 Scanning Electron Microscopy of Composites

SEM micrographs of the carbon nanotube filled composites are shown in Figure 4.29 and 4.30, in order to observe the effect of surface treatment on the dispersion and particle size of the carbon nanotubes in the composites. Carbon nanotube distribution and particle size might also affect the electrical and mechanical properties of the composites. Purification of carbon nanotubes results in larger agglomerate size when compared to composite containing ASCNT. The larger carbon nanotube agglomerates in the composites cause an increase in the stress concentration of their neighborhoods during mechanical testing. Composites prepared with modified carbon nanotubes exhibit smaller carbon nanotube agglomerate size. Especially individual carbon nanotubes can be observed in the SEM micrographs of the SDSCNT and PEG1000CNT containing composites. This might be due to the decrease in the reagglomeration of carbon nanotube particles during composite preparation in the presence of surfactants [177]. Moreover, carbon nanotube dispersion with a smaller particle size in the polymer matrix after surface modification results in improved mechanical properties (Figures 4.23-4.28). The dispersion of carbon nanotube particles seems to be homogeneous for all composites owing to the high shear induced during the composite preparation with extrusion process.

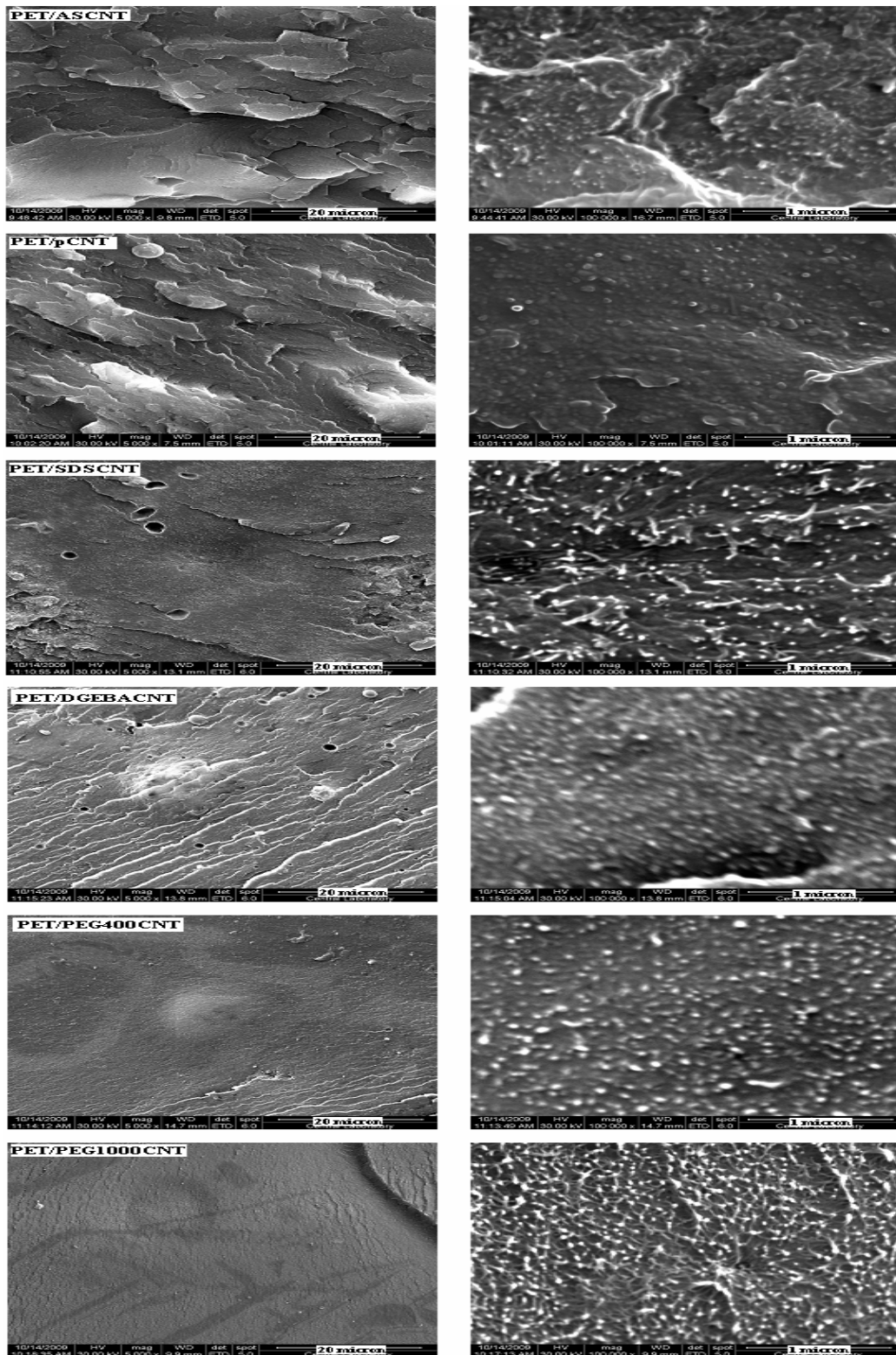


**Figure 4.29** SEM micrographs of 0.5 wt. % carbon nanotube containing PET/CNT composites (Micrographs on the right hand side are the magnified images of the micrographs on the left hand side)

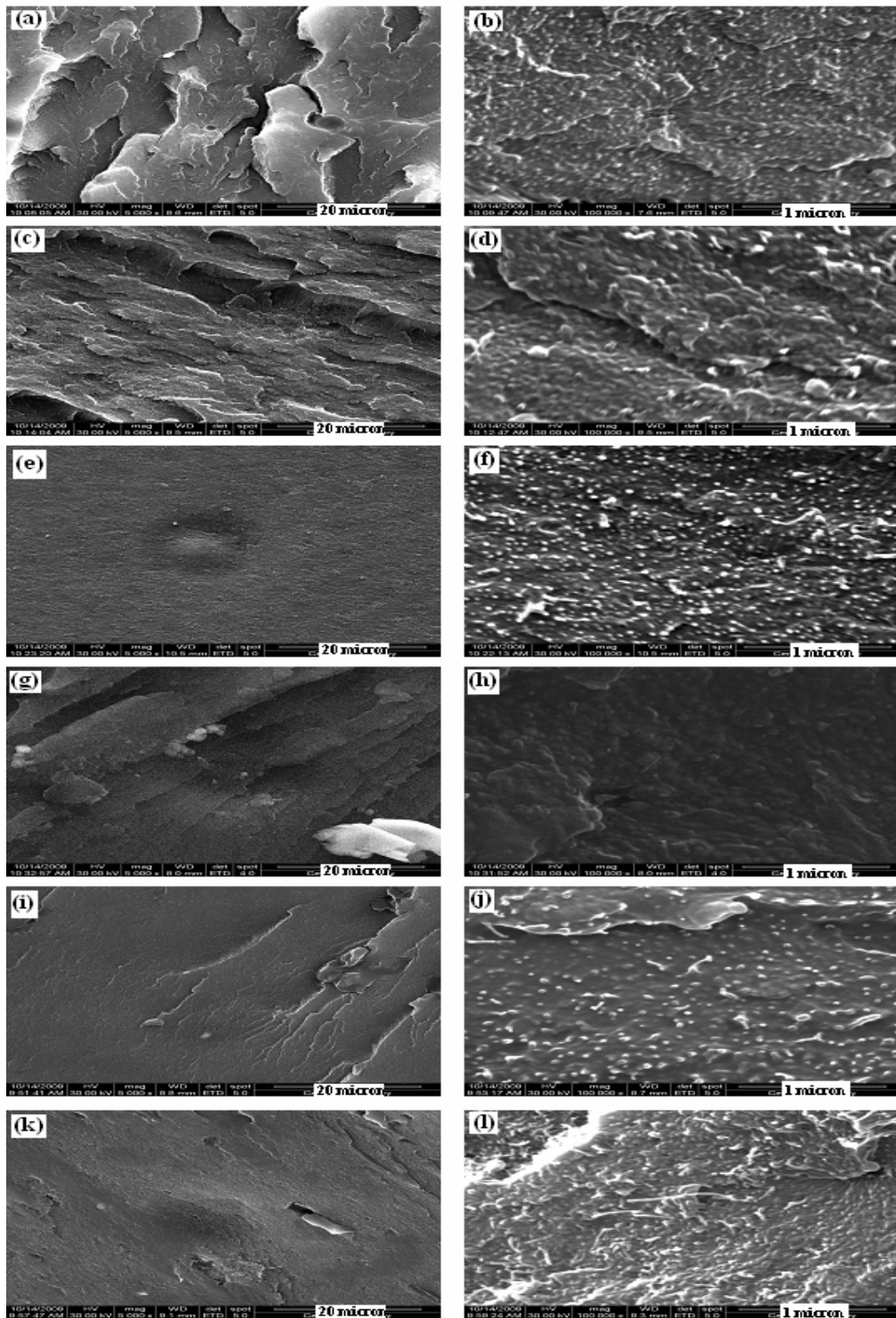


**Figure 4.30** SEM micrographs of PET/CNT composites (a) and (b) PET/ASCNT (1 wt. %), (c) and (d) PET/ASCNT (4 wt. %), (e) and (f) PET/pCNT (1 wt. %), (g) and (h) PET/pCNT (4 wt. %), (i) and (j) PET/PEG1000CNT (1 wt. %), (k) and (l) PET/PEG1000CNT (4 wt. %) (Micrographs on the right hand side are the magnified images of the micrographs on the left hand side)

## 4.2 Microfiber Reinforced High Density Polyethylene/Poly(ethylene terephthalate)/Carbon Nanotube Composites

Microfiber reinforced conductive polymer composites studies will be explained in two subsections. In the first part, the effects of the microfiber reinforcement, PET content in the composites and molding temperature on the morphology, electrical and mechanical properties of the microfibrillar HDPE/PET/CNT composites prepared with ASCNT will be discussed. In the second part, the effects of carbon nanotube surface treatment and content in the composites on the morphology, electrical and mechanical properties of the HDPE/PET/CNT composites prepared by using ASCNT, pCNT and PEG1000CNT will be explained.

### 4.2.1 Microfiber Reinforced High Density Polyethylene/Poly(ethylene terephthalate)/Carbon Nanotube Composites Prepared with As-Received Carbon Nanotubes

Morphological, electrical, mechanical and thermal characterization experiments of the microfiber reinforced polyethylene/poly(ethylene terephthalate)/carbon nanotube composites prepared with as-received carbon nanotubes will be explained in the following section.

#### 4.2.1.1 Surface Energy Measurements and Selective Localization of Carbon Nanotubes

Surface energies and melt viscosities of the polymers, mainly determine the location of the conductive filler in the polymer composites consisting of two immiscible polymers [212]. Surface energies of HDPE, PET and ASCNT, which are calculated from contact angle measurements (Equations 2.3-2.5), are shown in Table 4.9. They are also used in the determination of the surface tensions between the composite components.

**Table 4.9** Surface energy components of HDPE, PET and ASCNT (mN/m)

<b>Sample</b>	$\gamma_{\text{Solid}}$	$\gamma_{\text{Solid}}^{\text{d}}$	$\gamma_{\text{Solid}}^{\text{p}}$
<b>HDPE</b>	33.32	32.20	1.12
<b>PET</b>	36.96	29.06	7.90
<b>ASCNT</b>	46.14	35.67	10.47

Surface energy measurements show that ASCNT has higher surface energy ( $\gamma_{\text{Solid}}$ ) than HDPE and PET, due to its larger surface area and functional groups present on its surface. The polar component of HDPE ( $\gamma_{\text{Solid}}^{\text{p}}$ ) is near to zero, due to the lack of the functional groups. PET has higher polar surface energy component than that of HDPE, which can increase the affinity between ASCNT and PET by the reaction between the acidic end groups of PET and hydroxyl groups on ASCNT, rather than HDPE. Surface tensions, between PET and HDPE, PET and ASCNT, HDPE and ASCNT, are calculated as 5.28 mN/m, 1.05 mN/m, 7.74 mN/m, respectively (Equation 2.6). Wetting coefficient ( $w$ ) is calculated as 1.27 (Equation 2.7), which means that ASCNT particles should disperse in PET phase theoretically. In addition, lower interfacial tension between PET and ASCNT, makes the dispersion of ASCNT in PET phase easier [97]. This result is associated with the fact that carbon based conductive particles prefer to locate in the phase which has lower melt viscosity [5, 160, 212]. Rheological analyses show that PET has much lower melt viscosity than HDPE at the extrusion temperature (Figure 4.31). Also, SEM analysis reveals that ASCNT selectively disperse in the PET phase of HDPE/PET/ASCNT system (Figures 4.32 and 4.33). Individual carbon nanotubes are recognizable in carbon nanotube agglomerate, as long fibers with a diameter of around 10 nm. Figures 4.32 and 4.33 show the PET phase contacting with HDPE phase. As it can be seen from the figures, ASCNT particles are not distributed homogeneously in the composite. PET surface is rough, without any sign of elongation due to the brittle nature of PET and ASCNT particles selectively locate on its surface as fibrillar particles. On the other hand, HDPE phase is stretched due ductile nature with a smooth surface structure and it is very hard to observe any ASCNT particles on its surface.

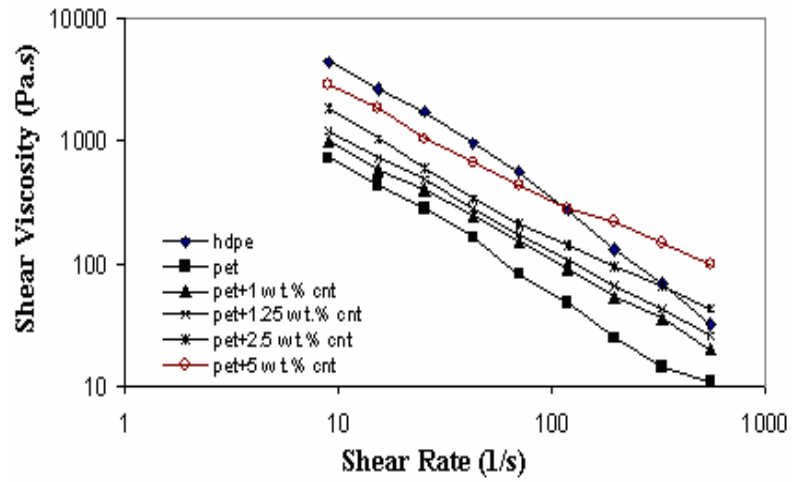


**Figure 4.31** Shear viscosity vs. shear rate graphs for HDPE, PET and PET/ASCNT composites

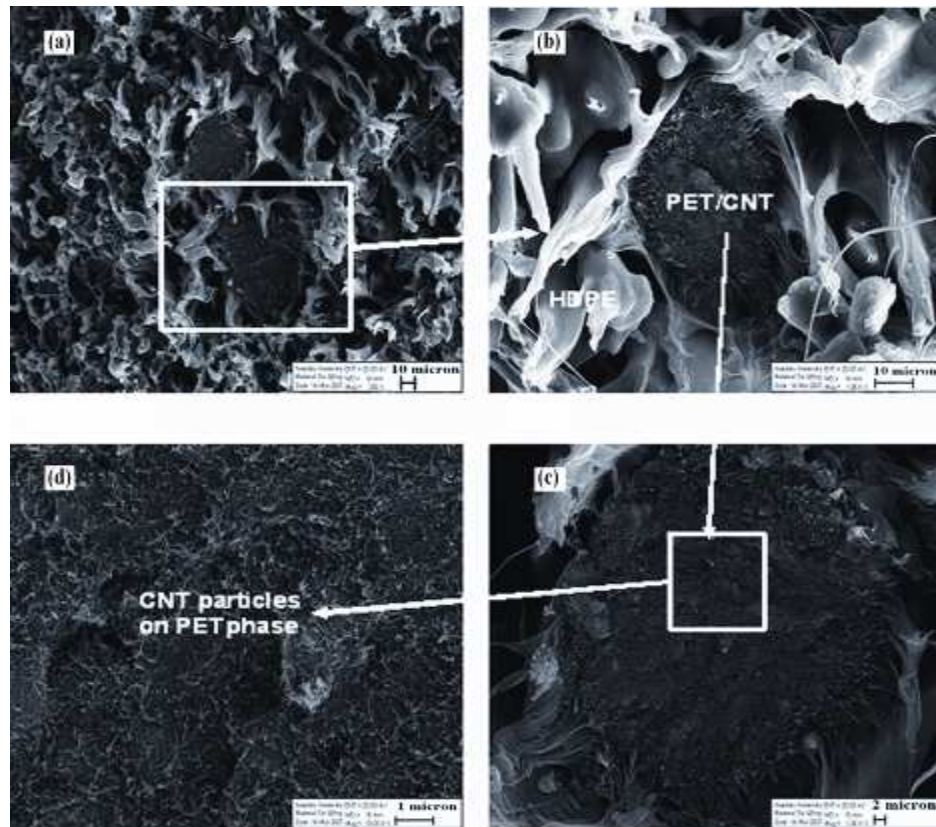


**Figure 4.32** SEM micrographs of the HDPE/PET/ASCNT (70/30/0.5) composite system

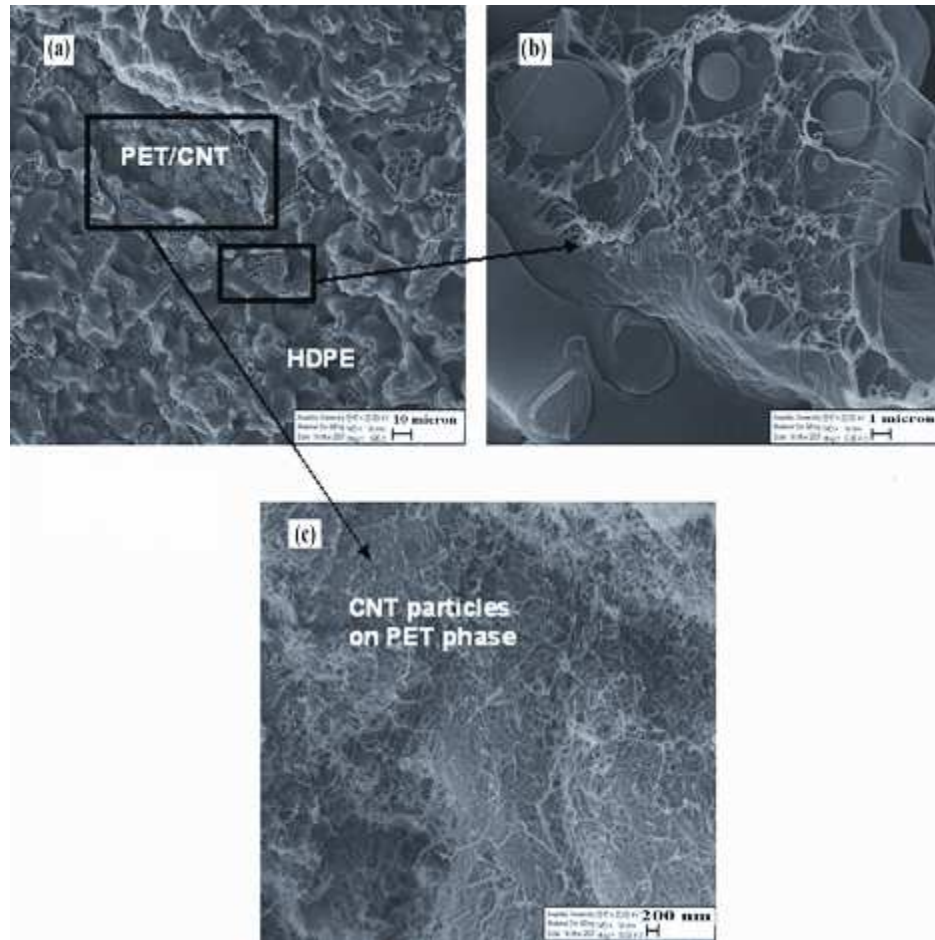


**Figure 4.33** SEM micrographs of the HDPE/PET/ASCNT (60/40/0.5) composite system

#### 4.2.1.2 Scanning Electron Microscopy of Composites

The SEM micrographs of the HDPE/PET blends and HDPE/PET/ASCNT composites (Figures 4.34 and 4.35) show that PET and PET/ASCNT phases disperse in HDPE up to 30 wt. % PET composition. A wide distribution of dispersed particle size is generally observed in the blends examined, due to the occurrence of coalescence phenomena of the minor phase during the melt mixing. The average diameter of PET and PET/ASCNT phases, which are etched away with trifluoro acetic acid, increases from 0.49  $\mu\text{m}$  to 1.41  $\mu\text{m}$  and 0.36  $\mu\text{m}$  to 0.84  $\mu\text{m}$ , respectively, as the PET content in the blend increases from 20 wt. % to 30 wt. %, respectively.

due to droplet coalescence (Table 4.10) [213-215]. PET/ASCNT domain sizes in composite systems are smaller than the PET domain sizes in the blend systems (Table 4.10). The decrease in the size of the PET phase after carbon nanotube addition to the HDPE/PET blends can be explained in terms of the reduction in the coalescence of the PET phase due to the presence of the rigid carbon nanotube particles in the PET phase and at the interface between the HDPE and PET. During the melt blending of the HDPE/PET/CNT composites, the interfaces act as solid like barriers which repulse each other, owing to the rigidity and lower mobility of the carbon nanotube particles. This lowers the melt coalescence of the PET/CNT phases. Moreover, carbon nanotube addition decreases the interfacial tension between the HDPE and PET, which can also cause a reduction in the size of PET phase. The interfacial tension between the HDPE and PET decreases from 5.28 mN/m to 5.04 mN/m in the presence of carbon nanotube particles. These phenomena can decrease the size of the PET/CNT phases in HDPE/PET/CNT composites when compared to size of the PET phase in HDPE/PET blends. This difference in PET domain size in the blends and composites affects the tensile properties of the samples. According to melt viscosity based morphology model (Paul and Barlow), which claims that the co-continuous morphology starts to form when the melt viscosity and the volume ratios of the polymer phases are equal to each other in a composite system, the co-continuous morphology start to develop after 30 wt. % and 40 wt. % PET loading for HDPE/PET and HDPE/PET/ASCNT systems, respectively. SEM results are in accordance with the Paul and Barlow model. A co-continuous morphology is observed when PET content in the blends and composites are 50 wt. % (Figures 4.34 and 4.35).

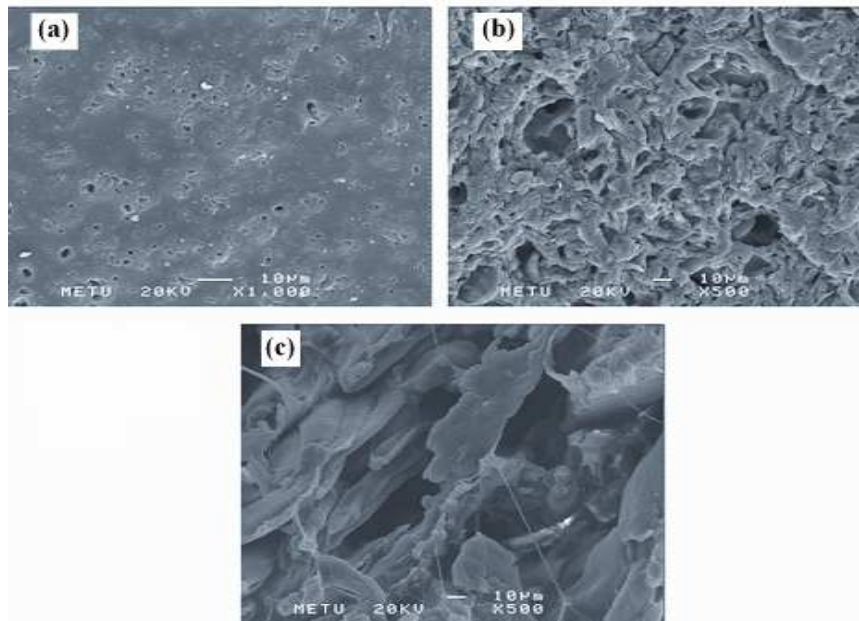


**Figure 4.34** SEM micrographs of the selected blend samples (HDPE/PET) (a) 80/20 (b) 70/30 (c) 50/50 (etched by trifluoro acetic acid)

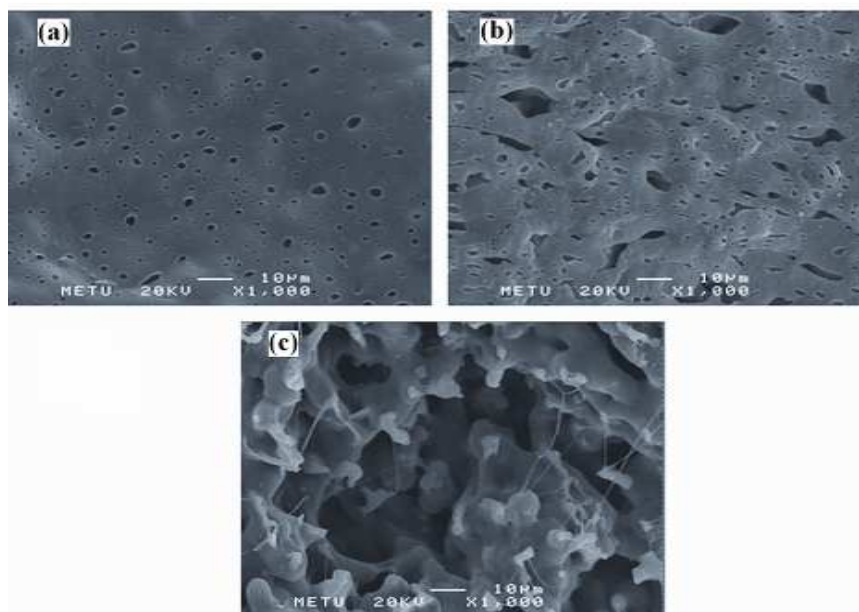


**Figure 4.35** SEM micrographs of the selected composite samples (HDPE/PET/CNT) (a) 80/20/0.5 (b) 70/30/0.5 (c) 50/50/0.5 (etched by trifluoro acetic acid)

**Table 4.10** Image analyses results of the selected samples

<b>Sample (HDPE/PET/CNT)</b>	<b>Morphology</b>	<b>Average Diameter (micron)</b>	<b>Minimum Diameter (micron)</b>	<b>Maximum Diameter (micron)</b>
<b>80/20 (Figure 4.34a)</b>	PET phase dispersed in HDPE	0.49	0.05	1.67
<b>70/30 (Figure 4.34b)</b>	PET phase dispersed in HDPE	1.41	0.09	23.13
<b>50/50 (Figure 4.34c)</b>	Co-continuous	-	-	-
<b>80/20/0.5 (Figure 4.35a)</b>	PET/CNT phase dispersed in HDPE	0.36	0.05	3.40
<b>70/30/0.5 (Figure 4.35b)</b>	PET/CNT phase dispersed in HDPE	0.84	0.05	10.29
<b>50/50/0.5 (Figure 4.35c)</b>	Co-continuous	-	-	-
<b>80/20/0.5 microfiber injection molded (Figure 4.37d)</b>	PET/CNT phase dispersed in HDPE	0.93	0.05	5.93
<b>80/20/0.5 injection molded (Figure 4.37e)</b>	PET/CNT phase dispersed in HDPE	0.94	0.06	10.85

Micrographs of the hot-stretched HDPE/PET/ASCNT systems (Figure 4.36) exhibit the in-situ PET/CNT microfiber structure formed in HDPE phase for all composites. However, the structure and concentration of the microfibers are different for all compositions [137, 138]. The changes in the surface structure of the microfibers are due to the diversity in the amounts of ASCNT in PET phase for various composite systems. Difference in the ASCNT concentration of the PET phase directly changes the microfiber structure [6]. Deformation of PET/ASCNT phase into microfibers during elongational flow, strongly depend on the interfacial

interactions between composite constituents and melt viscosity of the dispersed phase. The poor interfacial interactions between PET and HDPE, due to the incompatible nature of these polymers, do not create a remarkable resistance for the elongation of PET/ASCNT phase and enhance the formation of microfibers. However, the fibrillation of the PET phase in the presence of ASCNT particles also depends on the concentration of ASCNT in this phase. Carbon nanotubes are rigid particles, which limit the flow of the polymer melt and increase the melt viscosity (Figure 4.31). As the ASCNT amount in the PET phase decreases, hot stretching can facilitate the deformation and fibrillation of the dispersed PET/ASCNT phase in the composite, more effectively due to the lower melt viscosity of dispersed phase. The concentration of the microfibers grows up and the average diameter of them decreases as PET content of the composites increases (ASCNT content in PET phase decreases). The average diameters of the microfibers in the 80/20/0.5 microfiber and 50/50/0.5 microfiber systems are around 8 micron and 4 micron, respectively.

Microfiber reinforced composites are generally molded at a lower temperature than the melting temperature of the microfiber phase, in order to preserve the microfiber structure and perform the transformation of the composite into isotropic material reinforced with the microfibers [136, 139]. Figure 4.36 a, b show that the microfiber structure is protected in the composites which were molded at 210°C. This is necessary for the achievement of the desired electrical and mechanical properties. Moreover, most of the microfibers are oriented along the injection molding direction, since they leave a long section being vertical to the fracture surface (Figure 4.37 a) [140]. However at 240°C, some of the microfibers melt, since the molding temperature is close to the melting point of PET (Figure 4.37 c). When the molding temperature is raised to 280°C, microfiber structures totally disappear and is reconverted into randomly distributed spherical particles as a result of melting of the PET phase (Figure 4.37 d). SEM micrographs of the hot-stretched and conventional 80/20/0.5 composites, which are molded at 280°C, resemble each other (Figure 4.37 d, e) with the average diameters of the PET/ASCNT phases as 0.93 micron and 0.94 micron, respectively (Table 4.10).

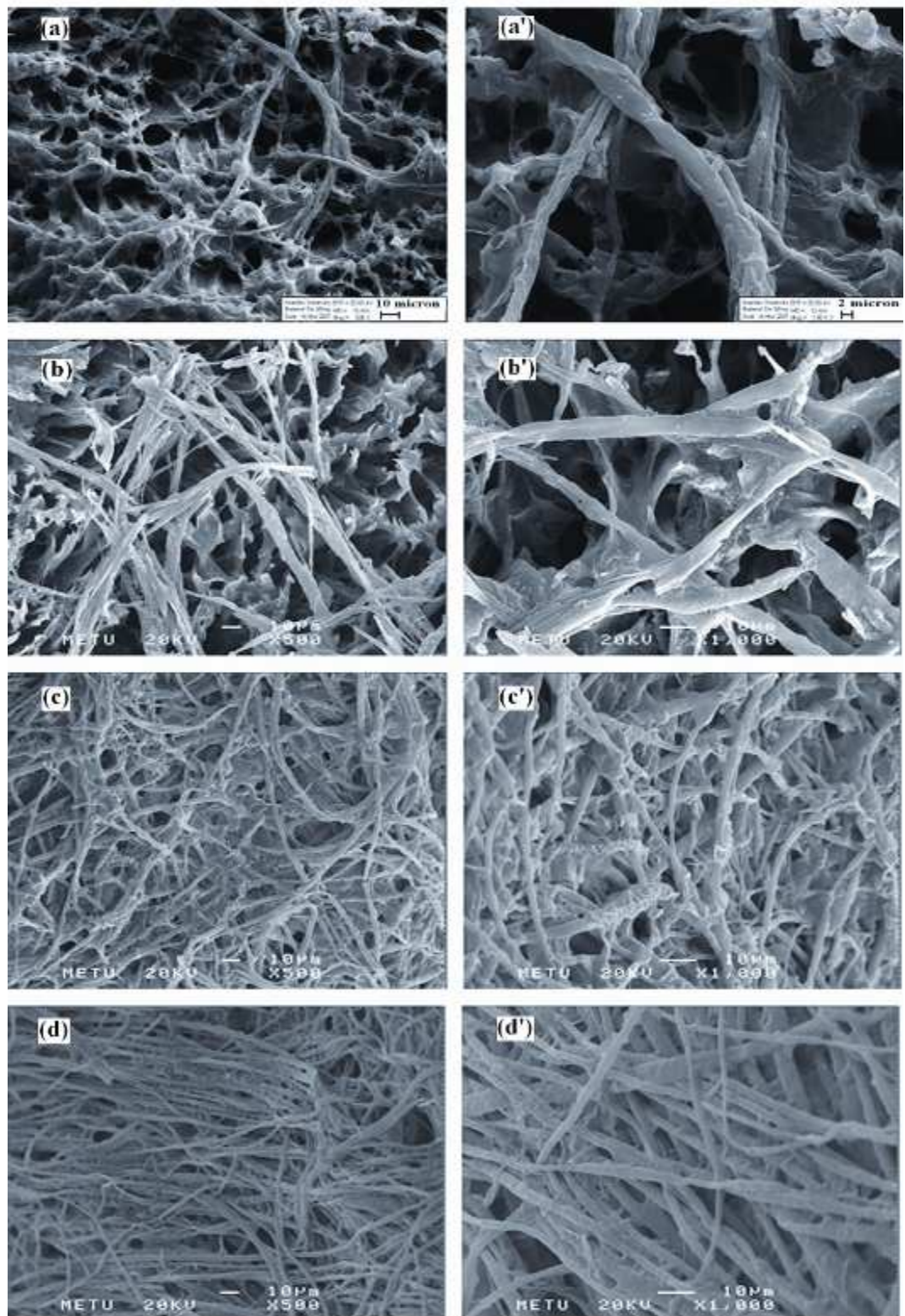


**Figure 4.36** SEM micrographs of the selected hot-stretched samples [(a), (a')] 90/10/0.5 microfiber [(b), (b')] 80/20/0.5 microfiber [(c), (c')] 70/30/0.5 microfiber [(d), (d')] 50/50/0.5 microfiber (etched by hot xylene)

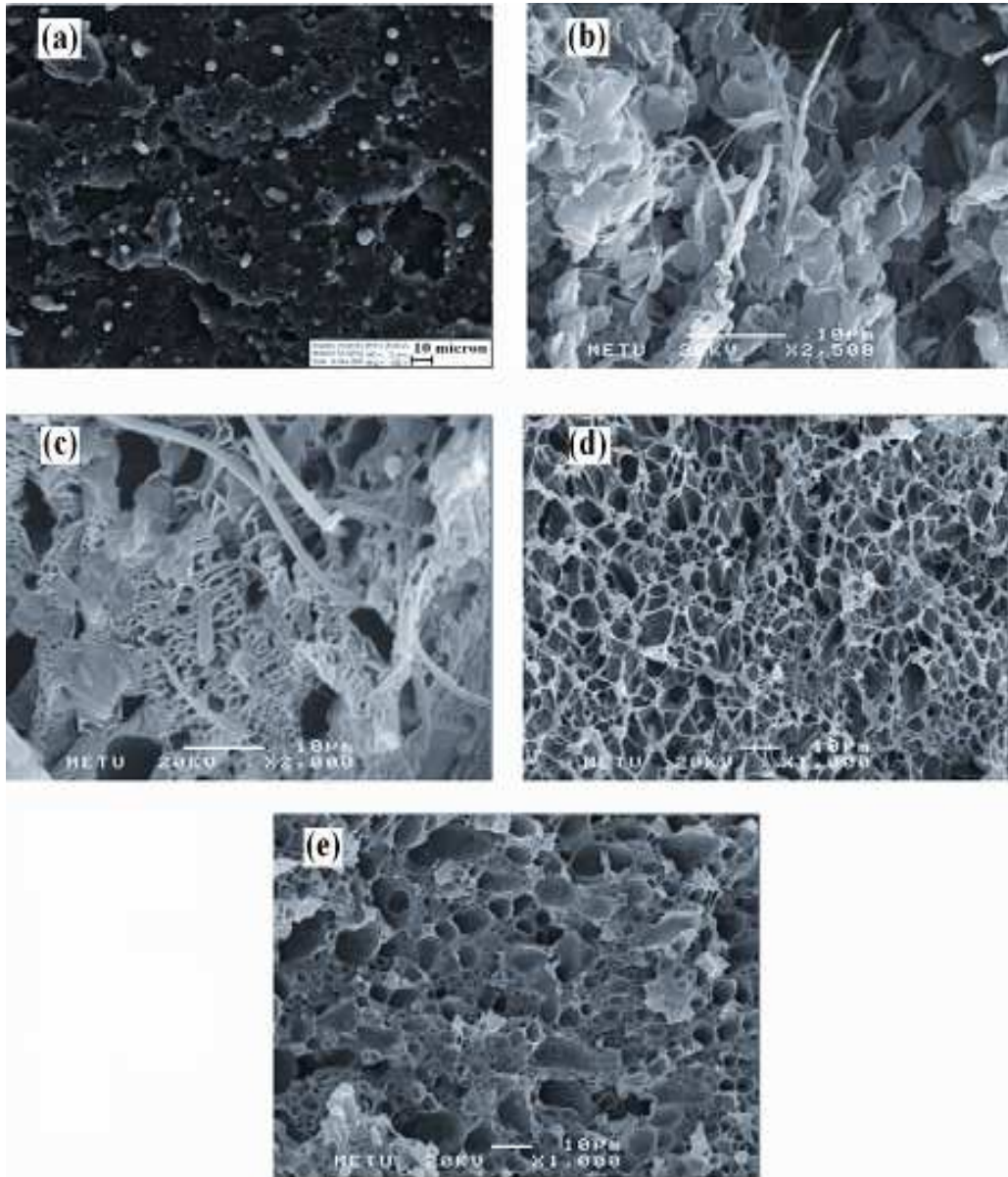


**Figure 4.37** SEM micrographs of the selected molded samples (a) 80/20/0.5 microfiber (210) (b) 80/20/0.5 microfiber (210) (etched by hot xylene) (c) 80/20/0.5 microfiber (240) (etched by hot xylene) (d) 80/20/0.5 microfiber (280) (etched by trifloro acetic acid) (e) 80/20/0.5 (etched by trifloro acetic acid)

#### 4.2.1.3 Electrical Resistivity Measurements of Composites

Electrical resistivity of HDPE/0.5 wt. % ASCNT composite is around  $10^{10}$  ohm.cm, which is in insulator range ( $>10^7$  ohm.cm). On the other hand, electrical resistivity of PET/ASCNT system containing same amount of CNT in it, is around  $10^2$  ohm.cm (Figure 4.38). This noticeable difference is due to the distinction between melt viscosities of these two polymers and affinities of the polymers to ASCNT. PET has higher affinity to ASCNT, due to the polar end groups present in the chemical structure and this improves the wetting of ASCNT by polymer matrix. Lower melt viscosity of PET causes a larger agglomerate size of ASCNT in the composite, which makes the conductive network formation and current conduction easier in PET matrix [215]. In addition, all the PET/ASCNT composites should exhibit low electrical resistivity ( $<100$  ohm.cm) above 0.5 wt. % ASCNT loading. This means that all the PET/ASCNT phases in the microfiber reinforced and conventional composites have enough electrical conductivity to form conductive networks in the samples.

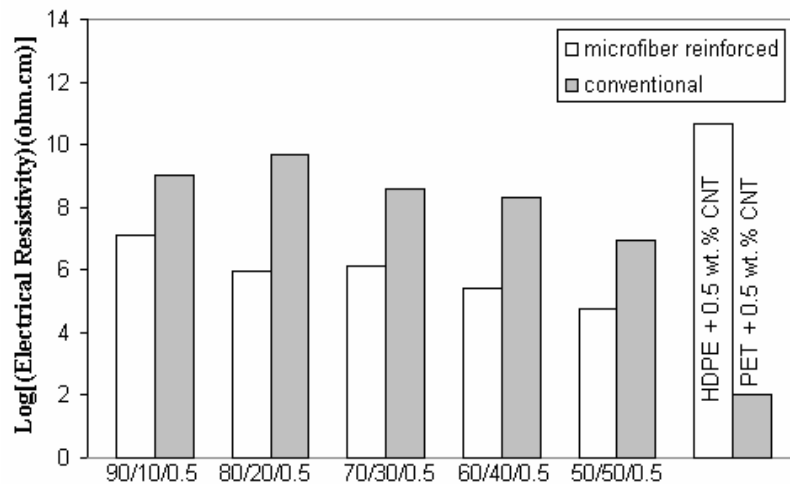


**Figure 4.38** Electrical resistivity values of the microfibrillar and conventional composites

In the microfibrillar and conventional HDPE/PET/ASCNT system, the percolation threshold concentration depend on two interconnected points; first one is the percolation threshold of nanotube particles in PET phase and the second one is the percolation threshold of PET/ASCNT phase in the HDPE matrix [5]. Before the percolation threshold concentration, tunneling distance is so much that HDPE dominates the conduction mechanism. Free charge carriers of conductive PET/ASCNT phase have to pass through micro spaces between microfibers, which are filled with insulating HDPE. However, beginning from percolation content, the conductive PET/CNT microfibers will dominate the current conduction mechanism. PET based composite containing 0.5 wt. % ASCNT has an electrical resistivity value of 100 ohm.cm. As a result of this, when PET/ASCNT phase forms a continuous structure in HDPE matrix, electrical conductivity of the composites passes from insulator range to semiconductor range ( $<10^7$  ohm.cm) as seen in Figure 4.38. Direct contact between the microfibers can dominate the electron conduction in the microfibrillar composite, since ASCNT particles can directly touch each other when individual fibers contact with other fibers [88, 216]. The percolation threshold of the PET/ASCNT microfibers in the microfiber reinforced composites is below 10 wt. % PET/ASCNT loading, since the electrical resistivity value of 90/10/0.5 microfiber (210) system is about  $10^7$  ohm.cm (Figure 4.38). Electrical resistivities of microfiber reinforced composites molded at 210°C decrease as the PET content in the composite is increased (Figure 4.39), due to the rise of the number of contact points between the microfibers providing the electron transportation [6]. However, the decrease in the ASCNT amount in the PET phase as the PET content in the composites increases, do not have a significant effect on the electrical resistivity results of the composites. On the other hand, electrical conductivities of the composites prepared without hot stretching and microfiber reinforced composites molded at 280°C are in the insulator range when PET/ASCNT content in the composite is below 40 wt. % (Figure 4.38). Since PET/ASCNT phase in the composite is not continuous below this composition (Figures 4.35 and 4.37), electrical conductivity of the composites are low and falls in the insulator range.

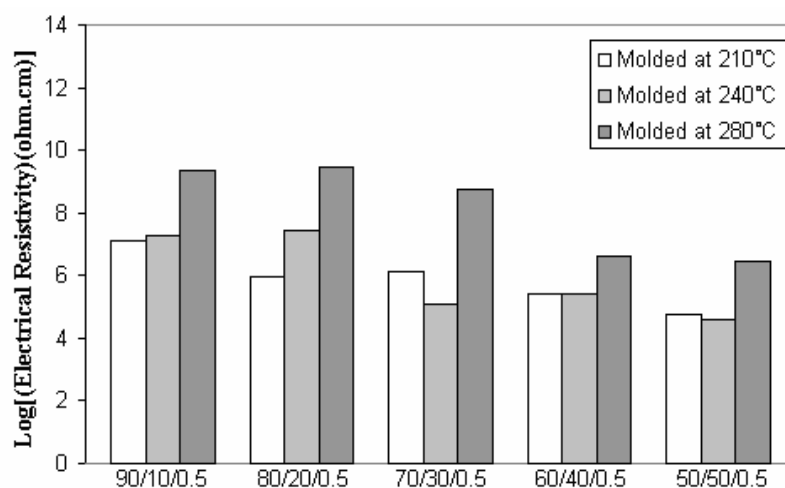


**Figure 4.39** Electrical resistivity values of the microfiber reinforced composites molded at different temperatures

Electrical resistivities of the microfiber reinforced composites increase when the molding temperature is increased from 210°C to 280°C (Figure 4.39). Molding temperatures above the melting point of PET, causes PET/ASCNT phase to melt and loose the microfiber characteristics. Thermodynamically when microfiber phases melt, they have a spherical shape (Figure 4.37) and continuity of the PET/ASCNT phase in the composite disappears below 40 wt.% PET loading (Figure 4.35). 80/20/0.5 microfiber (210) system has an electrical resistivity of  $10^6$  ohm.cm, whereas the electrical resistivity of the 80/20/0.5 microfiber (280) system is around  $10^{10}$  ohm.cm (Figure 4.39). Samples, which are molded at 240°C, have electrical resistivity values between the composites molded at 210°C and 280°C. Before the characterization experiments, it was expected that PET/ASCNT microfibers could soften and attach each other without damaging their structures when the molding temperature (240°C) is close to the melting point of PET, which may improve the current conduction by increasing the number of contact points between the microfibers. However, electrical conductivity results do not reveal a mechanism as explained above.

#### 4.2.1.4 Tensile and Impact Tests of Composites

SEM micrographs of the HDPE/PET/ASCNT composites show a typical incompatible morphology with discrete PET/ASCNT domains dispersed within a continuous phase of HDPE (Figures 4.32 and 4.33) [72]. No evidence of interfacial interactions or adhesion between both phases exists. The immiscible nature between two polymer phases leads to unstable morphology and poor mechanical properties in the composites. However, microfibrillar morphology can greatly improve the mechanical properties of the polymer/microfiber composites when the mechanical properties of the fibers with high aspect ratio are greater than the polymer matrix [95, 217, and 218]. Microfiber reinforcement improves the tensile strength and modulus of the samples compared to that of the blends and composites prepared without hot stretching up to 30 wt.% PET loading (Figures 4.40 and 4.41). Direct short fiber strengthening and residual thermal stress in microfibers are the main factors in reinforcement mechanism of in situ microfibrillar composites. The difference in the thermal expansion coefficients of HDPE and PET/ASCNT phases results in thermal residual stresses. During injection molding of composites at 210°C, PET/ASCNT microfibers are solid but HDPE is in molten phase. When the composite starts to cool from processing temperature to mold temperature, microfibers have little thermal contraction, whereas HDPE undergoes crystallization and contracts strongly [212]. The orientation of PET/ASCNT microfibers in the HDPE matrix is another factor that brings out enhancement of the tensile properties.

Microfiber reinforced composites including 40 and 50 wt.% PET could not be molded at 210°C and when these composites are molded at 240°C, their tensile strength and modulus are lower than the blends and conventional composites having the same composition, due to partial melting of the PET phase. Microfiber reinforced composites which are molded at 210°C, show a maximum for tensile strength and modulus values at 20 wt. % PET loading. Tensile strength and modulus values of 80/20/0.5 microfiber (210) are 44 MPa and 950 MPa, respectively. The optimum PET content for having improved mechanical properties is around 20-30 wt. % for HDPE/PET/ASCNT system, as also observed by other researchers before [219]. The increases in the concentration of the microfibers (Figure 4.36) do not improve the tensile strength and modulus, due to the poor

interfacial adhesion between HDPE and PET/ASCNT phase [218]. It can be concluded that; presence of more microfibers in the sample is not sufficient for increasing the tensile strength without the compatibility of the polymer phases after a certain PET composition (30 wt. %). Tensile strength values of the HDPE/PET/ASCNT composites are higher than HDPE/PET blends (Figure 4.40), as a result of the smaller domain size of the PET/ASCNT phase in the composites than the PET domain size in blends (Table 4.10) and presence of the reinforcing carbon nanotube particles in the composite structure.

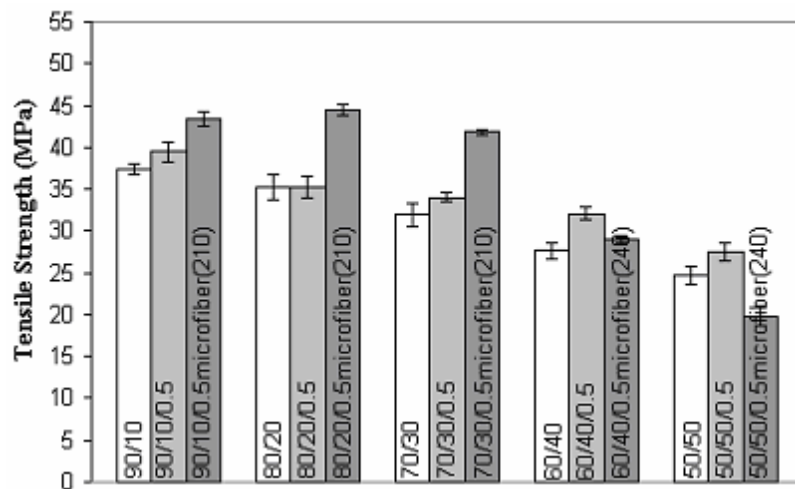


**Figure 4.40** Tensile strength values of the composites and blends

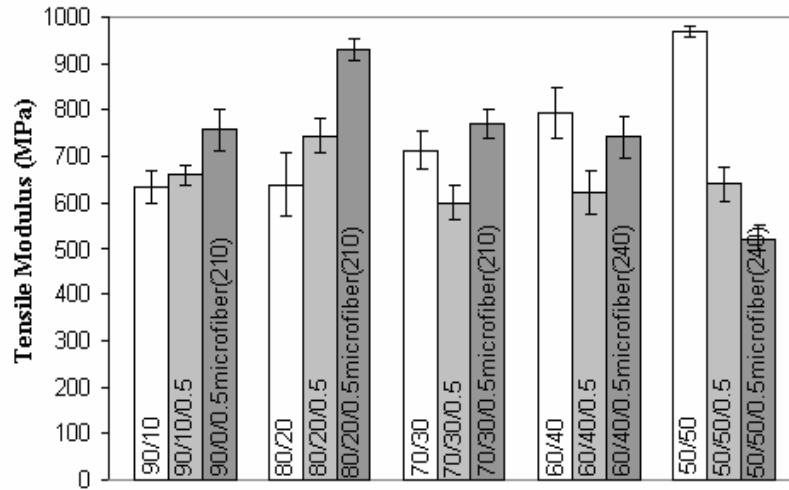


**Figure 4.41** Tensile modulus values of the composites and blends

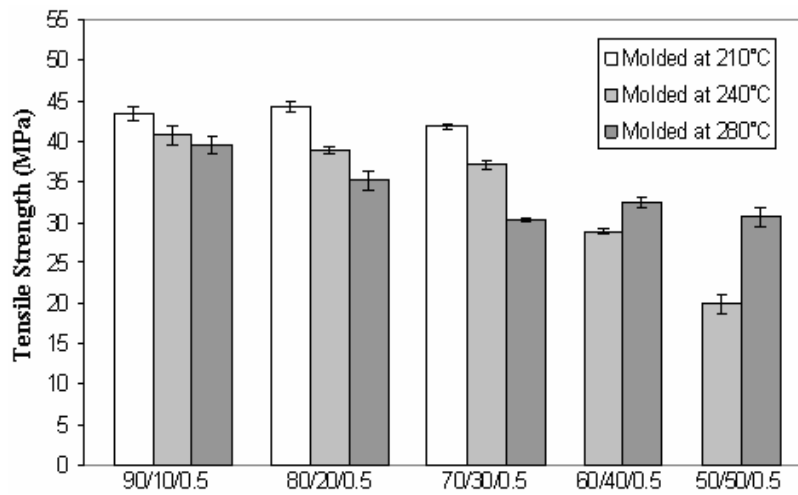


**Figure 4.42** Tensile strength values of the microfiber reinforced composites molded at different temperatures

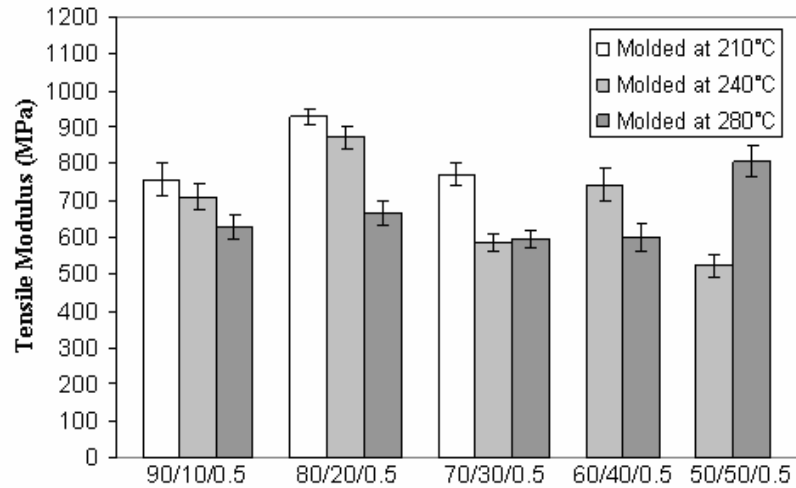


**Figure 4.43** Tensile modulus values of the microfiber reinforced composites molded at different temperatures

Increasing the molding temperature, decreases the tensile strength and modulus values of microfiber reinforced composites up to 30 and 40 wt.% PET loading, respectively (Figures 4.42 and 4.43). At high temperature molding, microfibers with high aspect ratio transform into spheres with low aspect ratio and the reinforcing effect of microfibers diminishes (Figure 4.37) [220]. Microfiber reinforced composites molded at 280°C and conventional composites have nearly the same values of tensile strength and the modulus. 80/20/0.5 microfiber (280) and 80/20/0.5 systems both have tensile strength of nearly 35 MPa. Also, 70/30/0.5 microfiber (280) and 70/30/0.5 systems both have tensile modulus of nearly 600 MPa.

Microfiber reinforcement enhances the impact strength values when compared to that of blends and composites prepared without hot stretching, except for 90/10 systems (Figure 4.44). Parallel to tensile strength and modulus results, 80/20/0.5 microfiber (210) system has the highest impact strength among the microfiber reinforced composites molded at 210°C. Microfibers present in the composite decrease the crack formation and propagation in the sample during the impact test. When the growing crack reaches the microfiber phase, the microfiber nucleates the formation of many tiny craze cracks, which produces a large free surface that

absorbs the mechanical energy as the potential surface energy [84]. As a result of this, when the microfiber concentration in the composite increases, the percent increase of the impact strength with respect to the blend without ASCNT also increases. The percent increase in impact strength values for 80/20/0.5 microfiber (210) and 70/30/0.5 microfiber (210) systems, when compared to the blend systems, are approximately 50 % and 350 %, respectively (Figure 4.44). However, when PET content in the composites is higher (40-50 wt. %), microfiber formation does not have a distinctive effect on the impact strength. The brittle nature of PET overcomes the microfiber reinforcement and decreases the impact strength. Molding temperature increment generally decreases the impact strength of the microfiber reinforced composites due to the melting of PET phase (Figure 4.45).

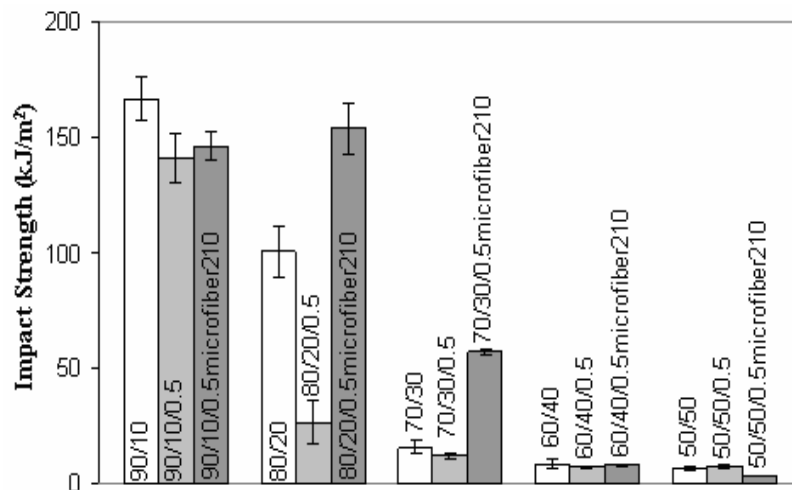


**Figure 4.44** Impact strength values of the composites and blends

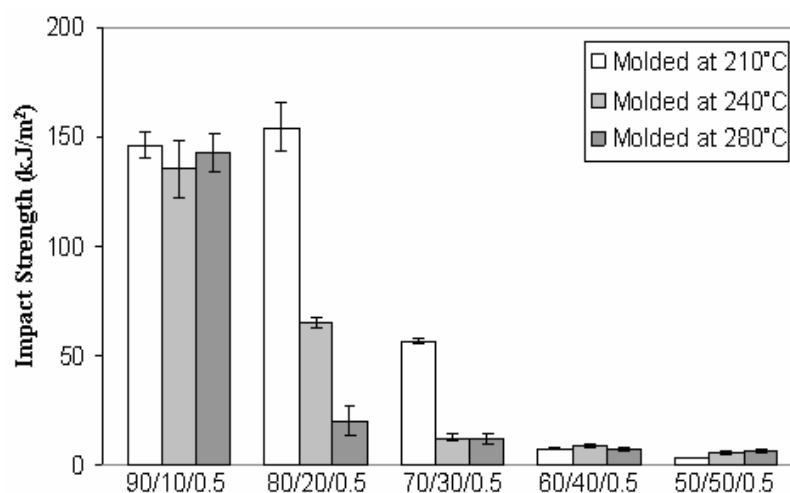


**Figure 4.45** Impact strength values of the microfiber reinforced composites molded at different temperatures

#### 4.2.1.5 Differential Scanning Calorimetry Analysis of Composites

Thermal properties of the polymer constituents of the selected composites and blends are investigated by using Differential Scanning Calorimetry (DSC). Melting points and percent crystallinities of HDPE and PET are given in Table 4.11. Melting temperatures ( $T_m$ ) of neat HDPE and PET are determined as 131 °C and 251 °C, respectively. Melting points of these two polymers are nearly the same with polymer constituents in the blends and composites. They show small fluctuations in the samples with different PET compositions [221]. Crystallization temperature for PET could not be detected, since it is very close to the melting point of HDPE (~ 130 °C). Percent crystallinities ( $X_c$ ) of the sample constituents are distinctive according to the composition of the sample. The observed changes in the crystallinities could be explained on the basis of the ASCNT in the PET phase and effect of the physical state of the second polymer phase in the samples [222]. Percent crystallinity ( $X_c$ ) of the HDPE phase decreases as the PET amount in the composite is increased. Crystallization of HDPE phase in the samples occurs in the presence of rigid PET phase due to the high melting temperature of PET (~ 250°C). This restricts the crystal growth in HDPE phase and descends the percent crystallinity [223]. However, percent crystallinities of the hot-stretched and

molded microfiber reinforced composites are nearly the same for both polymers. Degree of crystallinities of PET phases in the samples increases with the decreasing amount of HDPE. Crystallization of PET in the samples occurs in the presence of molten HDPE phase, which could again hinder the crystallization of PET phase and decrease the percent crystallinity [222]. In addition, presence of ASCNT in PET phase ascends the percent crystallinity. Carbon nanotubes are nano sized particles and they can enhance the crystallization of PET phase due to the nucleation effect [210]. Molding temperature does not have a distinctive effect on the crystallinity of both polymer phases (Table 4.11).

**Table 4.11** DSC results of the selected samples

<b>Sample (HDPE/PET/CNT)</b>	<b>T<sub>m</sub>(HDPE) (°C)</b>	<b>T<sub>m</sub>(PET) (°C)</b>	<b>X<sub>c</sub>(HDPE) (%)</b>	<b>X<sub>c</sub>(PET) (%)</b>
<b>80/20</b>	132	251	77.7	18.5
<b>70/30</b>	131	251	74.0	20.8
<b>50/50</b>	129	251	63.2	24.3
<b>80/20/0.5 microfiber</b>	130	251	72.8	24.8
<b>70/30/0.5 microfiber</b>	129	251	67.5	28.5
<b>50/50/0.5 microfiber</b>	129	252	62.8	30.3
<b>80/20/0.5 microfiber (210)</b>	130	249	72.4	25.4
<b>80/20/0.5 microfiber (240)</b>	132	250	74.9	25.6
<b>80/20/0.5 microfiber (280)</b>	130	250	75.4	25.5
<b>70/30/0.5 microfiber (210)</b>	131	250	65.6	27.4
<b>50/50/0.5 microfiber (210)</b>	130	250	63.4	30.8
<b>80/20/0.5</b>	131	251	72.8	26.2

#### 4.2.2 Microfiber Reinforced High Density Polyethylene/Poly(ethylene terephthalate)/Carbon Nanotube Composites Prepared with Surface Treated Carbon Nanotubes

Morphological, electrical and mechanical characterization experiments of the microfiber reinforced polyethylene/poly(ethylene terephthalate)/carbon nanotube composites prepared with as-received, purified and modified carbon nanotubes will be explained in the following section.

##### 4.2.2.1 Interfacial Tension and Wetting Coefficient Calculations

Surface energy components of the HDPE, PET, ASCNT, pCNT and PEG1000CNT are given in Tables 4.4 and 4.10. After the determination of the surface energy components for each material, surface tensions between the composite constituents are calculated. The surface tensions between the composite constituents are used during the wetting coefficient ( $w$ ) calculations to determine the location of carbon nanotube in the composites theoretically. The wetting coefficients for HDPE/PET/ASCNT, HDPE/PET/pCNT and HDPE/PET/PEG1000CNT composites are calculated as 1.27, 1.46 and 1.37, respectively. It is observed that the wetting coefficients for the composites prepared with all types of CNT are greater than 1, which means that carbon nanotube particles should disperse in PET phase theoretically. Wetting coefficients for pCNT and PEG1000CNT are greater than that of ASCNT due to the enhanced interactions between carbon nanotubes and PET after surface treatment. On the other hand, it is lower for PEG1000CNT than that of pCNT due to the possible chemical affinity between PEG and HDPE as a result of the common ethylene parts in their chemical structures. Moreover the incorporation of the nanoparticles into polymer blends can increase the compatibility of polymer phases by decreasing the interfacial tension between the phases [96]. Interfacial tensions between the HDPE and PET/CNT phases in HDPE/PET/ASCNT, HDPE/PET/pCNT, HDPE/PET/PEG1000CNT composites are calculated as 5.82, 5.04, 4.03 mN/m. They decrease with the carbon nanotube surface treatment when

compared to ASCNT based composite, which might show the enhanced miscibility between these phases.

#### 4.2.2.2 Melt Viscosity Measurements

Melt viscosities of the PET/CNT composites prepared with all types of carbon nanotube at 1.25, 3.75 and 7.5 wt. % compositions, neat HDPE and PET are measured and shown in Figure 4.46 (Equations 2.14-2.18). These analyses are performed to see the effect of interaction extent between the PET and carbon nanotubes on the melt viscosity of this phase. It is observed that the melt viscosity of neat PET is much lower than neat HDPE at the processing and hot-stretching temperature of the microfiber reinforced composites, which is a requirement for the formation of the satisfactory microfibers in an immiscible blend. Carbon nanotube addition to PET increased the melt viscosity and restricts the elongational flow in the presence of rigid carbon nanotube particles. Also, melt viscosities of the PET/CNT composites increase with the ascending amount of carbon nanotube in the composite which might limit the microfiber formation after 3.75 wt. % carbon nanotube loading due to the restrictions during deformation of the PET/CNT phase into microfibers. On the other hand, melt viscosities of the composites containing pCNT or PEG1000CNT are lower than those of ASCNT containing composites at all compositions. This indicates the difference in the distribution of the fillers in the polymer matrix, such as ASCNT might have larger agglomerate size and poorer dispersion in PET phase when compared to surface treated carbon nanotube (Figure 4.30).

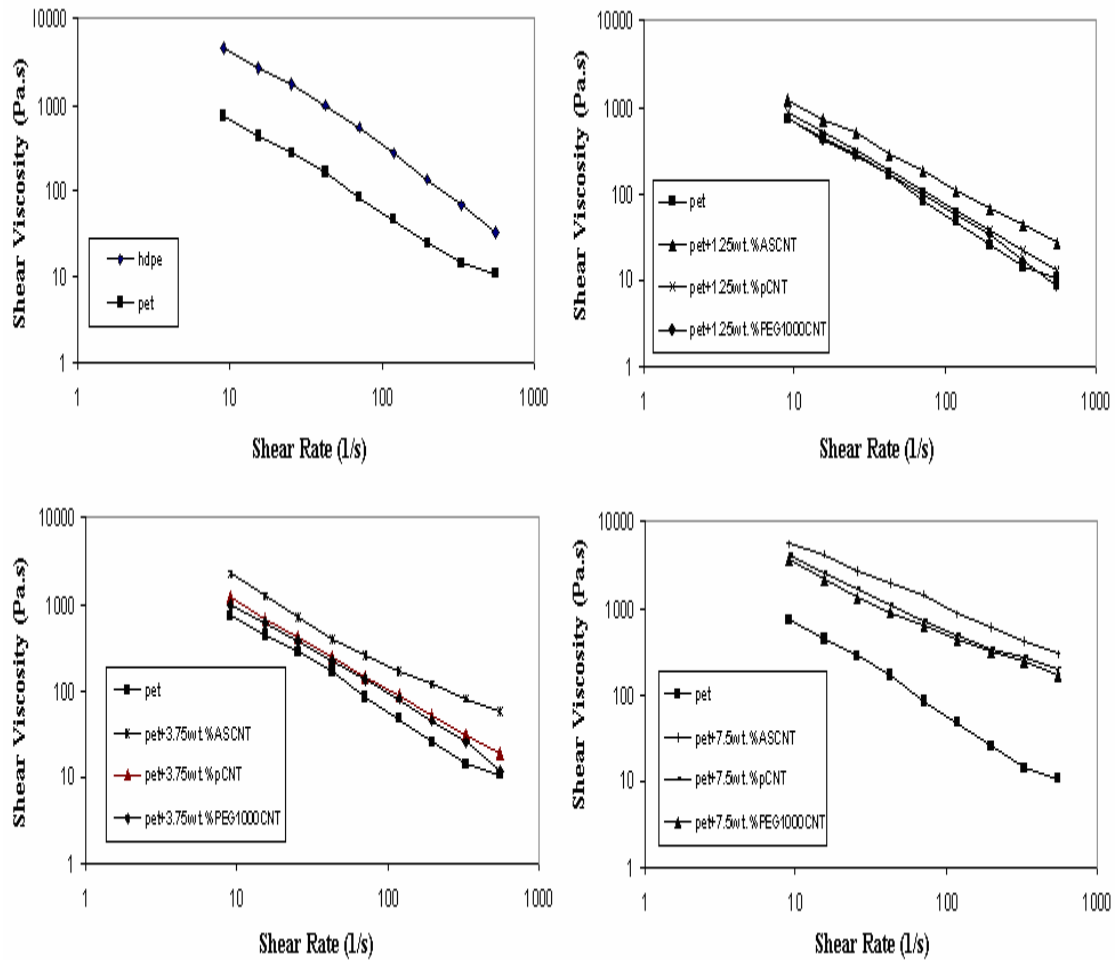


**Figure 4.46** Shear viscosity vs. shear rate graphs for HDPE, PET and PET/CNT composites

#### 4.2.2.3 Scanning Electron Microscopy of Composites

Figure 4.47 shows the distribution and domain sizes ( $d_{avg}$ ) of the PET/CNT phases in HDPE matrix for HDPE/PET/CNT composites. Micrographs exhibit that the PET/CNT phase is dispersed in the HDPE phase. The average sizes of PET/CNT phases in 1.5 wt. % (7.5 wt. % in PET phase) carbon nanotube containing composites are lower than those of 0.25 wt. % (1.25 wt. % in PET phase) carbon nanotube containing composites for all types of carbon nanotubes due to the reduction in the coalescence of the PET phase in the presence of the higher amount of rigid carbon nanotube particles in the PET phase and at the interface

between the HDPE and PET as carbon nanotube concentration increases [224]. PET/CNT phases seem to be dispersed more homogeneously for pCNT and PEG1000CNT based composites when compared to ASCNT based composites (Figure 4.47). However, the average PET/CNT phase sizes of the pCNT and PEG1000CNT based composites are larger than that of ASCNT based composite at the same carbon nanotube loadings. This might also show the distinctions in the carbon nanotube dispersion in PET phase after surface treatment. Surface treated carbon nanotube might distribute in PET phase with smaller agglomerate size which results in lower melt viscosity (Figure 4.46) [225] and decrease in the PET/CNT phase coalescence, during processing of composites [224].

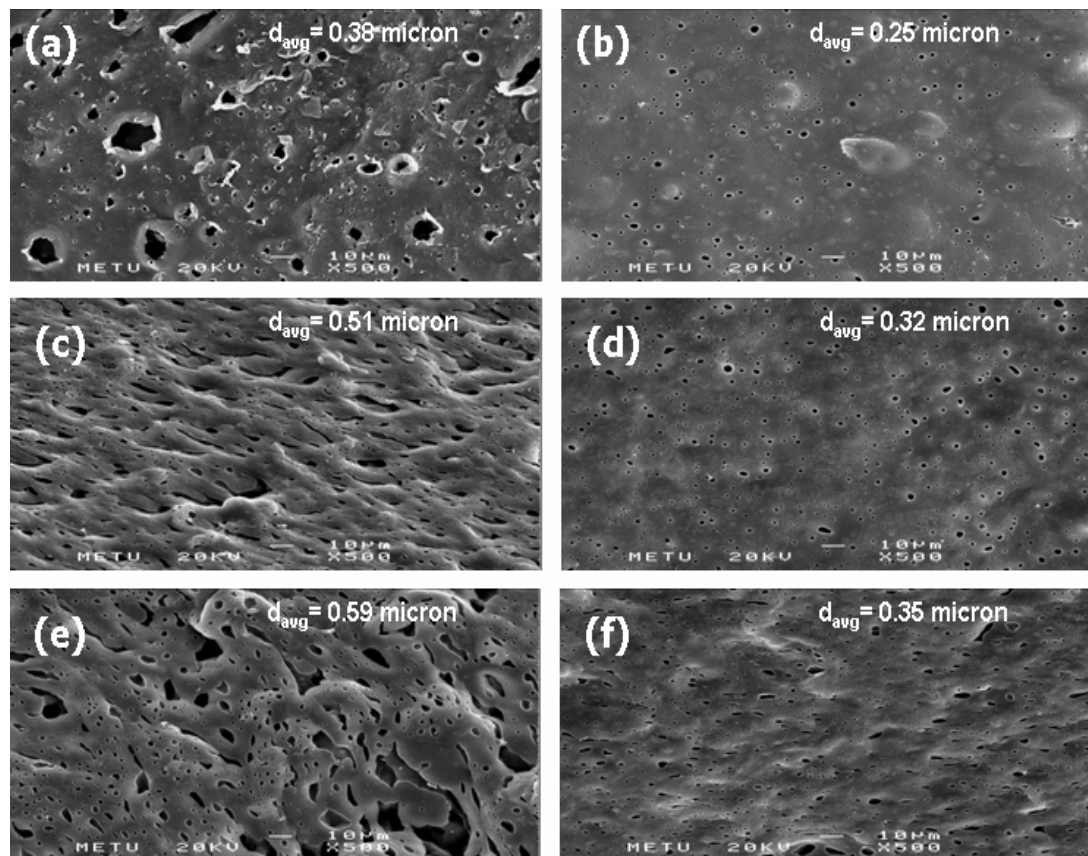


**Figure 4.47** SEM micrographs of the HDPE/PET/CNT composites a) 0.25 wt.% ASCNT, b) 1.5 wt.% ASCNT, c) 0.25 wt.% pCNT, d) 1.5 wt.% pCNT, e) 0.25 wt.% PEG1000CNT, f) 1.5 wt.% PEG1000CNT (samples were directly taken from the extruder die without hot-stretching and etched with trifluoro acetic acid)

The preferential distribution of the pCNT and PEG1000CNT in PET phase of HDPE/PET/CNT composites can be observed in Figure 4.48. In the figures, PET surface is rough, without any sign of elongation due to the brittle nature of PET and carbon nanotube particles selectively locate on its surface as fibrillar particles. On the other hand, HDPE phase is stretched due to ductile nature with a smooth surface structure and it is very hard to observe any carbon nanotube particles on its surface. These results are also coherent with the theoretical wetting coefficient calculations and previous findings which suggest that carbon based conductive filler particles prefer to locate in the phases with lower melt viscosity of polymer blends [160]. Rheological analysis showed that PET had much lower melt viscosity than HDPE at the composite mixing temperature (Figure 4.46). The selective dispersion of ASCNT in PET phase of HDPE/PET/CNT composites is shown in Figure 4.32 and 4.33.

Deformation of PET/CNT phase into microfibers during elongational flow strongly depends on the melt viscosity of the dispersed phase. However, the fibrillation of the PET phase in the presence of carbon nanotube particles depends on the concentration of carbon nanotube in this phase. Micrographs of the hot-stretched HDPE/PET/CNT composites (Figure 4.49 a-d) point out the in-situ PET/ASCNT microfiber structure in HDPE phase up to 0.75 wt. % carbon nanotube composition (3.75 wt. % carbon nanotube loading in PET phase). After this amount of carbon nanotube loading, increase in the melt viscosity of PET/ASCNT phase restricted the microfiber formation. On the other hand, hot-stretched HDPE/PET/CNT composites prepared with pCNT and PEG1000CNT show the successful formation of PET/CNT microfibrillar structure in HDPE phase up to 1 wt. % carbon nanotube loading (Figure 4.49 e-l). The remarkable melt viscosity difference between the PET/pCNT, PET/PEG1000CNT composites and PET/ASCNT composite for all carbon nanotube loadings (Figure 4.46) makes it possible to form microfibers more effectively at higher concentrations of pCNT and PEG1000CNT when compared to ASCNT. The smaller PET/CNT phase sizes of the 1.5 wt.% carbon nanotube containing composites for all types of CNT when compared to lower amount of carbon nanotube loadings (0.25 wt.%) (Figure 4.47), restrict the longer microfiber formation since narrower PET/CNT droplets deform into shorter microfibers during hot-stretching and a successful microfibrillar network can not be obtained inside the composite (Figure 4.49 d, h and l).

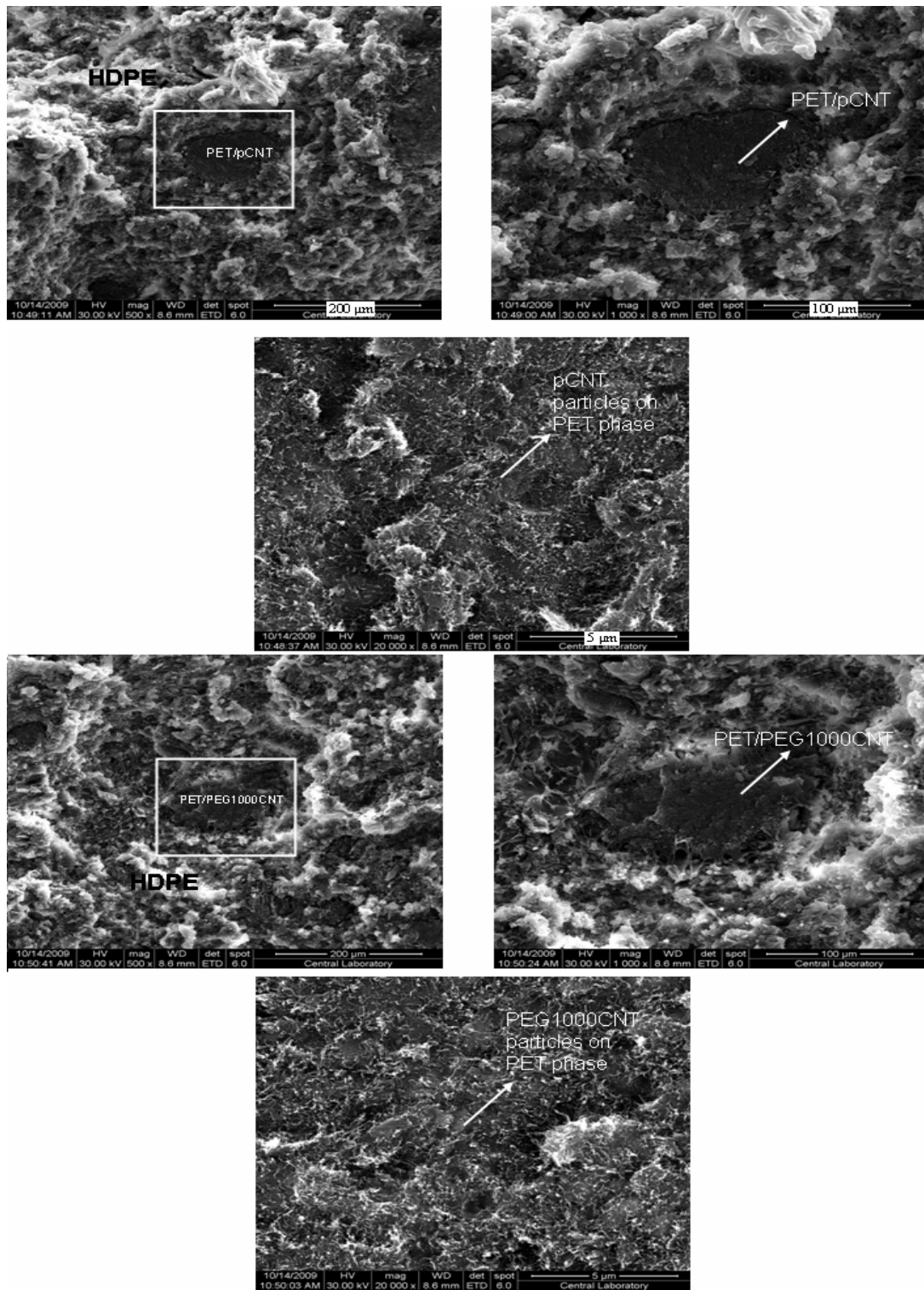


**Figure 4.48** SEM micrographs of the microfibrillar HDPE/PET/CNT composite systems containing 0.5 wt. % pCNT and PEG1000CNT containing (molded at 280°C and shows the selective localization of pCNT and PEG1000CNT in PET phase)

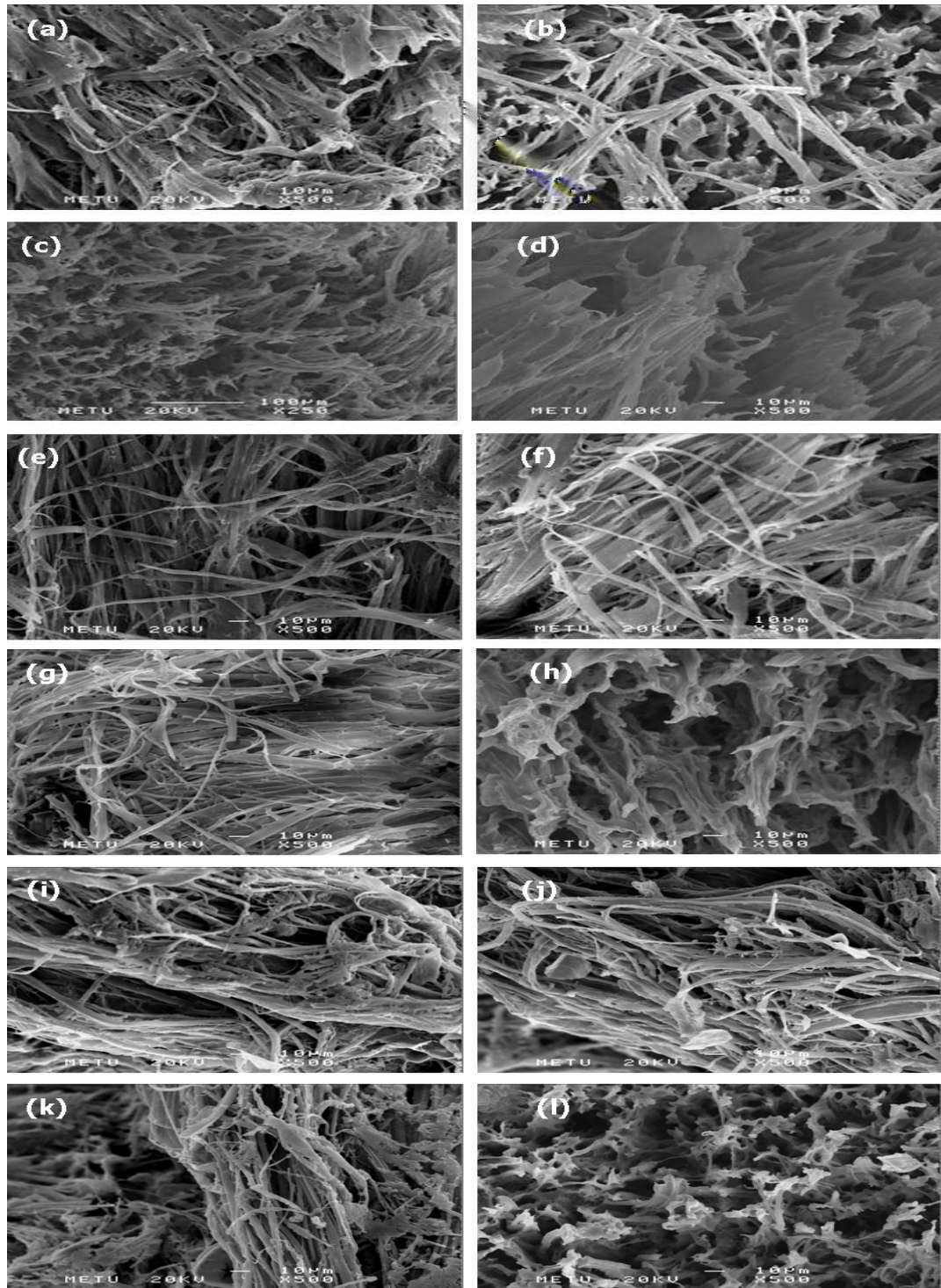


**Figure 4.49** SEM micrographs of the hot-stretched HDPE/PET/CNT composites a) 0.25 wt.% ASCNT, b) 0.5 wt.% ASCNT, c) 1 wt.% ASCNT, d)1.5 wt.% ASCNT, e) 0.25 wt.% pCNT, f) 0.5 wt.% pCNT, g) 1 wt.% pCNT, h)1.5 wt.% pCNT, i) 0.25 wt.% PEG1000CNT, j) 0.5 wt.% PEG1000CNT, k) 1 wt.% PEG1000CNT, l) 1.5 wt.% PEG1000CNT (etched with hot xylene)

The SEM micrographs of the injection molded (210 °C) specimens of the microfiber reinforced composites (Figure 4.50 a, c and e) reveal that the microfibrillar structure is preserved for the composites in which the microfiber formation was successful. On the other hand, micrographs of the molded (210°C) composites with inefficient microfiber formation (1.5 wt.% carbon nanotube composition) display only a few microfibers in their micrographs (Figure 4.50 b, d and f).

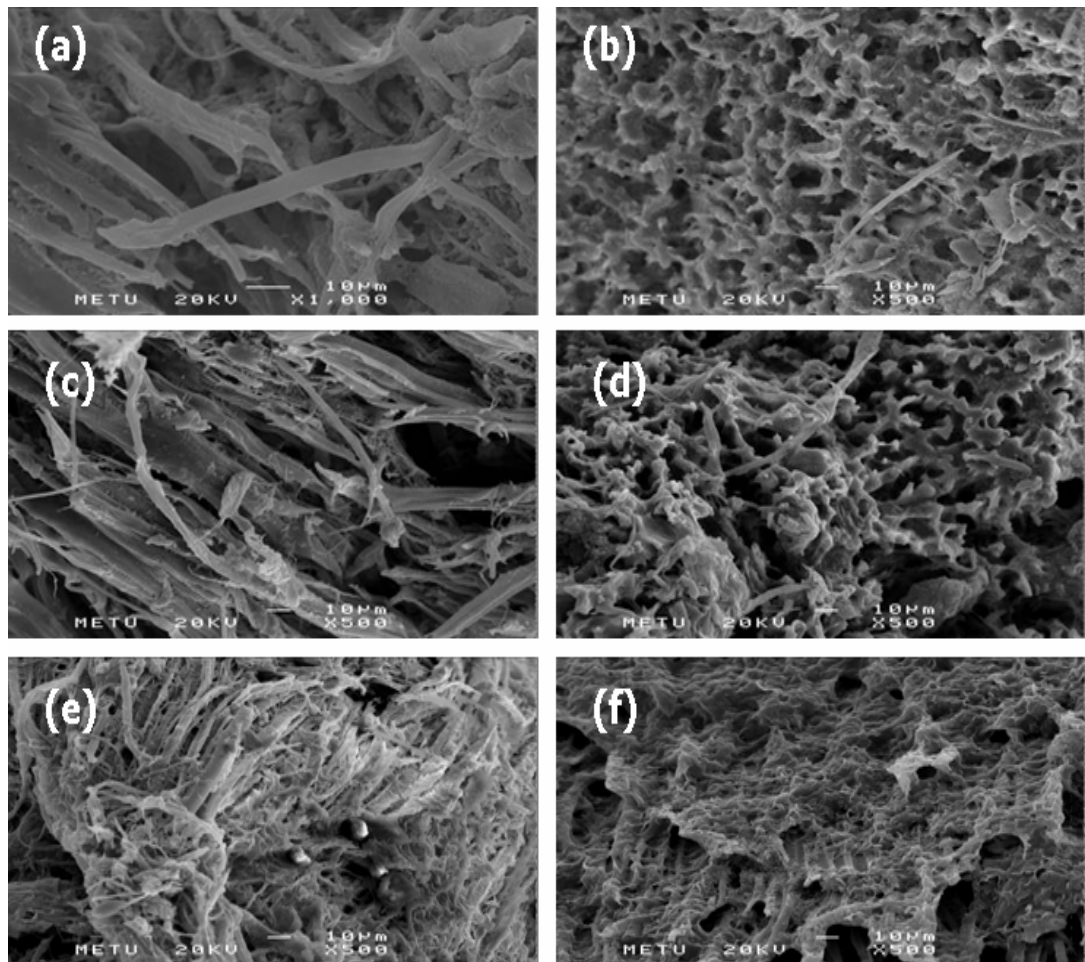


**Figure 4.50** SEM micrographs of the microfibrillar HDPE/PET/CNT composites a) 0.25 wt.% ASCNT, b) 1.5 wt.% ASCNT, c) 0.25 wt.% pCNT, d) 1.5 wt.% pCNT, e) 0.25 wt.% PEG1000CNT, f) 1.5 wt.% PEG1000CNT (molded at 210°C and etched with hot-xylene)

#### 4.2.2.4 Electrical Resistivity Measurements of Composites

PET/CNT composites have very high electrical conductivity and low percolation threshold concentration. The electrical resistivity values of the PET/CNT composites prepared with ASCNT, pCNT and PEG1000CNT are smaller than  $10^6$  ohm.cm at 0.25 wt. % carbon nanotube loading, which shows that the percolation threshold concentration of these composite systems are lower than this CNT concentration (Figure 4.22). Thus, when PET/CNT phase forms a continuous microfibrillar structure in HDPE matrix, electrical conductivity of the composites passes from insulator range to semiconductor range ( $< 10^8$  ohm.cm) (Figure 4.51 a). Microfibers with high electrical conductivity can contact with each other directly when the continuous microfiber network is formed in the composite, which makes the current conduction easier. Moreover, electrical resistivities of the composites decrease with the increasing amount of conductive filler until the successful microfiber network is present in the composites. Microfiber reinforced composites, which do not have a successful microfiber structure have higher electrical resistivities than those of the ones with microfibrillar morphology. The electrical resistivity value of the HDPE/PET/ASCNT composite is between  $10^5$  and  $10^6$  ohm.cm at 0.75 wt. % ASCNT composition. However, it increases to  $10^9$  ohm.cm when ASCNT content in the composite is 1 wt. % due to the lack of conductive microfiber network inside the composite (Figures 4.49 and 4.50). The same characteristic is also observed for pCNT and PEG1000CNT based composites. There is a remarkable increase in the electrical resistivity values of these composites between 1 wt. % and 1.5 wt. % carbon nanotube loadings. The transition of the composite's electrical conductivities from semiconductor to insulator range occurs at higher CNT concentrations for the composites prepared with surface treated carbon nanotubes when compared to ASCNT, due to the more effective microfiber formation induced by the lower melt viscosity of PET/CNT phases.

ASCNT based composites generally have lower electrical resistivity values than those of the composites based on the other two carbon nanotubes up to 0.75 wt. % carbon nanotube loading. The reason for this might be the lower electrical conductivities of PET/CNT phases prepared with surface treated carbon nanotube due to higher intrinsic electrical resistivities of the pCNT and PEG1000CNT when

compared to ASCNT. The electrical resistivity value of the 0.75 wt.% ASCNT containing microfibrillar composite is two times lower than that of the PEG1000CNT based composite (Figure 4.51 b). Molding temperatures above the melting point of PET (255 °C) cause PET/CNT phase to melt and loose the microfiber characteristics. Thermodynamically, when microfiber phases melt they have a spherical shape, PET/CNT phases are dispersed in the HDPE phase and a co-continuous morphology can not be obtained (Figures 4.47 and 4.48). Microfiber reinforced composites molded at 210 °C have lower electrical resistivity values than those of the composites molded at 280 °C for all carbon nanotube types (Figure 4.51 b), since higher temperature molded composites do not have a continuous PET/CNT network in their structures at 80/20 (HDPE/PET) ratio.

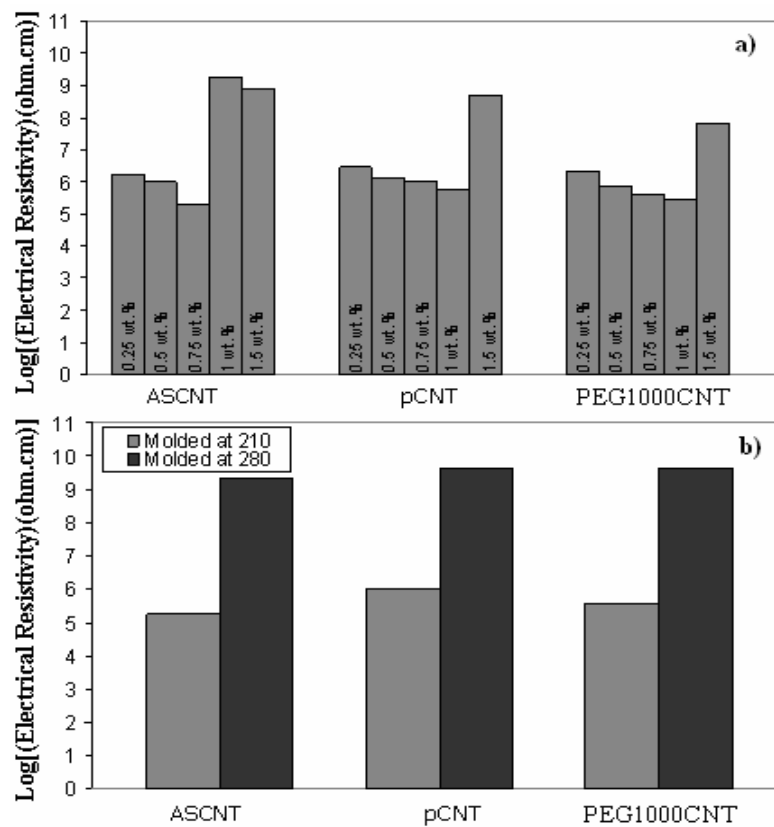


**Figure 4.51** Electrical resistivity values of the microfibrillar HDPE/PET/CNT composites a) effect of carbon nanotube surface treatment and amount (molded at 210°C), b) effect of molding temperature at 0.75 wt.% carbon nanotube containing microfibrillar composites

#### 4.2.2.5 Tensile and Impact Tests of Composites

The mechanical properties of the microfiber reinforced HDPE/PET/CNT composites mainly depend on the intrinsic mechanical properties of the matrix and microfiber phase; shape of the PET/CNT phase; degree of interfacial adhesion between the HDPE matrix and microfibrillar PET/CNT phase. Mechanical properties of the microfibrillar composites can be enhanced more effectively by the reinforcing effect of the microfibers with advanced mechanical strength. Microfiber formation in the presence of carbon nanotube particles improves the tensile strength and modulus when compared to those of the microfibrillar HDPE/PET blend (Figure 4.52). However, this reinforcement is limited for the ASCNT based composites due to the lower tensile properties of PET/ASCNT phase than PET/pCNT and PET/PEG1000CNT phases. PET/ASCNT composites generally suffer from the weak mechanical properties due to the weak interfacial adhesion between PET and carbon nanotube. After surface treatment the functional groups on carbon nanotube surface (Figure 4.10) can increase the chemical compatibility in the composite (Figure 4.19). Moreover, defect sites on the carbon nanotube surface can increase the mechanical interlocking and covalent bonding between carbon nanotube and PET matrix. These interactions between composite constituents improve the efficiency of load transfer from the PET to carbon nanotube [188] and mechanical strength of the composites prepared with pCNT and PEG1000CNT are higher than those of PET/ASCNT composite. As a result of these effects, tensile strength values of the pCNT and PEG1000CNT based composites are higher than that of the ASCNT containing composites for all compositions. Enhanced miscibility between HDPE and PET/CNT phases with the usage of pCNT and PEG1000CNT, which is confirmed by the decrease in the interfacial tensions theoretically, when compared to ASCNT, might be another reason for the improvement in mechanical properties of microfibrillar composites.

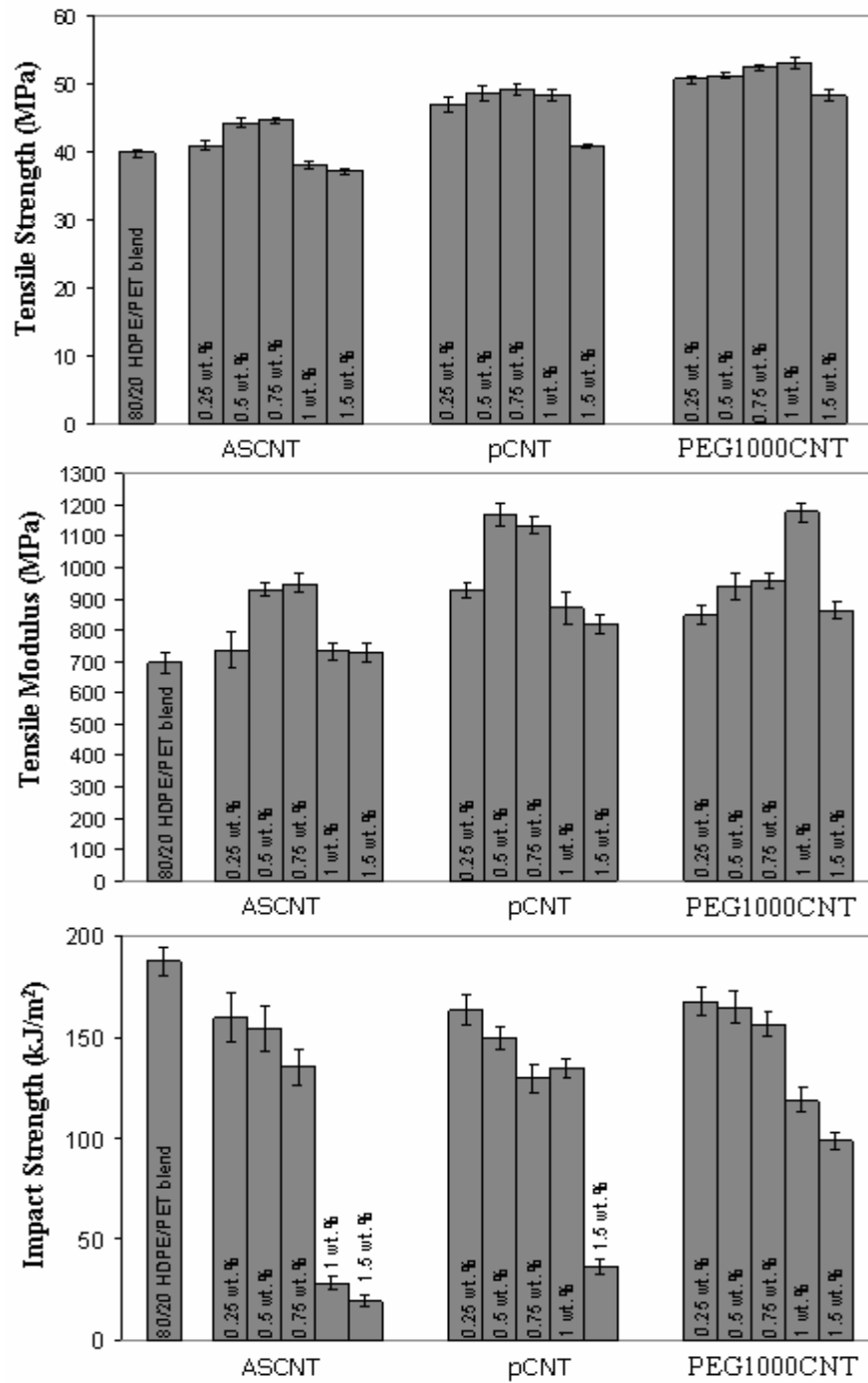


**Figure 4.52** Tensile strength, modulus and impact strength values of the microfibrillar HDPE/PET/CNT composites and HDPE/PET blend

Similar with the trend in the electrical resistivity results, generally a sharp decrease is observed for tensile modulus and impact strength values of the microfiber reinforced composites after 0.75 or 1 wt. % carbon nanotube loading due to the limited microfiber formation in these composites (Figures 4.49 and 4.50) and this decrease in the amount of microfibers in the structure diminishes the reinforcing effect of this phase. Tensile modulus values of the 0.75 and 1 wt. % pCNT containing composites are 1130 and 870 MPa, respectively. The incorporation of rigid CNT particles into HDPE/PET microfibrillar blends decreases the impact strength due to the brittle nature of carbon nanotube and this trend continues with ascending amount of carbon nanotube in the composites. Microfibers present in the composite decrease the crack formation and propagation in the sample during the impact test [84]. So, when the microfiber concentration in the composite decreases, a sudden decrease in the impact strength is also observed for all types of carbon nanotubes. Impact strength values of the 0.75 and 1 wt. % ASCNT containing composites are 135 and 30 kJ/m<sup>2</sup>, respectively (Figure 4.52). Molding temperature increment decreases the mechanical properties of the microfiber reinforced composites due to the melting of PET/CNT phase (Figure 4.53). At high temperature molding, PET/CNT microfibers with high aspect ratio transform into spherical particles with lower aspect ratio (Figure 4.48) and the reinforcing effect of this phase disappears.

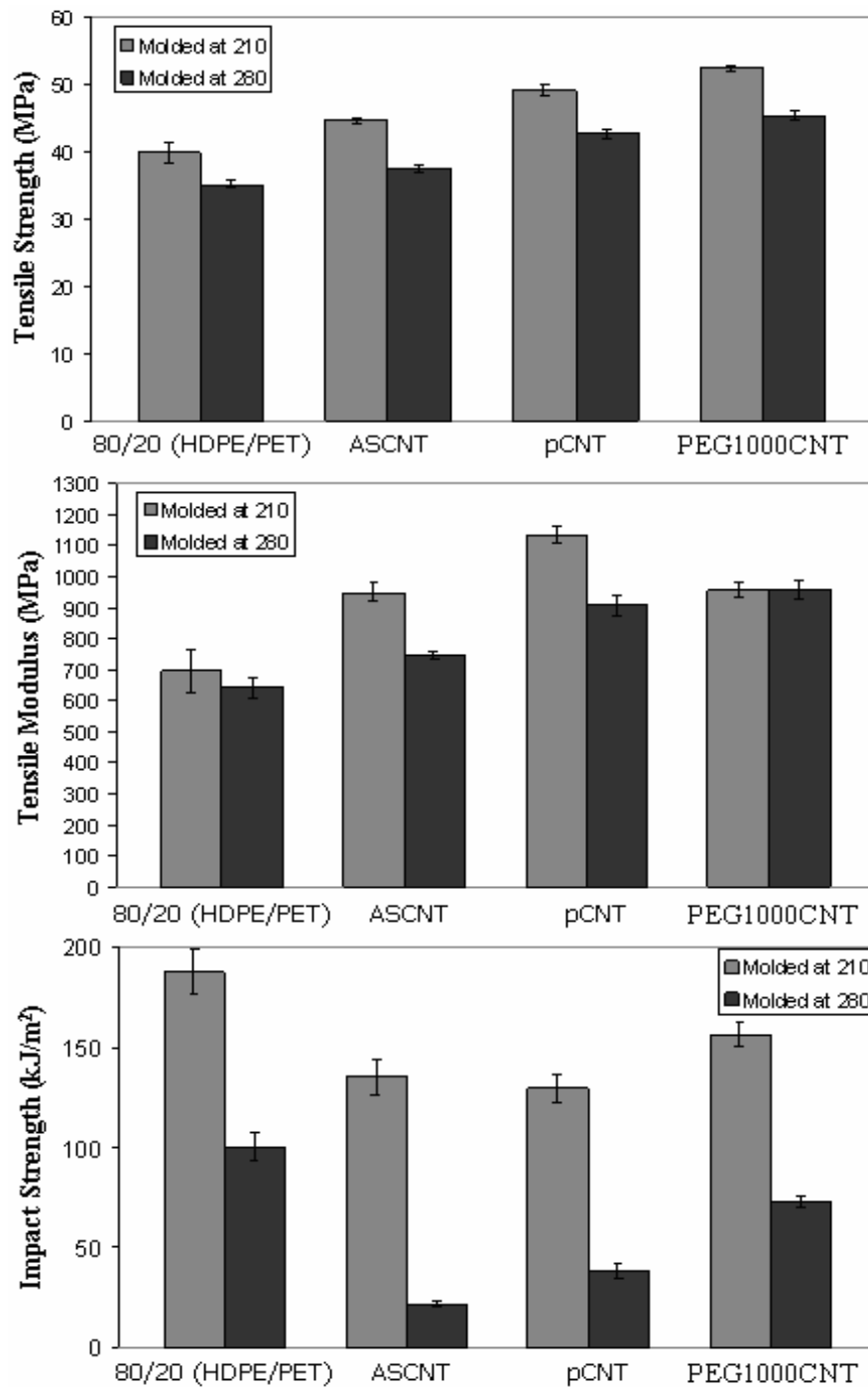


**Figure 4.53** Tensile strength, modulus and impact strength values of the microfibrillar HDPE/PET/CNT composites containing 0.75 wt. % carbon nanotube and HDPE/PET blends (effect of molding temperature)

### 4.3 Epoxy/Carbon Nanotube Composites and Epoxy/Carbon Nanotube/Glass Fiber Composite Panels

In this part of the dissertation, characterization studies of the epoxy/CNT composites and epoxy/CNT/glass fiber composite panels prepared with as-received carbon nanotube (ASCNT) and hexamethylene diamine (HMDA) treated carbon nanotubes (mCNT) will be explained in three subsections. The fiber reinforced composite panels are prepared as potential examples for the usage in the aerospace applications. In the first part, the characterization of the carbon nanotube samples will be discussed. Second part contains the characterization results of the epoxy/CNT composites. Finally, the properties of the epoxy/CNT/glass fiber composite panels will be explained in the last part.

#### 4.3.1 Characterization of Carbon Nanotubes

Carbon nanotubes were used as the conductive filler during the preparation of the epoxy/CNT composites and epoxy/CNT/glass fiber composite panels to increase the electrical conductivity and improve the damage sensing capability. In this part of the dissertation the effect of the amine modification on surface chemistry, morphology and suspension stability of the carbon nanotubes will be discussed.

##### 4.3.1.1 Fourier Transformed Infrared Spectroscopy of Carbon Nanotubes

Figure 4.54 shows the FTIR spectra of the untreated (ASCNT) and diamine treated (mCNT) carbon nanotubes. Peak at around  $3440\text{ cm}^{-1}$  in the FTIR spectrum of ASCNT shows the bending modes of hydroxyl groups and it is an evidence for the presence of oxygen containing functional groups on surfaces of carbon nanotubes before any surface treatment [106]. Moreover, the increase in the intensity of the peak at  $3440\text{ cm}^{-1}$  might show the increase in the amount of hydroxyl groups on the surface after chemical treatment [105]. Peaks at  $1450$ ,  $1589$  and  $3050\text{ cm}^{-1}$  of the mCNT spectrum correspond to  $\text{NH}_2$  and N-H bending and stretching vibrations

[106, 12, and 226]. They show the interactions between the amine groups of the surface modifier and functional groups on the surfaces of carbon nanotubes. Also, the presence of peak at around  $1180\text{ cm}^{-1}$  indicates the partial oxidation of the carbon nanotubes surface during diamine treatment.

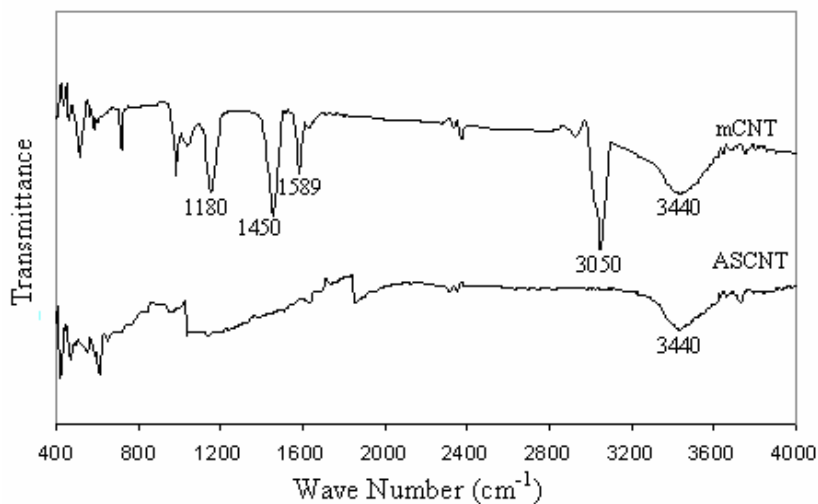


**Figure 4.54** FTIR spectra of the carbon nanotube samples

#### 4.3.1.2 X-Ray Diffraction and Scanning Electron Microscopy Analyses of Carbon Nanotubes

XRD patterns of ASCNT and mCNT are similar to each other and the characteristic peaks at  $26^\circ$  and  $43^\circ$  are observed for both samples (Figure 4.55), which means that the surface treated carbon nanotubes have the same cylinder wall and crystalline structure with untreated carbon nanotubes [184, 31]. Amine treatment does not cause a significant damage on crystalline wall structure of the carbon nanotubes. SEM micrographs of ASCNT show that carbon nanotubes are randomly entangled with each other in untreated carbon nanotubes (Figure 4.56). Chemically modified carbon nanotube structure is more compact and tubes are joined to each other. After surface treatment the length of the carbon nanotubes

are slightly shortened and the surface becomes rougher. The small differences in the morphologies of carbon nanotube samples are also observed in X-Ray patterns (Figure 4.55). Compact structure of carbon nanotubes and surface roughness are observed in the mCNT pattern as a very small shift to right in the place of the main peak and a slight decrease in the sharpness of this peak [184].

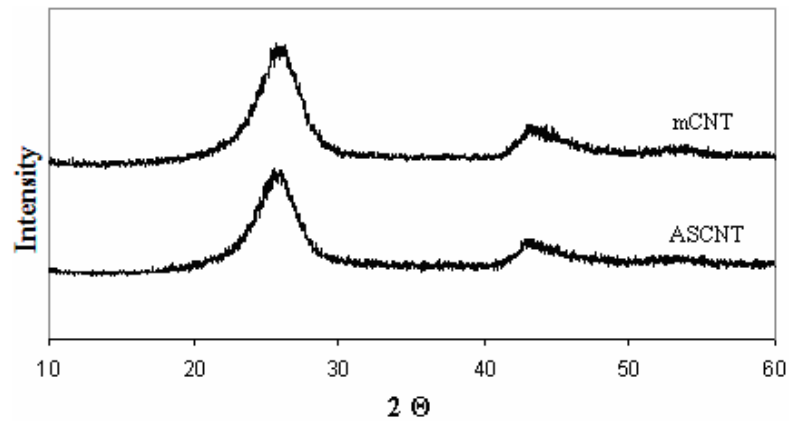


**Figure 4.55** XRD patterns of carbon nanotube samples

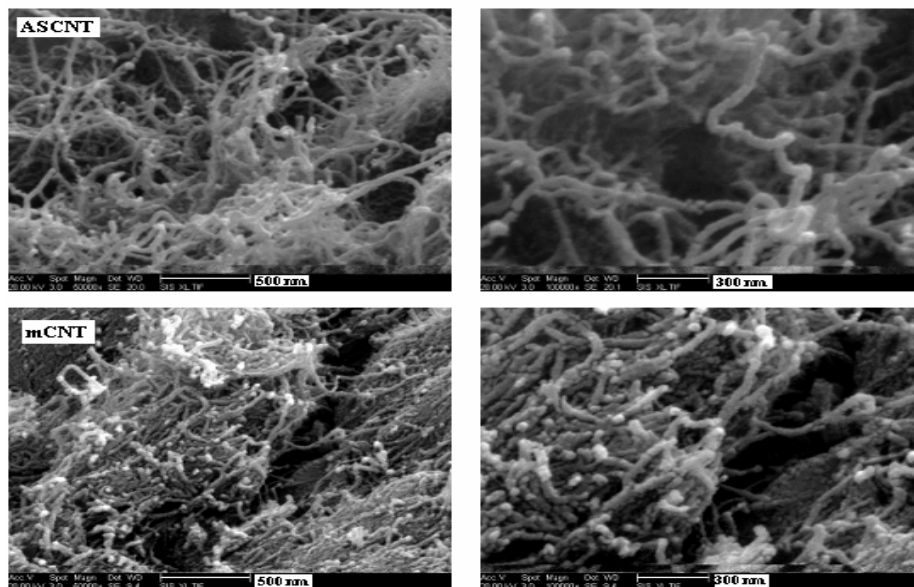


**Figure 4.56** SEM micrographs of carbon nanotube samples

#### 4.3.1.3 Suspension Stability Analysis of Carbon Nanotubes

Suspension stabilities of carbon nanotubes in acetone and ethyl alcohol (EA) are shown in Figure 4.57. Untreated carbon nanotube based suspension settles immediately due to the lack of enough surface functional groups to interact with the solvent. Amine treated carbon nanotube based suspension is stable up to 60 minutes, due to the enhanced interaction between the carbon nanotube and solvent as a result of the hydroxyl and amide groups present on the surface (Figure 4.54). Surfactant assisted suspensions are stable up to 48 hours, except the one with ASCNT and Triton X-100. The hydrophobic parts of the surfactant micelles adsorb on the surfaces of carbon nanotubes and decrease the surface tension. By this way, they can decrease the van der Waals interactions between the carbon nanotubes. Also, the electrostatic repulsions between the hydrophilic groups of the surfactants decrease the reagglomeration of carbon nanotubes. As a result, surfactants assist the homogeneous dispersion of carbon nanotubes in the solvents with a smaller particle size and increase the suspension stability [177]. Cationic cetyl pyridinium chloride (CPC) is more effective in terms of stabilizing the suspensions than nonionic Triton X-100, due to the better electrostatic interactions with the negatively charged surfaces of carbon nanotubes owing to the hydroxyl and amide groups formed after the surface treatment [67].

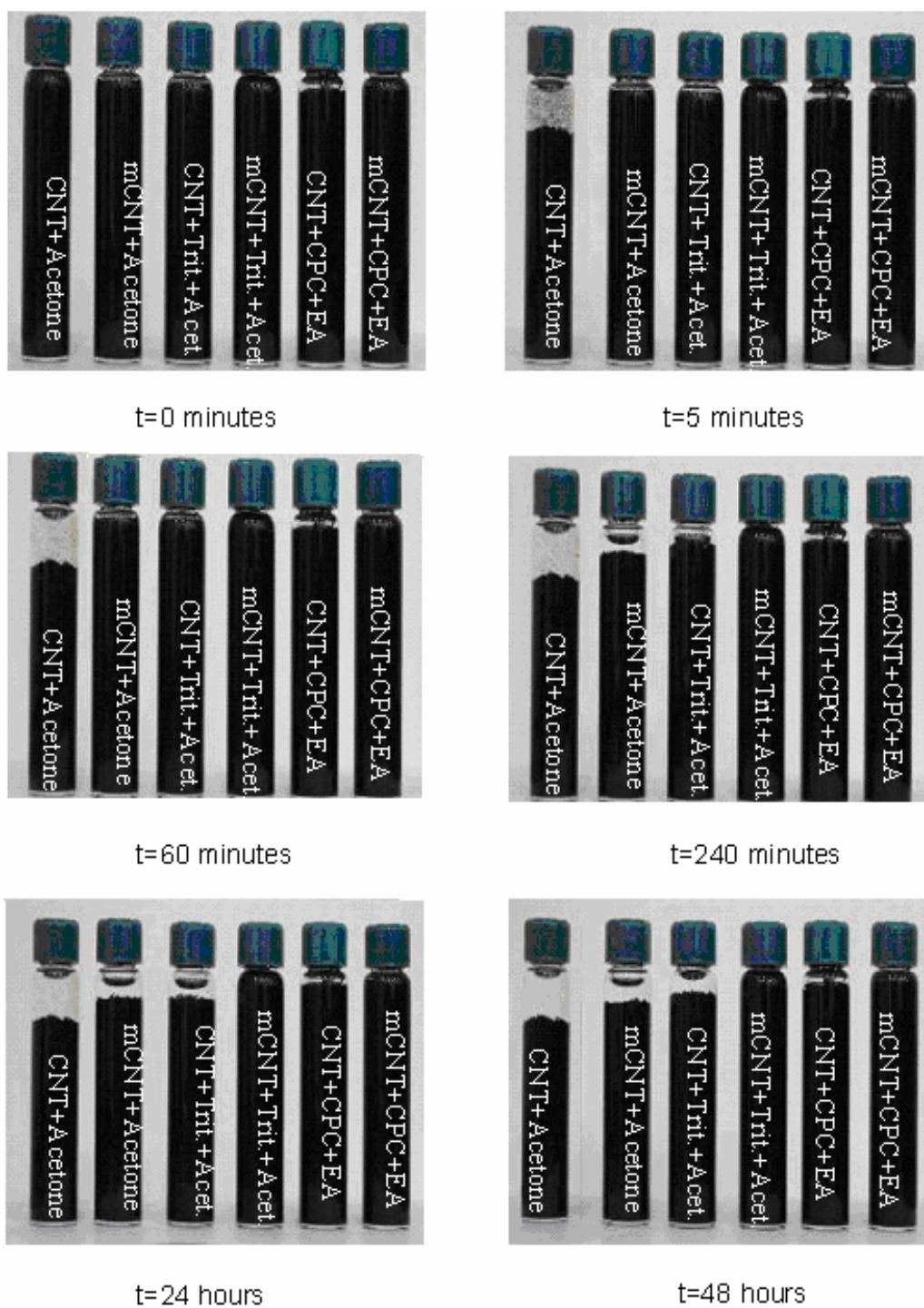


**Figure 4.57** Suspension stabilities of the carbon nanotube samples in acetone and ethyl alcohol (EA) with and without surfactant assistance

### 4.3.2 Characterization of Epoxy/Carbon Nanotube Composites

Epoxy/CNT composites were prepared with solvent assisted ultrasonication technique by using the as-received and modified carbon nanotubes. The effects of carbon nanotube surface modification and surfactant usage during composite preparation on the morphology, electrical and mechanical properties of the composites are discussed in this section of the dissertation.

#### 4.3.2.1 Scanning Electron Microscopy and Optical Microscopy of Composites

SEM micrographs of the epoxy/CNT composites show the morphologies of the fractured surfaces (Figure 4.58). The enhanced interfacial interactions between the epoxy and carbon nanotubes after the surface treatment result in a better dispersion of carbon nanotubes and a smaller particle size, in the composite with few larger agglomerates observed in the micrographs of mCNT based composite [226]. The carbon nanotubes observed on the fracture surface of the composite are shorter after the surface treatment due to the breakage of the carbon nanotubes during composite failure, instead of being pulled out of the surface, as a result of the better adhesion with the polymer matrix. Usage of surfactants also improves the dispersion of carbon nanotubes in the composites. During the composite preparation, the hydrophobic parts of the surfactants interact with the carbon nanotubes and on the other side the hydrophilic parts of the surfactants interact with the epoxy and form a chemical bridge between the carbon nanotubes and epoxy. By this way, carbon nanotubes adhere with the epoxy, instead of forming agglomerates by van der Waals interactions [67]. Moreover, CPC is more effective in terms of improving the dispersion of carbon nanotubes in composites than Triton X-100, due to enhanced electrostatic attraction forces between the functional groups on the surfaces of carbon nanotubes and CPC. Optical microscope images show the similar results with the SEM micrographs (Figure 4.59). It is observed that the agglomerate size of carbon nanotubes decreases with carbon nanotube surface treatment and surfactant usage, due to the lower possibility of the reagglomeration.

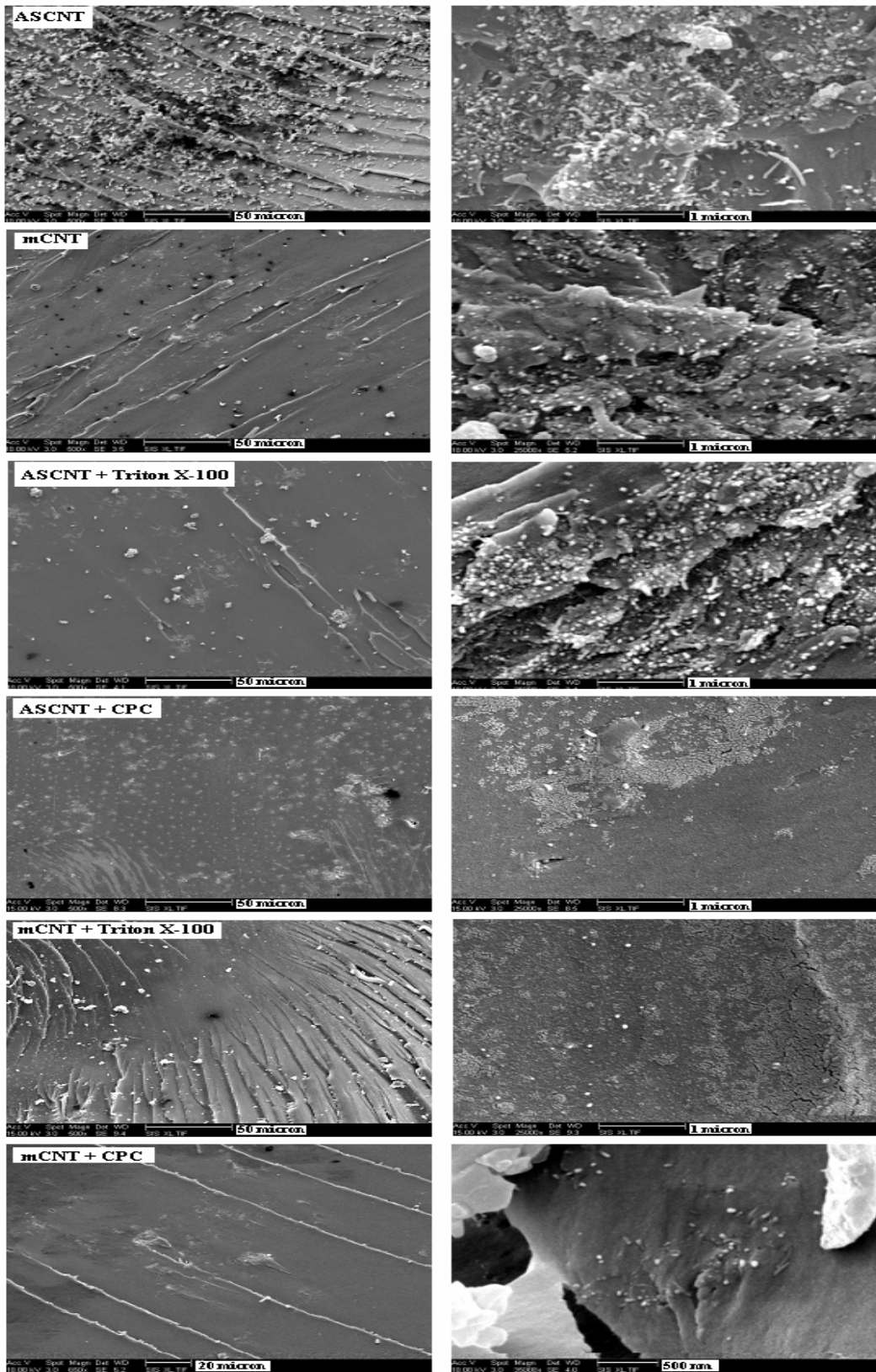


**Figure 4.58** SEM micrographs of the epoxy/CNT (0.5 wt. %) composites

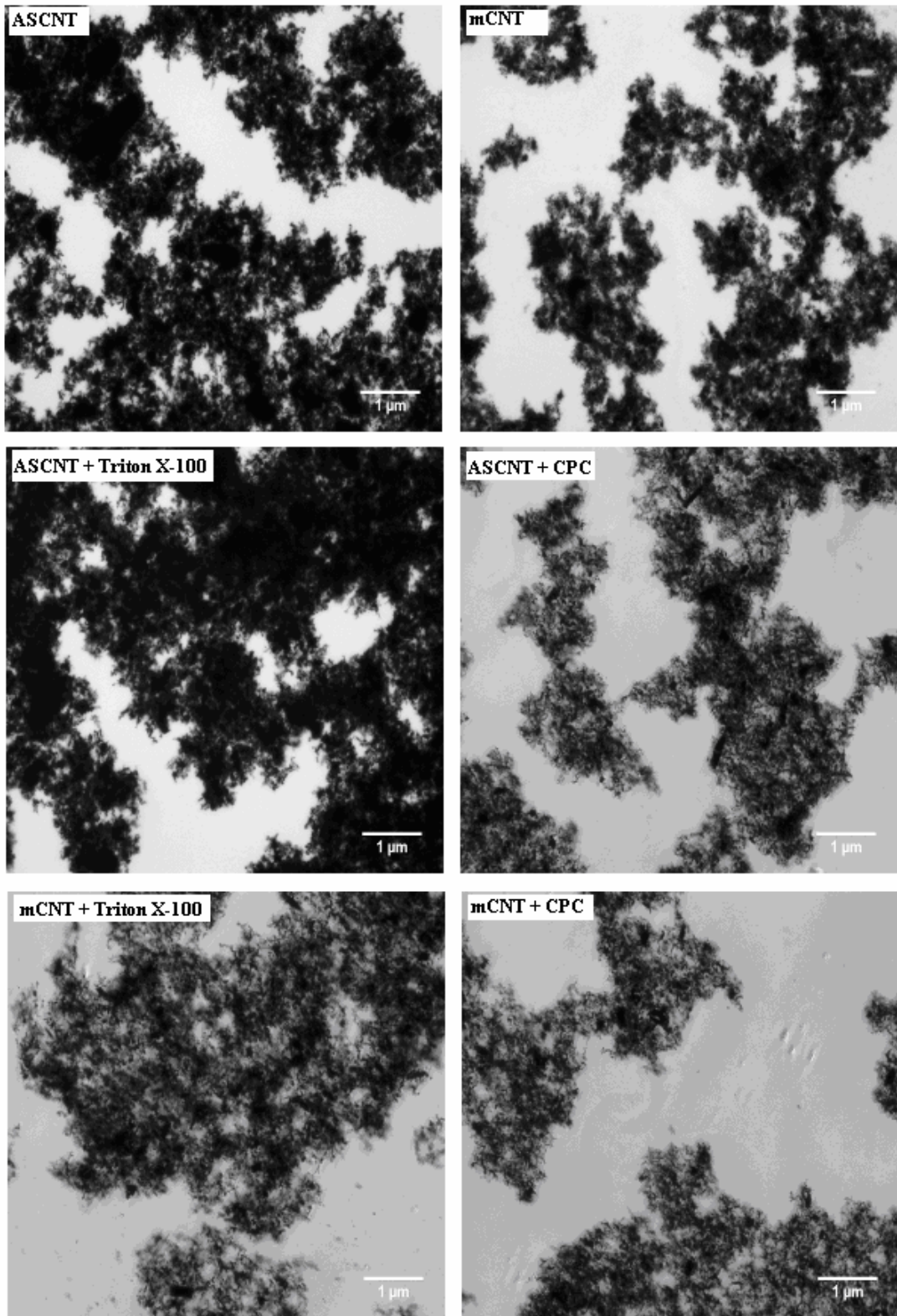


**Figure 4.59** Optical microscopy images of the epoxy/CNT (0.5 wt. %) composites

#### 4.3.2.2 Electrical Resistivity Measurements of Composites

The electrical resistivity value of the epoxy resins is around  $10^{13}$  ohm.cm [125]. The electrical resistivities of all the composites given in Figure 4.60 prepared with the ASCNT are lower than  $10^6$  ohm.cm, which means that the percolation threshold concentration of the epoxy/CNT system is lower than 0.25 wt.% CNT loading. The electrical resistivities of the composites decrease as the amount of the ASCNT in the composite increases. However, this improvement is limited after 0.5 wt.% ASCNT loading due to the larger agglomerate size of carbon nanotube and micron sized air bubbles which can not be removed totally due to the higher viscosity of the epoxy resin induced by the presence of carbon nanotubes.

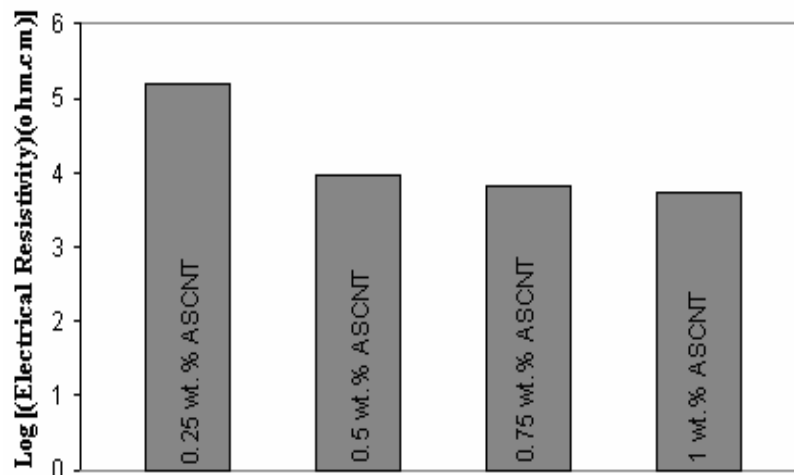


**Figure 4.60** Effect of carbon nanotube concentration on the electrical resistivity values of epoxy/ASCNT composites

Electrical resistivity of the conductive polymer composites mainly depend on the three main factors: specific electrical resistivity of carbon nanotubes, dispersion of carbon nanotubes in the composite and the agglomerate size of the carbon nanotubes. Composite prepared with mCNT have better carbon nanotube dispersion and smaller agglomerate size than the one with ASCNT (Figure 4.58).

However, the composite with mCNT has higher electrical resistivity than ASCNT based composite due to the increase in the specific electrical resistivities of carbon nanotubes after the surface treatment (Figure 4.61). The damage on the graphitic wall structure, induced by the surface treatment, decreases the electron transfer efficiency in the structure of carbon nanotubes. Moreover, the hydroxyl groups on the surface after chemical treatment constitute an insulating oxide layer and decrease the specific electrical resistivity of carbon nanotubes [32, 37 and 48]. Surfactant assisted composite preparation yields in lower electrical resistivity values due to the easier formation of conductive pathways in a well dispersed composite and higher surface area (contact area between carbon nanotube agglomerates) of carbon nanotubes with smaller agglomerate size [177]. Also, enhanced dispersion of carbon nanotubes in CPC assisted composites when compared to the ones with Triton X-100 results in lower electrical resistivity values. Surfactants (especially CPC) are more effective with mCNT than ASCNT in terms of descending the electrical resistivities of the composites due to higher number of charged functional groups on the surfaces of carbon nanotubes after the amine treatment (Figure 4.54).

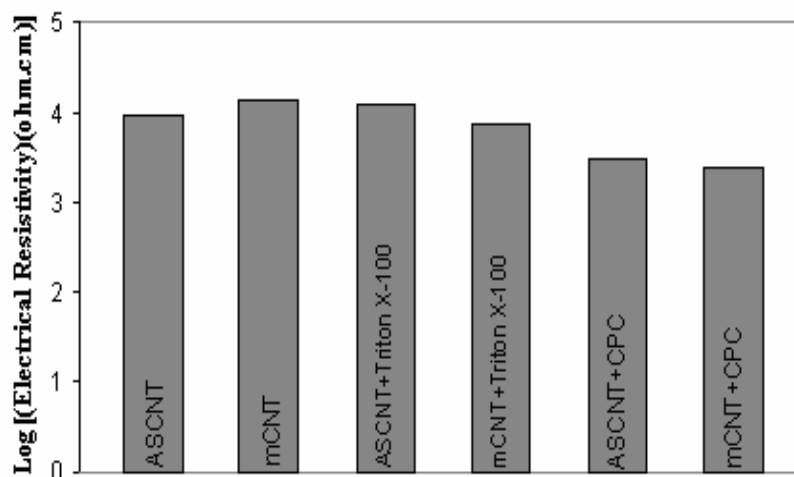


**Figure 4.61** Electrical resistivity values of the composites containing 0.5 wt.% carbon nanotubes

### 4.3.2.3 Tensile Tests of Composites

Tensile strength values of the epoxy/ASCNT composites are lower than the neat epoxy due to the inefficient load transfer caused by the low interfacial interactions between the epoxy and untreated carbon nanotubes (Figure 4.62). Carbon nanotubes come off the composite surface without breaking, during tensile loading (Figure 4.58). Moreover, larger carbon nanotube agglomerates in epoxy/CNT composite cause an increase in the stress concentration in their neighborhood and accelerate the rupture of the structure [7]. Carbon nanotube addition into epoxy improves the tensile modulus owing to the reinforcement effect of rigid fibrillar particles with high aspect ratio (Figure 4.63) [187]. However, this enhancement is limited in composites due to the large carbon nanotube agglomerates and air bubbles trapped inside the composites.

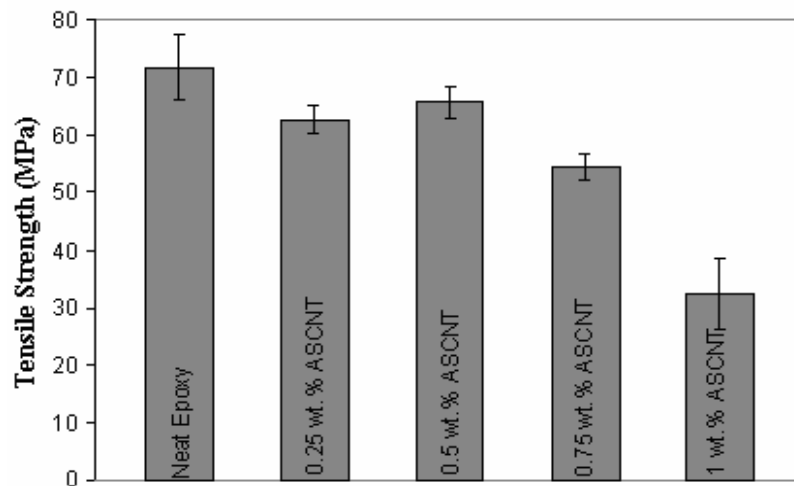


**Figure 4.62** Effect of carbon nanotube concentration on the tensile strength values of epoxy/ASCNT composites

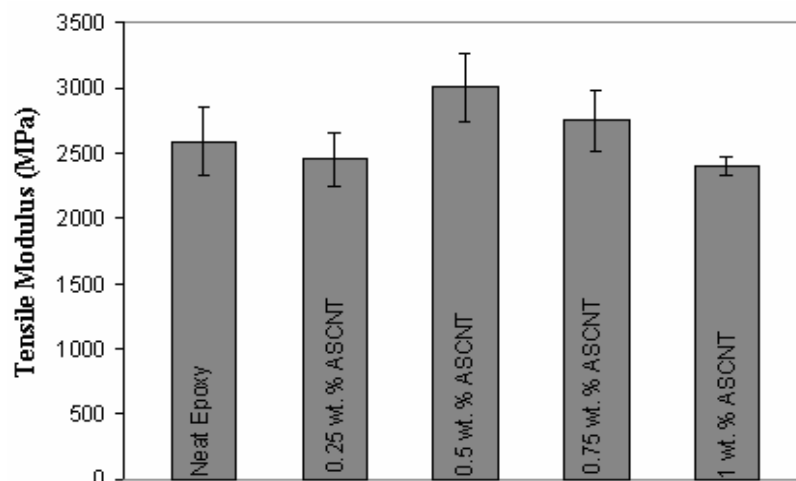


**Figure 4.63** Effect of carbon nanotube concentration on the tensile modulus values of epoxy/ASCNT composites

Tensile strength and modulus values of the mCNT based composites are higher than those of the neat epoxy and ASCNT based composite (Figures 4.64 and 4.65). The amide groups which are bonded to the surface during surface treatment form chemical bonds with the epoxide rings of epoxy resin and increase the miscibility of carbon nanotubes with epoxy [188]. The chemical and physical bonding between carbon nanotubes and epoxy develop the load transfer from the polymer matrix to carbon nanotubes and increase mechanical strength of the composite [227]. Moreover, the slightly changed bulk mechanical properties and aspect ratios of the carbon nanotubes as a result of the preserved graphitic wall structure during amine treatment make the enhancement of mechanical properties easier [26]. The usage of surfactants during composite preparation results in a homogeneous dispersion of carbon nanotubes with a smaller particle size (Figures 4.58 and 4.59). This decreases the number of stress concentrated points in the composite during the tensile tests and increases the tensile strength of the composites when compared to the composites prepared with the same kind of carbon nanotubes without surfactant usage. However, tensile moduli of the composites do not show an increase with the use of surfactants when compared to that of the composite based on mCNT, owing to the decrease in the effect of the particulate fillers (carbon nanotubes) on the tensile modulus, under a critical

particle size [8]. Cationic surfactant CPC is more effective than Triton X-100 in terms of ascending the mechanical strength of the composites due to the more effective interactions with carbon nanotubes which arise from the electrostatic attractions between the cationic head group of the surfactant and anionic surfaces of carbon nanotubes [65]. The nonionic Triton X-100 is unable to create such attractions. The enhanced surfactant-carbon nanotube interactions make it easier to break apart the carbon nanotube agglomerates and increase the tensile strength of the composites.

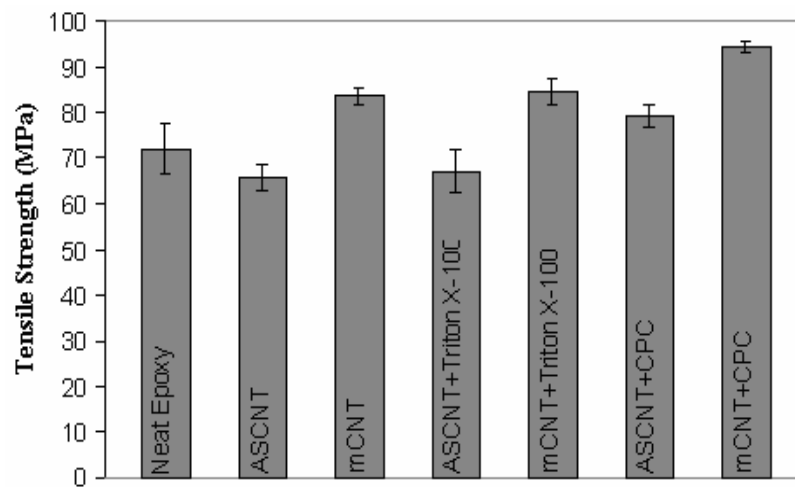


**Figure 4.64** Tensile strength values of the composites containing 0.5 wt. % carbon nanotubes

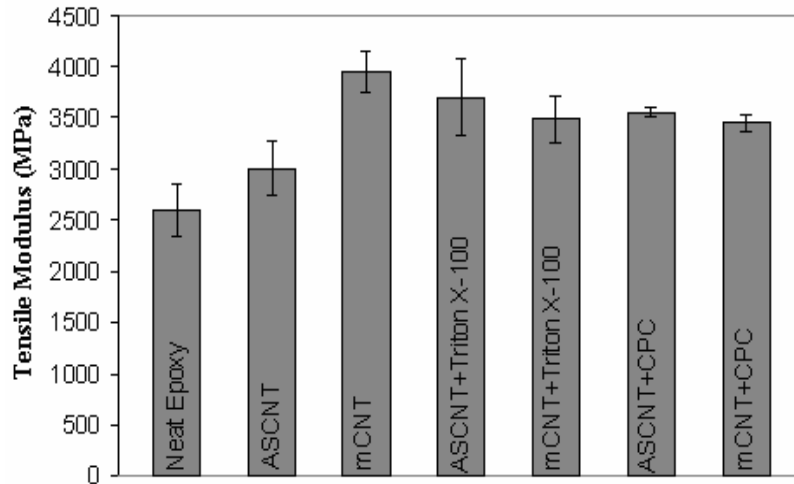


**Figure 4.65** Tensile modulus values of the composites containing 0.5 wt. % carbon nanotubes

### 4.3.3 Characterization of Epoxy/Carbon Nanotube/Glass Fiber Composite Panels

Glass fiber reinforced panels are planned to be used in the load bearing parts of the aerospace vehicles. So, the mechanical strength and damage sensitivities of these panels are very important for utilizing them in these applications. The effects of the carbon nanotube surface treatment and surfactant usage during panel preparation, on the damage sensing capabilities of the composite panels during impact, fatigue and tensile tests will be discussed in this section.

#### 4.3.3.1 Tensile Tests of Composite Panels

The coverage of the glass fibers with epoxy/carbon nanotube mixture, dispersion state and particle sizes of carbon nanotubes in epoxy matrix is very important for the properties of the composite panels. They should be optimized during the preparation of the composite panels [228]. SEM micrographs of the composite panel show that the glass fibers were coated with the epoxy/mCNT mixture. Carbon nanotubes can form the conductive network in the panels (Figure 4.66).

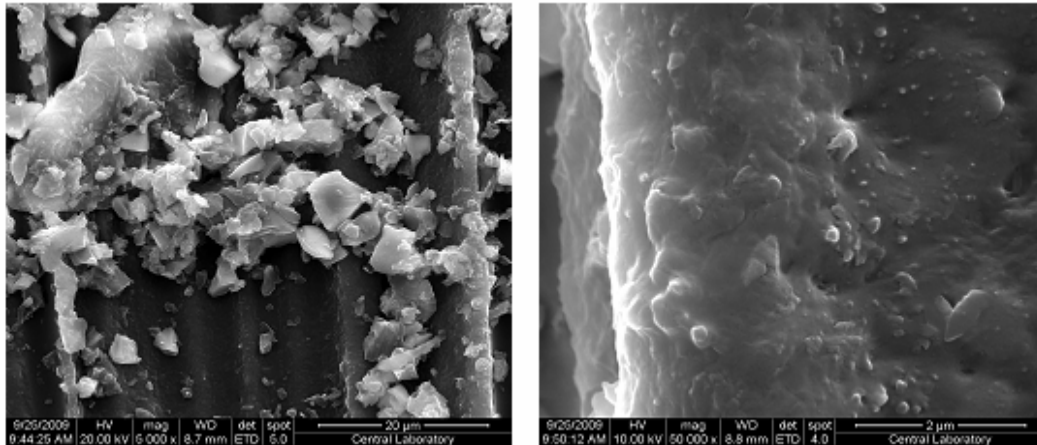


**Figure 4.66** SEM micrographs of the composite panel in which CPC assisted 0.5 wt. % carbon nanotubes containing epoxy/mCNT composite is used as matrix

Interfacial debonding, matrix cracking, fiber breakage and delamination are the mostly observed microscale damage modes in the fiber reinforced composite panels [228]. The mechanical strength of the panels which are prepared by using ASCNT are lower than that of the panel prepared with neat epoxy owing to the filtering effect resulted from the larger agglomerate size of the untreated carbon nanotubes (Figures 4.67 and 4.68). Larger ASCNT particles could not pass through the holes on the glass fiber fabric and could not penetrate the fiber bundles effectively and accumulate on the panel surface or fabric-matrix interface. These accumulations (larger carbon nanotube agglomerates), create stress concentrated parts in the composite panel during tensile testing; increase the easier and faster matrix cracking [175]. Moreover, carbon nanotube agglomerates ascend the interfacial debonding by decreasing the efficiency of the interfacial interactions between the epoxy and glass fibers. Smaller particle size of the mCNT results in more homogeneous distribution of carbon nanotubes in the composite panels. This decreases the stress concentrated weak points in the matrix, at the interface and load can be transferred from the matrix to the glass fibers more effectively. Fiber breakage and delamination are thought to be the dominant damage modes in these composite panels. Also, higher mechanical strength of the mCNT based composites when compared to neat epoxy and ASCNT based composites (Figures

4.64 and 4.65); increase the mechanical strength of the mCNT based composite panels.

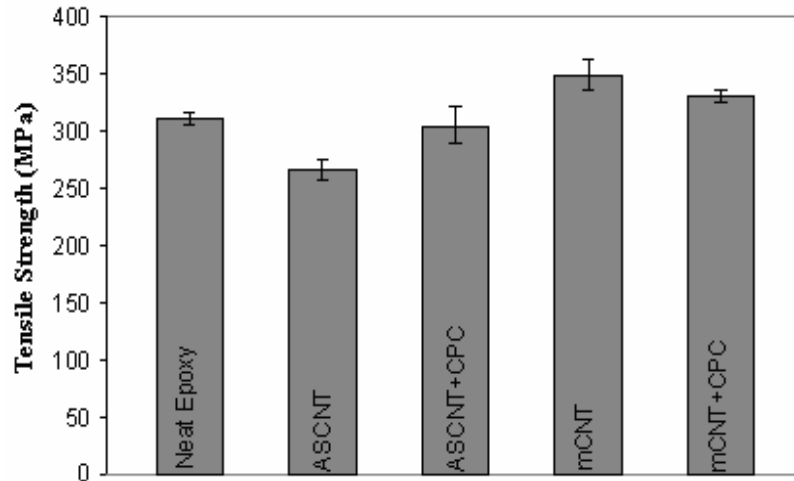


**Figure 4.67** Tensile strength values of the composite panels prepared by using neat epoxy and 0.5 wt. % carbon nanotubes containing epoxy based composites as matrix

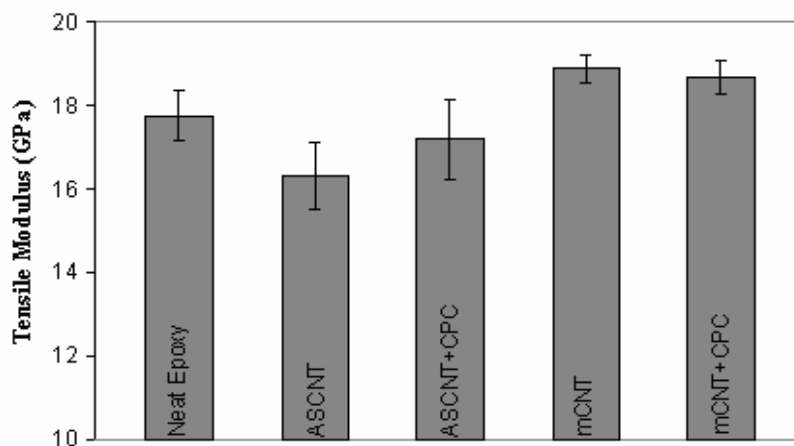


**Figure 4.68** Tensile modulus values of the composite panels prepared by using neat epoxy and 0.5 wt. % carbon nanotubes containing epoxy based composites as matrix

Poisson's ratios of the panels decrease with the usage of carbon nanotubes (Figure 4.69). This is due to the limitations of glass fiber movement in width direction induced by the carbon nanotube agglomerates and decrease in the elasticity of epoxy as a result of the rigid carbon nanotube particles. Poisson's ratio values of the carbon nanotube based composite panels get closer to that of the panel based on neat epoxy as the carbon nanotube particle size becomes smaller with the surfactant usage in the epoxy matrix (Figure 4.58).

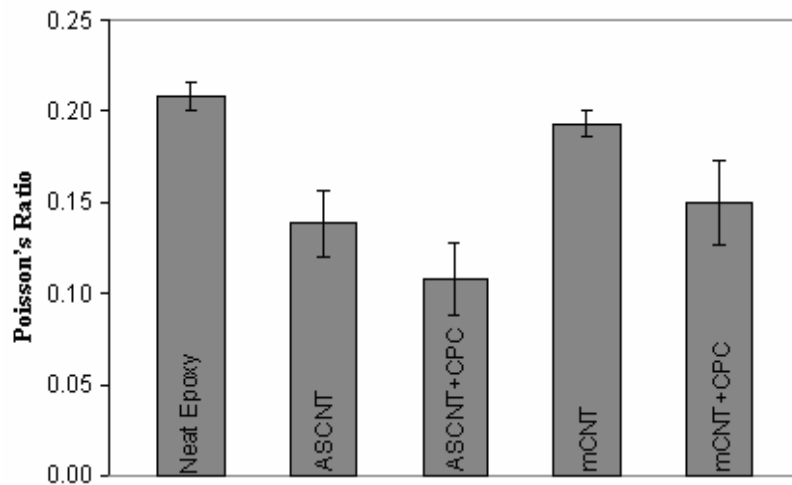


**Figure 4.69** Poisson's ratio values of the composite panels prepared by using neat epoxy and 0.5 wt. % carbon nanotubes containing epoxy based composites as matrix

#### 4.3.3.2 Impact Tests of Composite Panels

Carbon nanotubes are rigid particulate fillers and they generally decrease the elasticity of the polymer when they are used together in a composite structure. CPC assisted epoxy/mCNT panel needs more transferred impact energy for complete puncture when compared to the panel based on ASCNT (Figures 4.70 and 4.71). This might be due to the lower decrease in the elasticity of the epoxy matrix after carbon nanotube addition, as a result of the smaller and homogeneous

distribution of the carbon nanotube particles in epoxy. Thus, the panel based on mCNT is less affected from the damage modes like matrix cracking and delamination up to higher impact energy levels. The total area under the inelastic energy curve of the mCNT based panel is larger than that of the ASCNT based panel. This shows the higher impact resistance of the mCNT based composite panel. Moreover, higher elasticity of the CPC assisted epoxy/mCNT mixture provides more returned energy to the drop weight surface in the complete puncture region. Larger and easily noticeable damages can be observed on the surfaces of panels after 30 J transferred impact energy (50 and 70 J) for both types of panels.

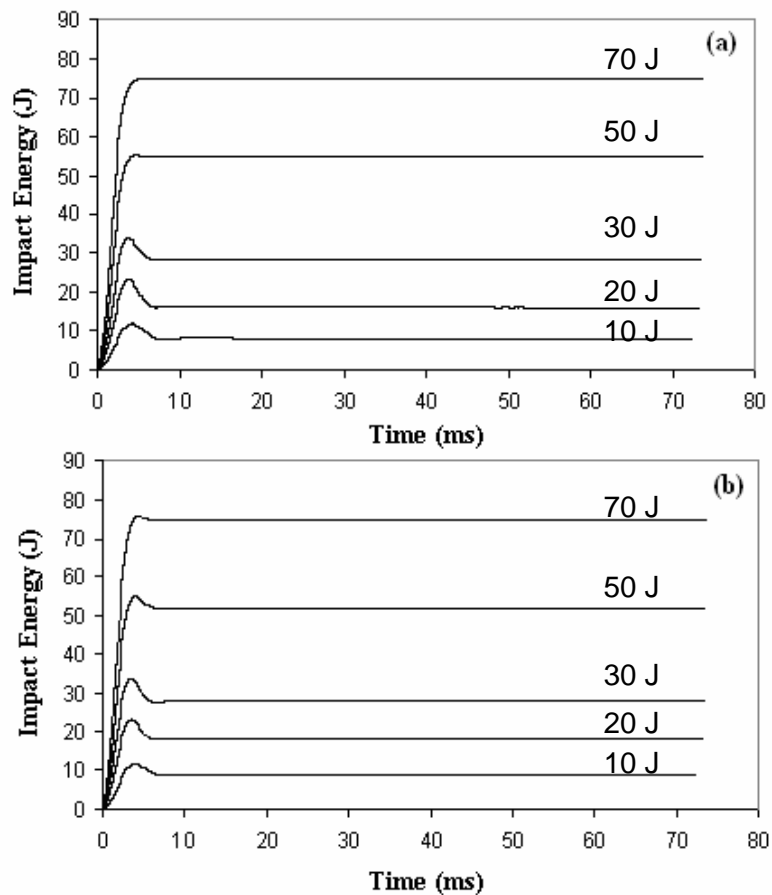


**Figure 4.70** The change in the impact energy of the panels prepared with (a) epoxy/ASCNT, (b) CPC assisted epoxy/mCNT as matrices during the impact test at different impact energies

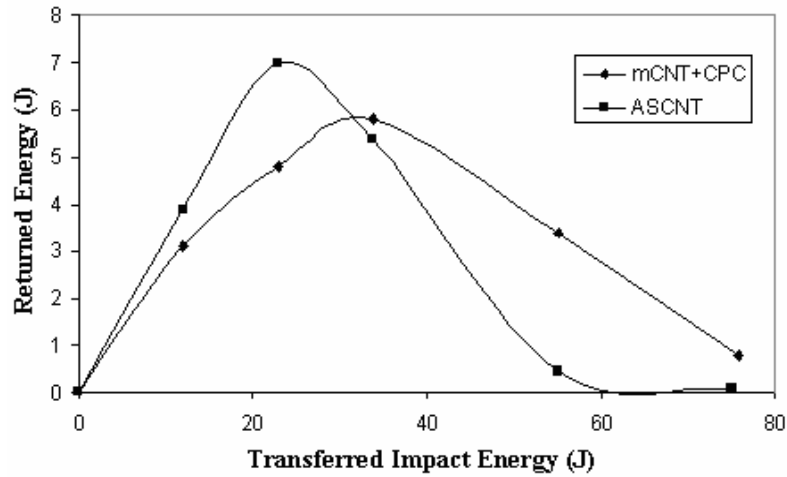


**Figure 4.71** Inelastic energy curves of the panels prepared with epoxy/ASCNT and CPC assisted epoxy/mCNT as matrices

#### 4.3.3.3 Electro-Mechanical Characterization During Impact Tests of Composite Panels

Extremely small sizes of the carbon nanotube particles when compared to the glass fiber fabrics make it possible to sense the small damages which can be developed inside the matrix, on the glass fibers or at the matrix-fiber interface with the electrical resistivity changes during different types of loadings [175]. At this point, it is very crucial to obtain homogeneous carbon nanotube distribution with small particle size throughout the composite panel specimens. Homogeneous carbon nanotube dispersion is important to obtain similar responses from the different parts of the samples and smaller carbon nanotube particle size is significant in terms of the migration of the carbon nanotubes through the holes on the glass fiber fabrics and effective coverage of the glass fiber surfaces with these carbon nanotubes. By this way, the measured electrical resistivity changes can reflect the physical changes inside the matrix, on the fibers and at the interfaces [228].

Electrical resistivity changes of the panels after the impact tests are determined by using the electrodes which are placed with silver paste on the top, bottom surfaces

and four edges of the specimens. These changes measured on the surfaces and through the cross-sectional areas of the specimens are shown in two different graphs (Figure 4.72), since they mainly occur with different damage modes. The damage like breaks and cracks in the epoxy/carbon nanotube mixture which covers the panel surface generally causes the surface electrical resistivity changes [175]. Thus, these resistivity differences on the surfaces do not give too much information about the extent of the damages which occur on the skeleton of the composite panel (glass fibers) during the impact testing. It is the easiest way to measure the electrical resistivity on the surfaces of the materials during their service lives and these electrical resistivity readings are very important in terms of relating the inside damage to the surface electrical resistivity changes. The core structure (glass fibers) damages such as fiber breakage and delamination mostly yield to the electrical resistivity changes through the cross-sectional areas [175]. Thus, the inside damages of the composites can be sensed directly with the resistivity measurements throughout the cross-sectional areas of the materials. However, these inspections might be harder to perform when compared to surface measurements, since the materials should be taken out from their service places for these tests. Moreover, the resistivity changes on the surfaces are higher than those through the cross-section of the specimen due to the more excessive damage formed on the surfaces [228].

The resistivity differences increase as the transferred impact energy to the specimens ascends (Figure 4.72). This shows us that the amounts of resistivity changes are proportional to the extent of the damages occurring in the panels [228]. Also, the trends in resistivity changes are in accordance with the inelastic energy curves of the composite panels. The major changes in the electrical resistivity are observed when the panels transform from elastic-inelastic yield region to complete puncture region (after 20 J for epoxy/ASCNT based panel, after 30 J for CPC assisted epoxy/mCNT based panel (Figure 4.71)). Generally, the resistivity differences are below 10 % when the impact energy was less than 20 J, where less noticeable damage is observed on the specimens. However, this does not show that there might be some small damages inside the specimens which might cause severe ruptures in the future. Thus, any small changes in the electrical resistivity values should be taken into account seriously and detailed investigations should be performed [175]. The smaller particle size of the carbon nanotube

agglomerates, and more homogeneous distribution observed after surface modification and surfactant usage (Figures 4.58 and 4.59), improve the damage sensing capability of the mCNT based panel when compared to ASCNT based panel. The homogeneous carbon nanotube dispersion regulates the electrical resistivity throughout the panel surface and increases the difference in the resistivity values during impact test due to the ascended number of the contact points between the carbon nanotube particles (Figure 4.72) [114]. Moreover, the integration of the carbon nanotube particles with glass fibers are more effective in mCNT based panel owing to the smaller carbon nanotube particle size (less filtering effect) (Figure 4.66). The wreckages occurred on the glass fibers disrupt the carbon nanotube conductive pathways more, inside the panel [175], and electrical resistivity changes are higher through the cross-sections of the specimens when compared to ASCNT based panel.

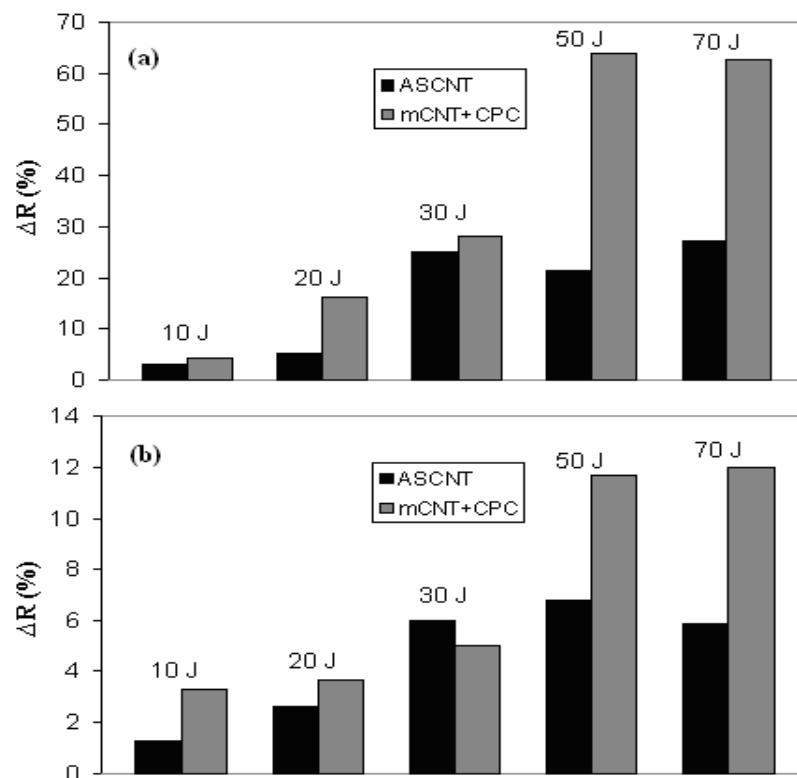


**Figure 4.72** Electrical resistivity changes (a) on the surfaces, (b) through the cross-sectional areas of the epoxy/ASCNT and CPC assisted epoxy/mCNT based panels for different transferred impact energies

#### 4.3.3.4 Electro-Mechanical Characterization During Tensile Tests of Composite Panels

The electrical resistivity changes increase as the composite panels are elongated during the static tensile tests (Figure 4.73). Epoxy/carbon nanotube mixtures which are used as matrices in the panels react with the change in the electrical resistivity to the strain and damages occurring in the specimens during tensile testing. The strain and damages corresponding to tensile loading cause increase in the distance between carbon nanotube particles throughout the composite panel. This decreases the number of contact points between the carbon nanotube agglomerates and ascends the electrical resistivity of the specimen by increasing the contact resistance between the carbon nanotube particles in the epoxy/carbon nanotube mixture [229]. The panels prepared with mCNT result in the higher electrical resistivity changes at the same strains when compared to the ones based on ASCNT owing to the better carbon nanotube - glass fiber integration. Although, panels based on mCNT might have lower extent of wreckage during testing due to their higher mechanical strengths (Figures 4.67), their reactions to these detriments are more noticeable in terms of electrical resistivity changes. This shows the better damage sensing capability of these panels. The electrical resistivity changes of the ASCNT based panels change linearly with strain, whereas those of the mCNT based panels increase parabolically as the samples are elongated during tensile testing. This might be due to the higher mechanical strength of the mCNT based panels and difference in dispersions of carbon nanotube particles in epoxy matrix corresponding to the distinctions in the surface functionalities and physical structures (Figures 4.54 - 4.56) between two different carbon nanotube samples.

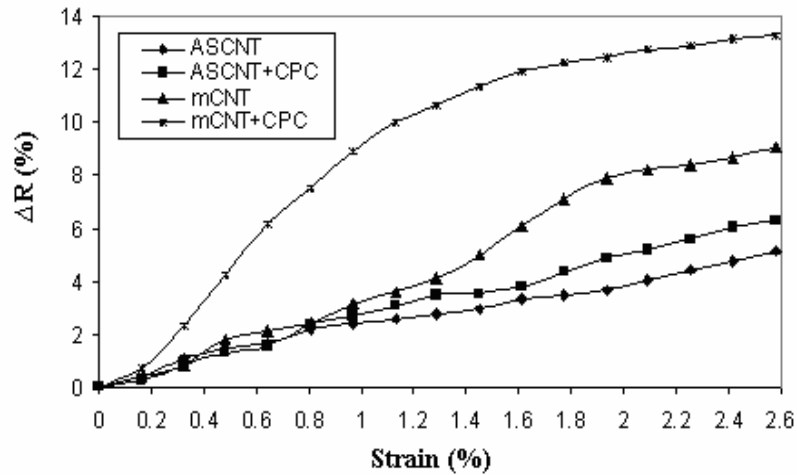


**Figure 4.73** Electrical resistivity changes of the composite panels during static tensile tests

#### 4.3.3.5 Electro-Mechanical Characterization During Fatigue Tests of Composite Panels

Another crucial factor which causes destruction of the composite materials is the fatigue resulting mostly from the cyclic loads. Thus, during the structural health monitoring of the composite panels, it is very important to determine the electrical resistivity changes which occurs from the residual strain and all types of damages as a result of the fatigue formed in the materials throughout their service lives. The total electrical resistivity differences in the samples during fatigue tests arise from the residual strain and damages formed in the specimens [230]. Residual strain is a plastic deformation which continues to stay in the body of the samples due to the exposed load cycles during the fatigue tests [8]. It increases as the number of load cycles ascends throughout testing. The deformations inside the composite panels cause an increase in the electrical resistivity of the specimens due to the separation of the carbon nanotube particles in the epoxy matrix. In other words, electrical resistivity changes during the fatigue tests are proportional to the number of load cycles and residual strain. The residual strains formed in the ASCNT based panels are greater than those of the mCNT based panels (Figure 4.74). This should be taken into account when comparing the electrical resistivity changes in

the panels with each other and relating the extent of the damages inside the materials during the fatigue tests to the electrical resistivity changes [230].

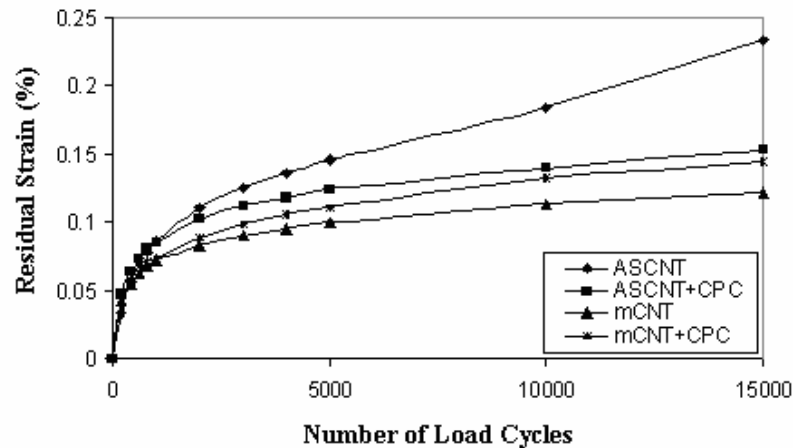


**Figure 4.74** Residual strain change of the composite panels during fatigue tests

Static tensile test results show that the mCNT based panels reflect the extent of the wreckages inside the composite panels at the same elongation values more effectively. Thus, the higher change in the resistivity of the ASCNT based panel when compared to that of the mCNT based panel at the same load cycle number is most probably caused by the higher residual strain formed in that panel, instead of the higher damage sensing capability of the panel (Figure 4.75 a). Electrical resistivity changes during fatigue tests are also proportional to the extent of the damages formed in the structures of the samples. The micron sized cracks formed at the interface of the composite panels and delamination between the layers are the most probable damage modes during the fatigue tests [231]. These matrix-fiber interface damages can be sensed more effectively with a carbon nanotube network which is formed from smaller sized carbon nanotube particles. So, the panel prepared with CPC assisted epoxy/mCNT mixture has the highest electrical resistivity changes as a result of the more effective increase in electrical resistivity resulting from the damages formed at the interfaces of the composite panel.

Moreover, the electrical resistivity changes of the mCNT based panels are higher than those of the ASCNT based panels at the same residual strain values (Figure 4.75 b). These results show that the carbon nanotube surface treatment and surfactant usage during epoxy/carbon nanotube mixture preparation improve the damage sensing capabilities of the composite panels.

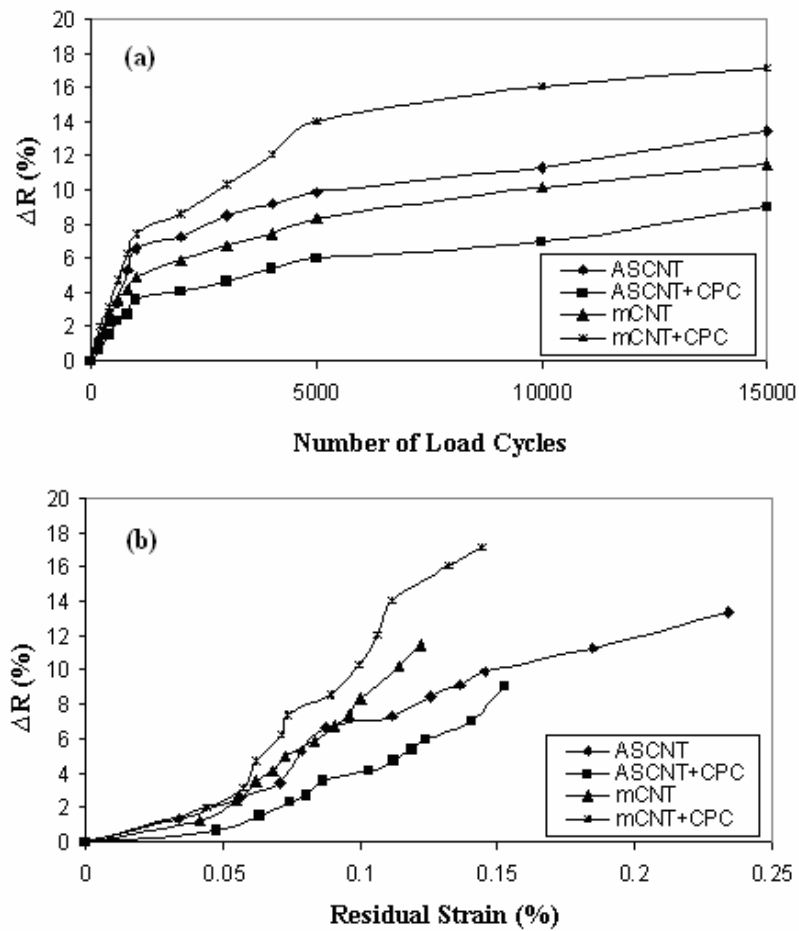


**Figure 4.75** Electrical resistivity changes of the composite panels during fatigue tests (a) vs. number of load cycles (b) vs. residual strains

## CHAPTER 5

### CONCLUSIONS

Carbon nanotube based conductive polymer composites were prepared and characterized in terms of morphology, electrical, mechanical and thermal properties. Surface treatment of carbon nanotubes improved the mechanical properties of the composites. Electrical resistivity values of the composites prepared with the surface treated carbon nanotubes were higher than those of the composites prepared with ASCNT. Microfiber reinforced composites and blends had higher electrical conductivities and mechanical strength when compared to conventional ones. The usage of surfactants during the preparation of the glass fiber reinforced composite panels enhanced the damage sensing capabilities of these panels. The following conclusions can be given for the separate sections of this dissertation:

#### 5.1 Purification of Carbon Nanotubes and Poly(ethylene terephthalate)/Carbon Nanotube Composites

- Surface energy measurements of the carbon nanotube samples showed that the acidic component of the surface energy increased after purification with acids and bases. The presence of peaks at around 1180, 1427, 1637, 1718  $\text{cm}^{-1}$  in FTIR spectra indicated the existence of carboxyl and quinone functional groups on carbon nanotube surface after treatment for all samples. The formation of hydroxyl groups could be seen from the peak at 3440  $\text{cm}^{-1}$ .
- ESCA results of purified carbon nanotubes pointed out an increase in the oxygen concentration on the surface. The formation of hydroxyl and carboxyl

based groups on the surface of carbon nanotubes during purification were also confirmed by the ESCA.

- Crystallite length of the carbon nanotubes decreased as the purification period increased in HNO<sub>3</sub>/H<sub>2</sub>SO<sub>4</sub> (1:3) mixture.
- Electrical resistivity values of the composites containing purified carbon nanotube were higher than that of PET/ASCNT composite, mainly due to the damage in the crystalline structure of carbon nanotubes and oxide layer present on the surfaces of purified carbon nanotubes.

## 5.2 Surface Modification of Carbon Nanotubes and Poly(ethylene terephthalate)/Carbon Nanotube Composites

- FTIR and ESCA spectra of the carbon nanotube samples indicated the existence of functional groups on carbon nanotube surface after modification.
- Surface treatment decreased the number of carboxylic acid groups on the carbon nanotube surface due to the consumption of these groups during reactions between modifiers and purified carbon nanotubes.
- After surface modification PEG and DGEBA could be observed as a distinct phase on carbon nanotube surface in SEM micrographs.
- The FTIR and NMR studies of the composites indicated the possible interactions between PET carboxylic end groups, aromatic group and hydroxyl; epoxide groups of PEG and DGEBA treated carbon nanotubes.
- Tensile strength, modulus and impact strength values of the composites increased after purification and modification when compared to the ASCNT based composites, due to the enhanced interactions between carbon nanotube and PET which improve the load transfer efficiency from PET to carbon nanotubes.

### 5.3 Microfiber Reinforced High Density Polyethylene/Poly(ethylene terephthalate)/Carbon Nanotube Composites Prepared with As-Received Carbon Nanotubes

- Microfiber reinforced HDPE/PET/ASCNT composites were prepared through extrusion and hot-stretching.
- According to surface energy measurements and SEM analyses, ASCNT particles were selectively located in PET phase of the composite.
- The concentration of the microfibers ascended as the amount of PET increased in the composites.
- The microstructures of the fibers were diverse for different PET compositions. The change in the structure of the microfibers was due to the difference in the amounts of ASCNT in PET phase for microfibrillar composites. The increase in the melt viscosity of PET phase influenced the microfiber formation and structure.
- Electrical conductivities of the microfibrillar composites were higher than those of the composites prepared without hot stretching due to the continuous PET/ASCNT microfiber network formed during hot-stretching.
- Microfiber reinforcement improved the tensile and impact strength of the samples, when compared to those of blend and conventional composite systems, up to 30 wt. % PET loading. After this amount, improvement in mechanical properties was diminished due to incompatible nature of HDPE and PET.

### 5.4 Microfiber Reinforced High Density Polyethylene/Poly(ethylene terephthalate)/Carbon Nanotube Composites Prepared with Surface Treated Carbon Nanotubes

- Wetting coefficient calculations and SEM micrographs of HDPE/PET/CNT composites showed the preferential distribution of all types of carbon nanotubes in PET phase.

- SEM micrographs of the hot-stretched composite samples revealed the efficient formation of PET/CNT microfibers up to 0.75 and 1 wt. % carbon nanotube loading for ASCNT and pCNT, mCNT, respectively.
- Sharp decreases were observed in electrical conductivity, tensile modulus and impact strength values of the composites after 0.75 or 1 wt. % carbon nanotube concentration owing to the limited microfiber formation. Electrical resistivity and tensile strength values of the composites prepared with pCNT and mCNT were higher than those of ASCNT based composites due to the advanced intrinsic electrical resistivity and tensile strength of PET/CNT phase in these composites.

## 5.5 Epoxy/Carbon Nanotube Composites and Epoxy/Carbon Nanotube/Glass Fiber Composite Panels

- Epoxy/carbon nanotube composites were prepared by using the solvent assisted sonication technique with the aid of carbon nanotube surface treatment and surfactant usage for the production of electrically conductive glass fiber reinforced composite panels.
- FTIR spectroscopy showed the formation of nitrogen and oxygen based functional groups on the surface of carbon nanotubes after diamine treatment.
- Surface treatment and surfactant assistance decreased the carbon nanotube particle size, improved the dispersion in the composites which increased the electrical conductivity and mechanical strength. These factors resulted in higher mechanical properties and better carbon nanotube–glass fiber integration for the composite panels prepared with modified carbon nanotubes and surfactant.
- Enhanced glass fiber coverage with carbon nanotubes increased the damage sensitivity of the panels. Higher electrical resistance changes were observed for the modified carbon nanotube based panels during mechanical tests when compared to the ones prepared with untreated carbon nanotubes.
- Measurements of the electrical resistivity changes can be used as an effective structural health monitoring tool for the determination of the mechanical damages in the carbon nanotube filled glass fiber reinforced composite panels.

## CHAPTER 6

### RECOMMENDATIONS

The main aim in this dissertation was to improve the mechanical and electrical properties of the conductive polymer composites. Different chemicals were used during the carbon nanotube surface treatment studies. The type of the surface modifier can be altered according to the polymer matrix. Moreover, different types of surfactants can be used to improve the carbon nanotube dispersion in the composites. The head group's charge, size and alkyl group's chain length of the surfactant are the factors which affect the surfactant selection for the composite preparation. Sodium dodecyl benzene sulfonate which is an anionic surfactant might be a good alternative for the surface treatment of carbon nanotubes.

During the microfiber reinforcement studies, PET/CNT microfibers were formed in high density polyethylene matrix by using a speed adjustable take-up device. The formation of the microfibers might be more effective with some modifications on the set-up which was used for the preparation of the microfiber reinforced composites. These modifications might be the usage of multiple take-up devices with different hot-stretching speeds and usage of multiple successive heating, cooling steps during the formation of the microfibers. The usage of advanced composite preparation methods can further improve mechanical and electrical properties of the composites. Significant decrease in the mechanical properties of the microfiber reinforced composites was observed after a certain PET content (30 wt. %) due to the incompatible nature of PET and HDPE. This problem can be solved if an elastomeric compatibilizer was used to enhance the miscibility between these two polymer phases. Improved interfacial adhesion between the polymer phases can enhance the mechanical strength of the composite by increasing the load transfer efficiency in the composite.

Epoxy/CNT composites were prepared by using solvent assisted ultrasonication technique. This method was effective up to a certain extent in terms of decreasing the carbon nanotube particle size and enhancing the carbon nanotube dispersion in the composites, with the help of surfactants. Smaller carbon nanotube particle size with more homogeneous dispersion in the composites can be obtained if different types of mixing methods (high shear mixers or high energy ball milling) were used during the preparation of the composites. Hand lay-up technique was used for production of the glass fiber reinforced composite panels. However, operator skills are very important for this method. It is very hard to obtain homogeneous materials with this technique. Alternative composite panel production methods such as vacuum assisted resin transfer molding (VARTM) can be used to achieve more homogeneous materials with advanced mechanical properties.

## REFERENCES

1. Mazumdar S.K., "Composites manufacturing: Materials, products and process engineering", CRC Press, New York (2002)
2. Jones R.M., "Mechanics of composite materials", Taylor & Francis Inc., London, (1999)
3. Hyde F. J., "Semiconductors", Macdonald & G. Ltd., London (1965)
4. Gul V.E., "Structure and Properties of Conducting Polymer Composites", VSP BV, The Netherlands (1996)
5. Xu X.B., Li Z.M., Yang M.B., Jiang S., Huang R., "The role of the surface microstructure of the microfibrils in an electrically conductive microfibrillar carbon black/poly(ethylene terephthalate)/polyethylene composite", Carbon, 43, 1479-1487 (2005)
6. Xu X.B., Li Z.M., Yu R.Z., Lu A., Yang M.B., Huang R., "Formation of in situ CB/PET microfibers in CB/PET/PE composites by slit die extrusion and hot stretching", Macromolecular Materials and Engineering, 289, 568-575 (2004)
7. Gojny F.H., Nastalczyk J., Roslaniec Z., Schulte K., "Surface modified multi-walled carbon nanotubes in CNT/epoxy composites", Chemical Physics Letters, 370, 820-824 (2003)
8. Nielsen L.E., Landel R.F., "Mechanical properties of polymer and composites", Marcel Decker Inc., New York (1994)
9. Ebbesen T.W., "Carbon nanotubes preparation and properties", CRC Press, Florida (1997)
10. Yuen S.M., Ma C.C.M., Lin Y.Y., Kuan H.C., "Preparation, morphology and properties of acid and amine modified multiwalled carbon nanotube/polyimide composite", Composites Science and Technology, 67, 2564–2573 (2007)
11. Young S.S., "Effect of Surface Treatment for Carbon Nanotubes on Morphological and Rheological Properties of Poly(ethylene oxide) Nanocomposites", Polymer Engineering and Science, 46, 1350-1357 (2006)

12. Yaping Z., Aibo Z., Qinghua C., Jiaoxia Z., Rongchang N., "Functionalized effect on carbon nanotube/epoxy nano-composites", *Materials Science and Engineering A*, 435-436, 145–149 (2006)
13. Shanmugaraj A.M., Bae J.H., Lee K.Y., Noh W.H., Lee S.H., Ryu S. H., "Physical and chemical characteristics of multiwalled carbon nanotubes functionalized with aminosilane and its influence on the properties of natural rubber composites" *Composites Science and Technology*, 67, 1813–1822 (2007)
14. Gupta S., Dixit M., Sharma K., Saxena N.S., "Mechanical study of metallized polyethylene terephthalate (PET) films", *Surface and Coatings Technology*, 204, 661–666 (2009)
15. Mahdi F., Abbas H., Khan A.A., "Strength characteristics of polymer mortar and concrete using different compositions of resins derived from post-consumer PET bottles", *Construction and Building Materials*, 24, 25–36 (2010)
16. Shen L., Gao X., Tong Y., Yeh A., Li R., Wu D., "Influence of different functionalized multiwall carbon nanotubes on the mechanical properties of poly(ethylene terephthalate) fibers", *Journal of Applied Polymer Science*, 108, 2865–2871 (2008)
17. Kobayashi H., Shioya M., Tanaka T., Irisawa T., Sakurai S., Yamamoto K., "A comparative study of fracture behavior between carbon black/poly(ethylene terephthalate) and multiwalled carbon nanotube/poly(ethylene terephthalate) composite films", *Journal of Applied Polymer Science*, 106, 152-160 (2007)
18. Shin D.H., Yoon K.H., Kwon O.H., Min B.G., Hwang C.I., "Surface resistivity and rheological behaviors of carboxylated multiwall carbon nanotube-filled PET composite film", *Journal of Applied Polymer Science*, 99, 900–904 (2006)
19. Crescenzo A.D., Demurtas D., Renzetti A., Siani G., Maria P.D., Meneghetti M., Pratod M., Fontana A., "Disaggregation of single-walled carbon nanotubes (SWNTs) promoted by the ionic liquid-based surfactant 1-hexadecyl-3-vinyl-imidazolium bromide in aqueous solution", *Soft Materials*, 5, 62-66 (2009)

20. Jiang B., Liu C., Zhang C., Liang R., Wang B., "Maximum nanotube volume fraction and its effect on overall elastic properties of nanotube-reinforced composites", *Composites Part B*, 40, 212-217 (2009)
21. Song Y.S., Youn J.R., "Influence of dispersion states of carbon nanotubes on physical properties of epoxy nanocomposites", *Carbon*, 43, 1378-1385 (2005)
22. Jin S.H., Yoon K.H., Park Y.B., Bang D.S., "Properties of surface-modified multiwalled carbon nanotube filled poly(ethylene terephthalate) composite films", *Journal of Applied Polymer Science*, 107, 1163–1168 (2008)
23. Wang S., "Optimum degree of functionalization for carbon nanotubes", *Current Applied Physics*, 9, 1146–1150 (2009)
24. Hou P.X., Liu C., Cheng H.M., "Purification of carbon nanotubes", *Carbon*, 46, 2003–2025 (2008)
25. Wang Y.B., Iqbal Z., Malhotra S.V., "Functionalization of carbon nanotubes with amines and enzymes" *Chemical Physics Letters*, 402, 96–101 (2005)
26. Coleman J.N., Khan U., Blau W.J., Gun'ko Y.K., "Small but strong: A review of the mechanical properties of carbon nanotube–polymer composites", *Carbon*, 44, 1624-1652 (2006)
27. Li J., Fang Z., Tong L., Gu A., Liu F., "Improving Dispersion of Multiwalled Carbon Nanotubes in Polyamide 6 Composites Through Amino-Functionalization", *Journal of Applied Polymer Science*, 106, 2898–2906 (2007)
28. Rothon R.N., "Particulate filled polymer composites", Rapra Technology Limited, Shawbury (2003)
29. Gojny F.H., Schulte K., "Functionalisation effect on the thermo mechanical behaviour of multi-wall carbon nanotube/epoxy-composites", *Composites Science and Technology*, 64, 2303–2308 (2004)
30. Gojny F.H., Wichmann M.H.G., Fiedler B., Schulte K., "Influence of different carbon nanotubes on the mechanical properties of epoxy matrix composites – A comparative study", *Composites Science and Technology*, 65, 2300–2313 (2005)
31. Zhang D., Shi L., Fang J., Li X., Dai K., "Preparation and modification of carbon nanotubes", *Materials Letters*, 59, 4044-4047 (2005)

32. Kim S.D., Kim J.W., Im J.S., Kim Y.H., Lee Y.S., "A comparative study on properties of multi-walled carbon nanotubes (MWCNTs) modified with acids and oxyfluorination", *Journal of Fluorine Chemistry*, 128, 60-64 (2007)
33. Ma P.C., Kim J.K., Tang B.Z., "Functionalization of carbon nanotubes using a silane coupling agent", *Carbon*, 44, 3232–3238 (2006)
34. Misra A., Tyagi P.K., Singh M.K., Misra D.S., "FTIR studies of nitrogen doped carbon nanotubes", *Diamond and Related Materials*, 15, 385-388 (2006)
35. Wen H.C., Yang K., Ou K.L., Wu W.F., Chou C.P., Luo R.C., Chang Y.M., "Effects of ammonia plasma treatment on the surface characteristics of carbon fibers", *Surface and Coatings Technology*, 200, 3166-3169 (2006)
36. Hill D.E., Lin Y., Rao A.M., Allard L.F., Sun Y.P., "Functionalization of carbon nanotubes with polystyrene", *Macromolecules*, 35, 9466-9471 (2002)
37. Gojny F.H., Wichmann M.H.G., Fiedler B., Kinloch I.A., Bauhofer W., Windle A.H., Schulte K., "Evaluation and identification of electrical and thermal conduction mechanisms in carbon nanotube/epoxy composites", *Polymer*, 47, 2036-2045 (2006)
38. Barros E.B., Souza A.G., Lemos V., Filho J.M., Fagan S.B., Herbst M.H., Rosolen J.M., Luengo J.A., Huber J.G., "Charge transfer effects in acid treated single-wall carbon nanotubes", *Carbon*, 43, 2495-2500 (2005)
39. Li W., Bai Y., Zhang Y., Sun M., Cheng R., Xu X., Chen Y., Mo Y., "Effect of hydroxyl radical on the structure of multi-walled carbon nanotubes", *Synthetic Metals*, 155, 509-515 (2005)
40. Bae J., Jang J., Yoon S.H., "Cure behavior of the liquid-crystalline epoxy/carbon nanotube system and the effect of surface treatment of carbon fillers on cure reaction", *Macromolecular Chemistry and Physics*, 203, 2196-2204 (2002)
41. Bikiaris D., Vassiliou A., Chrissafis K., Paraskevopoulos K.M., Jannakoudakis A., Docoslis A., "Effect of acid treated multi-walled carbon nanotubes on the mechanical, permeability, thermal properties and thermo-oxidative stability of isotactic polypropylene", *Polymer Degradation and Stability*, 93, 952-967 (2008)

42. Pompeo F., Resasco D.E., "Water solubilization of single-walled carbon nanotubes by functionalization with glucosamine", *Nano Letters*, 2, 369-373 (2002)
43. Xie X.L., Maia Y.W., Zhou X.P., "Dispersion and alignment of carbon nanotubes in polymer matrix: A review", *Materials Science and Engineering*, R 49, 89–112 (2005)
44. Wei H.F., Hsiue G.H., Liu C.Y., "Surface modification of multi-walled carbon nanotubes by a sol–gel reaction to increase their compatibility with PMMA resin", *Composites Science and Technology*, 67, 1018-1026 (2007)
45. Bhattacharyya A.R., Potschke P., "Mechanical properties and morphology of melt-mixed PA6/SWNT composites: Effect of reactive coupling", *Macromolecular Symposia*, 233, 161–169 (2006)
46. Peng F., Zhang L., Wang H., Lv P., Yu H., "Sulfonated carbon nanotubes as a strong protonic acid catalyst", *Carbon*, 43, 2397–2429 (2005)
47. Bryning M.B., Islam M.F., Kikkawa J.M., Yodh A.G., "Very low conductivity threshold in bulk isotropic single-walled carbon nanotube-epoxy composites", *Advanced Materials*, 17, 1186–1191 (2005)
48. Kim Y.J., Shin T.S., Choi H.D., Kwon J.H., Chung Y.C., Yoon H.G., "Electrical conductivity of chemically modified multiwalled carbon nanotube/epoxy composites", *Carbon*, 43, 23–30 (2005)
49. Chen L., Pang X.J., Yu Z.L., "Study on polycarbonate/multi-walled carbon nanotubes composite produced by melt processing", *Material Science and Engineering Part A*, 457, 287–291 (2007)
50. Mierczynska A., Mayne-L'Hermite M., Boiteux G., "Electrical and mechanical properties of carbon nanotube/ultrahigh-molecular-weight polyethylene composites prepared by a filler prelocalization method", *Journal of Applied Polymer Science*, 105, 158–168 (2007)
51. Zhang Q.H., Rastogi S., Chen D.J., Lippits D., Lemstra P.J., "Low percolation threshold in single-walled carbon nanotube/high density polyethylene composites prepared by melt processing technique", *Carbon*, 44, 778–785 (2006)
52. Dai J.F., Wang Q., Li W.X., Wei Z.Q., Xu G.J., "Properties of well aligned SWNT modified poly (methyl methacrylate) nanocomposites", *Materials Letters*, 61, 27–29 (2007)

53. Seo M.K., Park S.J., "Electrical resistivity and rheological behaviors of carbon nanotubes-filled polypropylene composites", *Chemical Physics Letters*, 395, 44–48 (2004)
54. Kim S.T., Choi H.J., Hong S.M., "Bulk polymerized polystyrene in the presence of multiwalled carbon nanotubes", *Colloidal Polymer Science*, 285, 593–598 (2007)
55. Shaffer M.S.P., Windle A.H., "Fabrication and characterization of carbon nanotube/poly(vinyl alcohol) composites", *Advanced Materials*, 11, 937–941 (1999)
56. Hu G.J., Zhao C.G., Zhang S.M., Yang M.S., Wang Z.G., "Low percolation thresholds of electrical conductivity and rheology in poly(ethylene terephthalate) through the networks of multi-walled carbon nanotubes", *Polymer*, 47, 480–488 (2006)
57. Tasis D., Tagmatarchis N., Georgakilas V., Prato M. "Soluble carbon nanotubes", *Chemistry European Journal*, 9, 4000-4008 (2003)
58. Feng H.Q., Caib L.X., Dong L.X., Xing H.B., Qing C.J., Jian S., "The surface fractal investigation on carbon nanotubes modified by the adsorption of poly(acrylic acid)", *Surface and Coatings Technology*, 190, 394–399 (2005)
59. Datsyuk V., Billon L., Pi ´ecourt C.G., Dagr´eou S., Boupatt N.P., Bourrigaud S., Guerret O., Couvreur L., "In situ nitroxide-mediated polymerized poly(acrylic acid) as a stabilizer/compatibilizer carbon nanotube/polymer composites", *Journal of Nanomaterials*, 2007, 1-12 (2007)
60. Qiu J., Wang G., Zhao C., "Preparation and characterization of amphiphilic multi-walled carbon nanotubes", *Journal of Nanoparticle Research*, 10, 659-663 (2008)
61. Qin S.H., Qin D.Q., Ford W.T., Herrera J.E., Resasco D.E., Bachilo S.M., "Solubilization and purification of single-wall carbon nanotubes in water by in situ radical polymerization of sodium 4-styrenesulfonate", *Macromolecules*, 37, 3965–3967 (2004)
62. Konyushenko E.N., Stejskal J., Trchova M., Hradil J., Kovarova J., Prokes J., Cieslar M., Hwang J.Y., Chen K.H., Sapurina I., "Multi-wall carbon nanotubes coated with polyaniline", *Polymer*, 47, 5715-5723 (2006)

63. Cui S., Canet R., Derre A., Couzi M., Delhaes P., "Characterization of multiwall carbon nanotubes and influence of surfactant in the nanocomposite processing", *Carbon*, 41, 797–809 (2003)
64. Haggemueller R., Gommans H.H., Rinzler A.G., Fischer J.E., Winey K.I., "Aligned single-wall carbon nanotubes in composites by melt processing methods", *Chemical Physics Letters*, 330, 219-225 (2000)
65. Islam M.F., Rojas E., Bergey D.M., Johnson A.T., Yodh A.G., "High weight fraction surfactant solubilization of single wall carbon nanotubes in water", *Nano Letters*, 3, 269-273 (2003)
66. Eitan A., Jiang K., Dukes D., Andrews R., Schadler L.S., "Surface modification of multiwalled carbon nanotubes: Toward the tailoring of the interface in polymer composites", *Chemistry of Materials*, 15, 3198-3201 (2003)
67. Vaisman L., Marom G., Wagner H.D., "Dispersions of surface-modified carbon nanotubes in water-soluble and water-insoluble polymers", *Advanced Functional Materials*, 16, 357–363 (2006)
68. Yang Z., Chen X., Pu Y., Zhou L., Chen C., Li W., Xu L., Yi B., Wang Y., "Facile approach to obtain individual-nanotube dispersion at high loading in carbon nanotubes/ polyimide composites", *Polymers for Advanced Technologies*, 18, 458–462 (2007)
69. Blighe F.M., Blau W.J., Coleman J.N., "Towards tough, yet stiff, composites by filling an elastomer with single-walled nanotubes at very high loading levels", *Nanotechnology*, 19 (2008)
70. Liao S.H., Weng C.C., Yen C.Y., Hsiao M.C., Ma C.C.M., Tsai M.C., Su A., Yen M.Y., Lin Y.F., Liu P.L., "Preparation and properties of functionalized multiwalled carbon nanotubes/polypropylene nanocomposite bipolar plates for polymer electrolyte membrane fuel cells", *Journal of Power Sources*, 195, 263–270 (2010)
71. Guerrero C., Lozano T., Gonzalez V., Arroyo E., "Properties and morphology of poly(ethylene terephthalate) and high-density polyethylene blends", *Journal of Applied Polymer Science*, 82, 1382–1390 (2001)
72. Kim D.H., Park K.Y., Kim J.Y., Suh K.D., "Improved compatibility of high-density polyethylene/poly(ethylene terephthalate) blend by the use of blocked isocyanate group" *Journal of Applied Polymer Science*, 78, 1017–1024 (2000)

73. Pracella M., Rolla L., Chionna D., Galeski A., "Compatibilization and properties of poly(ethyleneterephthalate)/polyethylene blends based on recycled materials", *Macromolecular Chemistry and Physics*, 203, 1473–1485 (2002)
74. Demir T., Tincer T., "Preparation and characterization of poly(ethylene terephthalate) powder-filled high-density polyethylene in the presence of silane coupling agents", *Journal of Applied Polymer Science*, 79, 827–835 (2001)
75. Fasce L., Seltzer R., Frontini P., Rodriguez Pita V.J., Pacheco E.B.A.V., Dias M.L., "Mechanical and fracture characterization of 50:50 HDPE/PET blends presenting different phase morphologies", *Polymer Engineering and Science*, 45, 354-363 (2005)
76. Torres N., Robin J.J., Boutevin B., "Study of compatibilization of HDPE–PET blends by adding grafted or statistical copolymers", *Journal of Applied Polymer Science*, 81, 2377–2386 (2001)
77. Xu H.S., Li Z.M., Yang S.Y., Pan J.L., Yang W., Yang M.B., "Rheological behavior comparison between PET/HDPE and PC/HDPE microfibrillar blends", *Polymer Engineering and Science*, 45, 1231-1238 (2005)
78. Pietrasanta Y., Robin J.J., Torres N., Boutevin B., "Reactive compatibilization of HDPE/PET blends by glycidyl methacrylate functionalized polyolefins", *Macromolecular Chemistry and Physics*, , 200, 142-149 (1999)
79. Lei Y., Wu Q., Zhang Q., "Morphology and properties of microfibrillar composites based on recycled poly(ethylene terephthalate) and high density polyethylene", *Composites: Part A*, 40, 904–912 (2009)
80. Dencheva N., Nunes T., Oliveira M.J., Denchev Z., "Microfibrillar composites based on polyamide/polyethylene blends.1. Structure investigations in oriented and isotropic polyamide6", *Polymer*, 46, 887–901 (2005)
81. Gordeyev S.A., Ferreira J.A., Bernardo C.A., Ward I.M., "A promising conductive material:highly oriented polypropylene filled with short vapour-grown carbon fibres", *Materials Letters*, 51, 32-36 (2001)
82. Zou Y., Feng Y., Wang L., "Processing and properties of MWNT/HDPE composites", *Carbon*, 42, 271–277 (2004)

83. Pötschke P., Dudkin M.S., Alig I., "Dielectric spectroscopy on melt processed polycarbonate multiwalled carbon nanotube composites", *Polymer*, 44, 5023–5030 (2003)
84. Meincke O., Kaempfer D., Weickmann H., "Mechanical properties and electrical conductivity of carbon-nanotubefilled polyamide-6 and its blends with acrylonitrile/butadiene/styrene", *Polymer*, 45, 739–748 (2004)
85. Yu J., Zhang L.Q., Rogunova M., Summers J., Hiltner A., Baer E., "Conductivity of polyolefins filled with high structure carbon black", *Journal of Applied Polymer Science*, 98, 1799-1805 (2005)
86. Koysuren O., Yesil S., Bayram G., "Effect of composite preparation techniques on electrical and mechanical properties and morphology of nylon 6 based conductive polymer composites", *Journal of Applied Polymer Science*, 102, 2520-2526 (2006)
87. Pötschke P., Bhattacharyya A.R., Janke A., "Carbon nanotube filled polycarbonate composites produced by melt mixing and their use in blends with polyethylene", *Carbon*, 42, 965-969 (2004)
88. Thongruang W., Spontak R.J., Balik C.M., "Bridged double percolation in conductive polymer composites: an electrical conductivity, morphology and mechanical property study", *Polymer*, 43, 3717-3725 (2002)
89. Evstatiev M., Fakirov S., "Microfibrillar reinforcement of polymer blends", *Polymer*, 33, 877-880 (1992)
90. Li, Z.M., Yang, M.B., Xie B.H., Feng J.M., Huang R., "In-situ microfiber reinforced composite based on PET and PE via slit die extrusion and hot stretching: Influences of hot stretching ratio on morphology and tensile properties at a fixed composition", *Polymer Engineering and Science*, Volume 43, 615-628 (2003)
91. Zhong G.J., Li Z.M., Li L.B., Mendes E., "Crystalline morphology of isotactic polypropylene (iPP) in injection molded poly(ethylene terephthalate) (PET)/iPP microfibrillar blends", *Polymer*, 48, 1729-1740 (2007)
92. Fakirov S., Evstatiev M., Friedrich K., "From polymer blends to microfibrillar reinforced composites", John Wiley, New York (2000)
93. Lin X.D., Cheung W.L., "Study on PET/PP microfibrillar composites. I. Morphological development in melt extrusion", *Journal of Applied Polymer Science*, 88, 3100–3109 (2003)

94. Zhong G.J., Li Z.M., Li L., Shen K., "Crystallization of oriented isotactic polypropylene (iPP) in the presence of in situ poly(ethylene terephthalate) (PET) microfibrils", *Polymer*, 49, 4271–4278 (2008)
95. Li Z.M., Yang M.B., Lu A., Feng J.M., Huang R., "Tensile properties of poly(ethylene terephthalate) and polyethylene in-situ microfiber reinforced composite formed via slit die extrusion and hot-stretching", *Materials Letters*, Volume 56, 756-762 (2002)
96. Li W., Schlarb A.K., Evstatiev M., "Study of PET/PP/TiO<sub>2</sub> microfibrillar-structured composites, Part 1: Preparation, morphology, and dynamic mechanical analysis of fibrillized blends", *Journal of Applied Polymer Science*, 113, 1471–1479 (2009)
97. Mallette J.G., Quej L.M., Marquez A., Manero O., "Carbon black-filled PET/HDPE blends: Effect of the CB structure on rheological and electric properties", *Journal of Applied Polymer Science*, 81, 562–569 (2001)
98. Dai K., Xu X.B., Li Z.M., "Electrically conductive carbon black (CB) filled in situ microfibrillar poly(ethylene terephthalate) (PET)/polyethylene (PE) composite with a selective CB distribution", *Polymer*, 48, 849-859 (2007)
99. Garmabi H., Naficy S., "Developing electrically conductive polypropylene/polyamide6/carbon black composites with microfibrillar morphology", *Journal of Applied Polymer Science*, 106, 3461–3467 (2007)
100. Naficy S., Garmabi H., "Study of the effective parameters on mechanical and electrical properties of carbon black filled PP/PA6 microfibrillar composites", *Composites Science and Technology*, 67, 3233–3241 (2007)
101. Ajayan P.M., Schadler L.S., Giannaris C., Rubio A., "Single-walled carbon nanotube polymer composites: Strength and weakness", *Advanced Materials*, 12, 750-753 (2000)
102. Thostenson E.T., Chou T.W., "On the elastic properties of carbon nanotube-based composites: modelling and characterization", *Journal of Physics Part D Applied Physics*, 36, 573-582 (2003)
103. Li S.N., Li B., Li Z.M., Fu Q., Shen K.Z., "Morphological manipulation of carbon nanotube/polycarbonate/polyethylene composites by dynamic injection packing molding", *Polymer*, 47, 4497–4500 (2006)
104. Shen J., Huang W., Wu L., Hu Y., Ye M., "Thermo-physical properties of epoxy nanocomposites reinforced with amino-functionalized multi-walled carbon nanotubes", *Composites: Part A*, 38, 1331–1336 (2007)

105. Wang J., Fang Z., Gu A., Xu L., Liu F., "Effect of amino-functionalization of multi-walled carbon nanotubes on the dispersion with epoxy resin matrix", *Journal of Applied Polymer Science*, 100, 97-104 (2006)
106. Chen X., Wang J., Lin M., Zhong W., Feng T., Chen X., Chen J., Xue F., "Mechanical and thermal properties of epoxy nanocomposites reinforced with amino-functionalized multi-walled carbon nanotubes", *Materials Science and Engineering A*, 492, 236-242 (2008)
107. Gong X., Liu J., Baskaran S., Voise R.D., Young J.S., "Surfactant-assisted processing of carbon nanotube/polymer composites", *Chemistry of Materials*, 12, 1049-1052, (2000)
108. Kim M., Park Y.B., Okoli O.I., Zhang C., "Processing, characterization, and modeling of carbon nanotube-reinforced multiscale composites", *Composites Science and Technology*, 69, 335-342 (2009)
109. Bekyarova E., Thostenson E.T., Yu A., Kim H., Gao J., Tang J., "Multiscale carbon nanotube-carbon fiber reinforcement for advanced epoxy composites", *Langmuir*, 23, 3970–3974 (2007)
110. Iwahori Y., Ishiwata S., Sumizawa T., Ishikawa T., "Mechanical properties improvements in two-phase and three-phase composites using carbon nanofiber dispersed resin" *Composites Part A*, 36, 1430–1439 (2005)
111. Thostenson E.S.T., Li W.Z., Wang D.Z., Ren Z.F., Chou T.W., "Carbon nanotube/carbon fiber hybrid multiscale composites", *Journal of Applied Physics*, 91, 6034–6037 (2002)
112. Park J.M., Kim D.S., Kim S.R., "Interfacial properties and microfailure degradation mechanisms of bioabsorbable fibers/poly-L-lactide composites using micromechanical and test and nondestructive acoustic emission", *Composite Science and Technology*, 63, 403–419 (2003)
113. Pham G.T., Park Y.B., Liang Z., Zhang C., Wang B., "Processing and modeling of conductive thermoplastic/carbon nanotube films for strain sensing", *Composites: Part B*, 39, 209–216 (2008)
114. Park J.M., Lee S.I., DeVries K.L., "Nondestructive sensing evaluation of surface modified single-carbon fiber reinforced epoxy composites by electrical resistivity measurement", *Composites: Part B*, 37, 612–626 (2006)
115. Hibberd R.G., "Solid-state electronics", Mc Graw-Hill Book Company, Texas (1968)

116. Riande E., Diaz Calleja R., "Electrical properties of polymers", Marcel Dekker Inc., New York (2004)
117. Gordeyev, S.A., Ferreira, J.A., Bernardo, C.A., Ward, I.M., "A promising conductive material: highly oriented polypropylene filled with short vapour-grown carbon fibres", *Materials Letters*, 51, 32-36 (2001)
118. Zhang W., Dehghani-Sanij A.A., Blackburn R.S., " Carbon based conductive polymer composites", *Journal of Material Science*, 42, 3408-3418 (2007)
119. Chodak I., Omastova M., Pionteck J., "Relation between electrical and mechanical properties of conductive polymer composites", *Journal of Applied Polymer Science*, 82, 1903-1906 (2001)
120. Pinto G., Martin A.J., "Conducting aluminum-filled nylon 6 composites", *Polymer Composites*, 22, 65-70 (2001)
121. Hierold C., "Advanced micro and nanosystems volume 8: Carbon nanotube devices", Wiley VCH, Weinheim (2008)
122. Meyyappan M., "Carbon nanotubes science and applications", CRC Press, Boca Raton (2005)
123. Yumura M., "The science and technology of carbon nanotubes", Elsevier Science Ltd., Amsterdam (1999)
124. Akovalı G., "The handbook of composite fabrication", Rapra Technology Ltd., Shawbury (2001)
125. Fried J.R., "Polymer science and technology", Prentice Hall, New Jersey (2003)
126. Billmeyer F.W., "Textbook of polymer science", John Wiley & Sons, New York (1984)
127. Seymour R.B., Carraher C.E., "Structure-property relationships in polymers", Plenum Press, New York (1984)
128. Gay D., Hoa S.V., Tsai H.W., "Composite materials design and applications", CRC Press, Boca Raton (2003)
129. Xanthos M., "Functional fillers for plastics", Wiley VCH, Weinheim (2005)
130. Ajayan P.M., Schadler L.S., Braun P.V., " Nanocomposite Science and Technology", Wiley VCH, Weinheim (2003)
131. Mai Y.W., Yu Z.Z., "Polymer nanocomposites", Woodhead Publishing Ltd., Cambridge (2006)
132. Mascia L., "Thermoplastic", Elsevier Applied Science, London (1989)

133. Joseph H.K., "Polymer nanocomposites", Mc-Graw Hill, New York (2006)
134. Charrier J.M., "Polymeric materials and processing", Carl Hanser Verlag, Munich (1990)
135. Mark H.F., "Encyclopedia of polymer science and technology", John Wiley & Sons, New York (2005)
136. Friedrich K., Evstatiev M., Fakirov S., Evstatiev O., Ishii M., Harrass M., "Microfibrillar reinforced composites from PET/PP blends: processing, morphology and mechanical properties", *Composites Science and Technology*, 65, 107–116 (2005)
137. Evstatiev M., Fakirov S., Friedrich K., "Effect of blend composition on the morphology and mechanical properties of microfibrillar composites" *Applied Composite Materials*, 2, 93-106 (1995)
138. Friedrich K., Evstatiev M., Fakirov S., Evstatiev O., "Effect of blend composition on the structure properties relationships on nanostructured polymer composites from polycondensate/polyolefin blends", *International Journal of Polymeric Materials*, 53, 211-227 (2004)
139. Evstatiev M., Fakirov S., Krasteva B., Friedrich K., Covas J.A., Cunha A.M., "Recycling of poly(ethyleneterephthalate) as polymer-polymer composites", *Polymer Engineering and Science*, 42, 826-835 (2002)
140. Li Z.M., Li S.N., Yang M.B., Huang R., "A novel approach to preparing carbon nanotube reinforced thermoplastic polymer composites", *Carbon*, 43, 2413–2416 (2005)
141. Ebewele R.O., "Polymer science and technology", CRC Press, Boca Raton (2000)
142. Ram A., "Fundamentals of polymer engineering", Plenum Press, New York (1997)
143. Tadmor Z., Gogos C.G., "Principles of polymer processing", John Wiley & Sons, New Jersey (2006)
144. Rosato D.V., Rosato D.V., Rosato M.G., "Injection molding handbook", Kluwer Academic Publishers, Boston (2000)
145. Middleman S., "Fundamentals of polymer processing", McGraw - Hill Inc., New York (1977)
146. Koshio A., Yudasaka M., Zhang M., Iijima S., "A simple way to chemically react single-wall carbon nanotubes with organic materials using ultrasonication", *Nano Letters*, 1, 361-363 (2001)

147. Paredes J.I., Burghard M., "Dispersions of individual single-walled carbon nanotubes of high length", *Langmuir*, 20, 5149-5152 (2004)
148. Crawford R.J., "Plastics engineering", Butterworth-Heinemann, Oxford (1998)
149. Strong A.B., "Plastics materials and processing", Pearson Prentice Hall, New Jersey (2006)
150. Kim Y., Kwon S.M., Kim D.Y., Kim H.S., Jin H.J., "Dispersity and stability measurements of functionalized multiwalled carbon nanotubes in organic solvents", *Current Applied Physics*, 9, 100–103 (2009)
151. Zhang J., Zou H., Qing Q., Yang Y., Li Q., Liu Z., Guo X., Du Z., "Effect of chemical oxidation on the structure of single-walled carbon nanotubes", *Journal of Physical Chemistry Part B*, 107, 3712-3718 (2003)
152. Špitalský Z., Krontiras C.A., Georga S.N., Galiotis C., "Effect of oxidation treatment of multiwalled carbon nanotubes on the mechanical and electrical properties of their epoxy composites", *Composites Part A*, 40, 778–783 (2009)
153. Datsyuk V., Kalyva M., Papagelis K., Parthenios J., Tasis D., Siokou A., Kallitsis I., Galiotis C., "Chemical oxidation of multiwalled carbon nanotubes", *Carbon*, 46, 833-840 (2008)
154. Hirsch A., "Functionalization of Single-Walled Carbon Nanotubes", *Angewandte Chemie International Edition*, Wiley VCH, Weinheim (2002)
155. Kahovec J., Fox R.B., Hatada K., "Nomenclature of regular single-strand organic polymers". *Pure and Applied Chemistry*, 74, 1921–1956 (2002)
156. Arpe H.J., "Ullmann's encyclopedia of industrial chemistry", Wiley VCH, Weinheim (2005)
157. Holmberg K., Jönsson B., Kronberg K., Lindman B., "Surfactants and polymers in aqueous solutions", John Wiley & Sons, West Sussex (2003)
158. Akovali G., Tosun T.T., Bayramli E., Erinc N.K., "Mechanical properties and surface energies of low density polyethylene-poly(vinyl chloride) blends", *Polymer*, 39, 1363-1368 (1998)
159. Hong Y.C., Shin D.H., Cho S.C., Uhm H.S., "Surface transformation of carbon nanotube powder into super-hydrophobic and measurement of wettability", *Chemical Physics Letters*, 427, 390–393 (2006)

160. Feng J., Chan C.M., Li J.X., "A method to control the dispersion of carbon black in an immiscible polymer blend", *Polymer Engineering and Science*, 43, 1058-1063 (2003)
161. Yacobi B.G., "Semiconductor materials: An introduction to basic principles", Kluwer Academic/Plenum Publishers, New York (2003)
162. Doering R., Nishi Y., "Handbook of semiconductor manufacturing technology", CRC Press, Boca Raton (2008)
163. Schroder D.K., "Semiconductor material and device characterization", John Wiley & Sons, New York (1998)
164. Ward I.M., Sweeney J., "The mechanical properties of solid polymers", John Wiley & Sons, West Sussex (2004)
165. Rydin R. W., Karbhari V. M., "Inelastic energy curves: A tool for evaluating the impact response of composite plates", *Journal of Reinforced Plastics and Composites*, 14, 1175-1198 (1995)
166. Rosen S.L., "Fundamental principles of polymeric materials", John Wiley & Sons, New York (1993)
167. Brundle C.R., Evans C.A., Wilson S., "Encyclopedia of material characterization", Butterworth-Heinemann, Stoneham (1992)
168. Cheremisinoff N.P., "Polymer characterization: Laboratory techniques and analysis", Noyes Publications, New Jersey (1996)
169. Gooch J.W., "Analysis and deformation of polymeric materials", Kluwer Academic Publishers, New York (2002)
170. Endo M., Kim Y.A., Takeda T., Hong S.H., Matusita T., Hayashi T., Dresselhaus M.S., "Structural characterization of carbon nanofibers obtained by hydrocarbon pyrolysis", *Carbon*, 39, 2003-2010 (2001)
171. Takeuchi K.J., Marschlok A.C., Lau G.C., Leising L.A., Takeuchi E.S., "Carbon structure/function relationships: Characterization and electrochemistry of carbon nanofibers", *Journal of Power Sources*, 157, 543-549 (2006)
172. Hatakeyama T., Quinn F.X., "Thermal analysis: Fundamentals and applications to polymer science", John Wiley & Sons, West Sussex (1999)
173. Speyer R.F., "Thermal analysis of materials", Marcel Dekker Inc., New York (1994)
174. Park J.M., Kim P.G., Jang J.H., Wanga Z., Kim J.W., Lee W.I., Park J.G., DeVries K.L., "Self-sensing and dispersive evaluation of single carbon

- fiber/carbon nanotube (CNT)-epoxy composites using electro-micromechanical technique and nondestructive acoustic emission”, *Composites: Part B*, 39, 1170–1182 (2008)
175. Boger L., Wichmann M.H.G., Meyer L.O., Schulte K., “Load and health monitoring in glass fibre reinforced composites with an electrically conductive nanocomposite epoxy matrix”, *Composites Science and Technology*, 68, 1886–1894 (2008)
  176. Brandrup J., Immergut E.H., “*Polymer handbook*”, Wiley-Interscience Pub., Canada (1989).
  177. Geng Y., Liu M.Y., Li J., Shi X.M., Kim J.K., “Effects of surfactant treatment on mechanical and electrical properties of CNT/epoxy nanocomposites”, *Composites: Part A*, 39, 1876-1883 (2008)
  178. Park S.J., Seo M.K., Nah C., “Influence of surface characteristics of carbon blacks on cure and mechanical behaviors of rubber matrix compoundings”, *Journal of Colloid and Interface Science*, 291, 229-235 (2005)
  179. Koysuren O., Yesil S., Bayram G., “Effect of surface treatment on electrical conductivity of carbon black filled conductive polymer composites”, *Journal of Applied Polymer Science*, 104, 3427-3433 (2007)
  180. Wu T.M., Lin Y.W., Liao C.S., “Preparation and characterization of polyaniline/multi-walled carbon nanotube composites”, *Carbon*, 43, 734-740 (2005)
  181. Chen X.H., Chen C.S., Xiao H.N., Chen X.H., Li W.H., Xu L.S., “Lipophilic functionalization of multi-walled carbon nanotubes with stearic acid”, *Carbon*, 43, 1800-1803 (2005)
  182. Porro S., Musso S., Vinante M., Vanzetti L., Anderle M., Trotta F., Tagliaferro A., “Purification of carbon nanotubes grown by thermal CVD”, *Physica E*, 37, 58-61 (2007)
  183. Maldonado S., Morin S., Stevenson K.J., “Structure, composition, and chemical reactivity of carbon nanotubes by selective nitrogen doping”, *Carbon*, 44, 1429-1437 (2006)
  184. Shen J., Huang W., Wu L., Hu Y., Ye M., “Study on amino-functionalized multiwalled carbon nanotubes”, *Materials Science and Engineering A*, 464, 151-156 (2007)
  185. Tamburri E., Orlanducci S., Terranova M.L., Valentini F., Palleschi G., Curulli A., Brunetti F., Passeri D., Alippi A., Rossi M., “Modulation of

- electrical properties in single-walled carbon nanotube/conducting polymer composites”, *Carbon*, 43, 1213-1221 (2005)
186. Chen J., Ramasubramaniam R., Xue C., Liu H., “A versatile, molecular engineering approach to simultaneously enhanced, multifunctional carbon nanotube–polymer composites”, *Advanced Functional Materials*, 16, 114-119 (2006)
  187. Coleman J.N., Khan U., Gun’ko Y.K., “Mechanical reinforcement of polymers using carbon nanotubes”, *Advanced Materials*, 18, 689-706 (2006)
  188. Wang M., Pramoda K.P., Goh S.H., “Enhancement of interfacial adhesion and dynamic mechanical properties of poly(methyl methacrylate)/multiwalled carbon nanotube composites with amine-terminated poly(ethylene oxide)”, *Carbon*, 44, 613-617 (2006)
  189. Han Z.J., Tay B.K., Shakerzadeh M., Ostrikov K., “Superhydrophobic amorphous carbon/carbon nanotube nanocomposites”, *Applied Physics Letters*, 94, 223106-223108 (2009)
  190. Jiang Z.X., Huang Y.D., Liu L., “Effects of functional group polarity on interfacial behavior of non-polar polyarylacetylene resin-silica glass composites”, *High Performance Polymers*, 21, 79–89 (2009)
  191. Hsu H.L., Jehng J.M., Sung Y., Wang L.C., Yang S.R., “The synthesis, characterization of oxidized multi-walled carbon nanotubes, and application to surface acoustic wave quartz crystal gas sensor”, *Materials Chemistry and Physics*, 109, 148-155 (2008)
  192. Wang Y., Xiong H., Gao Y., Li H., “Synthesis of poly(ethylene glycol) functionalized MWNTs and their inclusion complexes with  $\alpha$ -cyclodextrin”, *Journal of Materials Science*, 43, 5609–5617 (2008)
  193. Jung D.H., Kim B.H., Ko Y.K., Jung M.S., Jung S., Lee S.Y., Jung H.T., “Covalent attachment and hybridization of DNA oligonucleotides on patterned single-walled carbon nanotube films”, *Langmuir*, 20, 8886-8891 (2004)
  194. Lee W.H., Kim S.J., Lee W.J., Lee J.G., Haddon R.C., Reucroft P.J., “X-Ray photoelectron spectroscopic studies of surface modified single-wall carbon nanotube material”, *Applied Surface Science*, 181, 121-127 (2001)
  195. Cordella F., De Nardi M., Menna E., He’bert C., Loi M.A., “Tuning the photophysical properties of soluble single-wall carbon nanotube derivatives

- by co-functionalization with organic molecules”, *Carbon*, 47, 1264–1269 (2009)
196. Naeimi H., Mohajeri A., Moradi L., Rashidi A.M., “Efficient and facile one pot carboxylation of multiwalled carbon nanotubes by using oxidation with ozone under mild conditions”, *Applied Surface Science*, 256, 631-635 (2009)
  197. Kathi J., Rhee K.Y., Lee J.H., “Effect of chemical functionalization of multiwalled carbon nanotubes with 3-aminopropyltriethoxysilane on mechanical and morphological properties of epoxy nanocomposites”, *Composites Part A*, 40, 800-809 (2009)
  198. Avile’s F., Cauich-Rodríguez J.V., Moo-Tah L., May-Pat A., Vargas-Coronado R., “Evaluation of mild acid oxidation treatments for MWCNT functionalization”, *Carbon*, 47, 2970–2975 (2009)
  199. Yoo H.J., Jung Y.C., Cho J.W., “Effect of interaction between poly(ethylene terephthalate) and carbon nanotubes on the morphology and properties of their nanocomposites”, *Journal of Polymer Science: Part B: Polymer Physics*, 46, 900–910 (2008)
  200. Tzavalas S., Mouzakis D.E., Drakonakis V., Gregoriou V.G., “Polyethylene terephthalate–multiwall nanotubes nanocomposites: Effect of nanotubes on the conformations, crystallinity and crystallization behavior of PET”, *Journal of Polymer Science: Part B: Polymer Physics*, 46, 668–676 (2008)
  201. Fa’varo S.L., Rubira A.F., Muniz E.C., Radovanovic E., “Surface modification of HDPE, PP, and PET films with  $\text{KMnO}_4/\text{HCl}$  solutions”, *Polymer Degradation and Stability*, 92, 1219-1226 (2007)
  202. Phinyocheep P., Saelao J., Buzare J.Y., “Mechanical properties, morphology and molecular characteristics of poly(ethylene terephthalate) toughened by natural rubber”, *Polymer*, 48, 5702-5712 (2007)
  203. Zhang C., Zhu J., Ouyang M., Ma C., Sumita M., “Conductive network formation and electrical properties of poly(vinylidene fluoride)/multiwalled carbon nanotube composites: percolation and dynamic percolation”, *Journal of Applied Polymer Science*, 114, 1405–1411 (2009)
  204. Liu F., Zhang X., Li W., Cheng J., Tao X., Li Y., Sheng L., “Investigation of the electrical conductivity of HDPE composites filled with bundle-like MWNTs”, *Composites: Part A*, 40, 1717-1721 (2009)

205. Bauhofer W., Kovacs J.Z., "A review and analysis of electrical percolation in carbon nanotube polymer composites", *Composites Science and Technology*, 69, 1486–1498 (2009)
206. Roxana A., Ruseckaite J., Roberto J., Williams J., "Castor oil modified epoxy resins as model systems of rubber modified thermosets 1: Thermodynamic analysis of the phase separation", *Polymer International*, 30, 11-16 (1993)
207. Vandenburg H.J., Clifford A.A., Bartle K.D., Carlson R.E., Carroll J., Newton I.D., "A simple solvent selection method for accelerated solvent extraction of additives from polymers", *Analyst*, 124, 1707–1710 (1999)
208. Lemmouchi Y., Murariu M., Dos Santos A.M., Amass A.J., Schacht E., Dubois P., "Plasticization of poly(lactide) with blends of tributyl citrate and low molecular weight poly(D,L-lactide)-b-poly(ethylene glycol) copolymers", *European Polymer Journal*, 45, 2839–2848 (2009)
209. Svetec D.G., "Mechanical properties of polypropylene fibers produced from the binary polymer blends of different molecular weights", *Journal of Applied Polymer Science*, 75, 1211–1220 (2000)
210. Ou C.F., Ho M.T., Lin J.R., "The nucleating effect of montmorillonite on crystallization of PET/Montmorillonite nanocomposite", *Journal of Polymer Research*, 10, 127–132 (2003)
211. Vega J.F., Martı́nez-Salazar J., Trujillo M., Arnal M.L., Muller A.J., Bredeau S., Dubois Ph., "Rheology, processing, tensile Properties, and crystallization of polyethylene/carbon nanotube nanocomposites", *Macromolecules*, 42, 4719–4727 (2009)
212. Persson A.L., Bertilsson H., "Viscosity difference as distributing factor in selective absorption of aluminium borate whiskers in immiscible polymer blends", *Polymer*, 39, 5633-5642 (1998)
213. Cho Y.G., Kamal M.R., "Effect of the dispersed phase fraction on particle size in blends with high viscosity ratio", *Polymer Engineering and Science*, 42, 2005-2015 (2002)
214. Nunez R.G., Fong C.F., Favis B.D., Kee D.D., "Deformation of drops in extensional viscoelastic flow", *Journal of Applied Polymer Science*, 62, 1627-1634 (1996)

215. Foulger S.H., "Reduced percolation thresholds of immiscible conductive blends", *Journal of Polymer Science: Part B: Polymer Physics*, 37, 1899-1910 (1999)
216. Thostenson E.T., Ren Z., Chou T.W., "Advances in the science and technology of carbon nanotubes and their composites: a review", *Composites Science and Technology*, 61, 1899–1912 (2001)
217. Li Z.M., Yang M.B., Xie B.H., Feng J.M., Huang R., "In-situ microfiber reinforced composite based on PET and PE via slit die extrusion and hot stretching: Influences of hot stretching ratio on morphology and tensile properties at a fixed composition", *Polymer Engineering and Science*, 43, 615-628 (2003)
218. Evstatiev M., Schultz J.M., Fakirov S., Friedrich K., "In situ fibrillar reinforced PET/PA-6/PA-66 blend", *Polymer Engineering and Science*, 41, 192-204 (2001)
219. Li Z.M., Yang W., Xie B.H., Shen K.Z., Huang R., Yang M.B., "Morphology and tensile strength prediction of in situ microfibrillar poly(ethylene terephthalate)/ polyethylene blends fabricated via slit-die extrusion-hot stretching-quenching", *Macromolecular Materials Engineering*, 289, 349–354 (2004)
220. Fuchs C., Bhattacharyya D., Fakirov S., "Microfibril reinforced polymer–polymer composites: Application of Tsai-Hill equation to PP/PET composites", *Composites Science and Technology*, 66, 3161–3171 (2006)
221. Lin C.A. Chen C.C., An T.C., "Effect of blend ratio and draw ratio on the mechanical properties of PET/PP blended conjugate fibers", *Polymer-Plastics Technology and Engineering*, 45, 1339–1345 (2006)
222. Nadkarni V.M., Shingankuli V.L., Jog J.P., "Effect of blending on the crystallization behavior of PET", *Journal of Applied Polymer Science*, 46, 339-351 (1992)
223. Li Z.M., Yang W., Li L.B., Xie B.H., Huang R., Yang M.B., "Morphology and nonisothermal crystallization of in situ microfibrillar poly(ethylene terephthalate)/polypropylene blend fabricated through slit-extrusion, hot-stretch quenching", *Journal of Polymer Science: Part B: Polymer Physics*, 42, 374–385 (2004)
224. Hong J.S., Kim C., "Extension-induced dispersion of multi-walled carbon nanotube in non-Newtonian fluid", *Journal of Rheology*, 51, 833-850 (2007)

225. Jiang G., Huang H.X., "Microstructure and rheologic development of polypropylene/nano-CaCO<sub>3</sub> composites along twin-screw extruder", *Journal of Applied Polymer Science*, 114, 1687–1693 (2009)
226. Zhu J., Kim J.D., Peng H., Margrave J.L., Khabashesku V.N., Barrera E.V., "Improving the dispersion and integration of single-walled carbon nanotubes in epoxy composites through functionalization", *Nano Letters*, 3, 1107-1113 (2003)
227. Xianhong C., Jianfeng W., Ming L., Wenbin Z., Tao F., Xiaohua C., Jianghua C., Feng X., "Mechanical and thermal properties of epoxy nanocomposites reinforced with amino functionalized multi-walled carbon nanotubes", *Materials Science and Engineering A*, 492, 236–242 (2008)
228. Gao L., Thostenson E.T., Zhang Z., Chou T.W., "Sensing of damage mechanisms in fiber-reinforced composites under cyclic loading using carbon nanotubes", *Advanced Functional Materials*, 19, 123–130 (2009)
229. Thostenson E.T., Chou T.W., "Real-time in situ sensing of damage evolution in advanced fiber composites using carbon nanotube networks", *Nanotechnology*, 19, 215713-215718 (2008)
230. Nofar M., Hoa S.V., Pugh M.D., "Failure detection and monitoring in polymer matrix composites subjected to static and dynamic loads using carbon nanotube networks", *Composites Science and Technology*, 69, 1599-1606 (2009)
231. Thostenson E.T., Chou T.W., "Carbon nanotube networks: sensing of distributed strain and damage for life prediction and self healing", *Advanced Functional Materials*, 18, 2837–2841 (2006)

## APPENDIX A

### MECHANICAL PROPERTIES

**Table A.1** Tensile strength, tensile modulus, elongation at break and impact strength values of neat PET and PET/CNT composites prepared with as-received and purified carbon nanotubes at 0.5 wt. % carbon nanotube loading

Sample	Tensile Strength (MPa)	Tensile Modulus (MPa)	Elongation at Break (%)	Impact Strength (kJ/m <sup>2</sup> )
PET	49.1±2.0	1232±131	5.8±0.6	16.9±1.3
PET/ASCNT	24.4±2.2	1343±82	2.9±0.4	7.1±1.4
PET/CNT1	27.4±1.3	1441±129	3.1±0.2	7.1±1.3
PET/CNT2	45.2±1.2	1867±61	3.5±0.1	13.7±1.1
PET/CNT3	43.6±1.6	1701±53	3.6±0.5	13.6±1.3
PET/CNT4	35.6±1.8	1619±140	3.9±0.3	10.6±1.4
PET/CNT5	44.9±1.5	1830±85	3.1±0.3	14.4±1.3
PET/CNT6	38.1±1.4	1724±90	2.4±0.3	11.8±1.3
PET/CNT7	37.7±1.2	1700±98	3.0±0.3	13.2±1.4
PET/CNT8	30.1±1.3	1432±103	4.6±0.2	10.6±0.9

**Table A.2** Tensile strength, tensile modulus, elongation at break and impact strength values of PET/CNT composites prepared with modified carbon nanotubes at 0.5 wt. % carbon nanotube loading

<b>Sample</b>	<b>Tensile Strength (MPa)</b>	<b>Tensile Modulus (MPa)</b>	<b>Elongation at Break (%)</b>	<b>Impact Strength (kJ/m<sup>2</sup>)</b>
<b>PET/SDSCNT</b>	44.4±1.0	1894±82	3.4±0.8	12.6±0.5
<b>PET/DGEBACNT</b>	51.4±0.3	1586±55	9.7±1.4	18.0±1.8
<b>PET/PEG400CNT</b>	49.5±2.0	1791±31	4.5±0.2	16.8±1.5
<b>PET/PEG1000CNT</b>	58.3±0.8	1940±48	8.9±0.7	16.4±2.2

**Table A.3** Tensile strength, tensile modulus, elongation at break and impact strength values of PET/CNT composites prepared with as-received, purified and PEG1000 treated carbon nanotubes at different carbon nanotube loadings

<b>Sample</b>	<b>Tensile Strength (MPa)</b>	<b>Tensile Modulus (MPa)</b>	<b>Elongation at Break (%)</b>	<b>Impact Strength (kJ/m<sup>2</sup>)</b>
<b>ASCNT (0.25wt.%)</b>	22.3±1.8	1310±89	3.3±0.4	6.5±1.6
<b>ASCNT (1 wt.%)</b>	21.9±1.4	1344±146	2.4±0.5	5.3±0.6
<b>ASCNT (2 wt.%)</b>	19.7±1.5	1231±147	1.9±0.3	4.3±0.4
<b>ASCNT (4 wt.%)</b>	17.4±2.3	1245±113	1.7±0.2	3.9±0.3
<b>pCNT (0.25wt.%)</b>	36.0±1.9	1547±58	4.0±0.3	15.8±0.6
<b>pCNT (1 wt.%)</b>	44.5±1.5	1848±87	3.4±0.6	11.1±1.5
<b>pCNT (2 wt.%)</b>	41.3±0.7	1788±98	2.4±0.1	4.7±0.5
<b>pCNT (4 wt.%)</b>	30.5±0.5	1641±85	2.3±0.2	3.6±0.4
<b>PEG1000CNT(0.25wt.%)</b>	41.5±1.4	1483±82	11.6±0.1	15.6±0.3
<b>PEG1000CNT(1 wt.%)</b>	62.4±0.7	1887±88	6.2±0.2	17.8±0.8
<b>PEG1000CNT(2 wt.%)</b>	53.4±0.7	1844±65	3.3±0.1	9.0±0.5
<b>PEG1000CNT(4 wt.%)</b>	37.1±1.0	1708±61	2.5±0.2	6.7±0.2

**Table A.4** Tensile strength, tensile modulus, elongation at break and impact strength values of conventional HDPE/PET blends, HDPE/PET/CNT composites prepared with as-received carbon nanotubes

<b>Sample</b>	<b>Tensile Strength (MPa)</b>	<b>Tensile Modulus (MPa)</b>	<b>Elongation at Break (%)</b>	<b>Impact Strength (kJ/m<sup>2</sup>)</b>
<b>HDPE/PET (90/10)</b>	37.5±0.7	636±35	69±6	167±9
<b>HDPE/PET (80/20)</b>	35.2±1.5	640±69	58±7	100±11
<b>HDPE/PET (70/30)</b>	31.2±1.4	713±40	35±5	16±3
<b>HDPE/PET (60/40)</b>	27.6±0.9	795±54	16±3	8.4±1.8
<b>HDPE/PET (50/50)</b>	24.7±1.1	969±13	10±2	6.6±1.0
<b>HDPE/PET/CNT (90/10/0.5)</b>	39.5±1.2	660±21	40±5	141±10
<b>HDPE/PET/CNT (80/20/0.5)</b>	35.3±1.3	745±37	24±6	26±9
<b>HDPE/PET/CNT (70/30/0.5)</b>	34.0±0.6	601±37	24±4	12±1
<b>HDPE/PET/CNT (60/40/0.5)</b>	32.1±0.8	621±47	8.4±1.3	7.2±0.5
<b>HDPE/PET/CNT (50/50/0.5)</b>	27.5±1.0	641±36	8.1±1.5	7.0±0.8

**Table A.5** Tensile strength, tensile modulus, elongation at break and impact strength values of microfiber reinforced HDPE/PET/CNT composites prepared with as-received carbon nanotubes and molded at different temperatures

<b>Sample</b>	<b>Tensile Strength (MPa)</b>	<b>Tensile Modulus (MPa)</b>	<b>Elongation at Break (%)</b>	<b>Impact Strength (kJ/m<sup>2</sup>)</b>
<b>(90/10/0.5) 210 °C</b>	43.4±0.8	757±43	33±7	146±6
<b>(90/10/0.5) 240 °C</b>	40.8±1.1	710±34	31±8	135±13
<b>(90/10/0.5) 280 °C</b>	39.7±1.1	628±33	51±6	142±9
<b>(80/20/0.5) 210 °C</b>	44.4±0.6	930±23	27±1	154±11
<b>(80/20/0.5) 240 °C</b>	39.0±0.4	871±30	31±3	64±3
<b>(80/20/0.5) 280 °C</b>	35.3±1.2	664±33	19±3	19±7
<b>(70/30/0.5) 210 °C</b>	41.9±0.3	771±32	21±1	57±1
<b>(70/30/0.5) 240 °C</b>	37.2±0.5	586±25	20±2	12±1
<b>(70/30/0.5) 280 °C</b>	30.4±0.2	595±24	11±2	12±2
<b>(60/40/0.5) 210 °C</b>	-	-	-	7.8±0.5
<b>(60/40/0.5) 240 °C</b>	29.0±0.3	742±44	10±1	8.8±0.7
<b>(60/40/0.5) 280 °C</b>	32.5±0.6	600±38	12±2	7.3±0.8
<b>(50/50/0.5) 210 °C</b>	-	-	-	3.0±0.1
<b>(50/50/0.5) 240 °C</b>	19.9±1.2	523±30	7.3±1.4	6.0±0.9
<b>(50/50/0.5) 280 °C</b>	30.8±1.2	807±42	10±2	6.6±0.8

**Table A.6** Tensile strength, tensile modulus, elongation at break and impact strength values of microfiber reinforced HDPE/PET blend and HDPE/PET/CNT composites at (80/20 HDPE/PET ratio) prepared with as-received, purified and PEG1000 treated carbon nanotubes

<b>Sample</b>	<b>Tensile Strength (MPa)</b>	<b>Tensile Modulus (MPa)</b>	<b>Elongation at Break (%)</b>	<b>Impact Strength (kJ/m<sup>2</sup>)</b>
<b>HDPE/PET (80/20)</b>	39.9±0.5	694±34	36±3	187±7
<b>0.25 wt.% ASCNT 210 °C</b>	41.1±0.6	737±58	34±2	160±12
<b>0.75 wt.% ASCNT 210 °C</b>	44.6±0.5	949±29	22±2	135±9
<b>1 wt.% ASCNT 210 °C</b>	38.1±0.5	732±26	23±1	28±3
<b>1.5 wt.% ASCNT 210 °C</b>	37.1±0.4	726±31	20±4	20±3
<b>0.25 wt.% pCNT 210 °C</b>	47.0±1.0	927±25	20±1	163±7
<b>0.5 wt.% pCNT 210 °C</b>	48.7±1.1	1169±35	19±2	150±6
<b>0.75 wt.% pCNT 210 °C</b>	49.2±0.9	1132±26	18±1	130±7
<b>1 wt.% pCNT 210 °C</b>	48.3±0.8	869±51	19±3	134±5
<b>1.5 wt.% pCNT 210 °C</b>	40.9±0.3	821±29	15±2	37±4
<b>0.25 wt.% PEG1000CNT 210 °C</b>	50.8±0.6	847±31	26±4	167±7
<b>0.5 wt.% PEG1000CNT 210 °C</b>	51.2±0.5	940±40	23±5	165±8
<b>0.75 wt.% PEG1000CNT 210 °C</b>	52.5±0.4	958±23	24±3	156±6
<b>1 wt.% PEG1000CNT 210 °C</b>	53.2±0.9	1177±30	23±4	119±6
<b>1.5 wt.% PEG1000CNT 210 °C</b>	48.4±0.7	864±30	21±2	99±4
<b>0.75 wt.% ASCNT 280 °C</b>	37.5±0.5	745±14	25±2	22±2
<b>0.75 wt.% pCNT 280 °C</b>	42.8±0.8	907±33	21±2	38±4
<b>0.75 wt.% PEG1000CNT 280 °C</b>	45.4±0.8	957±32	33±3	73±3

**Table A.7** Tensile strength, tensile modulus and elongation at break values of neat epoxy and epoxy/CNT composites prepared with as-received carbon nanotubes at different compositions

<b>Sample</b>	<b>Tensile Strength (MPa)</b>	<b>Tensile Modulus (MPa)</b>	<b>Elongation at Break (%)</b>
<b>Epoxy</b>	71.9±5.6	2599±258	8.2±0.8
<b>Epoxy/ASCNT (0.25 wt.%)</b>	62.7±2.4	2448±205	7.0±0.5
<b>Epoxy/ASCNT (0.5 wt.%)</b>	65.8±2.9	3009±264	5.6±1.3
<b>Epoxy/ASCNT (0.75 wt.%)</b>	54.6±2.3	2756±237	4.8±0.6
<b>Epoxy/ASCNT (1 wt.%)</b>	32.4±6.3	2407±73	2.5±0.8

**Table A.8** Tensile strength, tensile modulus and elongation at break values of epoxy/CNT composites prepared with as-received and modified carbon nanotubes at 0.5 wt.% carbon nanotube loading

<b>Sample</b>	<b>Tensile Strength (MPa)</b>	<b>Tensile Modulus (MPa)</b>	<b>Elongation at Break (%)</b>
<b>mCNT</b>	83.6±1.9	3957±204	6.7±1.3
<b>ASCNT+Triton X100</b>	67.2±4.9	3710±384	5.6±1.3
<b>ASCNT+CPC</b>	79.3±2.5	3558±52	9.7±1.1
<b>mCNT+Triton X100</b>	84.5±3.0	3490±236	7.8±0.7
<b>mCNT+CPC</b>	94.3±1.4	3462±80	8.5±0.4

**Table A.9** Tensile strength, tensile modulus, elongation at break and Poisson's ratio values of glass fiber reinforced composite panels prepared by using neat epoxy and epoxy/CNT composites (0.5 wt.%) as matrix

<b>Sample</b>	<b>Tensile Strength (MPa)</b>	<b>Tensile Modulus (GPa)</b>	<b>Elongation at Break (%)</b>	<b>Poisson's Ratio</b>
<b>Epoxy</b>	311±5	17.7±0.6	3.3±0.2	0.21±0.01
<b>Epoxy/ASCNT</b>	267±9	16.3±0.8	2.7±0.1	0.14±0.02
<b>Epoxy/ASCNT/CPC</b>	306±15	17.2±1.0	3.1±0.2	0.11±0.02
<b>Epoxy/mCNT</b>	349±14	18.9±0.3	3.4±0.6	0.19±0.01
<b>Epoxy/mCNT/CPC</b>	331±5	18.7±0.4	3.1±0.3	0.15±0.02

## APPENDIX B

### ESCA SPECTRA

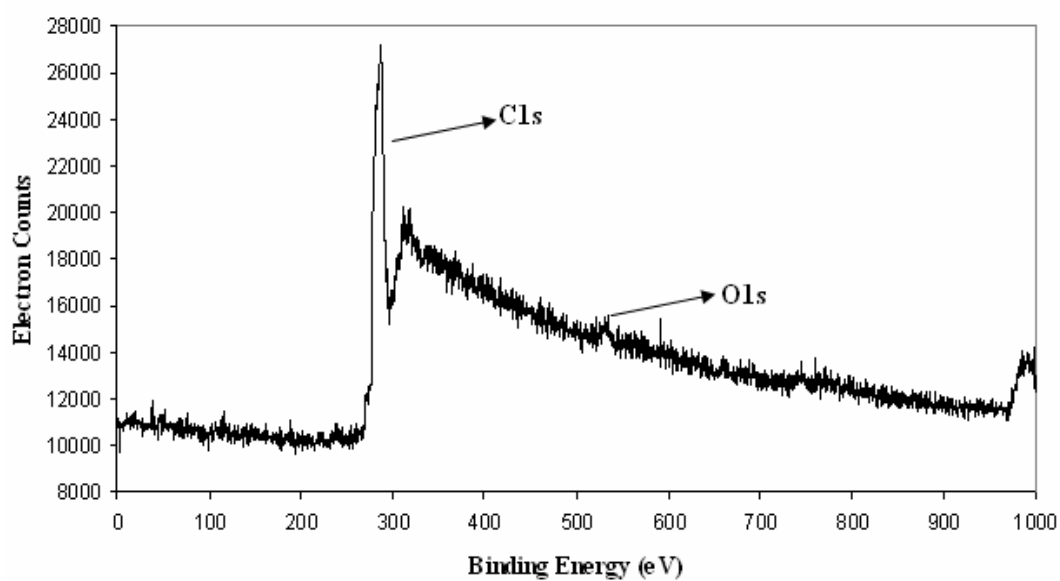


**Figure B.1** ESCA spectrum of ASCNT

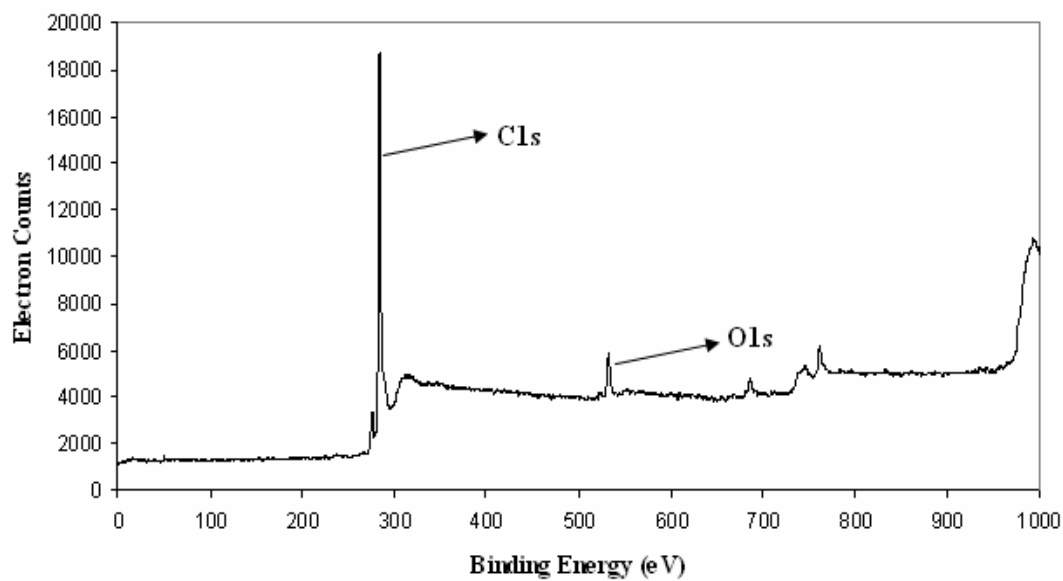


**Figure B.2** ESCA spectrum of CNT1

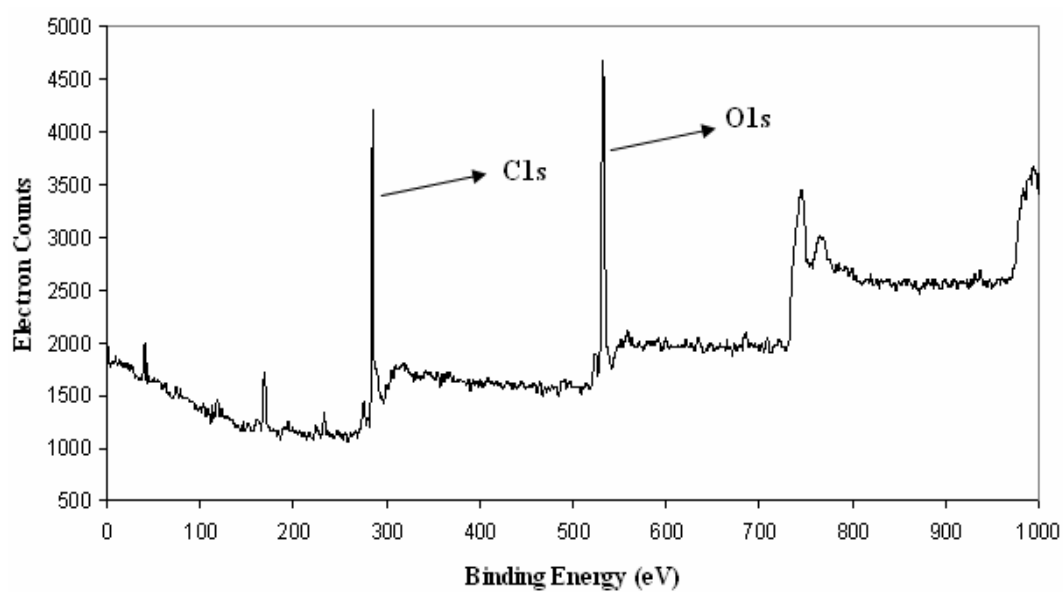


**Figure B.3** ESCA spectrum of CNT2

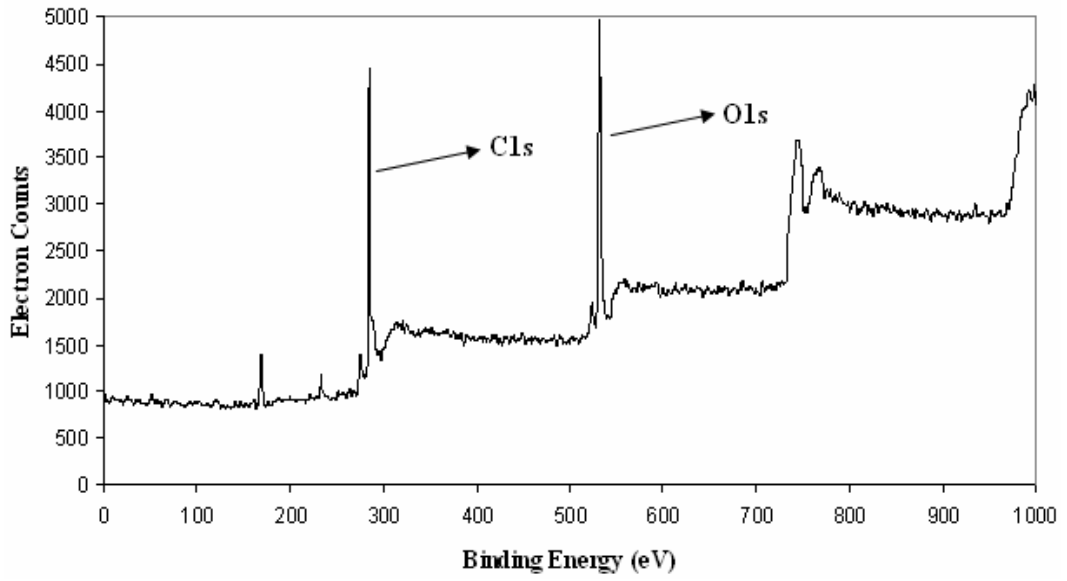


**Figure B.4** ESCA spectrum of CNT3

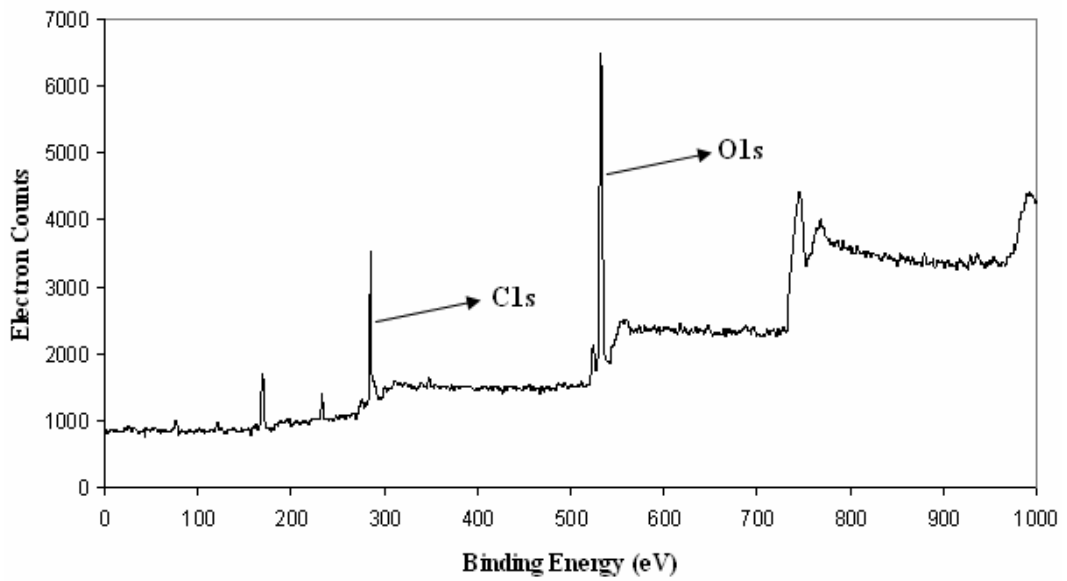


**Figure B.5** ESCA spectrum of CNT4

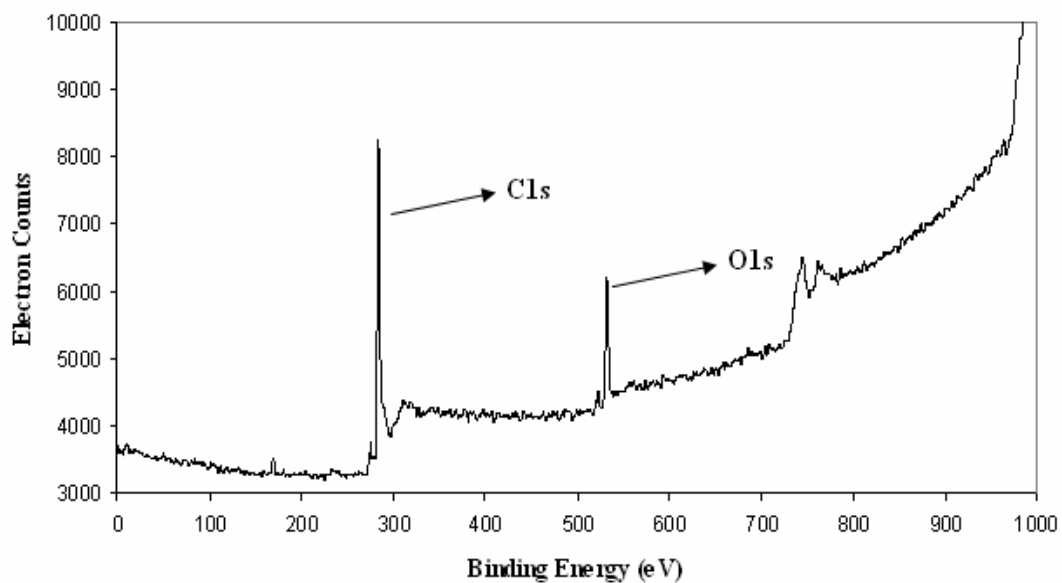


**Figure B.6** ESCA spectrum of CNT5

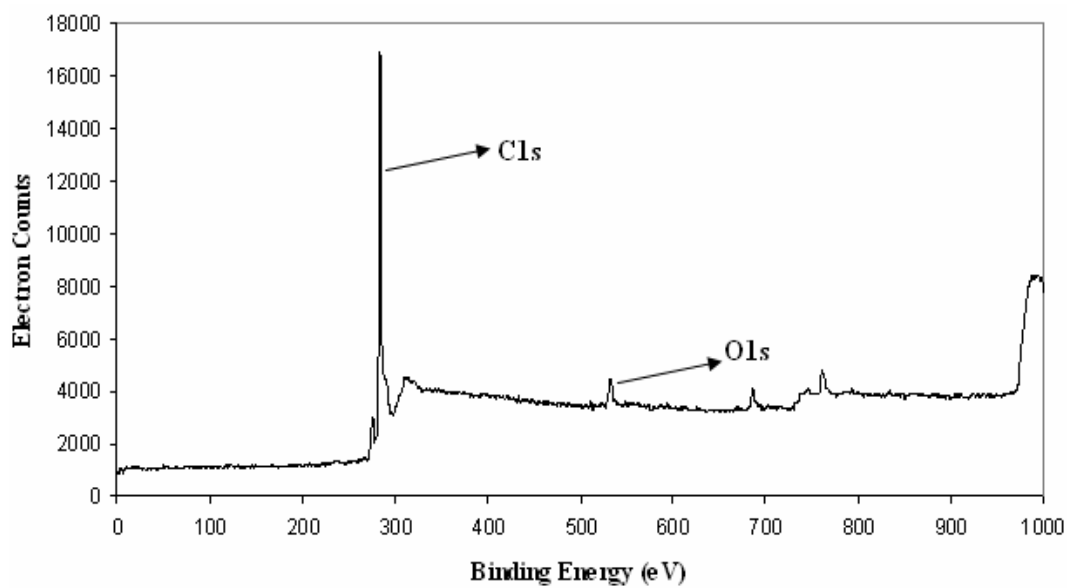


**Figure B.7** ESCA spectrum of CNT6

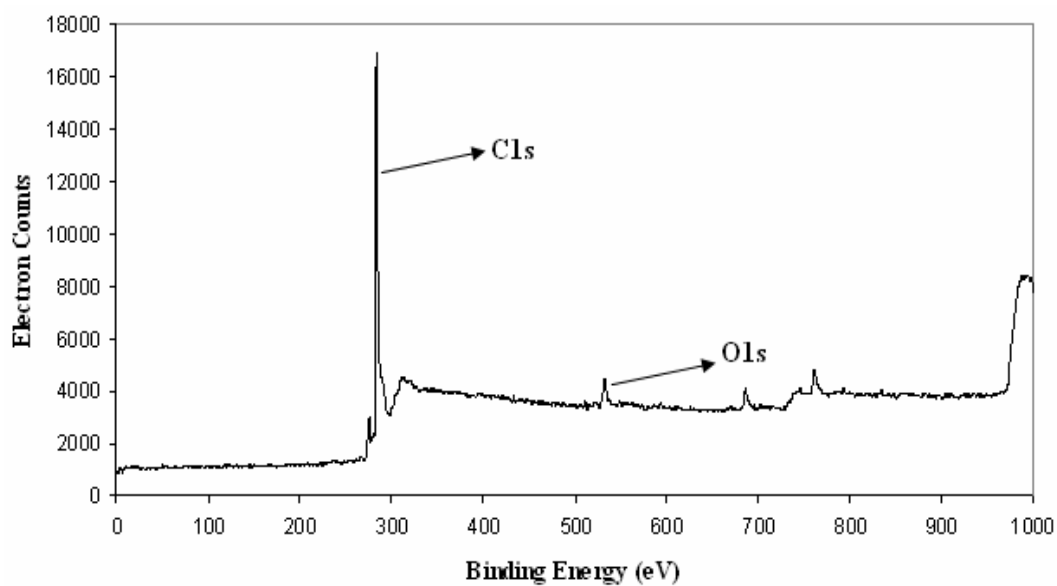


**Figure B.8** ESCA spectrum of CNT7

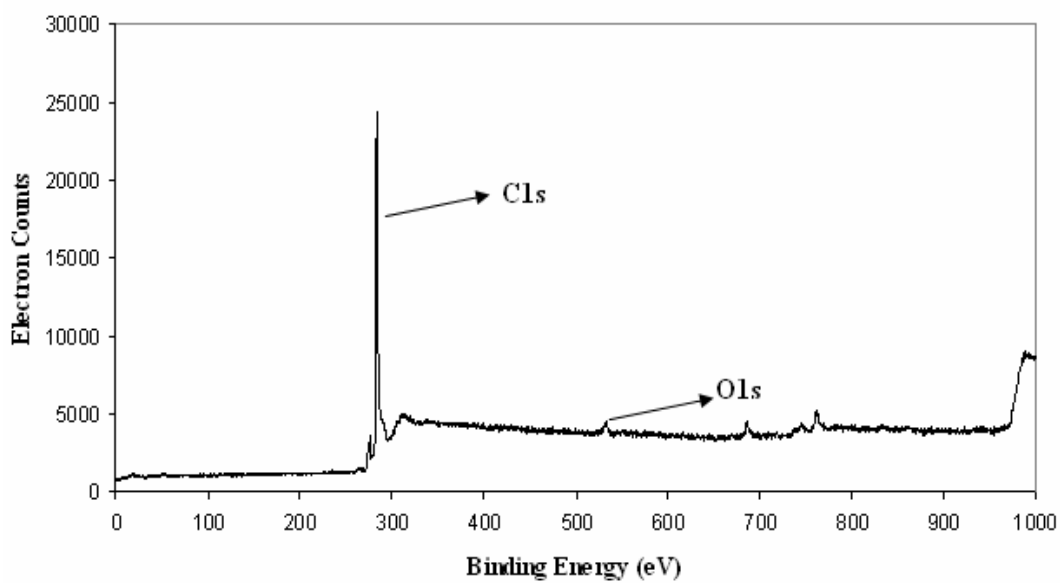


**Figure B.9** ESCA spectrum of CNT8

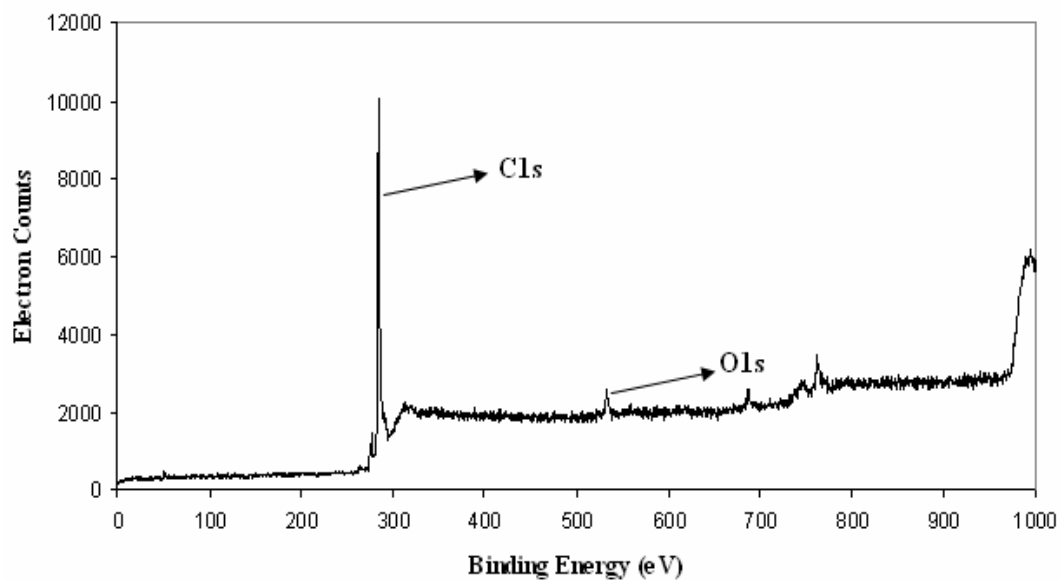


**Figure B.10** ESCA spectrum of SDSCNT

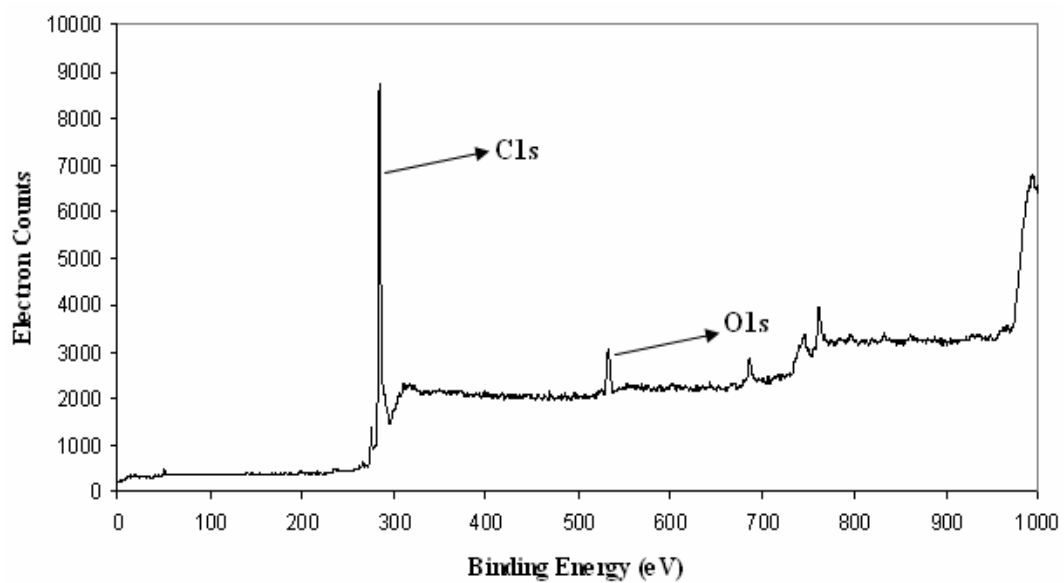


**Figure B.11** ESCA spectrum of DGEBCNT

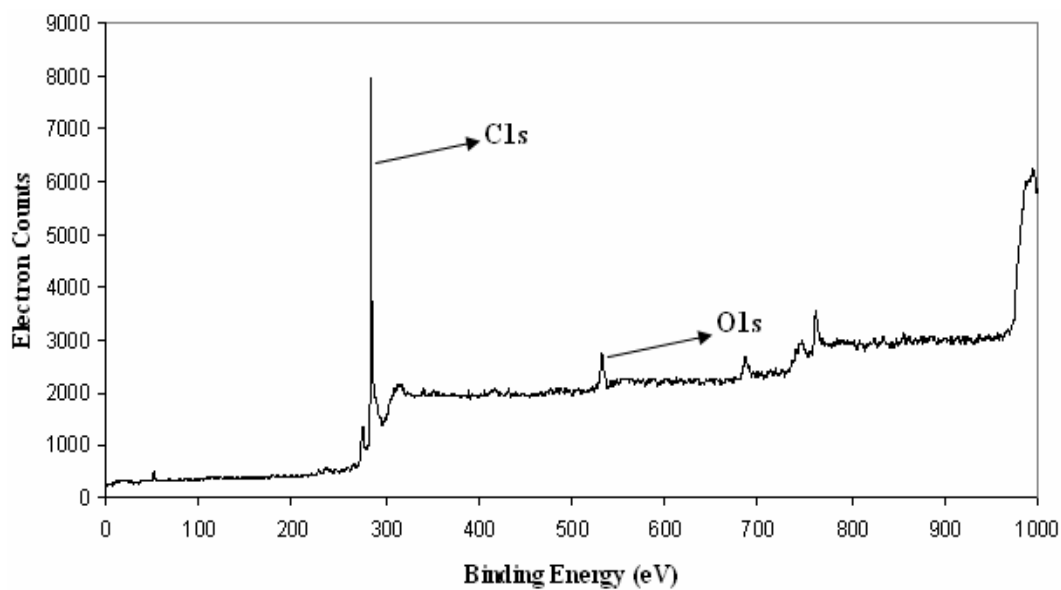


**Figure B.12** ESCA spectrum of PEG400CNT

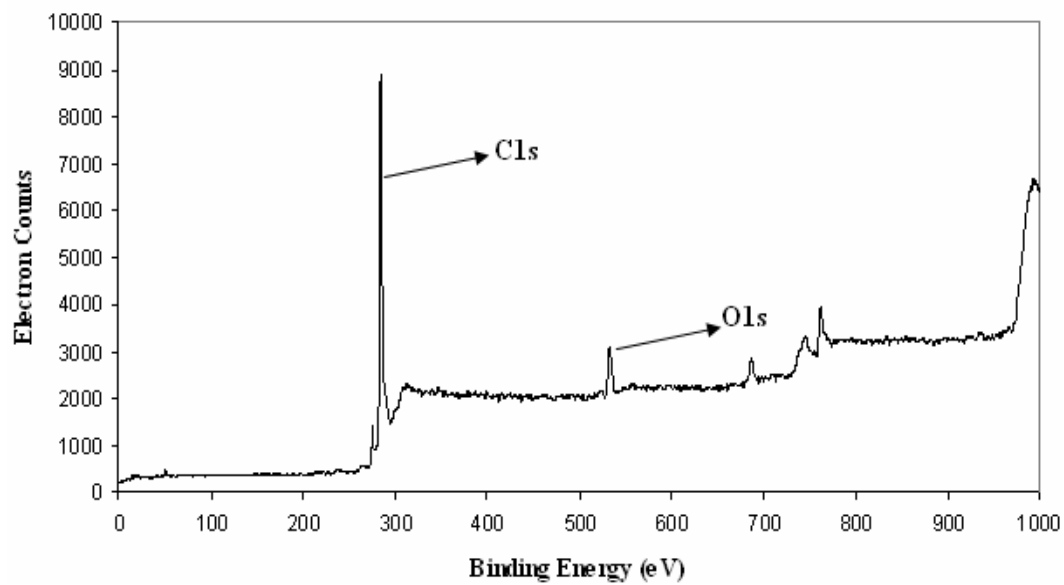


**Figure B.13** ESCA spectrum of PEG1000CNT

# APPENDIX C

## SOLID STATE NMR

Sample 1 <sup>13</sup>C CPMAS SPECTRUM  
Spin rate 5000Hz

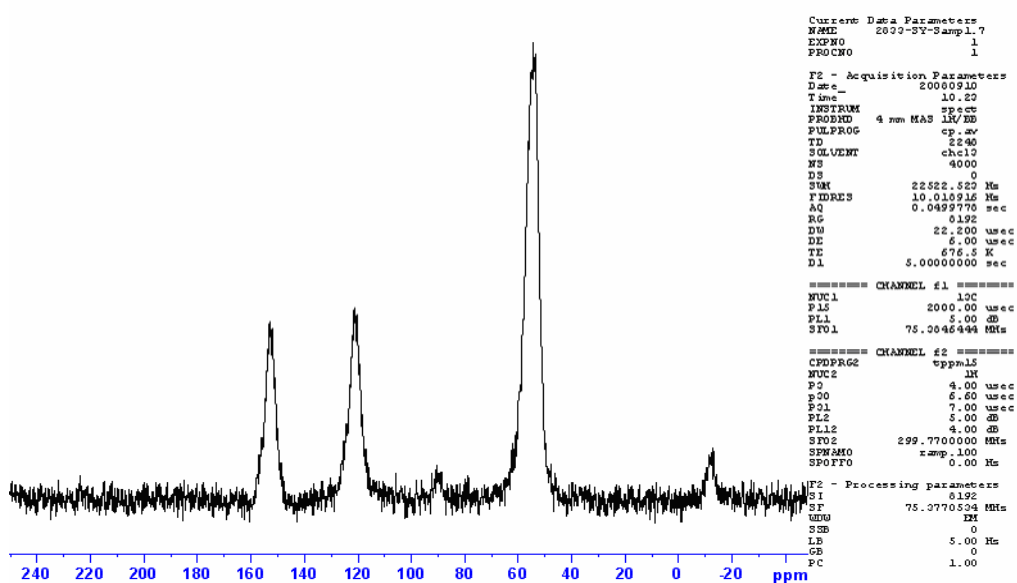


Figure C.1 <sup>13</sup>C NMR spectrum of PET

Sample 2 13C CPMAS SPECTRUM  
Spin rate 5000Hz

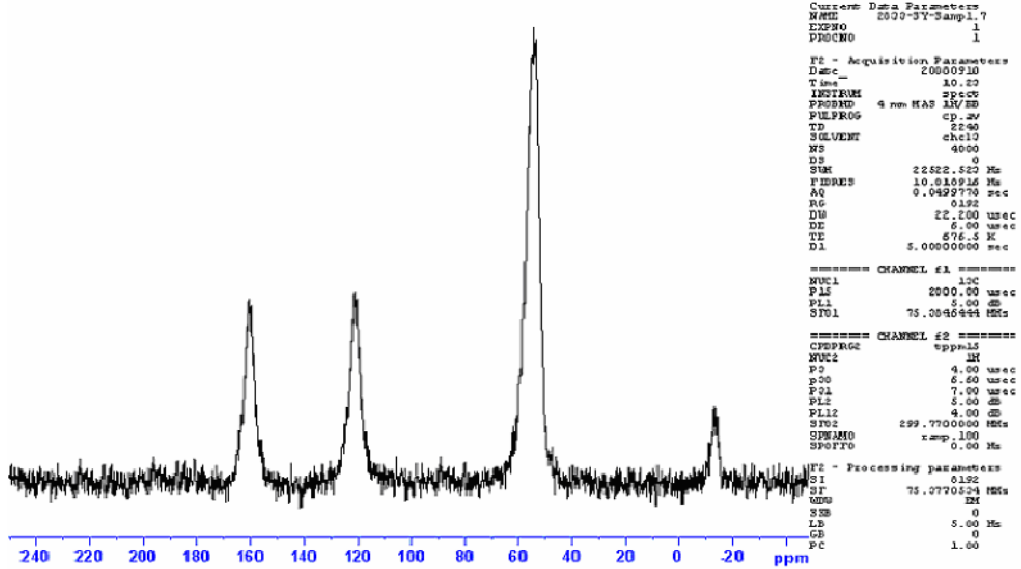


Figure C.2 <sup>13</sup>C NMR spectrum of PET/ASCNT composite

Sample 3 13C CPMAS SPECTRUM  
Spin rate 5000Hz

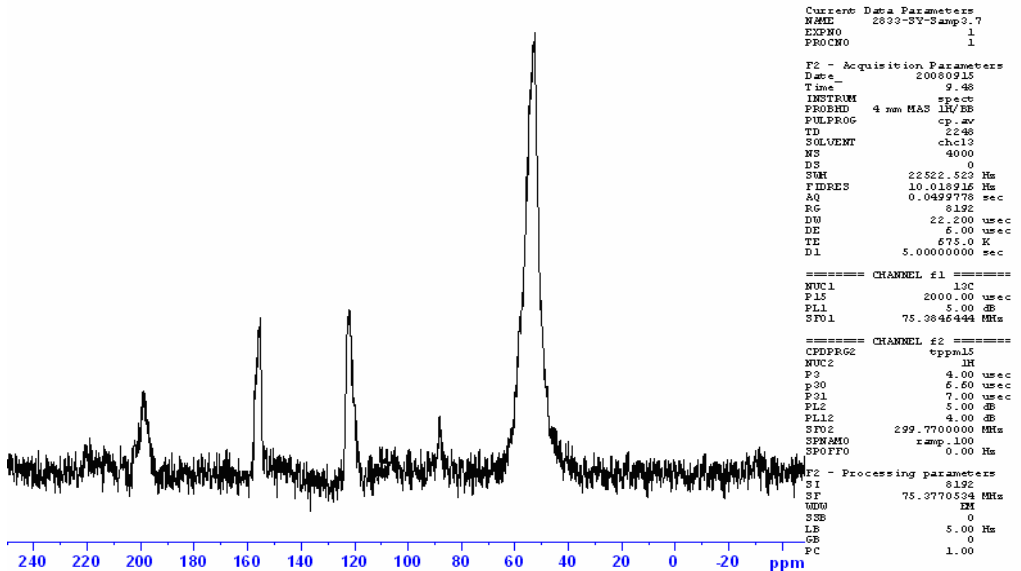


Figure C.3 <sup>13</sup>C NMR spectrum of PET/pCNT composite

Sample 7 13C CPMAS SPECTRUM  
Spin rate 5000Hz

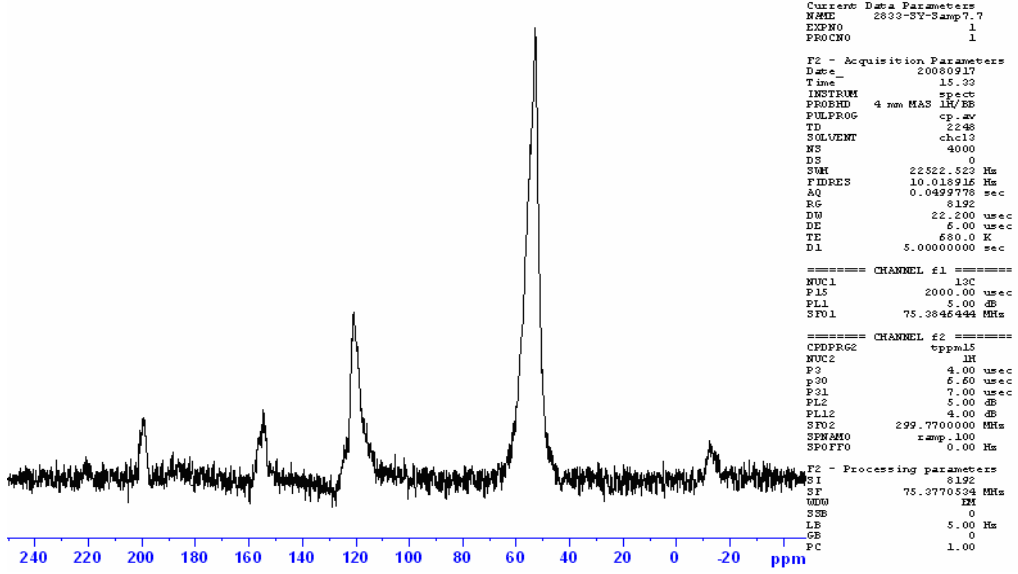


Figure C.4 <sup>13</sup>C NMR spectrum of PET/SDSCNT composite

Sample 6 13C CPMAS SPECTRUM  
Spin rate 5000Hz

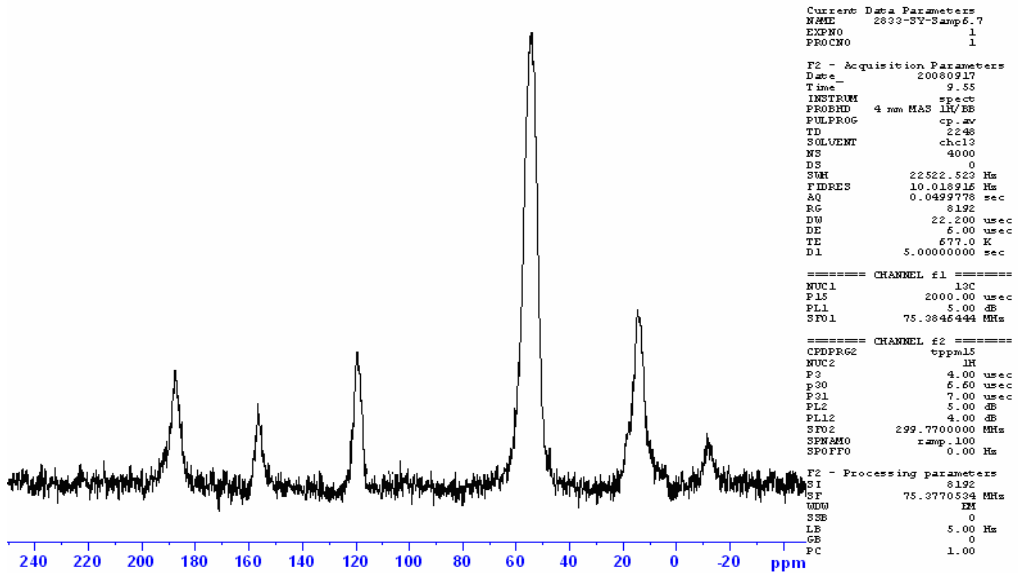


Figure C.5 <sup>13</sup>C NMR spectrum of PET/DGEBACNT composite

Sample 4 <sup>13</sup>C CPMAS SPECTRUM  
Spin rate 5000Hz

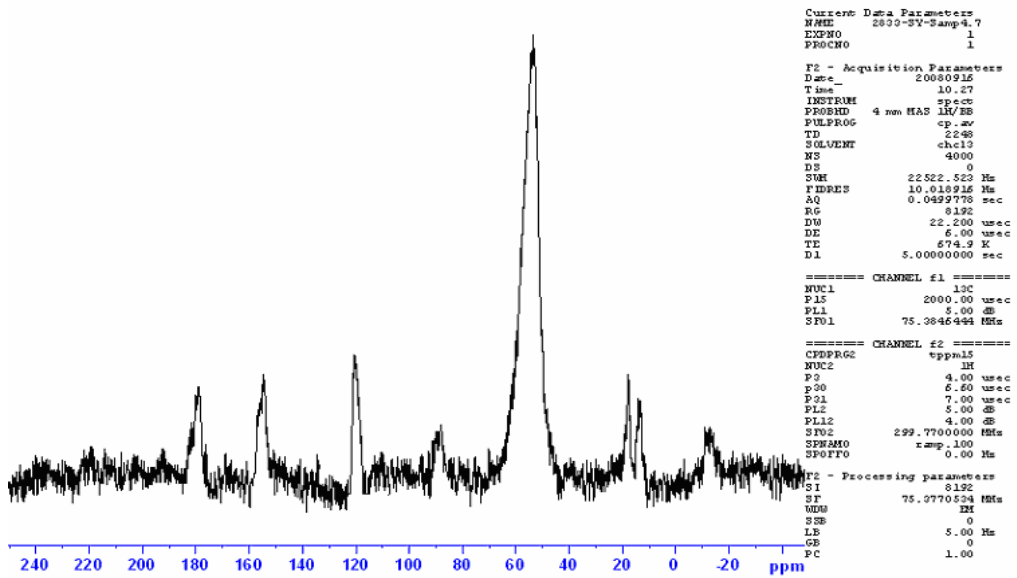


Figure C.6 <sup>13</sup>C NMR spectrum of PET/PEG400CNT composite

Sample 5 <sup>13</sup>C CPMAS SPECTRUM  
Spin rate 5000Hz

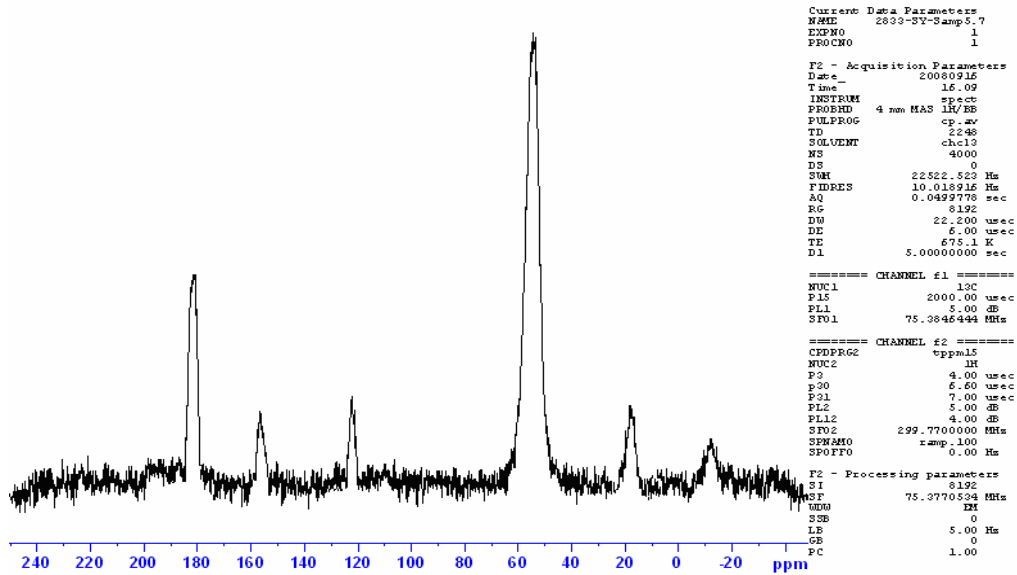


Figure C.7 <sup>13</sup>C NMR spectrum of PET/PEG1000CNT composite

## APPENDIX D

### DSC THERMOGRAMS

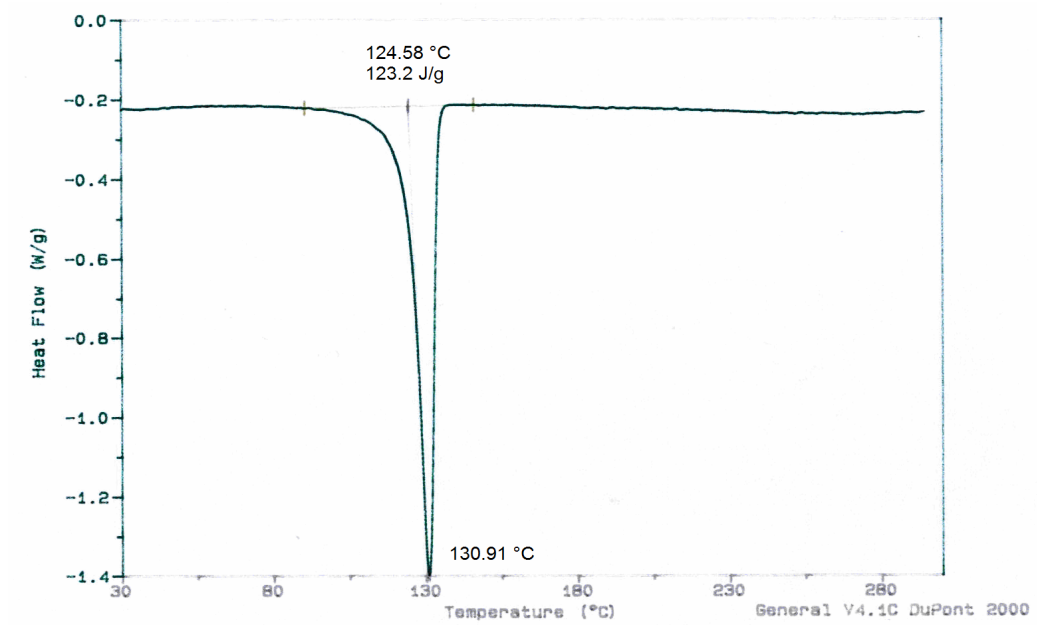
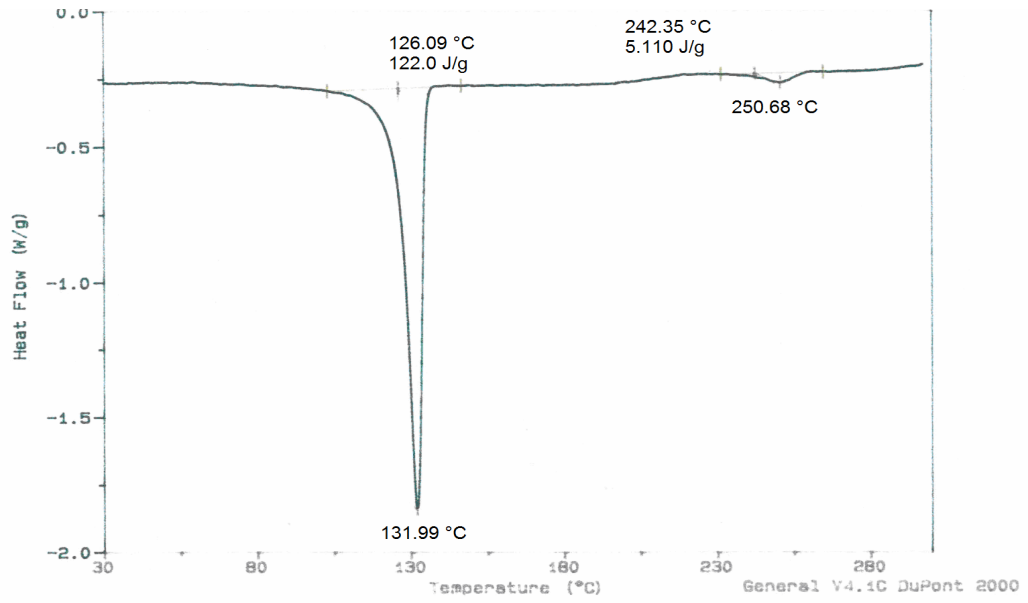
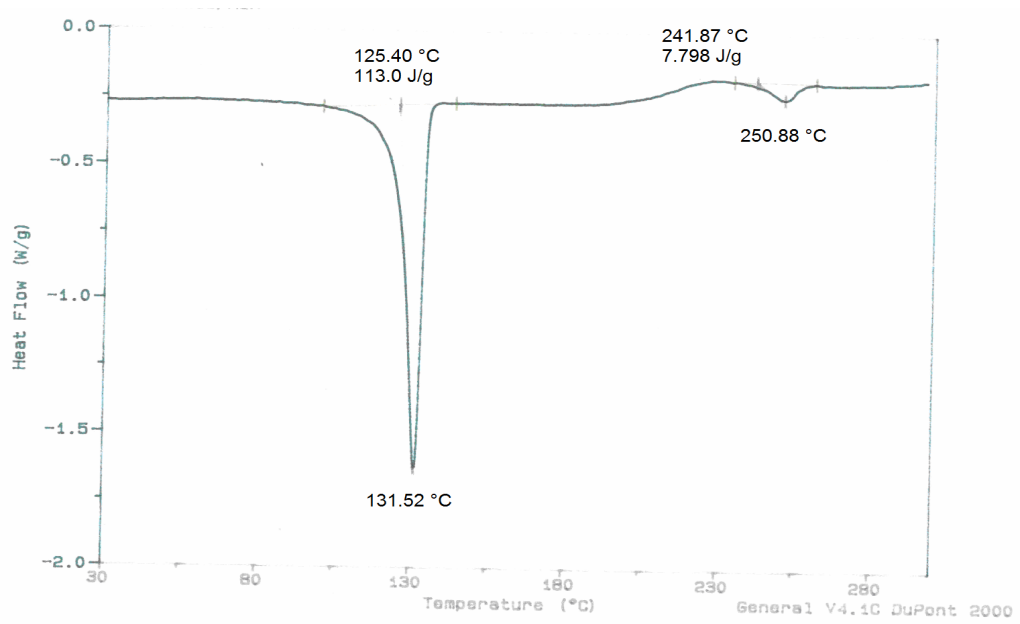


Figure D.1 DSC thermogram of HDPE



**Figure D.2** DSC thermogram of HDPE/PET (80/20) blend



**Figure D.3** DSC thermogram of HDPE/PET (70/30) blend

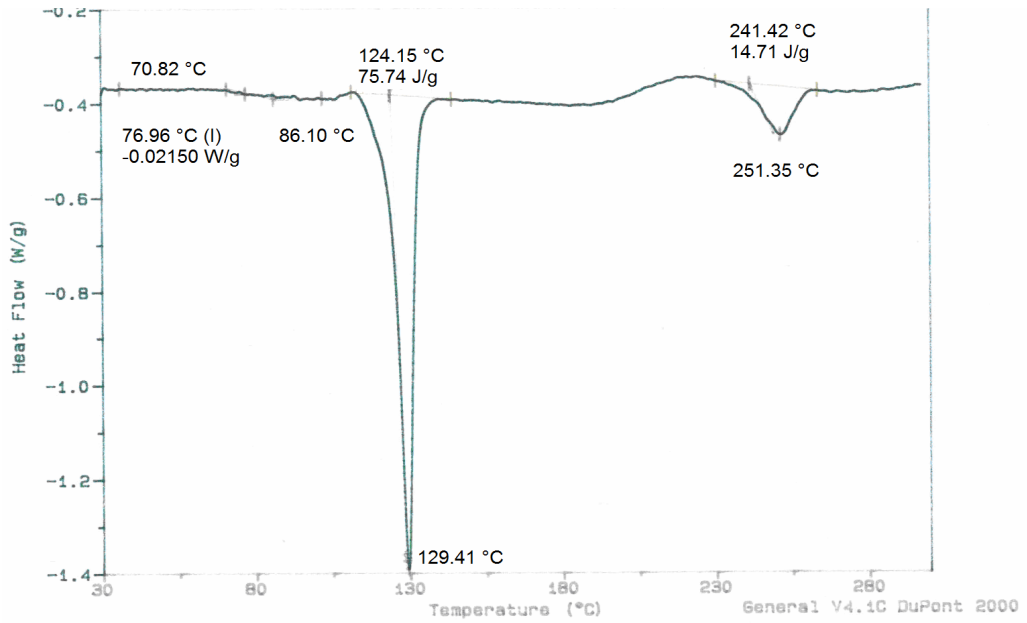


**Figure D.4** DSC thermogram of HDPE/PET (50/50) blend

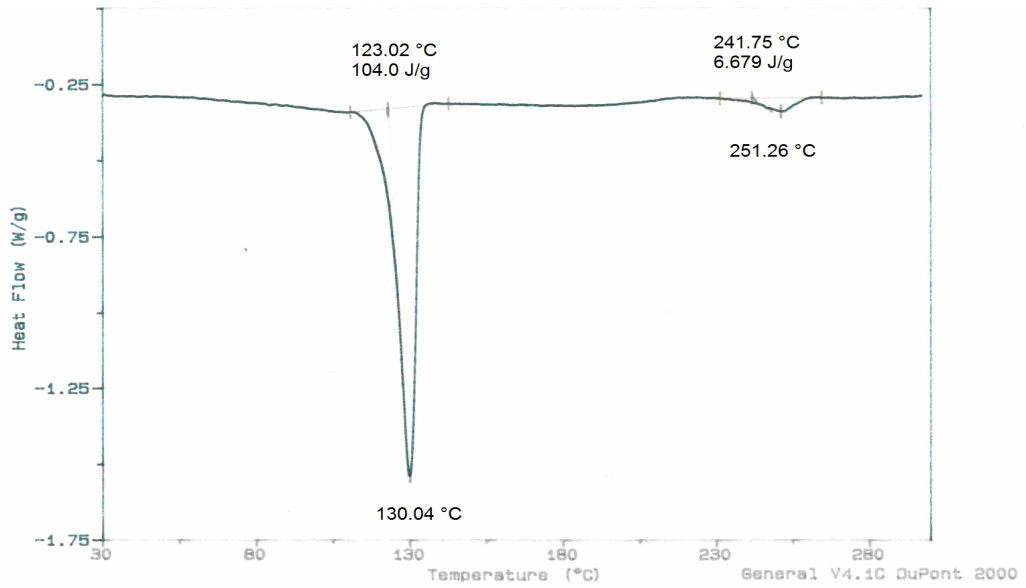


**Figure D.5** DSC thermogram of microfiber reinforced HDPE/PET/ASCNT (80/20/0.5) composite

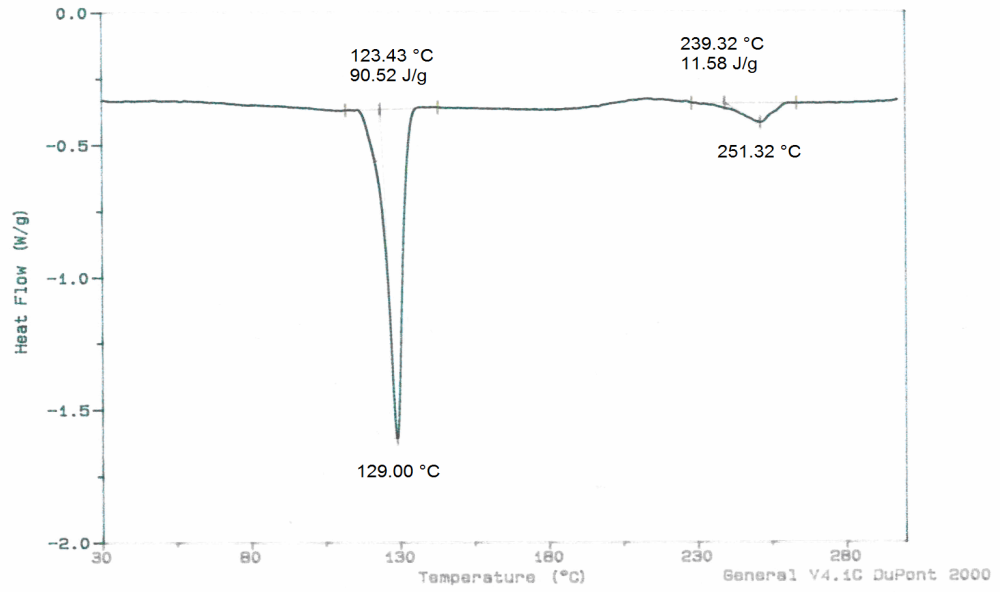


**Figure D.6** DSC thermogram of microfiber reinforced HDPE/PET/ASCNT (70/30/0.5) composite

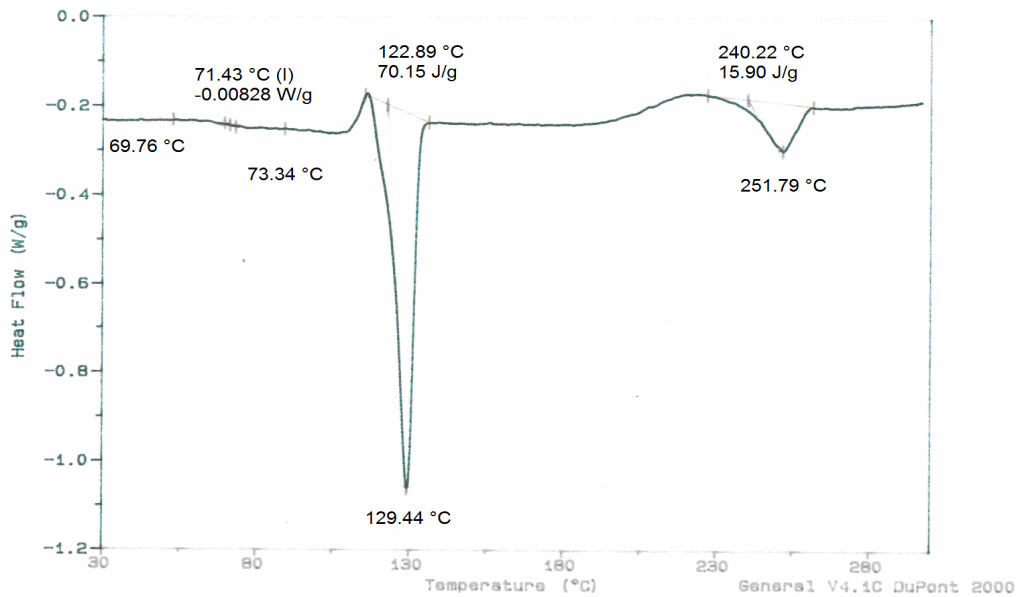


**Figure D.7** DSC thermogram of microfiber reinforced HDPE/PET/ASCNT (50/50/0.5) composite

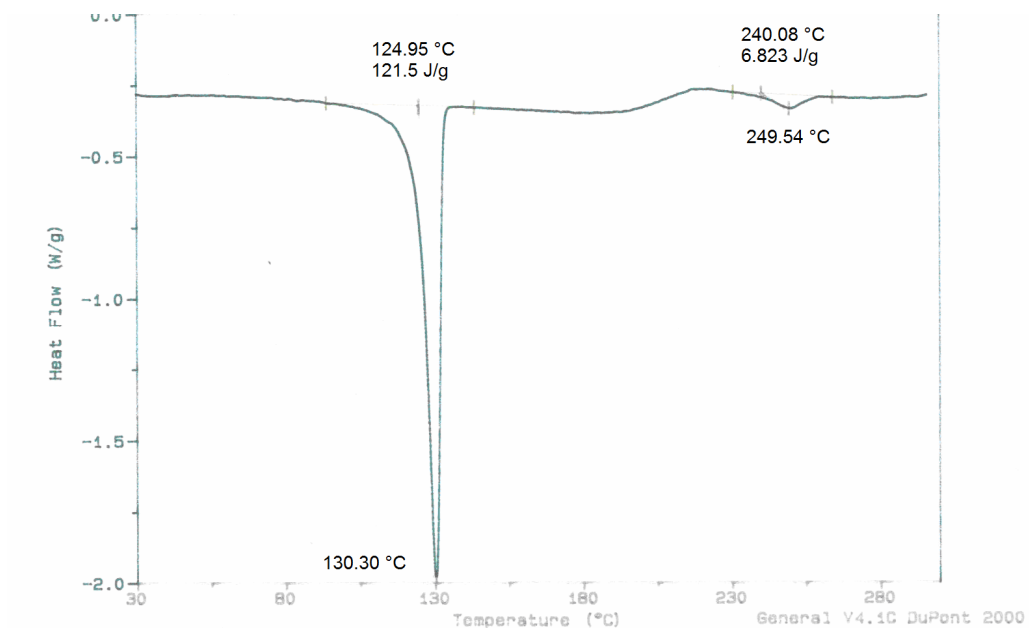


**Figure D.8** DSC thermogram of microfiber reinforced HDPE/PET/ASCNT (80/20/0.5) composite molded at 210 °C

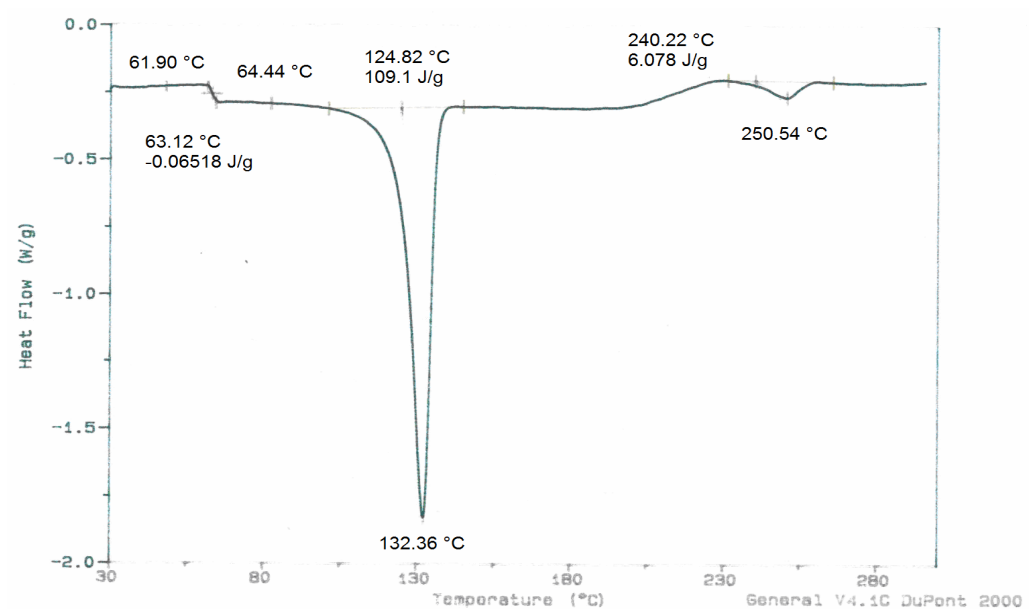


**Figure D.9** DSC thermogram of microfiber reinforced HDPE/PET/ASCNT (80/20/0.5) composite molded at 240 °C

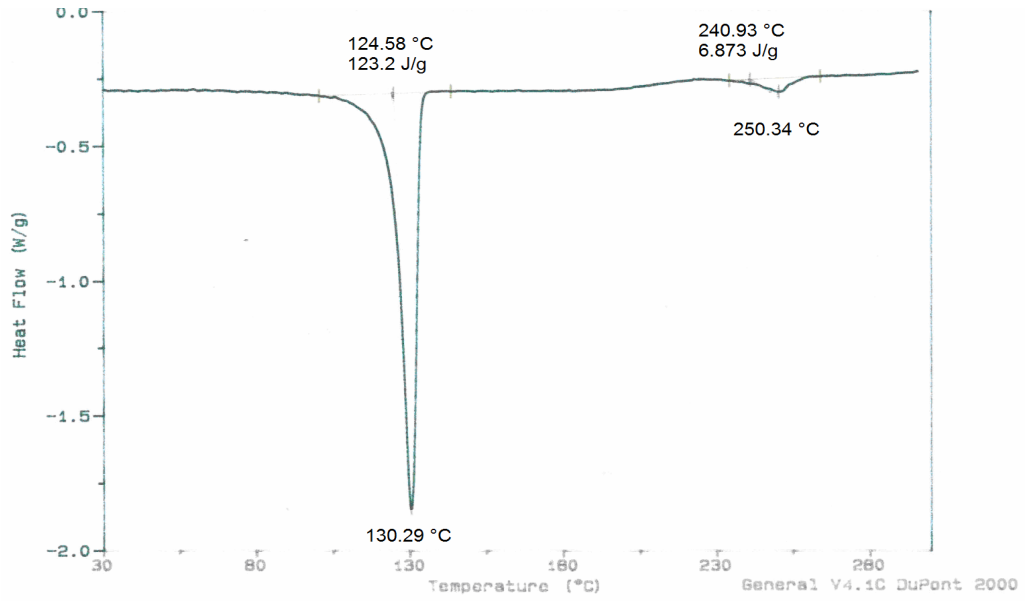


**Figure D.10** DSC thermogram of microfiber reinforced HDPE/PET/ASCNT (80/20/0.5) composite molded at 280 °C

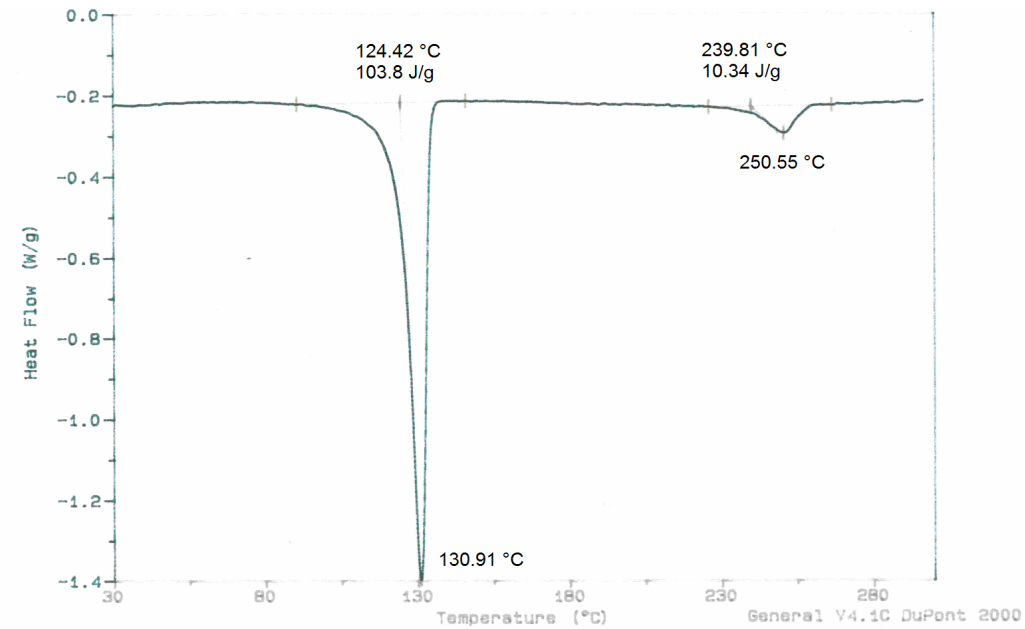


**Figure D.11** DSC thermogram of microfiber reinforced HDPE/PET/ASCNT (70/30/0.5) composite molded at 210 °C

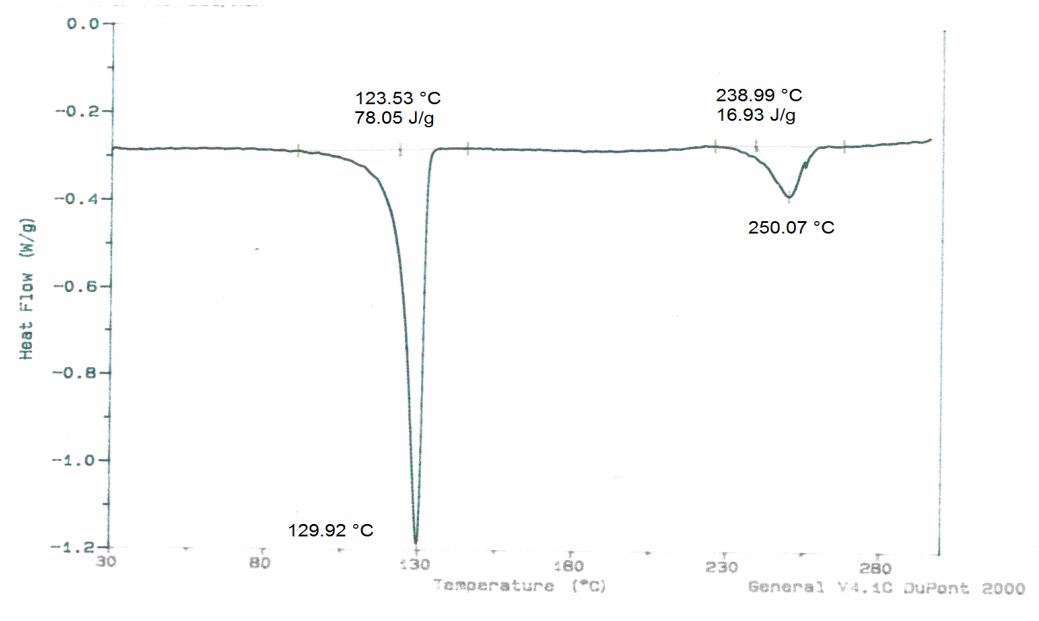


**Figure D.12** DSC thermogram of microfiber reinforced HDPE/PET/ASCNT (50/50/0.5) composite molded at 210 °C

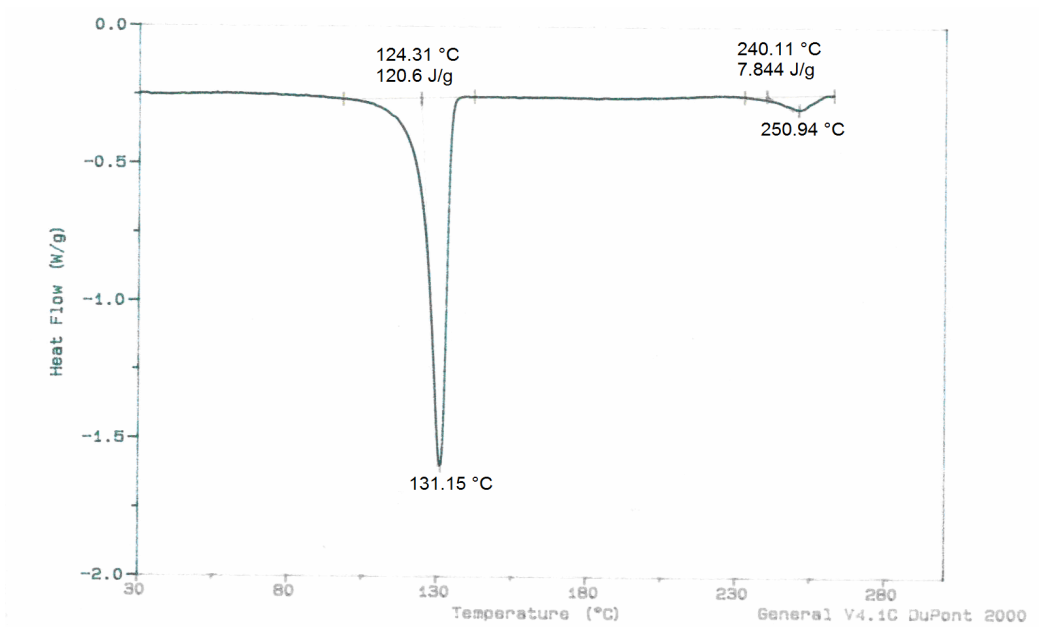


**Figure D.13** DSC thermogram of conventional HDPE/PET/ASCNT (80/20/0.5) composite

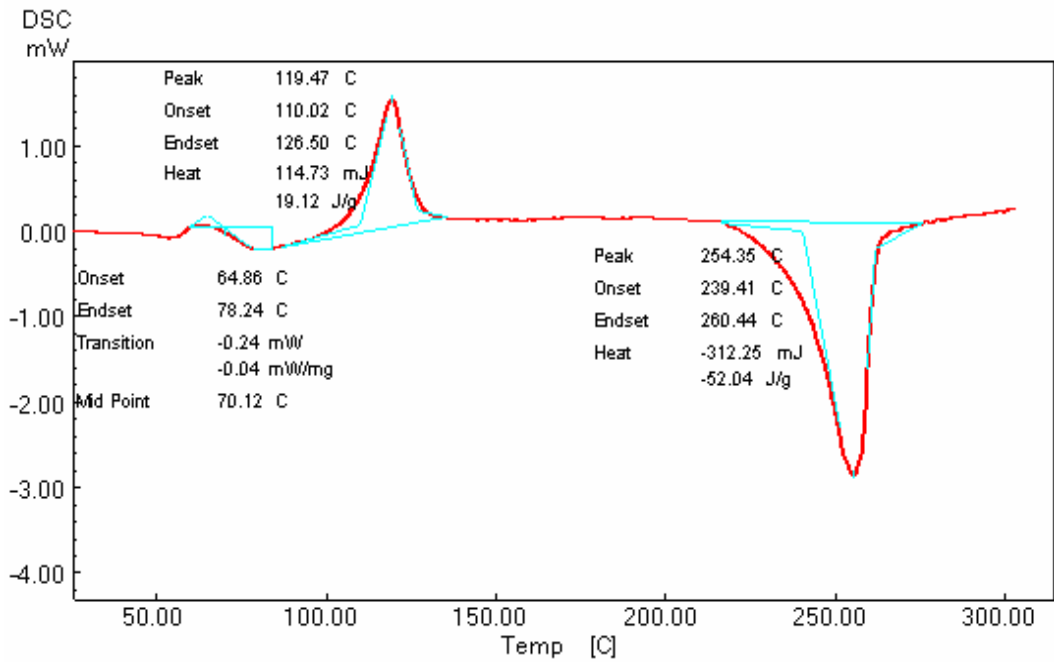


**Figure D.14** DSC thermogram of PET

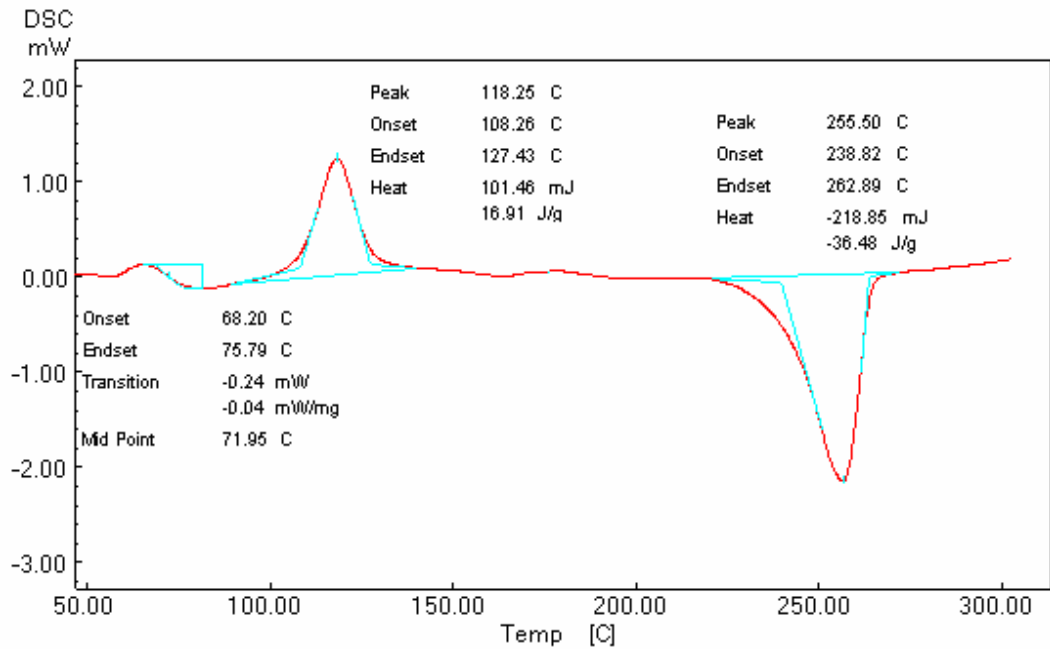


**Figure D.15** DSC thermogram of PET/ASCNT (0.5 wt. %) composite

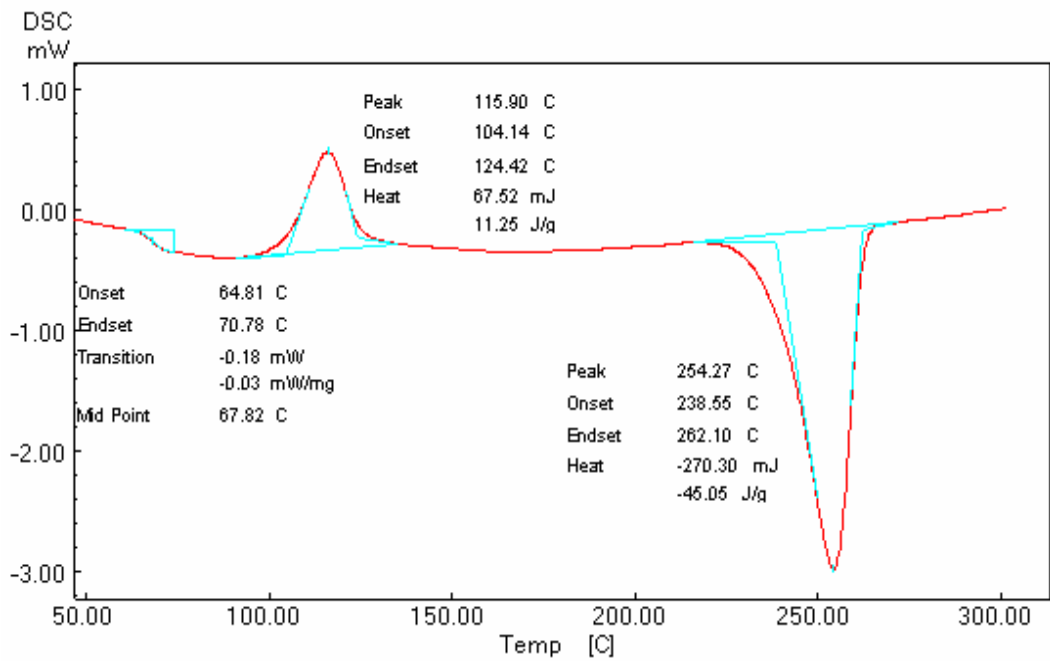


**Figure D.16** DSC thermogram of PET/pCNT (0.5 wt. %) composite

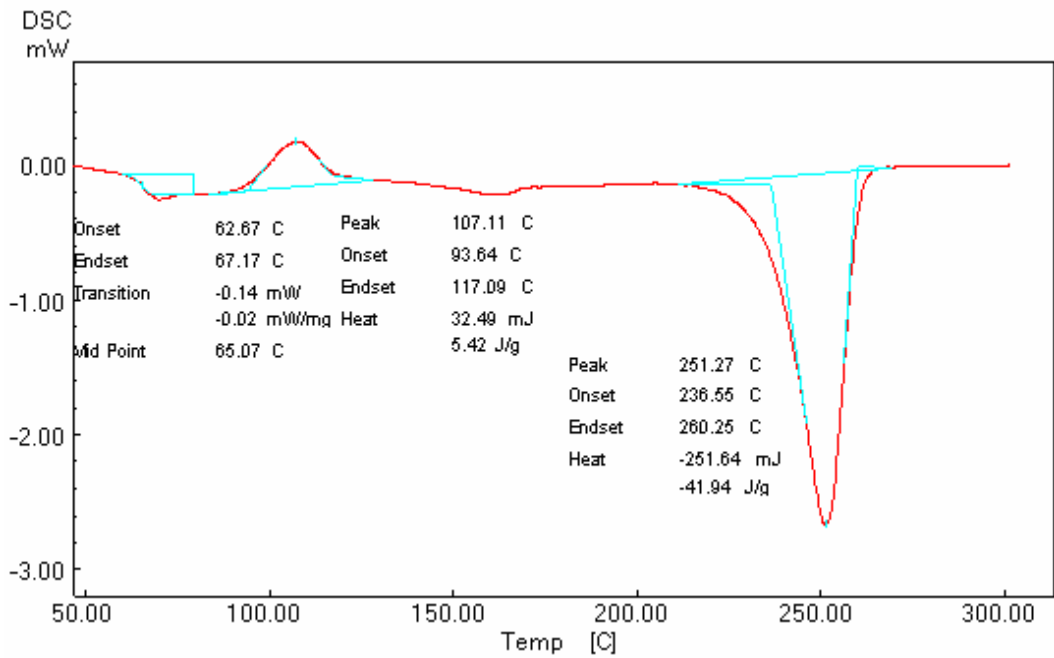


**Figure D.17** DSC thermogram of PET/SDSCNT (0.5 wt. %) composite

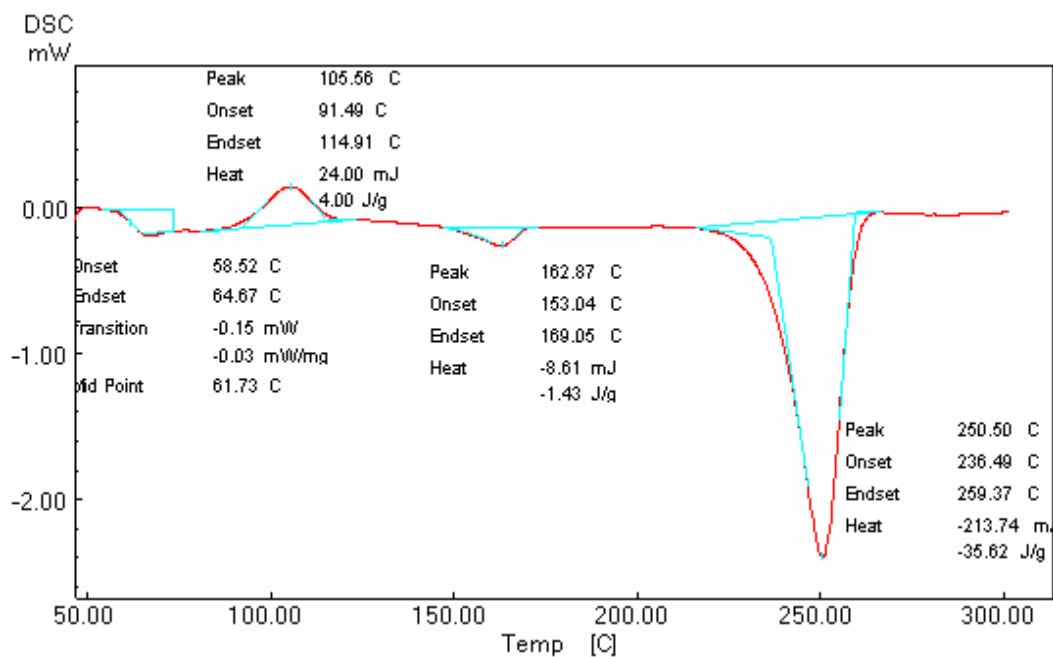


**Figure D.18** DSC thermogram of PET/DGEBACNT (0.5 wt. %) composite

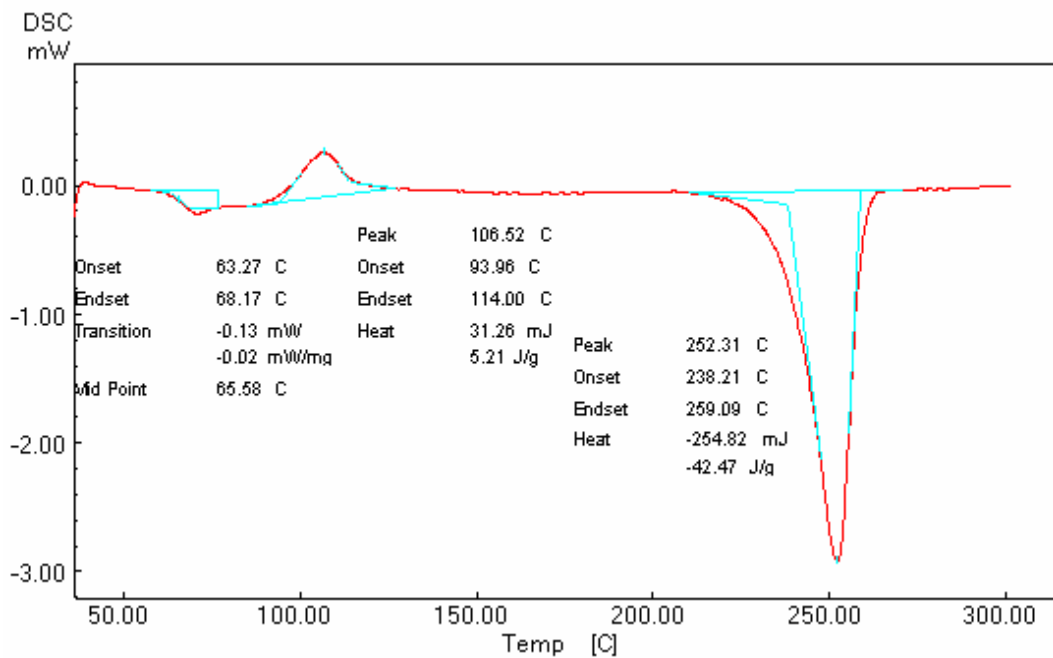


**Figure D.19** DSC thermogram of PET/PEG400CNT (0.5 wt. %) composite

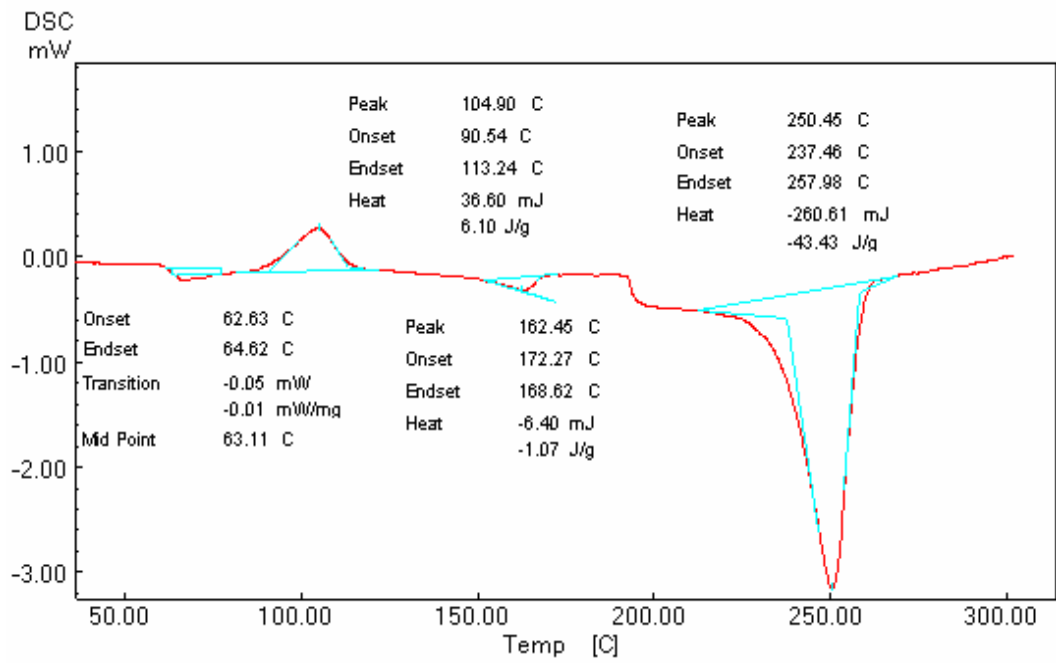


**Figure D.20** DSC thermogram of PET/PEG1000CNT (0.5 wt. %) composite

# CURRICULUM VITAE

## Personal Information

**Surname, Name:** Yeşil, Sertan

**Birth:** 1980, İzmir, Turkey

**Address:** Hedef Sokak. 9/7 Anittepe Ankara, TURKEY

**Nationality:** Turkish

**Marital Status:** Married

**E-mail:** syesil@metu.edu.tr

**Mobile:** + 90 505 455 89 90

## Education

**B.Sc.** (Chemical Engineering) (C.GPA: 3.49/4.00)

**[September 1998 - June 2003]**

**Middle East Technical University**, Department of Chemical Engineering, Ankara, Turkey

**High School**

**[September 1995 – February 1998]**

**Kocaeli Körfez Fen Lisesi**, Kocaeli, Turkey

## Professional Experience

**Research Assistant** (Chemical Engineering)

**[January 2004 - To date]**

**Middle East Technical University**, Department of Chemical Engineering, Ankara, Turkey

**Intern Chemical Engineer** (Summer Practice)

**[July 2002 – August 2002]**

**KORDSA**, Kocaeli, Turkey

**Intern Chemical Engineer** (Summer Practice)

**[June 2001 – July 2001]**

**DEPA, Kocaeli, Turkey**

### **Abroad Experience**

**Researcher**

**[February 2009 – August 2009]**

**University of California Davis**, Department of Mechanical and Aerospace Engineering, Davis CA, USA

### **Journal Publications**

- O. Koysuren, S. Yesil and G. Bayram, “Effect of Composite Preparation Techniques on Electrical and Mechanical Properties and Morphology of Nylon 6 Based Conductive Polymer Composites”, Journal of Applied Polymer Science, 102, pg. 2520, 2006.
- O. Koysuren, S. Yesil and G. Bayram, “Effect of Surface Treatment on Electrical Conductivity of Carbon Black Filled Conductive Polymer Composites”, Journal of Applied Polymer Science, 104, pg. 3427, 2007.
- O. Koysuren, S. Yesil, G. Bayram, M. Secmen and O.A. Civi, “Effect of a Carbon Black Surface Treatment on the Microwave Properties of PET/Carbon Black Composites”, Journal of Applied Polymer Science, 109, pg. 152, 2008.
- S. Yesil, O. Koysuren and G. Bayram, “Effect of Microfiber Reinforcement on the Morphology, Electrical, and Mechanical Properties of the Polyethylene/Poly(Ethylene Terephthalate)/Carbon Nanotube Composites”, Polymer Engineering and Science, (In Press), 2010.
- O. Koysuren, S. Yesil and G. Bayram, “Effect of Solid State Grinding on Properties of PP/PET Blends and Their Composites with Carbon Nanotubes”, Journal of Applied Polymer Science, (In Press), 2010.
- S. Yesil and G. Bayram, “Effect of Carbon Nanotube Purification on the Electrical and Mechanical Properties of Poly(ethylene terephthalate) Composites with Carbon Nanotubes in Low Concentration”, Journal of Applied Polymer Science, (In Press), 2010.

## **Conference Publications**

- O. Koysuren, S. Yesil and G. Bayram, "Preparation and Characterization of Nylon 6 Based Conductive Composites", Annual Technical Conference (ANTEC 2005), Boston, U.S.A., pg. 154, May 2005, (Poster Presentation).
- O. Koysuren, S. Yesil ve G. Bayram, "Karbon Bazlı Dolgu Maddesi İçeren Poli(Etilen Terftalat) Kompozitlerinin Mekanik ve Elektriksel Özellikleri", I. Ulusal Polimer Bilim ve Teknoloji Kongresi ve Sergisi, Ankara, Haziran 2006, (Oral Presentation).
- S. Yesil, M. Kilinc, and G. Bayram, "Poli(etilen tereftalat)/Poli(etilen naftalat) Bazlı Nanokompozitlerin Üretimi ve Karakterizasyonu", I. Ulusal Polimer Bilim ve Teknoloji Kongresi ve Sergisi, Ankara, Haziran 2006, (Oral Presentation).
- S. Yesil, O. Koysuren and G. Bayram, "Conductive Polymer Composites with Surface Modified Carbon Black", 22<sup>nd</sup> Annual Meeting of Polymer Processing Society (PPS 22), Yamagata, Japan, June 2006, (Poster Presentation).
- M. Kilinc, S. Yesil and G. Bayram, "Effect of Elastomer Type on Mechanical and Morphological Properties of PEN/PET Blend Based Composites", 22<sup>nd</sup> Annual Meeting of Polymer Processing Society (PPS 22), Yamagata, Japan, June 2006, (Oral Presentation).
- S. Yesil, O. Koysuren ve G. Bayram, "Karbon Bazlı Dolgu Maddeleri Katkılı Polipropilen Kompozitlerinin Mekanik ve Elektriksel Özellikleri", Yedinci Ulusal Kimya Mühendisliği Kongresi (UKMK 7), Eskişehir, Eylül 2006, (Poster Presentation).
- O. Koysuren, S. Yesil and G. Bayram, "Effect of Solid State Grinding Technique on Microstructured Blends of Incompatible Polymers", Somer Symposium Series I, Ankara, pg. 52, May 2007, (Poster Presentation).
- S. Yesil, O. Koysuren and G. Bayram, "In-Situ Microfiber Reinforcement of Conductive Polymer Composites", Somer Symposium Series I, Ankara, pg. 50, May 2007, (Poster Presentation).
- M. Kilinc, S. Yesil, G. Cakal, G. Bayram, S. Ozkar, and I. Eroglu "Production and Characterization of Hydrated Zinc Borate", Somer Symposium Series I, Ankara, pg. 51, May 2007, (Poster Presentation).

- M. Kilinc, S. Yesil, G. Cakal, G. Bayram, I. Eroglu, and S. Ozkar “Production and Characterization of 3.5 Mol Crystal Water Containing Zinc Borate on Pilot Scale”, 2. Ulusal Bor Sempozyumu, Ankara, Nisan 2008, (Oral presentation).
- S. Yesil, O. Koysuren and G. Bayram, “Processing and Characterization of Electrically Conductive In-situ Microfiber Polymer Composites”, 24<sup>th</sup> Annual Meeting of Polymer Processing Society (PPS 24), Salerno, Italy, June 2008, (Oral Presentation).
- O. Koysuren, S. Yesil, G. Bayram, M. Seçmen and O.A. Çivi, “Effect of Surface Treatment on Electrical and Microwave Properties of Carbon Black Filled PET Based Composites”, 24<sup>th</sup> Annual Meeting of Polymer Processing Society (PPS 24), Salerno, Italy, June 2008, (Poster Presentation).
- S. Yesil, O. Koysuren ve G. Bayram, “Poli(etilen tereftalat)/Karbon Nanotüp Kompozitlerinin Elektriksel ve Mekanik Özelliklerinin Geliştirilmesi”, Sekizinci Ulusal Kimya Mühendisliği Kongresi (UKMK 8), Malatya, Ağustos 2008, (Oral Presentation).
- S. Yesil and G. Bayram, “Surface Treatment of Carbon Nanotubes and Their Composites with Poly(ethylene terephthalate)”, 6th Chemical Engineering Conference for Collaborative Research in Eastern Mediterranean Countries (EMCC-6), Antalya, March 2010, (Poster Presentation).
- S. Yesil and G. Bayram, “Preparation and Characterization of Poly(ethylene terephthalate)/Carbon Nanotube Composites with Surface Modified Carbon Nanotubes”, Orlando, U.S.A., May 2010, (Poster Presentation).
- S. Yesil ve G. Bayram, “Mikrolifsel Güçlendirme Yöntemi Kullanılarak Hazırlanan Polietilen/Poli(etilen tereftalat)/Karbon Nanotüp Kompozitlerinin Elektriksel ve Mekanik Özelliklerinin İncelenmesi”, III. Ulusal Polimer Bilim ve Teknoloji Kongresi ve Sergisi, Kocaeli, Mayıs 2010, (Oral Presentation).

### **Research Projects**

- Preparation of Conductive Polymer Composites with the Addition of Conductive Fillers, TUBITAK (Scientific and Technological Research Council of Turkey) MISAG 271 (August 2004-February 2006), METU, Ankara, Turkey.

- Development of Production Techniques of Zinc Borate and Investigation of Its Uses as Flame Retardant Additive, BOREN (National Boron Research Foundation) BOREN-2005-07-G10-10 (July 2005-July 2007), METU, Ankara, Turkey.
- Conductive Polymer Composites: Production and Characterization, BAP-08-11-DPT2002K120510 (November 2003-November 2007), METU, Ankara, Turkey.

### **Honors, Prizes, and Awards**

- Kemal Kurdaş Academic Success Award, ODTÜ İstanbul Mezunlar Derneği, May 2002.
- Prof.Dr. Hasan Orbey Graduate Award, METU Chemical Engineering Department, December 2008.

### **Computer Related Experience and Skills**

- **Programming Languages:** FORTRAN 77
- **Operating Systems:** Windows 98/2000/XP/Vista
- **Commercial and Research Software Packages:** Matlab Simulink, Adobe Photoshop, Microsoft Office XP/2003/2007 (Word, Excel, PowerPoint, Outlook)

### **Languages**

**English:** Very good in reading and writing

**German:** Beginner